

# **Evaluation of the Broadband Impedance Spectroscopy Prognostic/Diagnostic Technique for Electric Cables Used in Nuclear Power Plants**

**The Boeing Company and  
Brookhaven National Laboratory**

**U.S. Nuclear Regulatory Commission  
Office of Nuclear Regulatory Research  
Washington, DC 20555-0001**



---

---

# Evaluation of the Broadband Impedance Spectroscopy Prognostic/Diagnostic Technique for Electric Cables Used in Nuclear Power Plants

---

---

Manuscript Completed: November 2005  
Date Published: June 2006

Prepared by  
D. Rogovin<sup>1</sup>, R. Lofaro<sup>2</sup>

<sup>1</sup> The Boeing Company  
Huntington Beach, CA 92647

<sup>2</sup> Brookhaven National Laboratory  
Upton, NY 11973-5000

J. Vora, NRC Project Manager

**Prepared for**  
**Division of Fuel, Engineering and Radiological Research**  
**Office of Nuclear Regulatory Research**  
**U.S. Nuclear Regulatory Commission**  
**Washington, DC 20555-0001**  
**NRC Job Code Y6410**



Intentionally Left Blank

## **ABSTRACT**

Aging mechanisms can lead to degradation of electric cables and resultant failures of critical functions, as well as losses of essential information for the decision-making process. Consequently, it would be highly desirable to have a single universally effective prognostic, diagnostic technique that can be used in situ to monitor the condition and predict the remaining useful life of installed electric cables of all types, in operating nuclear power plant applications and environments.

To address this issue, the U.S. Nuclear Regulatory Commission (NRC), Office of Nuclear Regulatory Research (RES), in collaboration with the Federal Aviation Administration (FAA) and the Boeing Company, initiated a research study to evaluate the effectiveness of the broadband impedance spectroscopy (BIS) technique for use in nuclear power plant cable diagnostics and condition monitoring. The results demonstrate the effectiveness of this nonintrusive, nondestructive technique, which uses low-voltage signals at varying frequencies to scan the length of an installed cable system to locate anomalies and degradation. Based upon this study's promising results, RES is considering follow-on collaborative research to demonstrate the effectiveness of the BIS technique in operating nuclear power plant environments.

Intentionally Left Blank

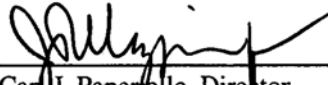
## FOREWORD

There is continued worldwide interest in the safety-related aspects of aging wire (cable) systems, including cables, splices, terminations, and electrical penetrations, in operating nuclear power plants. Aging of a wire system can result in a loss of critical functions of equipment energized by the system, or the loss of information that is critical to the decision-making process. Such losses can hamper operator actions and compromise plant safety. Therefore, condition monitoring of electric cables to verify their acceptability for continued service is of particular interest for applications in nuclear power plants, in which miles of electric cables are used to perform numerous operational and safety-related functions. However, there is currently no single in situ condition monitoring method that is universally effective in evaluating the condition of installed cables of all types, applications, and environments in operating nuclear power plants.

On November 15, 2000, the White House National Science and Technology Council, Committee on Technology, Wire System Safety Interagency Working Group, issued a report, entitled "Review of Federal Programs for Wire System Safety." That report concluded that safety of wire systems is a national issue that transcends various Government agencies and is important to public health and safety. Moreover, the interagency working group encouraged collaborative research among the various Federal agencies and develop a diagnostic technique that can be used in situ to monitor the condition of installed cable systems and predict their remaining useful life. Based on those recommendations, and in collaboration with the Federal Aviation Administration (FAA) and the Boeing Company, the U.S. Nuclear Regulatory Commission (NRC), Office of Nuclear Regulatory Research (RES), initiated a research program to evaluate the effectiveness of the broadband impedance spectroscopy (BIS) method for nuclear power plant cable diagnostics and condition monitoring. Toward that end, this report serves as a benchmark for interagency efforts to optimize research related to wire system aging.

The Boeing Company developed the BIS method in an FAA-sponsored research program to monitor the condition of installed aircraft wiring. The method utilizes impedance characteristics of the wiring to obtain information on the dielectric properties of wire insulation. The BIS method is a nonintrusive, nondestructive method that makes use of low-voltage signals at varying frequencies to scan the entire length of an installed cable system. The information extracted in this way can then be used to identify and locate anomalies and areas of degradation.

The RES-sponsored research program reported herein evaluated the BIS method for application to electric cables used in operating nuclear power plants. Research results demonstrate the effectiveness of the BIS method for detecting various types of anomalies and degradation in a commonly used type of low-voltage instrumentation and control electric cable. Notably, this research demonstrated the possibility of detecting and locating cable anomalies attributable to thermal hot spots, humidity, and abrasion. In addition, this report discusses considerations for follow-on research, preferably in a collaborative manner, to demonstrate the effectiveness of the BIS method in nuclear plant environments.

  
\_\_\_\_\_  
Carl J. Paperello, Director  
Office of Nuclear Regulatory Research  
U.S. Nuclear Regulatory Commission

Intentionally Left Blank

# TABLE OF CONTENTS

Page No.

ABSTRACT .....	iii
FOREWORD .....	v
TABLE OF CONTENTS .....	vii
LIST OF FIGURES .....	xi
LIST OF TABLES .....	xxiii
EXECUTIVE SUMMARY .....	xxv
ACKNOWLEDGMENTS .....	xxix
ABBREVIATIONS .....	xxxii
LIST OF SYMBOLS .....	xxxiii
1. INTRODUCTION .....	1
1.1 Background .....	1
1.2 Technical Issues .....	2
1.3 Objectives .....	4
1.4 Research Approach .....	4
1.5 Equipment Used .....	5
2. REVIEW OF CONDITION MONITORING TECHNIQUES .....	7
2.1 General Criteria for an Effective Technique .....	7
2.2 Mechanical Techniques .....	8
2.2.1 Visual Inspection .....	8
2.2.2 Elongation-At-Break .....	8
2.2.3 Compressive Modulus .....	9
2.3 Chemical Techniques .....	9
2.3.1 Oxidation Induction Time .....	10
2.3.2 Fourier Transform Infrared (FTIR) Spectroscopy .....	10
2.4 Electrical Techniques .....	11
2.4.1 Insulation Resistance .....	11
2.4.2 Dielectric Dissipation or Loss Factor .....	12
2.4.3 Voltage Withstand Test .....	13
2.4.4 Time-Domain Reflectometry .....	13
2.4.5 Partial Discharge Testing .....	14



2.5	Reasons to Focus on an Electrical Technique .....	14
3.	THEORY OF BROADBAND IMPEDANCE SPECTROSCOPY .....	15
3.1	Equivalent Circuit .....	15
3.2	Wire Properties and Wire Impedance Spectra .....	17
3.2.1	Approach to Extract Wire Properties from Impedance Data .....	17
3.2.2	Wire Properties from Impedance Data for Undamaged Wiring .....	21
3.2.3	Wire Properties from Impedance Data for Damaged Wiring .....	23
3.3	BIS Test Procedure .....	27
3.3.1	Procedure for Making Impedance Measurements .....	27
3.3.2	Analysis and Interpretation of Impedance Data .....	28
4.	PREPARATION AND BASELINE TESTING OF CABLE TEST SPECIMENS .....	31
4.1	Selection of Cable Types .....	31
4.2	Preparation of Test Samples .....	31
4.3	Baseline Testing of Test Samples .....	31
4.4	Accelerated Aging of Test Samples .....	32
5.	RESULTS OF BIS TESTING OF CABLE SAMPLES .....	37
5.1	Application of BIS to Thermally Aged Cables .....	37
5.1.1	Detection of Degradation on Cables with Global Thermal Aging .....	37
5.1.2	Development of Models for Cables with Thermal Degradation .....	40
5.1.3	Detection of Localized Degradation on Cables .....	54
5.1.4	Locating Localized Degradation on Cables .....	66
5.2	Application of BIS to Cables with Attached Loads .....	71
5.2.1	Test Specimens Used for Testing with Attached Loads .....	72
5.2.2	Low Frequency BIS Tests for Cables with Attached Loads .....	72
5.2.3	High Frequency BIS Tests for Cables with Attached Loads .....	75
5.2.4	Phenomenological Models of Cables with Attached Loads .....	77
5.2.5	Locating a Hot-Spot on a Cable with an Attached Load .....	83
5.3	Application of BIS to Cables with Abrasion Damage .....	84
5.3.1	Abrasion Test Specimens .....	84
5.3.2	Evaluation of Low Frequency BIS Results on Cables with Abrasion ..	85
5.3.3	Evaluation of High Frequency BIS Results on Cables with Abrasion .	101
5.3.4	Detection of Abrasion Damage Using BIS .....	110
5.3.5	Location of Abrasion Damage Using BIS .....	113
5.4	Application of BIS to Cables with Cracking Damage .....	122
5.4.1	Test Specimens Used for Testing of Cables with Cracking .....	123
5.4.2	Low Frequency BIS Measurements of Cables with Cracking .....	124
5.4.3	High Frequency BIS Measurements of Cables with Cracking .....	128
5.5	Application of BIS to Cables with Varying Environments .....	130
5.5.1	Specimens Tested to Evaluate BIS for Cables with a Varying Environment .....	130
5.5.2	Low Frequency BIS Results .....	131

5.5.3	Phenomenological Models of Cables with Varying Environment	137
6.	EVALUATION OF THE BIS METHOD FOR NUCLEAR PLANT CABLES	149
6.1	Results for Global Thermal Aging	149
6.2	Results for Global Plus Localized Thermal Aging (Hot-Spot)	150
6.3	Results for Global Thermal Aging with an Attached Load	151
6.4	Results for Global Plus Localized Abrasion Damage	152
6.5	Results for Global Thermal Aging with Cracking Damage	153
6.6	Results for Global Thermal Aging with a Varying Environment	153
7.	CONCLUSIONS AND CONSIDERATIONS FOR FOLLOW-ON RESEARCH	155
7.1	Conclusions on the Effectiveness of the BIS Method	155
7.2	Considerations for Follow-On Research to Demonstrate the Effectiveness of the BIS Method in Nuclear Plant Environment	156
8.	REFERENCES	157
Appendix A:	BIS Test Results for Cables with Global Thermal Aging Simulating 20 years and 40 years of Service	159
Appendix B:	BIS Test Results for Cables with Localized Thermal Aging (Hot Spots)	203

Intentionally Left Blank

## LIST OF FIGURES

	<u>Page No.</u>
Figure 1	Wire system equivalent circuit ..... 15
Figure 2	Low frequency impedance spectra log magnitude for a 10 meter poly-x twisted pair wire ..... 19
Figure 3	Low frequency impedance spectra phase angle for a 10 meter poly-x twisted pair wire ..... 20
Figure 4	High frequency impedance spectra magnitude for a 10 meter poly-x twisted pair wire ..... 21
Figure 5	High frequency impedance spectra phase angle for a 10 meter poly-x twisted pair wire ..... 21
Figure 6	Frequency-dependent wire resistance and inductance ..... 22
Figure 7	Micro picture of a poly-x wire cross section ..... 22
Figure 8	Real and imaginary components of the wire insulation dielectric function (open circuited) ..... 23
Figure 9	Log magnitude and phase of the impedance spectra for moist and dry wiring (open circuited) ..... 24
Figure 10	Ratio of the impedance spectra magnitude for moist and dry wiring (open circuited) ..... 25
Figure 11	Ratio of the resistance and inductance for moist and dry wiring as a function of frequency (R is $\Omega/m$ and L is H/m - open circuited) ..... 25
Figure 12	Ratio of the real and imaginary components of the wiring insulation's dielectric function for moist and dry wiring as a function of frequency ..... 27
Figure 13	Equipment and test setup for making impedance measurements ..... 28
Figure 14	Typical aging chamber loading for global and hot-spot aging of cable test specimens ..... 32
Figure 15	Measured low frequency impedance phase spectra for cables with global thermal aging to simulate 60 years of service at various temperatures ..... 38

Figure 16	Measured high frequency impedance phase spectra for cables with global thermal aging to simulate 60 years of service at various temperatures . . . . .	39
Figure 17	Expanded view of impedance phase and magnitude per unit length spectra over the frequency range from 78 MHz to 86 MHz for cables with global thermal aging to simulate 60 years of service at various service temperatures . . .	40
Figure 18	Characteristic impedance magnitude per unit length and phase spectra for cables with global thermal aging to simulate 60 years of service at various temperatures . . . . .	42
Figure 19	Imaginary component and real component of propagation function for cables with global thermal aging to simulate 60 years of service at various temperatures . . . . .	42
Figure 20	Resistance per unit length and change in resistance per unit length for cables with global thermal aging to simulate 60 years of service at various temperatures . . . . .	43
Figure 21	Comparison of resistance per unit length predicted by analytical model to that extracted from measured impedance for cable with global thermal aging to simulate 60 years of service at 70°C . . . . .	45
Figure 22	Inductance per unit length and change in inductance per unit length for cables with global thermal aging to simulate 60 years of service at 70°C . . . . .	45
Figure 23	Comparison of inductance per unit length predicted by analytical model to that extracted from measured impedance for cable with global thermal aging to simulate 60 years of service at 70°C . . . . .	47
Figure 24	Capacitance per unit length and change in capacitance per unit length for cables with global thermal aging to simulate 60 years of service at various temperatures . . . . .	48
Figure 25	Conductance-to-frequency ratio per unit length and change in conductance-to-frequency ratio per unit length for cables with global thermal aging to simulate 60 years of service at various temperatures . . . . .	49
Figure 26	Comparison of capacitance per unit length predicted by analytical model to that extracted from measured impedance for cable with global thermal aging to simulate 60 years of service at 70°C . . . . .	50

Figure 27	Comparison of conductance-to-frequency ratio per unit length predicted by analytical model to that extracted from measured impedance for cable with global thermal aging to simulate 60 years of service at 70°C .....	51
Figure 28	Comparison of characteristic impedance magnitude per unit length and phase spectra predicted by analytical model to that extracted from measured impedance for cable with global thermal aging to simulate 60 years of service at 70°C .....	52
Figure 29	Comparison of the imaginary component and real component of the propagation function predicted by analytical model to that extracted from measured impedance for cable with global thermal aging to simulate 60 years of service at 70°C .....	52
Figure 30	High frequency characteristic impedance magnitude and phase spectra extrapolated from low frequency spectra for cables with thermal aging to simulate 60 years of service at various temperatures .....	53
Figure 31	Imaginary and real components of the high frequency propagation function determined from the extrapolated characteristic impedance for cables with thermal aging to simulate 60 years of service at various temperatures .....	54
Figure 32	Impedance magnitude and phase spectra over the frequency range of 14MHz to 22MHz for cables with global thermal aging to simulate 60 years of service at 50°C, plus additional thermal aging to simulate hot-spots of different severity .....	56
Figure 33	Impedance magnitude and phase spectra over the frequency range of 39MHz to 45MHz for cables with global thermal aging to simulate 60 years of service at 50°C, plus additional thermal aging to simulate a hot-spot .....	57
Figure 34	Impedance magnitude and phase spectra over the frequency range from 14MHz to 22MHz for cables with global thermal aging to simulate 60 years of service at 50°C, plus additional thermal aging to simulate hot-spots of different sizes .....	58
Figure 35	Impedance magnitude and phase spectra over the frequency range of 39MHz to 45MHz for cables with global thermal aging to simulate 60 years of service at 50°C, plus additional thermal aging to simulate hot-spots of different sizes .....	59

Figure 36	Impedance magnitude and phase spectra over the frequency range from 14MHz to 22MHz for cables with global thermal aging to simulate 60 years of service at 50°C, plus additional thermal aging to simulate hot-spots at different locations . . . . .	60
Figure 37	Impedance magnitude and phase spectra over the frequency range from 39MHz to 45MHz for cables with global thermal aging to simulate 60 years of service at 50°C, plus additional thermal aging to simulate hot-spots at different locations . . . . .	60
Figure 38	Example of average impedance phase spectrum over the frequency range from 100kHz to 100MHz for cable with global thermal aging . . . . .	63
Figure 39	Schematic model of a cable with a hot-spot . . . . .	67
Figure 40	Impedance phase and magnitude error functions for cable with thermal aging to simulate a 1 meter hot-spot located 7.0 to 8.0 meters from the cable end representing 60 years of service at 70°C . . . . .	69
Figure 41	Impedance phase zero crossing error functions for cable with thermal aging to simulate a 1.0 meter hot-spot located 7.0 to 8.0 from the cable end representing 60 years of service at 70°C . . . . .	70
Figure 42	Impedance phase and magnitude error functions for cable with thermal aging to simulate a 1 meter hot-spot 2.0 to 3.0 meters from the end of the cable representing 60 years of service at 70°C . . . . .	70
Figure 43	Impedance phase zero crossing error functions for cable with thermal aging to simulate a 1 meter hot-spot located 2.0 to 3.0 meters from the end representing 60 years of service at 70°C . . . . .	71
Figure 44	Comparison of measured impedance magnitude for cable with and without an attached load . . . . .	73
Figure 45	Comparison of the impedance phase spectra for cables with and without a load attached . . . . .	74
Figure 46	Comparison of impedance phase in the frequency range from 116kHz to 123kHz for cables with and without a load attached . . . . .	74
Figure 47	Change in impedance phase for cable system with a hot-spot from cable system without a hot-spot . . . . .	75

Figure 48	Comparison of $\Pi(\omega)$ parameter in the vicinity of the first zero crossing for cable systems with and without a hot-spot . . . . .	77
Figure 49	Schematic of model for thermally aged cable with a load attached . . . . .	78
Figure 50	Comparison of low frequency measured and predicted impedance magnitude for a cable system with no hot-spots and an attached load . . . . .	79
Figure 51	Comparison of low frequency measured and predicted impedance phase spectra for a cable system with no hot-spots and an attached load . . . . .	79
Figure 52	Comparison of high frequency measured and predicted impedance magnitude and phase for a cable system with a hot-spot and an attached load . . . . .	80
Figure 53	Schematic of a cable system with a hot-spot and an attached load . . . . .	80
Figure 54	Comparison of measured and modeled impedance magnitude for cable system with a hot-spot and an attached load . . . . .	81
Figure 55	Comparison of low frequency measured and modeled impedance phase spectra for a cable system with a hot-spot and an attached load . . . . .	82
Figure 56	Comparison of high frequency impedance magnitude and phase spectra for cable system with a hot-spot and an attached load . . . . .	82
Figure 57	Prediction of hot-spot location for a cable system with a load attached . . . . .	83
Figure 58	Schematic of four cases studied to evaluate BIS for detecting and locating abrasion . . . . .	85
Figure 59	Low frequency impedance phase spectra for cables with and without abrasion exposed to an environment of 20% Relative Humidity . . . . .	86
Figure 60	Low frequency impedance phase spectra for cables with and without abrasion exposed to an environment of 85% Relative Humidity . . . . .	87
Figure 61	Impedance magnitude for cables with and without abrasion plus a conductive contaminant exposed to an environment of 85% RH . . . . .	88
Figure 62	Impedance phase spectra for cables with and without abrasion plus a conductive contaminant exposed to an environment of 85% RH. . . . .	88



Figure 63	Low frequency characteristic impedance magnitude for cables with and without abrasion exposed to an environment of 85% RH .....	89
Figure 64	Low frequency characteristic impedance phase spectra for cables with and without abrasion exposed to an environment of 85% RH .....	90
Figure 65	Imaginary component of the low frequency propagation function for cables with and without abrasion exposed to an environment of 85% RH .....	91
Figure 66	Real component of the low frequency propagation function for cables with and without abrasion exposed to an environment of 85% RH .....	91
Figure 67	Capacitance per unit length extracted from measured low frequency impedance spectra for cables with and without abrasion exposed to an environment of 85% RH .....	92
Figure 68	Conductance per unit length extracted from measured low frequency impedance spectra for cables with and without abrasion exposed to an environment of 85% RH .....	92
Figure 69	Low frequency characteristic impedance magnitude for cables with and without abrasion plus a conductive contaminant exposed to an environment of 85% RH .....	93
Figure 70	Low frequency characteristic impedance phase spectra for cables with and without abrasion plus a conductive contaminant exposed to an environment of 85% RH .....	94
Figure 71	Imaginary component of the low frequency propagation function for cables with and without abrasion plus a conductive contaminant exposed to an environment of 85% RH .....	95
Figure 72	Real component of the low frequency propagation function for cables with and without abrasion plus a conductive contaminant exposed to an environment of 85% RH .....	95
Figure 73	Capacitance per unit length extracted from measured low frequency impedance spectra for cables with and without abrasion plus a conductive contaminant exposed to an environment of 85% RH .....	96
Figure 74	Conductance per unit length extracted from measured low frequency impedance spectra for cables with and without abrasion plus a conductive contaminant exposed to an environment of 85% RH .....	97

Figure 75	Schematic of the localized cable interaction model for abraded cables plus a conductive contaminant .....	97
Figure 76	Schematic representation of abraded cable with a conductive path between conductors .....	98
Figure 77	Impedance magnitude of conductivity path for abraded cable with conductive path between conductors at various locations .....	99
Figure 78	Comparison of magnitude for total impedance, interaction impedance, and conductivity path impedance for abraded cable with a conductivity path at various locations .....	100
Figure 79	Comparison of conductivity path impedance phase, $\xi(\omega)$ , cable impedance phase, $\eta(\omega)$ , and total impedance phase, $\Phi(\omega)$ , for abraded cable with a conductivity path .....	101
Figure 80	Comparison of high frequency impedance magnitude and phase spectra for cables with and without abrasion .....	102
Figure 81	Comparison of high frequency impedance magnitude and phase spectra for the frequency range from 8.4 MHz to 9.6MHz for cables with and without abrasion .....	103
Figure 82	Comparison of high frequency impedance magnitude and phase spectra in the frequency range from 64MHz to 65.5MHz for cables with and without abrasion .....	103
Figure 83	Imaginary component of the high frequency propagation function for cables with abrasion plus a conductive contaminant .....	105
Figure 84	Real component of the high frequency propagation function for cables with abrasion plus a conductive contaminant .....	106
Figure 85	Resistance spectra for abraded cables in the high frequency range from phenomenological model .....	108
Figure 86	Inductance spectra for abraded cables in the high frequency range from phenomenological models .....	108
Figure 87	Capacitance spectra for abraded cables in the high frequency range from phenomenological models .....	109

Figure 88	Conductance spectra for abraded cables in the high frequency range from phenomenological models .....	109
Figure 89	Slope of the equation representing the imaginary component of the high frequency propagation function for abraded cables .....	111
Figure 90	Comparison of zero crossings in the frequency range 4.4MHz to 4.8MHz for the second derivative of the impedance phase, $\ddot{\Pi}(\omega)$ , for cables with and without abrasion .....	112
Figure 91	Comparison of the zero crossings of the second derivative of the impedance phase, $\ddot{\Pi}(\omega)$ , in the frequency range from 22.4MHz to 23.8MHz for cables with and without abrasion .....	112
Figure 92	Comparison of predicted and measured impedance phase in the range from 2.55MHz to 10.04MHz for unabraded cable (Specimen 15) .....	115
Figure 93	Comparison of predicted and measured impedance magnitude in the range from 2.55MHz to 10.04MHz for unabraded cable (Specimen 15) .....	116
Figure 94	Characteristic impedance magnitude in the frequency range from 2.55MHz to 10.04MHz for cables with and without abrasion .....	117
Figure 95	Characteristic impedance phase spectra in the frequency range from 2.55MHz to 10.04MHz for cables with and without abrasion .....	117
Figure 96	Imaginary component of the propagation function in the frequency range from 2.55MHz to 10.04MHz for cables with and without abrasion .....	118
Figure 97	Real component of the propagation function in the frequency range from 2.55MHz to 10.04MHz for cables with and without abrasion .....	118
Figure 98	Measured impedance phase spectra in the frequency range from 4.048MHz to 15.04MHz for cables with and without abrasion on one conductor .....	120
Figure 99	Predicted location of abrasion damage for cable with one conductor abraded ..	121
Figure 100	Measured impedance phase spectra in the frequency range from 4.048MHz to 15.04MHz for cables with and without abrasion on both conductors .....	122
Figure 101	Predicted location of abrasion damage on cable with both conductors abraded ..	123
Figure 102	Schematic of cable with cracking damage .....	124

Figure 103	Comparison of impedance phase for cables with and without cracking . . . . .	125
Figure 104	Characteristic impedance log magnitude and phase for cables with and without cracking . . . . .	126
Figure 105	Imaginary and real components of the propagation function for cables with and without cracking . . . . .	126
Figure 106	Resistance per unit length for cables with and without cracking . . . . .	127
Figure 107	Inductance per unit length for cables with and without cracking . . . . .	127
Figure 108	Comparison of capacitance per unit length for cable with and without cracks . .	128
Figure 109	Conductance per frequency per unit length for cable with and without cracks . .	129
Figure 110	Comparison of second derivative of the impedance spectra, $\Pi(\omega)$ , for cables with and without cracking . . . . .	129
Figure 111	Schematic of test setup for cables with varying environment . . . . .	131
Figure 112	Impedance magnitude for 100 meter cable with no aging or hot-spot and external temperatures of 24°C (75°F), and 42°C (107.6°F) . . . . .	132
Figure 113	Impedance phase spectra for 100 meter cable with no aging or hot-spot and external temperatures of 24°C (75°F), and 42°C (107.6°F) . . . . .	132
Figure 114	Impedance phase spectra for 100 meter cable with no aging or hot-spot and external temperatures of 24°C (75°F) low humidity, and 29°C (85°F) and 85% RH. . . . .	133
Figure 115	Impedance phase spectra for 100 meter cable with 1 meter hot-spot and external temperatures of 24°C (75°F), and 42°C (107.6°F) . . . . .	134
Figure 116	Impedance phase spectra for 100 meter cables with and without a 1 meter hot-spot, and an external temperature of 24°C (75°F) . . . . .	134
Figure 117	Expanded view of the impedance phase spectra in the frequency range from 425kHz to 445kHz for 100 meter cables with and without a 1 meter hot-spot, and an external temperature of 24°C (75°F) . . . . .	135
Figure 118	Expanded view of the impedance phase spectra in the frequency range from 425kHz to 445kHz for 100 meter cables with and without a 1 meter hot-spot, and an external temperature of 42°C . . . . .	136

Figure 119	Summary comparison of impedance phase spectra for 100 meter cables with and without a 1-meter hot-spot and external temperatures of 24°C (75°F) and 42°C (107.6°F) .....	136
Figure 120	Comparison of impedance magnitude in the frequency range from 1kHz to 1MHz for cables aged to simulate 60 yrs @ 50°C and 60 yrs @ 90°C .....	137
Figure 121	Comparison of impedance phase spectra for 10 meter cables aged to simulate 60 yrs @ 50°C and 60 yrs @ 90°C .....	138
Figure 122	Comparison of extracted characteristic impedance magnitude for 10 meter cables aged to simulate 60 yrs. @ 50°C and 60 yrs @ 90°C .....	139
Figure 123	Comparison of extracted characteristic impedance phase spectra for 10 m cables aged to simulate 60 yrs.@50°C and 60 yrs@90°C .....	139
Figure 124	Comparison of imaginary component of the propagation function for 10 m cables aged to simulate 60 yrs.@50°C and 60 yrs@90°C .....	140
Figure 125	Comparison of the real component of the propagation function for 10 meter cables aged to simulate 60 yrs. @ 50°C and 60 yrs @ 90°C .....	140
Figure 126	Comparison of resistance per unit length and relative difference in resistance per unit length for 10-meter cables aged to simulate 60 yrs. @ 50°C and 60 yrs @ 90°C .....	141
Figure 127	Comparison of inductance per unit length and relative difference in inductance per unit length for 10m cables aged to simulate 60yrs.@50°C and 60yrs@90°C .....	142
Figure 128	Comparison of capacitance per unit length and relative difference in capacitance per unit length for 10m cables aged to simulate 60 yrs @50°C and 60 yrs@90°C .....	143
Figure 129	Comparison of conductance per unit length and relative difference in conductance per unit length for 10m cables aged to simulate 60 yrs @50°C and 60 yrs@90°C .....	144
Figure 130	Schematic of model for 100-meter cable containing a hot-spot .....	144
Figure 131	Error in predicted impedance phase as a function of assumed hot-spot location .....	146

Figure 132 Error in predicted impedance phase as a function of assumed hot-spot location over the cable length from 90 meters to 99 meters ..... 147

Intentionally Left Blank

## LIST OF TABLES

		<u>Page No.</u>
Table 1	Cable Test Specimens for Broadband Impedance Spectroscopy Research . . . . .	33
Table 2	Specimens tested to evaluate BIS for detecting global thermal aging . . . . .	38
Table 3	Parameters for analytical model of resistance for cables thermally aged to simulate 60 years of service at various service temperatures . . . . .	44
Table 4	Parameter values for analytical model of inductance for cables aged to simulate 60 years of service at various service temperatures . . . . .	46
Table 5	Parameter values for dielectric function analytical model for cables thermally aged to simulate 60 years of service at various service temperatures . . . . .	50
Table 6	Specimens tested to evaluate BIS for locating localized areas of thermal aging . . . . .	55
Table 7	Average impedance phase magnitude for cables with global thermal aging to simulate 60 years of service at 50°C, plus additional thermal aging to simulate hot-spots . . . . .	64
Table 8	Differences in zero crossing frequencies between cable with no hot-spot (cable 26) and cables with hot-spots (cables 27 to 30) at odd number zero crossings . . . . .	65
Table 9	Impedance phase zero crossing line spacing for cables with global thermal aging to simulate 60 years of service, with and without hot-spots . . . . .	66
Table 10	Specimens tested to evaluate BIS for testing cables with attached loads . . . . .	72
Table 11	Specimens tested to evaluate BIS for detecting abrasion . . . . .	84
Table 12	Fitting constants for equation representing the real component of the high frequency propagation function for cables with abrasion plus a conductive contaminant . . . . .	105
Table 13	Fitting constants for equations representing the high frequency electrical properties of abraded cables . . . . .	107
Table 14	Specimens tested to evaluate BIS for testing cables with a varying environment . . . . .	131



Intentionally Left Blank

## EXECUTIVE SUMMARY

Aging of electric cables has been studied for decades and it is well known that aging degradation can lead to failures of electric cable systems. Periodic replacement of installed cables is not practical due to the costs involved, and the potential for introducing unforeseen anomalies due to installation deficiencies and modifications. As such, a prognostic/diagnostic technique that can be used in situ to monitor the condition of installed electric cables and predict their remaining useful life is highly desirable. While a number of prognostic/diagnostic techniques are currently available to test installed cables, each has its limitations on the types of cables for which it can be used and the extent of the age-related degradation it can detect. Currently, there is no single viable in situ technique available that can be used to monitor the condition of all types of electric cables in a nuclear power plant, especially the low-voltage instrumentation and control (I&C) cables.

Existing regulatory requirements relevant to electric cables:

- 10CFR, part 50, Appendix A, GDC 18 - Inspection and testing of electric power systems.

Electric power systems important to safety shall be designed to permit appropriate periodic inspection and testing of important areas and features, such as, wiring, insulation, connections, and switchboards, to assure the continuity of the systems and the condition of their components. The systems shall be designed with a capability to test periodically the operability and functional performance of the components of the systems, such as onsite power sources, relays, switches, and buses, and the operability of the system as a whole.

- 10CFR, part 50, Appendix B, Criterion XI

A test program shall be established to assure that all testing required to demonstrate that structures, systems and components will perform satisfactorily in service is identified and performed in accordance with written test procedures which incorporate the requirements and acceptance limits contained in applicable design documents.

- 10CFR, Part 54, License Renewal, GALL Report - XI E3 Inaccessible medium voltage cables not subject to 10CFR 50.49 environmental qualification requirements

Testing and condition monitoring based aging management program is acceptable to the staff.

The utilization of the research results and the applicability of an effective diagnostics and condition monitoring method for installed cable systems in operating nuclear power plants:

- The research results show that the BIS method has potential for being a non-intrusive, non-destructive and an effective in situ diagnostics and condition monitoring method for installed cable systems in operating nuclear power plants.

- The BIS method has potential for satisfying the aging management requirements of inaccessible/underground cables for the current license term and for license renewal considerations.
- The research results provide technical bases for:
  - (a) evaluating the licensees programs for aging management of cables within the scope of license renewal (10CFR Part 54),
  - (b) supporting the development of appropriate IEEE standards, and
  - (c) for the development of a dedicated regulatory guide on cable diagnostics and condition monitoring

The BIS technique - applied to electric cable diagnostics and condition monitoring:

The Broadband Impedance Spectroscopy (BIS) technique was developed by the Boeing Company under the sponsorship of the United States Federal Aviation Administration (FAA) to monitor the condition of installed aircraft wiring. In the study reported herein, which was sponsored by the Office of Nuclear Regulatory Research (RES) of the U.S. Nuclear Regulatory Commission (NRC), the BIS technique was evaluated for application to electric cables used in nuclear power plants. Cable samples, which are representative of a commonly used type of low-voltage instrumentation and control cable in nuclear power plants, were prepared and received accelerated aging to simulate various types of degradation expected in actual plant service conditions, including the following:

- Global thermal degradation,
- Global thermal degradation plus localized hot-spots,
- Thermal degradation with cracking, and
- Abrasion damage

The cable samples were then tested in the laboratory using the BIS method, and the data were analyzed to draw conclusions on the effectiveness of the method. Several test configurations were evaluated, including:

- Constant temperature and humidity along the cable with no load attached,
- Constant temperature and humidity along the cable with a load attached, and
- Varying environments along the length of the cable with no load attached

For the cable type tested, pre-aging measurements were used to develop models that represent the impedance response of the cable. These models were then used to determine the post-aging condition of the cables. In applying the BIS method, a model is useful for each type of cable to be tested.

The results demonstrated that the BIS method can be used on nuclear power plant cables, and may represent a breakthrough in the prognostics and diagnostics of installed cable systems. The technique provides a non-destructive means of monitoring cable systems in their installed configuration. Age-related degradation can be detected in an incipient stage prior to failure.

Specific conclusions from this research are:

- The BIS method was clearly able to detect the presence of thermal degradation associated with the cables used in this study. Specifically, the impedance phase spectra of the cables tested were observed to increase as the amount of thermal degradation on the cable increased. This increase can be used as an indicator of global thermal degradation.
- The BIS method was able to detect the presence of localized thermal degradation, or hot-spots on the cables. Specifically, a shift in the zero crossings of the impedance phase spectra was observed when a hot-spot was present on the cable.
- An approach was developed for locating hot-spots within a cable using models of the cable's electrical properties. The models were able to predict the hot-spot location within  $\pm 10\%$ .
- The BIS method was not sensitive enough to distinguish between the different severities and sizes of hot-spots simulated at low frequencies. However, high frequency data were able to distinguish between the severity levels. Additional research is warranted to establish the sensitivity limits for this technique.
- The BIS method was able to detect and locate the presence of abrasion-related damage on a cable. The models and approach used are similar to that for detecting and locating thermal hot-spots.
- The BIS method was demonstrated to be effective for detecting and locating degradation on cables with an attached load. This is important since it is desirable to have a technique that can test cables in their installed configuration, without having to disconnect them from attached equipment.
- The BIS method was able to detect simulated cracking damage on cables. However, the simulation method used in this study was determined not to accurately represent the cracking phenomena. Additional research is warranted to more accurately evaluate the BIS method on actual cable cracking.
- The BIS method was able to detect the presence of localized thermal degradation, or hot-spots on the cables even with a varying environment along the external surface of the cables. For the example presented herein, the model's prediction of hot-spot location is within a few percent of the correct position.

While the BIS method shows great promise as a prognostic and diagnostic technique for installed cable systems, additional research is desirable before it can be applied in the field. Specifically, the following additional items should be considered for future research:

- Research on the detection and location of cracking damage in cables using more realistic simulation of the cracking damage,
- The technique should be demonstrated on additional types of cable to determine its usefulness for other materials and cable configurations,
- The technique should be demonstrated in an actual plant environment to determine the impact of the various environmental factors that may impact the BIS measurements, and
- The technique should be demonstrated on blind test samples in which the type, severity, size, and location of the degradation are unknown

Based upon the promising results obtained from this research effort, the Office of Nuclear Regulatory Research is considering follow-on research, preferably in a collaborative manner, to demonstrate the applicability of the BIS method in nuclear plant environment.

## ACKNOWLEDGMENTS

The authors would like to thank the NRC program manager, Jitendra Vora for his technical guidance and support throughout this project.

We would also like to thank Martin Kendig of Rockwell Scientific for his assistance in the performance of the impedance measurements, and the processing of the data.

We also thank Michael Villaran of Brookhaven National Laboratory for his assistance in reviewing the report and providing technical comments.

The assistance of Louis Gerlach in the preparation of the cable test specimens is also greatly appreciated.

We also express our appreciation to Susan Signorelli for her assistance in the preparation of this manuscript.

Intentionally Left Blank

## ABBREVIATIONS

AWG	American Wire Gauge
BIS	Broadband Impedance Spectroscopy
BNL	Brookhaven National Laboratory
CM	Condition Monitoring
DZC	Detection Zero Crossing
EAB	Elongation-at-Break
EPR	Ethylene Propylene Rubber
FAA	Federal Aviation Administration
FTIR	Fourier Transform Infrared Spectroscopy
I&C	Instrumentation and Control
IR	Insulation Resistance
NRC	Nuclear Regulatory Commission
OIT	Oxidation Induction Time
OSTP	White House Office of Science and Technology Policy
RES	U.S. NRC, Office of Nuclear Regulatory Research
TDR	Time Domain Reflectometry
XLPE	Cross-Linked Polyethylene



Intentionally Left Blank

## LIST OF SYMBOLS

$d$	Diameter of cable conductors (cm/in.)
$l$	total length of cable (meters/ft.)
$l_a$	length to start of defect (meters/ft.)
$l_b$	length to end of defect (meters/ft.)
$l_c$	length to abraded portion of cable (meters/ft.)
$r_i$	Inside radius of coaxial cable insulation (cm/in.)
$r_o$	Outside radius of coaxial cable insulation (cm/in.)
$r$	Radius of cable conductor (cm/in.)
$s$	Center-to-center distance of cable conductors (cm/in.)
$x$	Distance along cable specimen (meters/feet)
$C$	Capacitance (Farads)
$G$	Conductance (mho)
$I$	Current (Amperes)
$L$	Inductance (Henries)
$L_k$	Inductance for cable aged to simulate service temperature $k$ (Henries)
$R$	Resistance (Ohms)
$R_s$	Resistance of a single conductor (Ohms)
$R_k$	Resistance of a cable aged to simulate service temperature $k$ (Ohms)
$V$	Voltage (Volts)
$Z$	Impedance (Ohms)
$Z_0$	Characteristic Impedance (Ohms)
$\delta$	Difference between parameters
$\delta_s$	Depth of conductor skin effect (cm/in)
$\epsilon_0$	Dielectric constant of vacuum
$\epsilon_1$	Real component of the dielectric function
$\epsilon_2$	Imaginary component of the dielectric function
$\gamma^i$	Imaginary component of the propagation function
$\gamma^r$	Real component of the propagation function
$\zeta$	Slope of linear function representing imaginary component of propagation function
$\tau$	Time constant (seconds)
$\Lambda$	Structure factor
$\Pi$	Second derivative of the impedance phase
$\Phi$	Impedance phase (Degrees)
$\Psi$	Characteristic impedance phase (Degrees)
$\omega$	Frequency (Hertz)
$\omega_k$	Frequency for cable aged to simulate service temperature $k$ (Hertz)

Intentionally Left Blank

# 1. INTRODUCTION

## 1.1 Background

Condition monitoring of electric cables is of particular interest for application to nuclear power plants, in which miles of electric cables are used to perform numerous operational and safety functions. Aging studies have shown that, as these cables age, there is the possibility that their performance may degrade making them susceptible to failure (Lofaro, et al., 2002; Villaran and Lofaro, 2003). Since replacement of all the cables would be expensive and impractical, an effective technique to characterize their condition is highly desirable. To be useful, the technique would have to be unobtrusive, non-destructive and able to be performed in situ. Currently, there is no single in situ condition monitoring technique that has been proven to be effective at determining the installed condition and the remaining useful service life of all the various types of electric cables, particularly low-voltage instrumentation and control (I&C) cables, in a typical nuclear power plant.

The issue of cable system safety was brought to the forefront with the issuance of the U.S. White House Office of Science and Technology Policy (OSTP) Report containing a review of Federal Programs related to the safety of installed electric cable systems, which was published in November 2000. The report concluded that cable system safety is an important public health and safety issue that transcends government agencies. One of the recommendations from that report is to perform collaborative research to develop effective condition monitoring techniques.

In response to the White House OSTP report recommendation, the U.S. Nuclear Regulatory Commission, Office of Nuclear Regulatory Research (NRC/RES) organized the International Conference on Wire System Aging in April 2002 [Lofaro, November 2002] to provide a forum for researchers from around the world to meet and discuss issues related to wire system aging, including promising new condition monitoring techniques for cable systems. One of the techniques discussed was broadband impedance spectroscopy.

Broadband impedance spectroscopy (BIS) is a technique being developed by the Boeing Company, under the sponsorship of the U.S. Federal Aviation Administration (FAA) to monitor the condition of wiring in aircraft. It utilizes impedance measurements of the wiring to obtain information on the dielectric properties of the wire insulation. Impedance measurements are made in situ at relatively low voltages and over a broad range of frequencies. Using algorithms and computer models developed by Boeing, the dielectric properties are extracted from these impedance measurements to characterize the condition of the wiring. The information extracted can be used to identify and locate areas of degradation.

Based on the initial success of the FAA research, NRC/RES sponsored a research program to evaluate the feasibility of using BIS to monitor nuclear power plant cables. While the construction of nuclear plant cables is different than aircraft wiring, conceptually there are similarities; therefore, condition monitoring techniques developed for aircraft may be suitable for use in nuclear power plants. The feasibility study demonstrated that BIS was able to distinguish

between aged and un-aged nuclear plant electric cables. Also, the technique was able to locate localized areas of degradation. Based on these results it was determined that BIS is a promising new technique for application to nuclear plant cables and further research was initiated to evaluate this technique in more detail. This report documents the results of this research.

In this report, an overview of the types of electric cables used in nuclear power plants is presented. The theory behind BIS is then discussed, along with the procedures for performing the test and evaluating the data. Finally, results from tests on actual nuclear plant cables are presented, from which conclusions regarding the effectiveness of the technique are drawn. Recommendations are made for future research, as well as demonstrations of the BIS method in nuclear plant environments.

## **1.2 Technical Issues**

There are several important technical issues related to condition monitoring of cables in nuclear power plants that should to be addressed through research. These include the following:

- Detection of age-related degradation that could impact cable performance,
- Location of localized damage due to “hot-spots” along the cable route,
- Handling of connected loads to allow testing cables in situ without de-termination,
- Identification and location of localized damage, such as abrasion or cracking, and
- Handling of varying environments along a cable due to routing through different areas and environmental zones of the plant

The first issue relates to the ability to determine the installed condition of a cable. Typically, electric cables used in nuclear power plants perform numerous operational and safety functions in the plant. The service environments to which the cables are exposed vary from benign indoor conditions, to adverse localized environments, including high temperatures, humidity, radiation, and pressures. Some safety-related cables are expected to operate under harsh environments and accident conditions. These cables must be qualified through testing to provide assurance that they can perform their safety function for the licensed life of the plant. Once qualified, the cables are typically installed and receive minimal attention thereafter. For license renewal, acceptable options are provided for demonstrating continued qualification for qualified cables. Aging management programs are required for non-qualified cables that are in the scope of license renewal.

As plants approach the end of their original licensed life, many utilities are applying for license extensions to continue operation of the plant. The basis for the license renewal is that aging degradation will be managed through the implementation of effective aging management programs. For electric cables, current aging management programs rely on visual inspection of cables to determine their condition and whether they are fit for continued service. While visual

inspections provide some assurance that the cables are not damaged, these inspections provide very little information on sections of the cables that are not visible. For these hidden sections of cable, techniques that can interrogate an entire cable system would be useful to detect degradation that could potentially cause a loss of function.

The second technical issue that must be addressed is related to areas along the cable route that expose the cable to adverse localized environments. Such areas can be caused by routing of a cable near a hot steam pipe, or through a high radiation area. Installations that place the cables in areas with localized adverse environments, or “hot-spots,” can result in localized damage to a cable. Even though the majority of a cable may appear to be in good condition, a hot-spot can cause localized degradation of the cable that can impair its performance. Therefore, a viable and preferred condition monitoring technique must be able to locate localized damage caused by these hot-spots.

Another important issue related to condition monitoring of cables is the ability to test the cables in situ without disturbing them. Ideally, the cable would not have to be de-terminated from its load for the testing process since this could introduce undesirable stresses on the cable and its connectors due to repeated disconnecting and re-connecting of the terminations. Since each cable will have a load attached, it is desirable that the condition monitoring technique be able to correct for the impact of the load on any measurement data obtained from the cable.

Studies have shown that exposure to aging stressors can degrade the insulating materials commonly used in the construction of electric cables. This degradation can be global in nature, such as a reduction in ductility of the insulation, or it can be localized, such as cracking. Mechanical damage has also been observed on installed cables, such as due to abrasion. This localized damage can adversely impact the ability of a cable to perform its function, particularly under abnormal operating or accident conditions when moisture is present. Therefore, it is important that a condition monitoring technique be able to detect localized damage, such as cracking and abrasion.

Finally, the cable runs in nuclear power plants can be very long, and one cable can traverse many different areas of the plant. As such, the environment along the cable may vary. Therefore, it is important that the condition monitoring technique be capable of accounting for this varying environment along the cable.

Each of these technical issues was addressed in the research program discussed herein.

### **1.3 Objectives**

The objectives of the research program reported herein were to evaluate the effectiveness and sensitivity of the BIS technique with respect to the technical issues discussed above. To maintain a manageable scope for this effort, the issues were reviewed and selected ones were chosen to be addressed in this program based on their importance to demonstrating the usefulness of the BIS method for nuclear plant cables. For this research effort the objectives were to evaluate the BIS technique capabilities for the following:

- Detecting and locating areas of localized degradation (hot-spots) on nuclear plant cables caused by stressors commonly found in nuclear plants.
- Detecting and locating localized damage on nuclear plant cables with a load attached
- Detecting and locating localized damage on nuclear plant cables in the form of abrasion and cracking
- Detecting and locating localized damage on nuclear plant cables with a varying environment along the length of the cable

Additional issues not covered in this program are intended to be addressed in future research.

#### **1.4 Research Approach**

The research approach used to meet the project objectives involved the testing of cable samples that were exposed to accelerated thermal aging to simulate degradation caused by exposure to service conditions. A test matrix was developed that included tests of cable specimens to address each of the issues identified above. The testing was divided into five sections; 1) detection and location of thermal degradation (both global and localized), 2) detection of degradation with attached loads on the cable, 3) detection of abrasion damage, 4) detection of cracking damage, and 5) detection of degradation with varying environments along the cable. In each case, appropriate test specimens were prepared and broadband impedance measurements were made.

Analytical models were developed, the data were analyzed, and correlations were established.

The cable test specimens were prepared and baseline tested at BNL. Once preparation of the cable test specimens was completed, the specimens were shipped to the Boeing test facilities in Thousand Oaks, California. There, BIS testing of the specimens was performed and the data obtained were analyzed. Measurements were made on un-aged cable specimens, and the data were used to develop models that represent the impedance response of the un-damaged cables. The models were then validated by comparison of the model predictions to the actual data obtained. These models can be used to identify the level and location of degradation on other cables constructed of similar materials and with similar conductor configurations. The theory and process for developing and using the models is discussed in Section 3 of this report.

Once the models were completed, testing of the aged specimens was performed. The models were then used to analyze the data obtained and predict the aged condition of the cables.

## **1.5 Equipment Used**

The impedance measurements were made using a commercially available instrument, and an instrument built for the FAA for BIS measurements. The former instrument was used for low-frequency measurements ranging from 100Hz to 1MHz. The later instrument was used for the high-frequency measurements ranging from 1MHz to 100MHz. Both instruments were controlled by laptop computer using a LabVIEW® software graphical interface. Data were downloaded and stored on the laptop for subsequent distribution and analysis.



(This page intentionally left blank)

## **2. REVIEW OF CONDITION MONITORING TECHNIQUES**

In this section a discussion on what constitutes effective cable condition monitoring is presented, along with a brief overview of several currently available condition monitoring techniques. The techniques are categorized as mechanical, chemical, and electrical based on the properties they monitor. The advantages and limitations of each technique are discussed. The purpose of this discussion is to present the current state-of-the-art in cable monitoring at the time of this research. This section is not intended to be a comprehensive listing of all condition monitoring techniques. It is acknowledged that there are other techniques available, and significant advancements are being made in the refinement of the existing technologies. However, thus far these techniques are subject to similar limitations as the techniques discussed herein.

### **2.1 General Criteria for an Effective Technique**

Condition monitoring of an electric cable involves the observation, measurement, or trending of one or more indicators, which can be correlated to the condition or functional performance of the cable. The intention is to provide information that can be used to determine the current ability of a cable to perform within specified acceptance criteria, as well as to make predictions about its remaining useful life. Ideally, the technique should have the following attributes:

- Non-destructive and non-intrusive (i.e., it does not require that the cable be disconnected or disturbed),
- Capable of measuring property changes or indicators that are trendable and can be consistently correlated to functional performance during normal service,
- Applicable to cable types and materials commonly used in existing nuclear power plants,
- Capable of being performed in situ under field conditions,
- Capable of detecting age-related degradation at levels that are low enough to allow sufficient time to take corrective actions prior to cable failure,
- Capable of locating localized areas of degradation on a cable due to hot-spots, and
- Provides information that can be used to predict the remaining useful life of the cable.

In practice, there are no condition monitoring techniques currently available that have all of the above attributes. Each has its own uses, as well as limitations that make it unsuitable as a general tool for monitoring installed cables.

The following sections provide an overview of several currently available techniques. The advantages of each technique are discussed, along with its limitations.

### **2.2 Mechanical Techniques**

Techniques classified as mechanical involve the measurement or monitoring of some physical attribute of the cable. Examples of mechanical techniques include visual inspections, elongation-at-break, and compressive modulus measurement. Each of these techniques is discussed below.

### **2.2.1 Visual Inspection**

Visual inspection is an effective technique for providing a qualitative assessment of a cable's condition. While no quantitative data is obtained, the results can be trended to provide an assessment of how fast a cable is degrading under the operating conditions to which it is exposed. This technique can be used to evaluate the condition of a cable and determine if more extensive testing is required to characterize its condition. Past studies have found that, in most cases, cables that appear to be in good physical condition through visual inspection show acceptable electrical performance.

The major advantage of the visual inspection is that it is inexpensive to perform and it does not require any expensive equipment. It is recommended that a standardized procedure be developed to ensure that a consistent inspection approach is used and that all of the important cable attributes are inspected.

The most serious limitation of this technique is that the cable to be inspected must be accessible and visible. In some cases, cables may be installed in closed conduits or buried beneath other cables in a cable tray. In these cases, visual inspection would not be directly useful. Also, even for visually accessible cables, usually only the jacket can be seen. Therefore, inspection of the insulation would probably not be possible. However, visual inspection of representative cables that are accessible could be used to provide an indirect measure of the condition of the inaccessible cables.

### **2.2.2 Elongation-At-Break**

Elongation-at-break (EAB) is a measure of a material's resistance to fracture under an applied tensile stress. It is often termed the "ductility" of a material and is defined as the percent increase in elongation at the time of fracture. EAB is a valuable parameter for monitoring aging in cable materials because of its sensitivity to microstructural changes in polymers brought about by service aging. It is a widely accepted measure of polymer aging and is used as a reference in evaluating other techniques.

In general, EAB measurements provide a useful quantitative assessment of the remaining integrity of a cable. As the EAB decreases to a low value, and crack initiation and propagation become possible from in-service stresses, moisture intrusion and current leakage could become a problem. At this time there does not appear to be any commonly accepted criterion for the minimum EAB of a cable material that will define the end of its useful service life. A conservative value of  $\geq 50$  percent has been used as an acceptance criterion, even though there is usually some useful service life remaining.

The major concern with EAB testing is that it is a destructive test, and relatively large amounts of cable are required. They can only be obtained if cable is removed from service, or if sacrificial cable samples are available for periodic evaluation.

### **2.2.3 Compressive Modulus**

Compressive modulus is a material property defined as the ratio of compressive stress to compressive strain below the proportional limit. As cable insulation and jacket materials age they tend to harden, which will cause the compressive modulus of the materials to increase. By monitoring this change in compressive modulus, an estimate of the degradation rate of the material can be made. Compressive modulus is measured using a device developed by EPRI known as the polymer indenter.

In many instances, cables are not easily accessible in nuclear plants. Often they may be stacked in cable trays or run through conduits, which severely limits access to perform CM testing. For cables which are accessible, the indenter can be used to determine the modulus of the outer jackets. For those cables that are not accessible, it is not desirable nor possible, in some instances, to excessively handle the cables to permit indenter testing. To monitor the modulus of individual jackets or insulation, access would be desirable at a termination point. This is not the optimum situation, since the termination points may be physically located in a different plant location and exposed to very different ambient conditions than the remainder of the cable.

Measurement of compressive modulus is a non-destructive test that does not affect the continued operation of the cable. The indenter is computer controlled and the software prevents the probe from penetrating the material being tested, from leaving residual marks, or from causing any other type of damage. It is suitable for use on various materials (XLPE, EPR, Hypalon<sup>®</sup> and Neoprene). However, not every material produces significant age-induced changes in compressive modulus that can easily be correlated with thermal or radiation exposure. For low levels of aging, relatively small modulus changes can be seen, which, in the absence of baseline measurements, might be difficult to correlate with aging. Cable construction and manufacture were also found to produce different modulus results for the same aging. Compressive modulus data correlate well with EAB measurements, which is an indication of this technique's usefulness.

## **2.3 Chemical Techniques**

Techniques classified as chemical involve the measurement or monitoring of some attribute of the cable's insulation related to changes in its chemistry or molecular makeup. Examples of chemical techniques include oxidation induction time (OIT) and Fourier Transform Infrared Spectroscopy (FTIR). Each of these techniques is discussed below.

### **2.3.1 Oxidation Induction Time**

Polymeric materials used to insulate cable conductors typically include an anti-oxidant in their formulation to mitigate oxidation, which will degrade the polymer over time. As the cables age, the anti-oxidant additives are gradually lost from the polymers due to diffusion and volatilization from the surface. As the additives are depleted, oxidation will gradually increase.

Oxidation induction time is a technique for measuring the time required for a polymer to begin to oxidize under controlled conditions. When compared to values from new cables, the OIT provides an indication of the amount of aging on the cable. The process involves the controlled heating of a small scraping of insulation material from the cable. As the sample is heated under an oxygen environment, the amount of energy liberated is measured. An increase in this energy indicates the onset of oxidation, which is an exothermic reaction. The time to oxidation onset is measured and represents the oxidation induction time.

OIT has been shown to provide useful correlations to EAB values for some cable insulation materials. However, access to the cable is required to obtain the test specimen. Also, the test must be performed in a laboratory setting, and the results only provide data on a localized portion of the cable.

### **2.3.2 Fourier Transform Infrared (FTIR) Spectroscopy**

FTIR Spectroscopy is a technique for analyzing the structure of molecules. The principle involves the measurement of absorbance or transmittance of infrared radiation by molecular structures, including those for polymers. As the radiation passes through a polymer, atoms absorb radiation and begin to vibrate. For a particular chemical bond, maximum vibration occurs for a specific wavelength of radiation. Therefore, by irradiating a specimen with a continuous spectrum of infrared radiation, and measuring the peaks (wavelengths) at which maximum absorbance or transmittance occurs, the chemical bonds that are vibrating may be identified from standard wavelengths that are available from the open literature. The presence of certain molecular bonds that develop as a result of oxidation can be used as an indicator of aging.

One of the potential problems with the FTIR spectroscopy technique is that it is a surface examination procedure in which the infrared radiation passes into the surface of the specimen and is refracted back into the crystal. By analyzing the intensity of the incident and reflected rays, the transmittance is determined. Since accelerated thermal aging at elevated temperatures will produce an oxidation gradient at the specimen surface, the spectroscope will detect a higher amount of oxidation than the average bulk value. The technique would, therefore, be expected to give a more accurate estimate of bulk aging for naturally-aged specimens, for which oxidation gradients will be minimized at the lower service aging temperatures.

## **2.4 Electrical Techniques**

Techniques classified as electrical involve the measurement or monitoring of some electrical property of the cable. Examples of electrical techniques include insulation resistance (IR), dielectric loss, voltage withstand testing, time-domain reflectometry, and partial discharge testing. Each of these techniques is discussed below.

### **2.4.1 Insulation Resistance**

Insulation resistance measurements are commonly performed to determine the current condition of cable insulation. By applying a voltage from the conductor to ground, the resistance of the insulation separating them can be measured. The advantages of this test are that it is relatively easy to perform and requires inexpensive equipment. If the insulation resistance decreases in a predictable manner as the insulation ages, trending of this parameter could be useful as a condition monitoring technique for electric cables.

When a dc voltage is applied to a test specimen, the total current flowing in the insulation from the conductor to ground is equal to the sum of the capacitive charging current, leakage current, and dielectric absorption current. These three component currents change with time. The capacitive charging current and the dielectric absorption current will initially be relatively high when the test voltage is first applied to the test specimen. Once the insulation, which behaves like a capacitor, is energized and charges have aligned across the insulation, these currents will taper off and eventually approach zero. However, leakage current will typically start at zero and gradually increase. In high integrity insulation, leakage current will reach and maintain a steady value after a certain amount of time. If the insulation is badly deteriorated, wet, or contaminated, the leakage current will be greater than that found in good insulation and it could continue to increase over time. As a result, the total current flowing in a test specimen will start out high when a test voltage is first applied, and taper off in different ways over the next several minutes depending on the condition of the insulation.

In high integrity insulation the insulation resistance will gradually increase after the test voltage is applied, then a steady value will be reached. Because of this behavior, insulation resistance measurements are taken using an ohmmeter first at one minute and again at ten minutes. The ratio of the insulation resistance at ten minutes to the value measured at one minute is called the polarization index.

One disadvantage of making insulation resistance measurements is that the cable under test must be disconnected in order to attach the test instrument. However, this can be controlled by test procedures with independent verification steps, as are commonly used for surveillance and maintenance procedures in nuclear power plants.

The major factor affecting insulation resistance measurements is temperature. The effect of temperature is predictable and can be corrected by normalizing the raw insulation resistance readings to a common temperature, such as 16°C (60°F), for purposes of comparison. Using the ratio of the 10 minute insulation resistance to the 1 minute reading, the polarization index can provide a measure of dielectric condition that eliminates temperature effects. Consequently, in

order to collect data that are trendable, accurate time and temperature data must accompany the raw quantitative insulation resistance measurements. For this reason, plant personnel often look upon the insulation resistance test as a simple pass/fail test for the dielectric integrity of electrical equipment and cables, but too irregular for trendable condition monitoring.

#### **2.4.2 Dielectric Dissipation or Loss Factor**

When a steady-state ac test voltage is applied to an insulated cable, the resulting apparent total current that flows consists of a charging current due to the capacitance of the cable insulation and a leakage current. The phase angle between the applied test voltage and the total current is known as the dielectric phase angle. The complement of the phase angle is called the dielectric loss angle.

The leakage current for electric cables is normally much smaller than the charging current, but it is more sensitive to the condition of the insulation. As insulation deteriorates it is expected that the leakage current will increase, while the capacitive current remains approximately constant. Thus, the ratio of the magnitudes will increase. The ratio is called the dielectric dissipation factor and is commonly used as a measure of insulation condition. Another means of describing insulation condition is the dielectric power factor, expressed as the cosine of the dielectric phase angle. At very low power factors (<10 percent), the dielectric power factor is approximately equal to the dielectric dissipation factor.

Dielectric loss measurement is a very simple and straightforward condition monitoring technique. Using a signal analyzer, an internal source provides an applied ac voltage signal to the test specimen over a range frequencies, while measuring and recording the dielectric phase angle at each increment. The phase angle data can then be used to calculate the dielectric loss or power factor. Studies have shown that dielectric loss can be correlated to cable degradation.

Another advantage of this test is that it can be used to interrogate an entire cable system. The data obtained provide information on the global condition of the cable, and can provide insights into the condition of the entire cable system.

Some of the factors that affect the dielectric loss measurement technique include cable length, humidity or moisture within the cable and insulation, and electrical equipment operating in the vicinity of the test cable. The effect of length is very uniform and predictable, resulting in a relative increase in insulation power factor as the length of cable increases. This effect is most easily accounted for by making in situ baseline measurements for each cable to be monitored to serve as a standard for comparison with similar measurements in the future. The effect of other operating electrical equipment or energized cables in the same tray is typically concentrated at the frequency of the operating equipment. In most cases, this is the 60Hz power frequency and it has a more pronounced effect on longer cables than short ones. This problem can be avoided by making measurements at an applied ac test voltage with a frequency below 50Hz or above 70Hz.

The major advantage of the dielectric loss technique is that the cable being tested does not have to be completely accessible. The test equipment can be connected to the ends of the cable, and the test can be performed without physically touching the length of the cable. Also, no material samples are taken from the cable.

A disadvantage of the dielectric loss technique is that the cable under test must be disconnected in order to attach the test instrument. However, this can be controlled by test procedures with independent verification steps, as are commonly used for surveillance and maintenance procedures in nuclear power plants.

### **2.4.3 Voltage Withstand Test**

The high potential voltage withstand test is a measure of a cable insulation's ability to withstand a high applied voltage stress. To perform this test, the cable is connected to a source of high voltage. The test voltage is applied to each individual conductor of the cable specimen and held for five minutes, during which time the leakage current between the conductor and electrical ground is recorded. The leakage current provides a measure of the insulation's condition.

As with any electrical test, an advantage of this test is that it can interrogate an entire cable system to identify weak points.

A disadvantage of this test is that, due to the high voltages applied, the test itself can degrade the insulation. If this test is repeated a number of times, the dielectric strength may become so weakened that the cable could fail because of the testing. As such, this test would not normally be used in situ by nuclear power plant technicians to assess and trend the dielectric integrity of a cable's insulation system. Since it is a high voltage test, it has the potential to destroy a cable if a voltage breakdown should occur. Even at lower levels of applied test voltage, within the voltage rating of the cable, the cable insulation is incrementally weakened by each high potential test. Thus, the risks of causing either catastrophic or incipient damage to cable insulation make this an unsuitable condition monitoring method.

### **2.4.4 Time-Domain Reflectometry**

Time-domain reflectometry (TDR) works on the same principle as radar. A pulse of low-voltage energy is transmitted down a cable and the reflected waveform is captured on the instrument scope. When the pulse reaches the end of the cable, or a fault along the cable, part or all of the pulse energy is reflected back to the instrument. The TDR measures the time it takes for the signal to travel down the cable and reflect back. The TDR then converts this time to distance and displays the information as a waveform and/or distance reading. Knowing the length of the cable, the reflected pulse can be interpreted as the end of the cable, or a fault in the cable.

The primary use of the TDR is for locating defects in a cable. Little information is provided on the condition of un-faulted cable insulation.



## **2.4.5 Partial Discharge Testing**

Another type of electrical test is the partial discharge test. When an insulation defect such as a void is present, the defect will display a localized corona or ionization during exposure to a high-voltage stress. As voltage builds up across a void, once the partial discharge inception voltage is reached, the gas in the void will ionize and a discharge will occur. The discharge redistributes electrical charge within the dielectric and is known as partial discharge.

The inception voltage for these voids tends to be constant, so that the measurement of total charge being redistributed within the dielectric is believed to be a good indicator of the size of the voids and their likelihood of becoming an incipient failure. Partial discharge testing requires the measurement of small current pulses ( $<5$  pC) while applying a relatively high test voltage.

## **2.5 Reasons to Focus on an Electrical Technique**

From the previous overview of currently available condition monitoring techniques it can be seen that there are advantages and limitations to each. Of the three categories of techniques presented, the electrical techniques appear to have the highest potential of meeting the criteria for an effective in situ technique discussed previously. Advantages of the electrical techniques are the following:

- An entire cable system can be interrogated with one test to detect degradation,
- The cable does not have to be accessible along its entire length,
- Results can be correlated to other monitoring parameters, such as EAB,
- The data obtained can be used to locate localized defects,
- Hardware can be installed to provide continuous on-line monitoring without connecting test equipment, and
- Material samples are not required to perform the test
- Loads at either end of an installed cable system can remain connected
- Non-intrusive, non-destructive voltage signals can be applied for examination

Based on these advantages, an electrical technique was focused on for this research. In particular, broadband impedance spectroscopy was selected for evaluation.

### 3. THEORY OF BROADBAND IMPEDANCE SPECTROSCOPY

This section presents an overview of the theory behind broadband impedance spectroscopy (BIS), and how impedance measurements are used to determine the electrical properties of cables.

#### 3.1 Equivalent Circuit

Over the past 70 years or more electric impedance models enabled the analysis of the dielectric properties for numerous materials (for example, see Vaughan, 1969). Figure 2 depicts the system being analyzed, which consists of two wires of length  $\ell$  with a voltage potential  $V(\omega)$  across them.

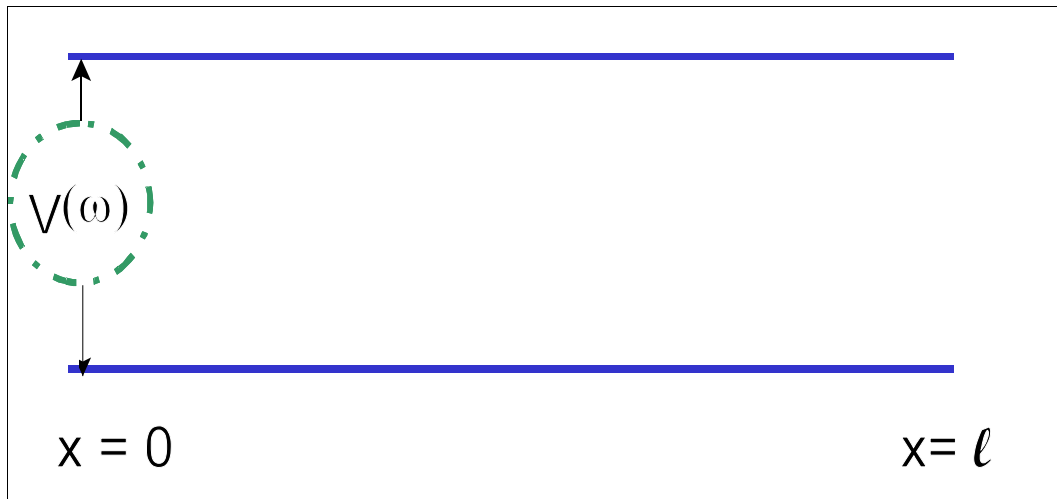


**Figure 2** Wire system equivalent circuit

The core concept of transmission theory is that a set of wires can be viewed as a distributed system that is endowed with a frequency dependent resistance,  $R(\omega)$  per meter, inductance,  $L(\omega)$  per meter, conductance,  $G(\omega)$  per meter, and capacitance,  $C(\omega)$  per meter. Note, the conductance and capacitance are related to the wire insulation dielectric function,  $\varepsilon(\omega)$  via

$$G(\omega) + i \omega C(\omega) = i \Lambda \omega \varepsilon(\omega) \quad (3.1-1)$$

Here “ $i$ ” represents the imaginary operator (square root of -1), and “ $\Lambda$ ” is a structure factor that is independent of frequency and is a real number. For example, for two identical wires whose diameter is “ $d$ ” and the center-to-center separation between the conductors is “ $s$ ” the structure factor would be:

$$\Lambda = \frac{\pi}{\cosh^{-1}(s/d)} \quad (3.1-2a)$$

If the system is a coaxial cable, with inner and outer radii  $r_0$  and  $r_1$ , respectively, then

$$\Lambda = \frac{2\pi}{\ln\left(\frac{r_0}{r_1}\right)} \quad (3.1-2b)$$

If a voltage is established between the wires, then the system's electrodynamics obey the following equations (Durney and Johnson, 1969):

$$\frac{\partial}{\partial x} V(x, t) = -R I(x, t) - L \frac{\partial}{\partial t} I(x, t) \quad (3.1-3)$$

$$\frac{\partial}{\partial x} I(x, t) = -G V(x, t) - C \frac{\partial}{\partial t} V(x, t) \quad (3.1-4)$$

Here,  $V(x, t)$  is the voltage established between the two wires at the space-time point  $(x, t)$  and  $I(x, t)$  is the current flowing in the wires. The solutions of these equations define a set of normal modes  $A(x, t)$

$$A(x, t) = \exp[\gamma_{\pm}(\omega) x - i(\omega t)] \quad (3.1-5)$$

The propagation function is defined as follows:

$$\begin{aligned} \gamma_{\pm}(\omega) &= \pm \sqrt{[R(\omega) + i\omega L(\omega)][G(\omega) + i\omega C(\omega)]} \\ &= \pm[\alpha(\omega) + i\beta(\omega)] \end{aligned} \quad (3.1-6a)$$

Here  $\alpha(\omega)$  is the dissipation (per meter) and  $2\pi/\beta(\omega)$  is the wavelength of the normal mode. Furthermore, we can rewrite the propagation function as

$$\gamma_{\pm}(\omega) = \pm \sqrt{[R(\omega) + i \omega L(\omega)] i \Lambda \varepsilon(\omega)} \quad (3.1-6b)$$

The impedance for open-circuited and short-circuited wires is given by the following equations:

$$Z_{open}(\omega) = Z_0(\omega) \text{Coth}[\gamma(\omega) \ell] \quad (3.1-7a)$$

$$Z_{short}(\omega) = Z_0(\omega) \text{Tanh}[\gamma(\omega) \ell] \quad (3.1-7b)$$

Here the wire length is  $\ell$ , and  $Z_0(\omega)$ , the characteristic impedance, is given by the following equation:

$$Z_0(\omega) = \sqrt{\frac{R(\omega) + i \omega L(\omega)}{G(\omega) + i \omega C(\omega)}} \quad (3.1-8)$$

## 3.2 Wire Properties and Wire Impedance Spectra

In this section, the approach for extracting wire properties from impedance data is presented. An example is then given describing how this approach is used for wire prognostics by extracting the wire properties from the impedance data of healthy wiring and from damaged wiring. Specifically, the cases of damage due to (1) humidity and (2) abrasion are examined. The data presented in this section were obtained from a research program sponsored by the FAA, as well as Boeing's IR&D on aircraft wiring and are used herein for demonstration purposes.

### 3.2.1 Approach to Extract Wire Properties from Impedance Data

First, the wire properties are extracted from the measured broadband impedance spectra for the following wiring configurations: open-circuited and short-circuited. The product of the short-circuited and open-circuited impedances and their ratio yield the characteristic impedance and the propagation function, as follows:

$$Z_o^2(\omega) = Z_{short}(\omega) Z_{open}(\omega) \quad (3.2-1a)$$

$$\gamma(\omega) \ell = \text{Tanh}^{-1} \sqrt{\frac{Z_{short}(\omega)}{Z_{open}(\omega)}} \quad (3.2-1b)$$

Using equations (3.1.6b) and (3.1.8) for the propagation function and characteristic impedance, respectively, the above equations can be written as:

$$\gamma(\omega) Z_0(\omega) = R(\omega) + i \omega L(\omega) \quad (3.2-2a)$$

$$\frac{\gamma(\omega)}{Z_0(\omega)} = i \Lambda \omega \varepsilon(\omega) \quad (3.2-2b)$$

Therefore, the wire properties per length are related to the characteristic impedance and the propagation function via the following equations:

$$R(\omega) = \text{Re} [\gamma(\omega) Z_0(\omega)] \quad (3.2-3a)$$

$$L(\omega) = \frac{1}{\omega} \text{Im} [\gamma(\omega) Z_0(\omega)] \quad (3.2-3b)$$

$$\varepsilon_1(\omega) = \text{Re} \left[ \frac{\gamma(\omega)}{\omega \Lambda Z_0(\omega)} \right] \quad (3.2-3c)$$

$$\varepsilon_2(\omega) = -\text{Im} \left[ \frac{\gamma(\omega)}{\omega \Lambda Z_0(\omega)} \right] \quad (3.2-3d)$$

Here,  $\varepsilon_1(\omega)$  and  $\varepsilon_2(\omega)$  are the real and imaginary portion of the dielectric function, respectively.

Before an example of a wiring system is presented, the behavior of the characteristic impedance and propagation function will be discussed, as well as the open-circuited and short-circuited impedance spectra. At low frequencies, the characteristic impedance is dominated by the wire's capacitance and therefore is large. Conversely, the propagation function is very small such that  $\gamma(\omega) \ell \ll 1$ . Thus, the open-circuited and short-circuited impedance spectra approach the following limiting forms at low frequencies:

$$Z_{open}(\omega) \rightarrow \frac{1}{i \omega \Lambda \ell \varepsilon(\omega)} \quad (3.2-4a)$$

$$Z_{short}(\omega) \rightarrow \ell [R(\omega) + i \omega L(\omega)] \quad (3.2-4b)$$

Thus, at low frequencies the open-circuited wire impedance is dominated by the wire's capacitance. The magnitude of the open-circuited impedance depends nearly inversely on the frequency and, therefore is large, whereas its phase is determined by the ratio  $\epsilon_2(\omega)/\epsilon_1(\omega)$ . On the other hand, at low frequencies the short-circuited impedance is independent of frequency ( $\omega \rightarrow 0$ ), is dominated by the wire's resistance, and is small. At higher frequencies, the short-circuited impedance exhibits a linear dependence on frequency with a slope determined by the wire's inductance. Thus, the low frequency portion of these spectra is completely dominated by the wire's electrical properties.

As an example, Figures 3 and 4 depict the log magnitude and phase of the impedance spectra at low frequencies for a ten meter poly-x twisted pair wire that was open-circuited and short-circuited. Here, the frequency ranges from 1kHz to 1MHz.

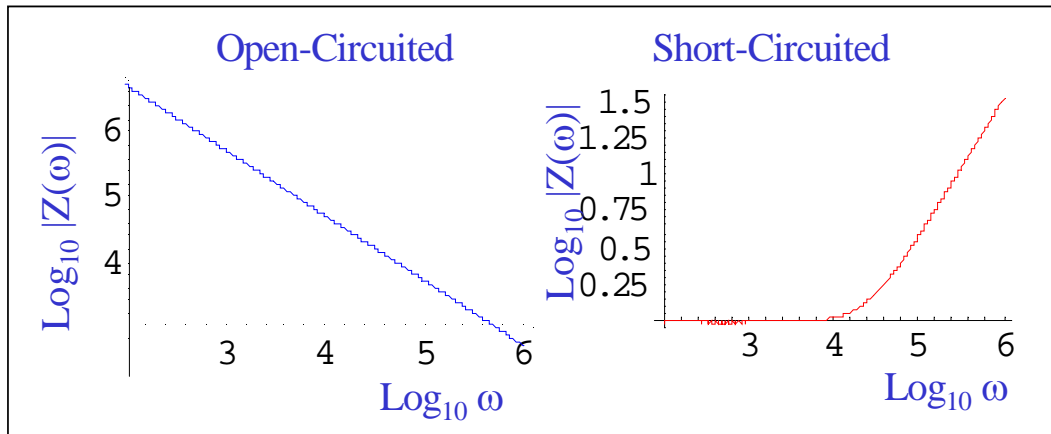


**Figure 3** Low frequency impedance spectra log magnitude for a 10 meter poly-x twisted pair wire

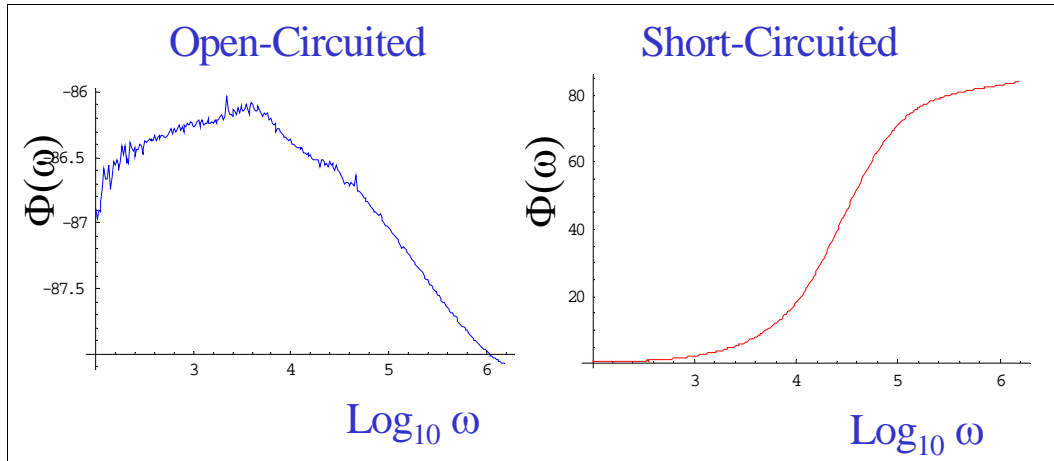


**Figure 4** Low frequency impedance spectra phase angle for a 10 meter poly-x twisted pair wire

In the region where  $\gamma(\omega) \ell > \pi$ , the impedance spectra exhibit oscillations with a period of  $2\pi/[\gamma(\omega) \ell]$ . Electrical waves now propagate on the wiring and the impedance is dominated by wave interference. Furthermore, noting that  $\epsilon_1(\omega) \gg \epsilon_2(\omega)$ , the characteristic impedance and the propagation function approach the following limits:

$$Z_0 \rightarrow \sqrt{\frac{L(\omega)}{\Lambda \epsilon_1(\omega)}} \quad (3.2-5a)$$

$$\gamma(\omega) \rightarrow i \omega \sqrt{\Lambda \epsilon_1(\omega) L(\omega)} \quad (3.2-5b)$$

Examination of the open-circuited and short-circuited cable impedances, described by Equations (3.1.7a) and (3.1.7b), reveal that the period of these oscillations is determined by the inductance and the real component of the dielectric function. Information on the location of defects, such as “hot-spots,” is contained in this portion of the impedance spectrum.

As an example, Figures 5 and 6 depict the impedance magnitude and phase spectra at high frequencies for a ten meter poly-x twisted pair wire that was open-circuited and short-circuited. Here the frequency ranged from 1MHz to 40MHz.

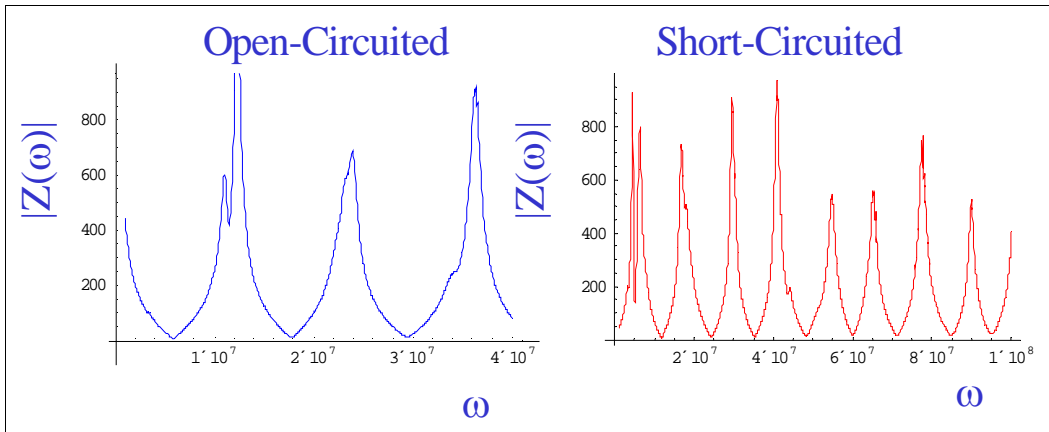


**Figure 5** High frequency impedance spectra magnitude for a 10 meter poly-x twisted pair wire

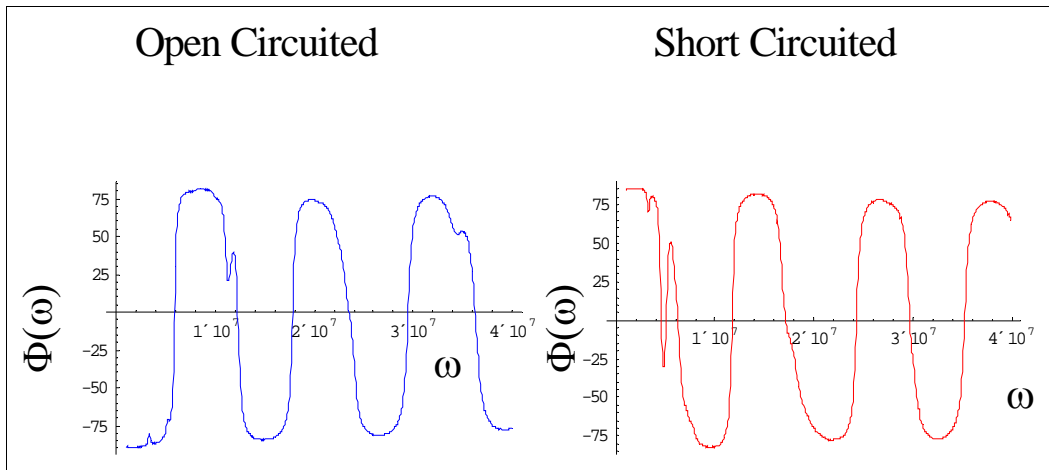


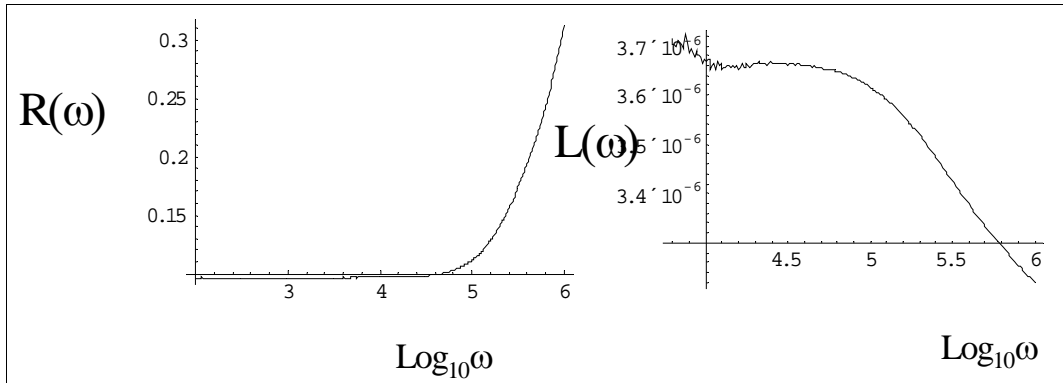
**Figure 6** High frequency impedance spectra phase angle for a 10 meter poly-x twisted pair wire

### 3.2.2 Wire Properties from Impedance Data for Undamaged Wiring

The wire electrical properties can be extracted from impedance data using equations (3.2-3a) through Eq. (3.2-3d). The frequency dependent resistance and inductance are shown in Figure 7.

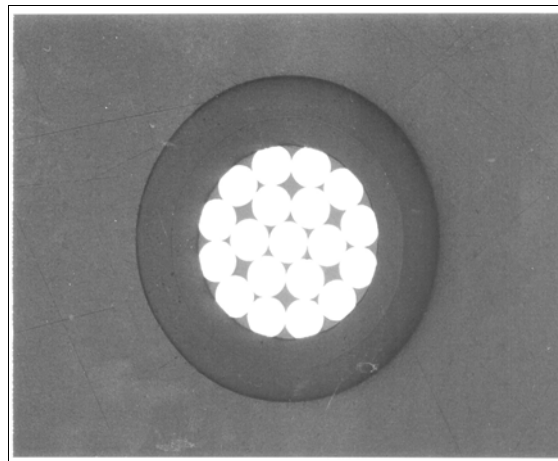
Examination of the resistance,  $R(\omega)$ , shows that it increases significantly at frequencies over 50kHz due to the skin effect. Analysis shows that the resistance varies as  $\omega^{1/2}$ , as expected. The skin effect manifests itself when the conductor's skin depth,  $\delta_s(\omega)$ , is on the order or less than the radius of the conductor,  $r$  (here  $r \sim 10^{-4}m$ ), i.e.  $\delta_s(\omega) < r$ . At that point, the electrical currents are confined near the surface of the conductor within the skin depth. This occurs when  $\omega \approx 50kHz$ .





**Figure 7** Frequency-dependent wire resistance and inductance

The inductance also exhibits frequency dependence. However,  $L(\omega)$  does not follow the usual skin effect frequency dependence due to the wire's complex microstructure, depicted in Figure 8. Specifically, there are nineteen strands, all of which conduct current, and their associated magnetic fields interfere with each other. Furthermore, their individual radii are over twenty times smaller than the wire conductor itself. Thus, the skin depth is on the order of  $100\mu\text{--}300\mu$ . As a result, the frequency dependence is very weak. Finally, the low frequency behavior (100Hz-1kHz) of the inductance (shown in Figure 7) is probably not valid. In particular, the contribution of the inductance to the wire's impedance is very small compared to that of the resistance and dielectric function. As a result, the low-frequency portion of the inductance (100Hz-1kHz) suffers from noise.



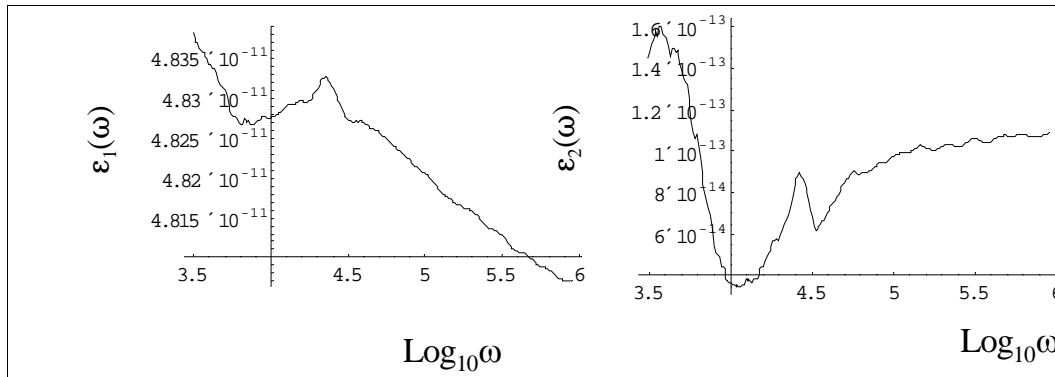
**Figure 8** Micro picture of a poly-x wire cross section

Figure 9 depicts the real and imaginary components of the wire's dielectric function (times the structure factor,  $\Lambda$ ) in the frequency range from 100kHz to 1MHz. Examination of this figure

reveals that the real component is about 500-1000 times larger than the imaginary component. Note that both components exhibit significant frequency dependence in the vicinity of 100Hz. These structures arise from a slow, Debye ion process on the order of 100ms, in which ions move in response to the ac electric fields associated with the probe voltage,  $V(\omega)$ . Furthermore, there is a broad background that arises from very fast electronic processes, on the order of  $0.1\mu\text{s}$ . Analysis of the dielectric data reveals that this process is nearly independent of frequency and is the largest contribution to the dielectric function. This electronic dielectric process follows the fraction power law, in which the following relationship applies:

$$\epsilon_{\text{electronic}}(\omega) \approx \frac{A_1 \epsilon_0}{[1 + (i \omega \tau)^p]} \quad (3.2-6)$$

Here  $A_1$  is a fitting constant representing the strength of the process with a typical value ranging from 2 to 4,  $\epsilon_0$  is the dielectric constant of vacuum,  $\tau$  is the time scale of the electronic dielectric process, and  $p$  is a fitting constant  $\approx 0.05$ . Note that as the frequency increases, the wire insulation becomes more lossy. Finally, there is a small structure in the vicinity of 30kHz that mirrors another process that is midway between the electronic and ion dielectric processes. The origin of this process is unclear.



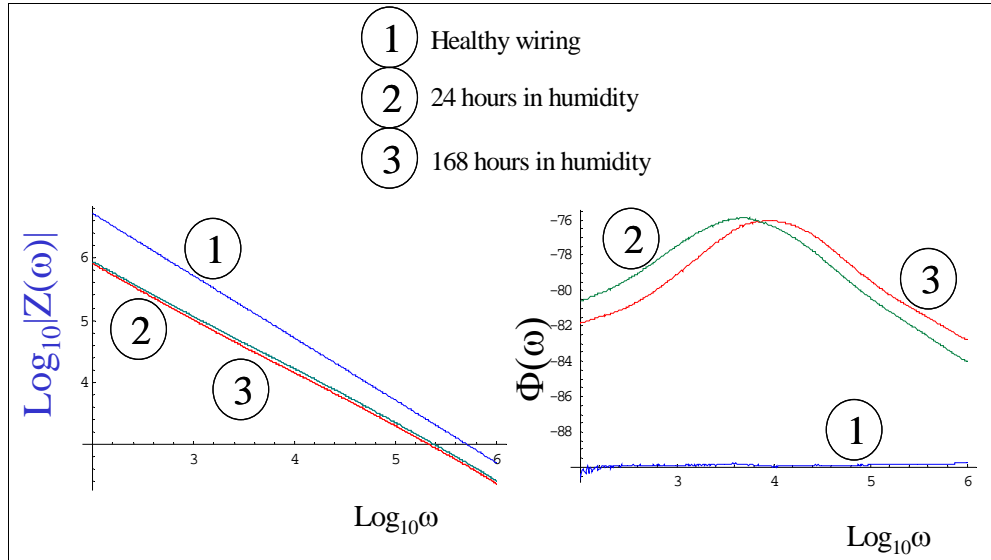
**Figure 9** Real and imaginary components of the wire insulation dielectric function (open circuited)

### 3.2.3 Wire Properties from Impedance Data for Damaged Wiring

An important element of a successful cable condition monitoring technique is its ability to detect damage on the cable due to exposure to a stressor. As part of the initial feasibility study for this project, impedance data were evaluated for wiring that was damaged by exposure to elevated humidity levels. Humidity was chosen as the damage stressor since models were already available for this damage mechanism from previous research on aircraft wires (Rogovin and Kendig, 2002).

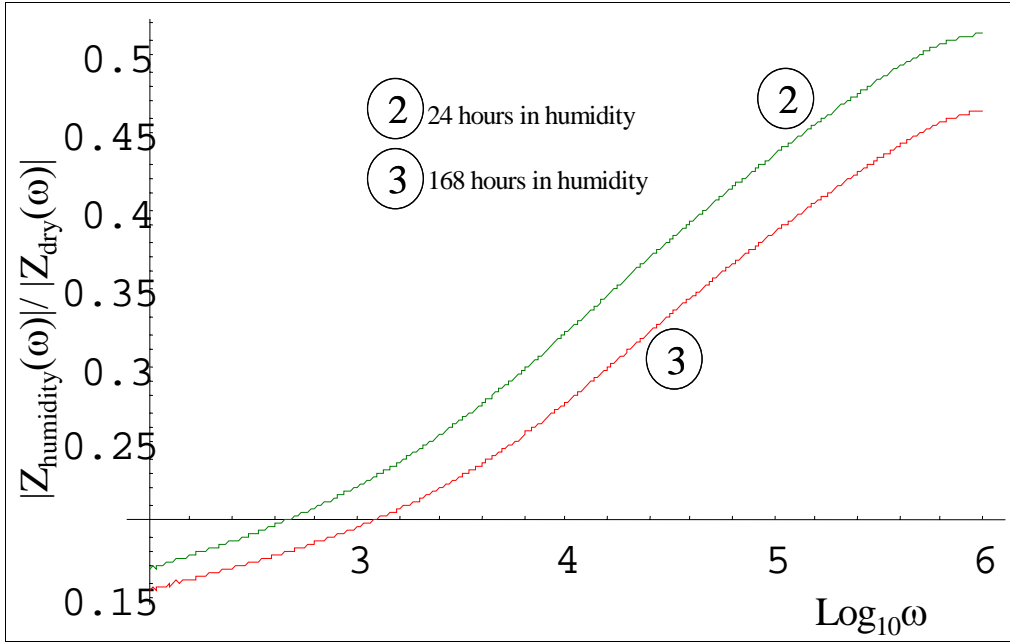
If the wiring is damaged by exposure to elevated levels of humidity, corrosion and other new microscopic processes may occur that are reflected in the wire's electrical properties. As an example, the case of poly-x twisted pair wiring exposed to humidity is examined.

Figure 10 depicts the log magnitude and phase of the impedance over the low frequency portion (100Hz-1MHz) of the spectra for the cases in which the wires are open-circuited. Three conditions are evaluated: (1) healthy wiring, (2) wiring exposed to 85%/85°F for 24 hours, and (3) wiring exposed to 85%/85°F for 168 hours.



**Figure 10** Log magnitude and phase of the impedance spectra for moist and dry wiring (open circuited)

Examination of Figure 10 reveals that humidity changes the impedance spectra significantly. Specifically, at low frequencies the impedance phase for the healthy wire  $\Phi_{dry}(\omega) \approx -90^\circ$ , which implies that little energy is dissipated in the wiring. When the wiring is exposed to humidity for a period of time, the impedance phase migrates to more dissipative states where its value varies from  $-85^\circ < \Phi_{humidity}(\omega) < -75^\circ$ . Furthermore, the magnitude of the impedance is reduced drastically. This is shown in Figure 11 where the ratio of the magnitude of the impedances are plotted as a function of frequency. Note that the longer the wiring is exposed to humidity the more conductive it becomes. Clearly, the wire's dielectric properties can be seriously compromised by humidity.



**Figure 11** Ratio of the impedance spectra magnitude for moist and dry wiring (open circuited)

Next, the electrical properties for dry and moist wiring are compared. Figure 12 depicts the resistance and inductance of dry and moist wiring in the frequency range from 100Hz to 1MHz.

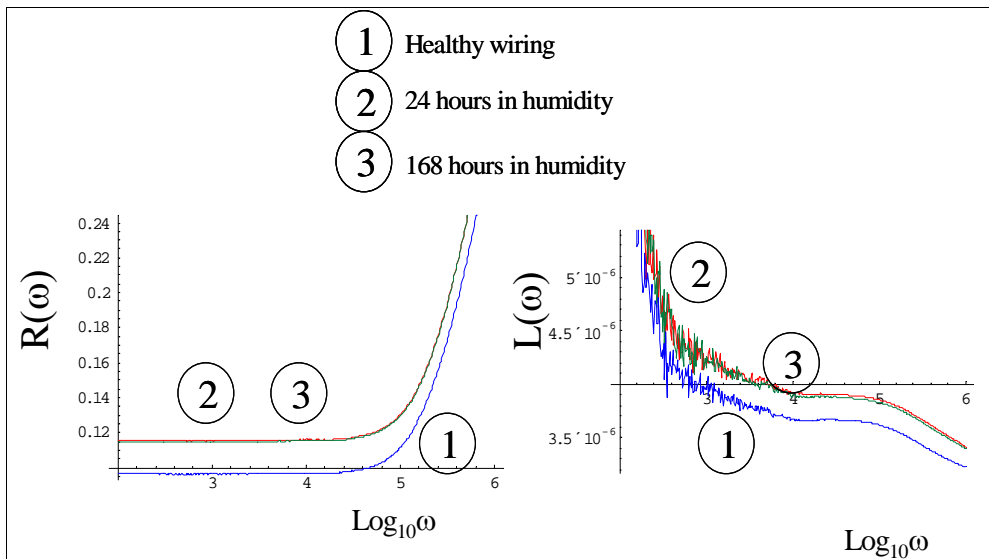


**Figure 12** Ratio of the resistance and inductance for moist and dry wiring as a function of frequency (R is  $\Omega/m$  and L is H/m - open circuited)

Referring to Figure 11, it should be noted that both of these electric properties are changed by humidity. For example, the resistance of moist wiring is about 20% larger than dry wiring. To understand this, the following model describing the resistance for a pair of twisted wires is examined:

$$R(\omega) = \frac{2 R_s(\omega)}{\pi d} \left[ \frac{s/d}{\sqrt{(s/d)^2 - 1}} \right] \quad (3.2-7)$$

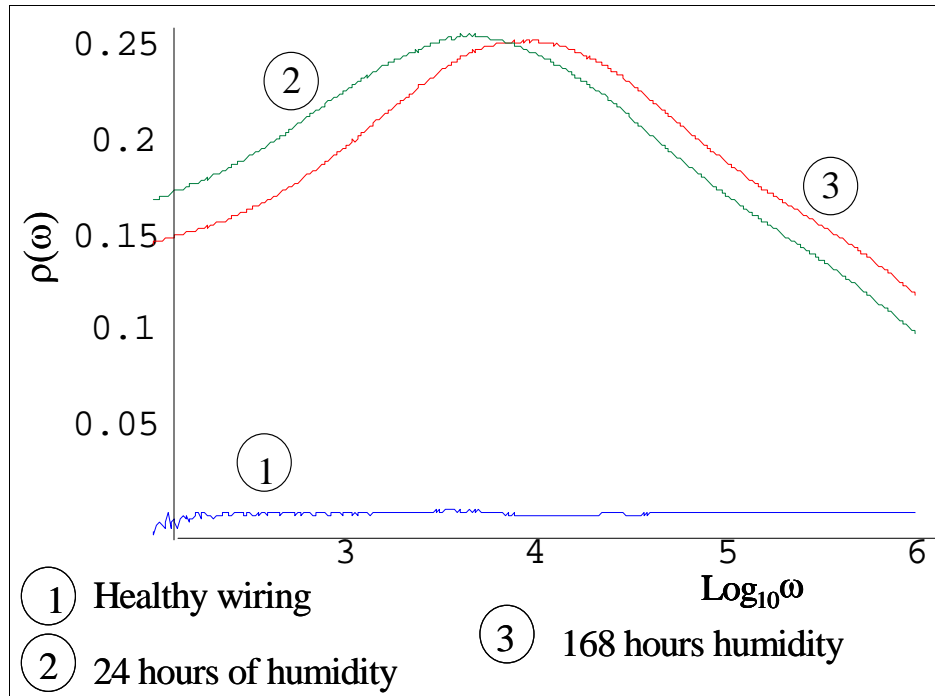
Here “s” is the distance between the wire centers,  $R_s(\omega)$  is the resistance for a single wire ( $s \rightarrow \infty$ ) and “d” is the diameter of the wire insulation. Note that equation (3.2-7) demands that the resistance will increase as s/d increases. Since humidity swells the wire’s insulation, the resistance will increase, as shown in Figure 12.

Figure 13 compares the real and imaginary components of the wire insulation’s dielectric function. Note that the imaginary component increases by a factor of several hundred to over one thousand with exposure to humidity. This behavior implies that new and significant microscopic processes occur. These processes occur throughout the spectrum, implying both ionic and electronic dielectric processes. Note that the real component of the dielectric function has increased as well.

More important, these processes are different than those that occur in a dry wire. This can be seen by examining the ratio of the imaginary to the real component of the dielectric function,

$$\rho = \varepsilon_2(\omega) / \varepsilon_1(\omega) \quad (3.2-8)$$

Examination of Figure 13 reveals that the ratio increases from  $10^{-3}$  for dry wire to the range of  $0.15 < \rho(\omega) < 0.25$  for wire exposed to humidity. Clearly, the exponent (p), response time ( $\tau$ ) and the strength ( $A_1$ ) in the fraction power law, as represented by Eq. (3.2-6), have changed. Furthermore, the imaginary component of the dielectric function shows structure near  $\omega \approx 10^4$ Hz. Note that the longer the wiring is exposed to humidity, the further this peak migrates to higher frequencies.



**Figure 13** Ratio of the real and imaginary components of the wiring insulation's dielectric function for moist and dry wiring as a function of frequency

### 3.3 BIS Test Procedure

The process for using the BIS technique to evaluate a cable's condition involves two steps; 1) performing impedance measurements on the cable, and 2) analysis and interpretation of the impedance data obtained using analytical models. Each of these steps is discussed in the following sections.

#### 3.3.1 Procedure for Making Impedance Measurements

Impedance measurements were made on the cable being evaluated over a broad range of frequencies in the open circuited configuration. In this study, frequencies ranging from 100 Hz to 100 MHz were used. The measurements were broken up into two frequency ranges; low frequency, which included frequencies from 100Hz to 1MHz, and high frequencies, which included frequencies from 1MHz to 100MHz. The use of two frequency ranges was determined to be the best approach for taking impedance measurements due to the limitations of the test equipment available. In the low frequency range, a Hewlett-Packard instrument was used since it provided better impedance data accuracy in this range of frequencies. However, at higher frequencies, the impedance data obtained from the HP instrument were "noisy" and lacked adequate resolution. Therefore, in the high frequency range, an Eclipse instrument was used

that was specially designed to provide accurate impedance measurements at high frequencies. Figure 14 shows the Eclipse instrument (top) and the HP instrument (bottom) used to perform the impedance measurements.



**Figure 14** Equipment and test setup for making impedance measurements

For the laboratory measurements, the cable being evaluated was prepared by stripping approximately  $\frac{1}{2}$  inch of insulation from the ends of each conductor. The conductors were then connected to terminals on the instrument being used for the impedance measurement, as discussed above. The actual impedance measurements were performed automatically by a laptop computer based software program, which controlled the actual measurements and downloading of the data obtained. The measurements involved the input of a sinusoidal voltage signal into the cable with an amplitude of 1-volt. The frequency of the input signal was varied over the desired range of measurement. Data points were obtained at 2000 discrete frequencies in each measurement range, and included the impedance magnitude and phase angle. The data points were downloaded to the computer for subsequent retrieval and analysis.

### **3.3.2 Analysis and Interpretation of Impedance Data**

After the impedance measurements were obtained, the data were analyzed using analytical models. Different models were developed for each specific type of degradation being evaluated, and were used to interpret the data for purposes of detecting and locating degradation on the cable.

In practice, the application of BIS would involve starting with a known condition of the cable in an un-degraded (baseline) state. The impedance measurements of the cable after being degraded would be compared to the baseline condition. An appropriate model would then be selected to explain any differences in the cable's impedance. Based on the model that best fits the data, the type of degradation would be identified.

The development of analytical models for various types of cable degradation was one of the main objectives of this research effort, and is discussed in the following sections of this report. It should be noted that only one cable type was evaluated in this study. Therefore, the models developed may not be applicable to other types of cables. The suitability of the models developed in this study to other cable types is the subject of a future research program.



(This page intentionally left blank)

## **4. PREPARATION AND BASELINE TESTING OF CABLE TEST SPECIMENS**

This section of the report discusses the process used to prepare the cable test specimens that were used in this study.

### **4.1 Selection of Cable Types**

A number of different types of cables are used in nuclear power plants, and a great deal of knowledge is available concerning their construction and performance (see for example Thue, 1999; Moore, 1997; and Grayson, 2000). For this research, cable samples were prepared using Rockbestos Firewall® III, 2/C #12 AWG instrumentation and control cable, which is a commonly used type of cable in nuclear power plants. The cables had a cross-linked polyethylene (XLPE) insulation on each conductor, and an overall Neoprene jacket covering the bundle of insulated conductors. The testing was limited to one type of cable to allow a full range of testing to be performed within the budget and schedule allocated for this study. Future research is desirable to investigate the effectiveness of the BIS technique on other types of cables.

### **4.2 Preparation of Test Samples**

The test specimens were prepared using a single reel of cable stored at BNL. The cable reel was obtained from the warehouse stock of a decommissioned nuclear power plant as part of a previous research program for the NRC. A single reel of cable was used as the source of all of the test specimens for this study to avoid differences in cable properties that can occur between different batches of cable.

Lengths of cable were cut from the reel to prepare the test specimens. The test specimens ranged in length from 10 meters (32.8 feet) to 100 meters (328 feet). Approximately 15 cm (6 inches) of the outer jacket was stripped from each end of the test specimen, along with approximately 2.5 cm (1 inch) of insulation from each conductor end.

### **4.3 Baseline Testing of Test Samples**

Prior to aging, each test specimen was tested to determine its baseline performance. The tests used were insulation resistance and dielectric loss. These tests were chosen since they are well established, traditional tests that can be used for comparison purposes with the BIS test data. The tests were repeated after aging of the test specimens was completed.

#### 4.4 Accelerated Aging of Test Samples

Thermal aging was applied to the cable test specimens using convection ovens at BNL to simulate exposure to a service temperature of 50°C (122°F) for durations of 20 years, 40 years, and 60 years. The aging duration was determined using the Arrhenius equation with an activation energy of 1.33 eV, which is the value used in the original qualification tests for these cables. The thermal aging was applied globally to the entire length of the test specimen. Cable specimens with no thermal aging were also tested to provide baseline data on the cable performance.

In addition to global aging, selected specimens received thermal aging over a portion of their length to simulate exposure to hot-spots at predetermined locations on the cable. The hot-spot lengths simulated were 0.5 meters (1.64 feet) and 1.0 meters (3.3 feet) long. The hot-spots were simulated by inserting only a portion of the test specimen in the aging chamber. Figure 15 shows a typical aging chamber loading used to perform the global and hot-spot aging. Table 1 provides a matrix of the test specimens prepared for this study.



**Figure 15** Typical aging chamber loading for global and hot-spot aging of cable test specimens

**Table 1** Cable Test Specimens for Broadband Impedance Spectroscopy Research

Cable Type = Rockbestos I&C, 2 Conductor, #12 AWG with XLPE Insulation and Neoprene Outer Jacket

No.	Specimen ID No.	Length meters (inches)	Global Accelerated Thermal Aging Applied <sup>1</sup>		Localized Accelerated Thermal Aging Applied <sup>1</sup>			
			Aging Parameters (hours @ Temp)	Service Life Simulated (years @ Temp.)	Aging Parameters <sup>2</sup> (hours @ Temp.)	Size (meters)	Hot-Spot Simulated (years @ Temp.)	Hot-Spot Location <sup>3</sup> (meters)
1.	PNI-79-RB-188-801	1.0 (39.4)	None	None	None	-	None	-
2.	PNI-79-RB-188-802	2.0 (78.7)	None	None	None	-	None	-
3.	PNI-79-RB-188-803	9.0 (354.3)	None	None	None	-	None	-
4.	PNI-79-RB-188-804	1.0 (39.4)	31.6 @ 121°C (250°F)	20 @ 50°C (122°F)	None	-	None	-
5.	PNI-79-RB-188-805	2.0 (78.7)	31.6 @ 121°C (250°F)	20 @ 50°C (122°F)	None	-	None	-
6.	PNI-79-RB-188-806	9.0 (354.3)	31.6 @ 121°C (250°F)	20 @ 50°C (122°F)	None	-	None	-
7.	PNI-79-RB-188-807	1.0 (39.4)	63.1 @ 121°C (250°F)	40 @ 50°C (122°F)	None	-	None	-
8.	PNI-79-RB-188-808	2.0 (78.7)	63.1 @ 121°C (250°F)	40 @ 50°C (122°F)	None	-	None	-
9.	PNI-79-RB-188-809	9.0 (354.3)	63.1 @ 121°C (250°F)	40 @ 50°C (122°F)	None	-	None	-
10.	PNI-79-RB-188-810	1.0 (39.4)	94.7 @ 121°C (250°F)	60 @ 50°C (122°F)	None	-	None	-
11.	PNI-79-RB-188-811	2.0 (78.7)	94.7 @ 121°C (250°F)	60 @ 50°C (122°F)	None	-	None	-
12.	PNI-79-RB-188-812	9.0 (354.3)	94.7 @ 121°C (250°F)	60 @ 50°C (122°F)	None	-	None	-
13.	PNI-79-RB-188-813	10.0 (393.7)	None	None	None	-	None	-
14.	PNI-79-RB-188-814	10.0 (393.7)	None	None	None	-	None	-
15.	PNI-79-RB-188-815	10.0 (393.7)	None	None	None	-	None	-

**Table 1** Cable Test Specimens for Broadband Impedance Spectroscopy Research (continued)

No.	Specimen ID No.	Length meters (inches)	Global Accelerated Thermal Aging Applied <sup>1</sup>		Localized Accelerated Thermal Aging Applied <sup>1</sup>			
			Aging Parameters (hours @ Temp)	Service Life Simulated (years @ Temp.)	Aging Parameters <sup>2</sup> (hours @ Temp.)	Size meters (inches)	Hot-Spot Simulated (years @ Temp.)	Hot-Spot Location <sup>3</sup> (meters)
16.	PNI-79-RB-188-816	10.0 (393.7)	31.6 @ 121°C (250°F)	20 @ 50°C (122°F)	None	-	None	-
17.	PNI-79-RB-188-817	10.0 (393.7)	31.6 @ 121°C (250°F)	20 @ 50°C (122°F)	6.96 @ 150°C (302°F)	1.0 (39.4)	20 @ 60°C (140°F)	8.0 - 9.0
18.	PNI-79-RB-188-818	10.0 (393.7)	31.6 @ 121°C (250°F)	20 @ 50°C (122°F)	6.96 @ 150°C (302°F)	0.5 (19.7)	20 @ 60°C (140°F)	8.0 - 8.5
19.	PNI-79-RB-188-819	10.0 (393.7)	31.6 @ 121°C (250°F)	20 @ 50°C (122°F)	33.1 @ 150°C (302°F)	1.0 (39.4)	20 @ 70°C (158°F)	8.0 - 9.0
20.	PNI-79-RB-188-820	10.0 (393.7)	31.6 @ 121°C (250°F)	20 @ 50°C (122°F)	33.1 @ 150°C (302°F)	0.5 (19.7)	20 @ 70°C (158°F)	8.0 - 8.5
21.	PNI-79-RB-188-821	10.0 (393.7)	63.1 @ 121°C (250°F)	40 @ 50°C (122°F)	None	-	None	-
22.	PNI-79-RB-188-822	10.0 (393.7)	63.1 @ 121°C (250°F)	40 @ 50°C (122°F)	13.9 @ 150°C (302°F)	1.0 (39.4)	40 @ 60°C (140°F)	1.0 - 2.0
23.	PNI-79-RB-188-823	10.0 (393.7)	63.1 @ 121°C (250°F)	40 @ 50°C (122°F)	13.9 @ 150°C (302°F)	0.5 (19.7)	40 @ 60°C (140°F)	1.5 - 2.0
24.	PNI-79-RB-188-824	10.0 (393.7)	63.1 @ 121°C (250°F)	40 @ 50°C (122°F)	66.2 @ 150°C (302°F)	1.0 (39.4)	40 @ 70°C (158°F)	1.0 - 2.0
25.	PNI-79-RB-188-825	10.0 (393.7)	63.1 @ 121°C (250°F)	40 @ 50°C (122°F)	66.2 @ 150°C (302°F)	0.5 (19.7)	40 @ 70°C (158°F)	1.5 - 2.0
26.	PNI-79-RB-188-826	10.0 (393.7)	94.7 @ 121°C (250°F)	60 @ 50°C (122°F)	None	-	None	-
27.	PNI-79-RB-188-827	10.0 (393.7)	94.7 @ 121°C (250°F)	60 @ 50°C (122°F)	20.9 @ 150°C (302°F)	1.0 (39.4)	60 @ 60°C (140°F)	7.0 - 8.0
28.	PNI-79-RB-188-828	10.0 (393.7)	94.7 @ 121°C (250°F)	60 @ 50°C (122°F)	20.9 @ 150°C (302°F)	0.5 (19.7)	60 @ 60°C (140°F)	7.0 - 7.5
29.	PNI-79-RB-188-829	10.0 (393.7)	94.7 @ 121°C (250°F)	60 @ 50°C (122°F)	99.3 @ 150°C (302°F)	1.0 (39.4)	60 @ 70°C (158°F)	7.0 - 8.0
30.	PNI-79-RB-188-830	10.0 (393.7)	94.7 @ 121°C (250°F)	60 @ 50°C (122°F)	99.3 @ 150°C (302°F)	0.5 (19.7)	60 @ 70°C (158°F)	7.0 - 7.5
31.	PNI-79-RB-188-831	10.0 (393.7)	31.6 @ 121°C (250°F)	20 @ 50°C (122°F)	418.8 @ 150°C (302°F)	1.0 (39.4)	20 @ 90°C (194°F)	8.0 - 9.0
32.	PNI-79-RB-188-832	10.0 (393.7)	31.6 @ 121°C (250°F)	20 @ 50°C (122°F)	418.8 @ 150°C (302°F)	0.5 (19.7)	20 @ 90°C (194°F)	8.0 - 8.5
33.	PNI-79-RB-188-833	10.0 (393.7)	63.1 @ 121°C (250°F)	40 @ 50°C (122°F)	837.6 @ 150°C (302°F)	1.0 (39.4)	40 @ 90°C (194°F)	1.0 - 2.0
34.	PNI-79-RB-188-834	10.0 (393.7)	63.1 @ 121°C (250°F)	40 @ 50°C (122°F)	837.6 @ 150°C (302°F)	0.5 (197)	40 @ 90°C (194°F)	1.5 - 2.0

**Table 1** Cable Test Specimens for Broadband Impedance Spectroscopy Research (continued)

No.	Specimen ID No.	Length meters (inches)	Global Accelerated Thermal Aging Applied <sup>1</sup>		Localized Accelerated Thermal Aging Applied <sup>1</sup>			
			Aging Parameters (hours @ Temp)	Service Life Simulated (years @ Temp.)	Aging Parameters <sup>2</sup> (hours @ Temp.)	Size meters (inches)	Hot-Spot Simulated (years @ Temp.)	Hot-Spot Location <sup>3</sup> (meters)
35.	PNI-79-RB-188-835	10.0 (393.7)	94.7 @ 121°C (250°F)	60 @ 50°C (122°F)	1256.4 @ 150°C (302°F)	1.0 (39.4)	60 @ 90°C (194°F)	7.0 - 8.0
36.	PNI-79-RB-188-836	10.0 (393.7)	94.7 @ 121°C (250°F)	60 @ 50°C (122°F)	1256.4 @ 150°C (302°F)	0.5 (19.7)	60 @ 90°C (194°F)	7.0 - 7.5
37.	PNI-79-RB-188-837	10.0 (393.7)	9.1 @ 121°C (250°F)	20 @ 60°C (140°F)	None	-	None	-
38.	PNI-79-RB-188-838	10.0 (393.7)	35.3 @ 121°C (250°F)	20 @ 70°C (158°F)	None	-	None	-
39.	PNI-79-RB-188-839	10.0 (393.7)	18.3 @ 121°C (250°F)	40 @ 60°C (140°F)	None	-	None	-
40.	PNI-79-RB-188-840	10.0 (393.7)	70.6 @ 121°C (250°F)	40 @ 70°C (158°F)	None	-	None	-
41.	PNI-79-RB-188-841	10.0 (393.7)	27.4 @ 121°C (250°F)	60 @ 60°C (140°F)	None	-	None	-
42.	PNI-79-RB-188-842	10.0 (393.7)	105.8 @ 121°C (250°F)	60 @ 70°C (158°F)	None	-	None	-
43.	PNI-79-RB-188-843	10.0 (393.7)	1256.4 @ 150°C (302°F)	60 @ 90°C (158°F)	None	-	None	-
44.	PNI-79-RB-188-847	100.0 (3937)	None	-	1256.4 @ 150°C (302°F)	1.0 (39.4)	60 @ 90°C (194°F)	96.0 -97.0
45.	PNI-79-RB-188-848	100.0 (3937)	None	-	None	-	None	-

1. Calculations based on activation energy of 1.33 eV.

2. Hot-spot aging time is in addition to global aging time.

3. Measured from right end of cable, as determined by orienting wording on cable so it can be read normally from left to right.

(This page intentionally left blank)

## **5. RESULTS OF BIS TESTING OF CABLE SAMPLES**

This section presents the results of the BIS tests performed on the cable test specimens with various types of degradation. The models developed for each type of degradation are presented and, comparisons with actual test data are made.

### **5.1 Application of BIS to Thermally Aged Cables**

The initial research to evaluate BIS was focused on the detection of degradation on cables that had been exposed to thermal aging. This is a fundamental requirement of an effective cable condition monitoring technique for nuclear plant cables since thermal aging is one of the predominant stressors in such plants. Section 5.1.1 presents the results of tests on cables that received global thermal aging to simulate various service conditions. These cables were tested to characterize their impedance spectra, and demonstrate the capability of the BIS method for detecting thermal degradation. Subsequently, models were developed to represent the measured impedance spectra and the electrical properties of the cables.

In Section 5.1.2, the results from tests on cables with localized thermal aging, or hot-spots, is presented. These tests were performed to determine if the BIS technique is capable of locating localized degradation on a cable. The models and process used to locate degradation are presented and discussed.

#### **5.1.1 Detection of Degradation on Cables with Global Thermal Aging**

The BIS technique was evaluated for its ability to detect global thermal aging on cables using the test specimens shown in Table 2. These cables were aged to simulate 20, 40 and 60 years of service at service temperatures of 50°C (122°F), 60°C (140°F), and 70°C (158°F). For each test specimen, broadband impedance measurements were made over the low frequency range (100 Hz to 1 MHz) and over the high frequency range (1 MHz to 100 MHz).

Figure 16 shows the measured impedance phase spectra in the low frequency range for the cables aged to simulate 60 years of service (Specimens 26, 41, and 42). In performing these measurements, the cables were placed in a humidity chamber, which was maintained at a constant temperature of 25° (77°F) and a pressure of 1 atmosphere to minimize atmospheric effects on the measurements. The cables were tested with the conductors connected to the test instrument on one end, and “open” (unconnected) at the opposite end.

Referring to Figure 16, it is seen that as the amount of degradation on the cable increases, which is represented by the higher simulated service temperature, the greater the cable’s impedance phase shifts away from -90 degrees. This suggests that as the degradation on the cable increases, the cable becomes more dissipative, which is expected. Similar results were obtained for cables aged to simulate 20 years and 40 years of service (Appendix A).



**Table 2** Specimens tested to evaluate BIS for detecting global thermal aging

No.	Specimen ID	Length meters (inches)	Service Life Simulated	Hot-Spot Simulated
16.	PNI-79-RB-188-816	10 (393.7)	20 @ 50°C (122°F)	None
37.	PNI-79-RB-188-837	10 (393.7)	20 @ 60°C (140°F)	None
38.	PNI-79-RB-188-838	10 (393.7)	20 @ 70°C (158°F)	None
21.	PNI-79-RB-188-821	10 (393.7)	40 @ 50°C (122°F)	None
39.	PNI-79-RB-188-839	10 (393.7)	40 @ 60°C (140°F)	None
40.	PNI-79-RB-188-840	10 (393.7)	40 @ 70°C (158°F)	None
26.	PNI-79-RB-188-826	10 (393.7)	60 @ 50°C (122°F)	None
41.	PNI-79-RB-188-841	10 (393.7)	60 @ 60°C (140°F)	None
42.	PNI-79-RB-188-842	10 (393.7)	60 @ 70°C (158°F)	None

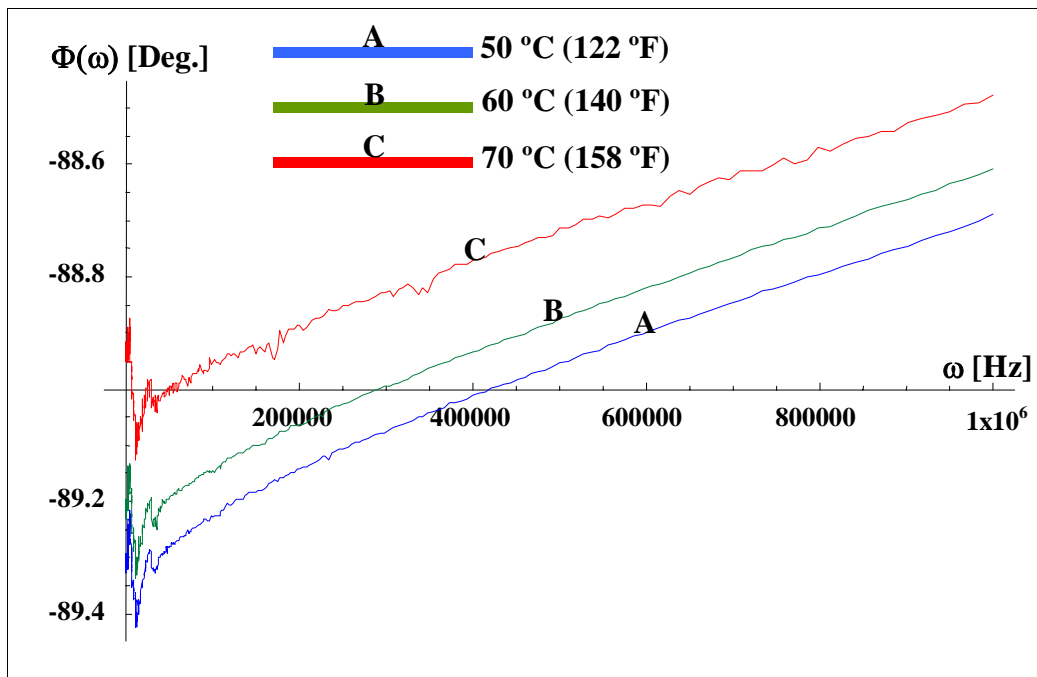


**Figure 16** Measured low frequency impedance phase spectra for cables with global thermal aging to simulate 60 years of service at various temperatures

Figure 17 shows the impedance phase spectra for these cables in the high frequency range. Examination of this figure reveals that the impedance phase for these cables differs significantly as degradation increases, particularly for frequencies above 60MHz where large differences in the zero crossings of the impedance phase spectra are seen. An expanded view for the frequency range from 78 MHz to 86 MHz is shown in Figure 18 for both the impedance phase and magnitude. The shift in both phase and magnitude to lower frequencies with increasing degradation is readily observed. Similar results were obtained for cables aged to simulate 20 years and 40 years of service (Appendix A).

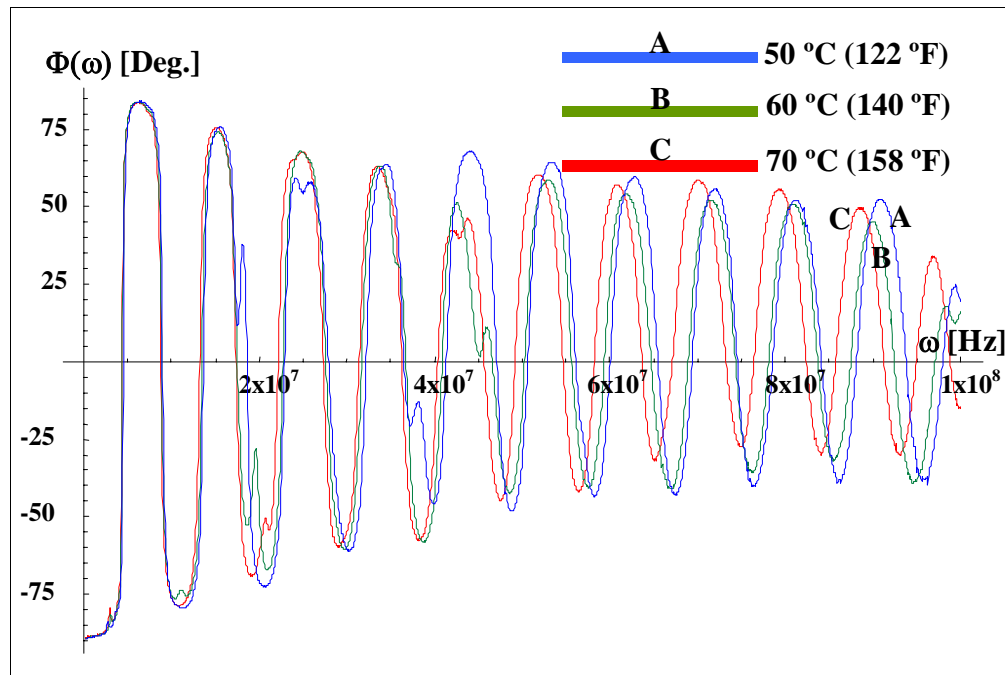


**Figure 17** Measured high frequency impedance phase spectra for cables with global thermal aging to simulate 60 years of service at various temperatures

These results demonstrate that thermal degradation has an impact on a cable’s electrical impedance spectra. By measuring the impedance over a range of frequencies and comparing the impedance spectra to a known spectra for an undamaged cable, changes in the impedance phase and magnitude can be observed and used as an indicator of cable degradation.

In the next section, models are developed that can be used to describe the changes in the impedance spectra. These models can be used to characterize a cable’s electrical properties after being exposed to global thermal degradation. The models can also be used to locate localized areas of degradation on the cable, such as would be caused by environmental “hot-spots” along the cable.

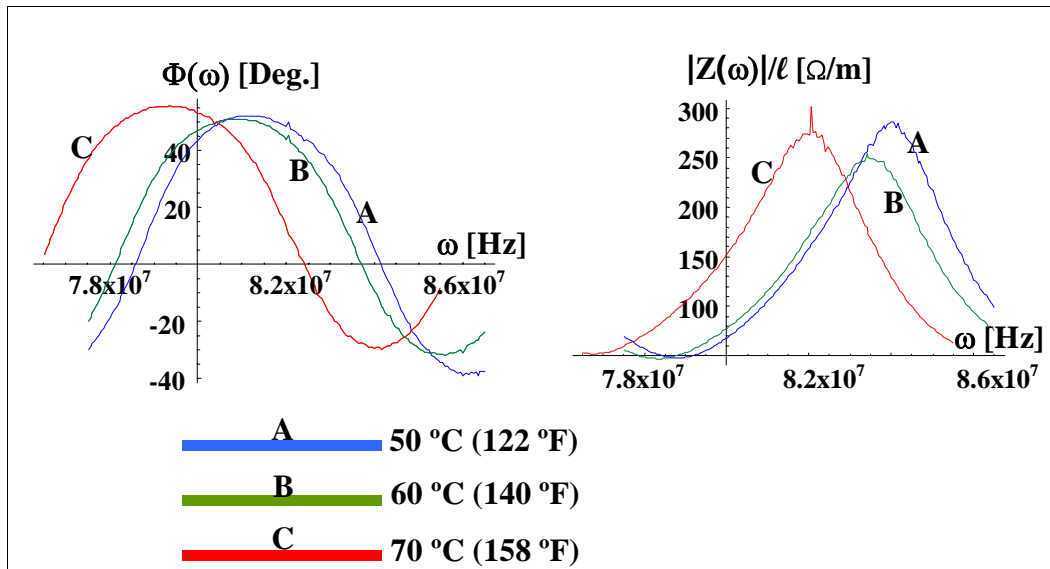


**Figure 18** Expanded view of impedance phase and magnitude per unit length spectra over the frequency range from 78 MHz to 86 MHz for cables with global thermal aging to simulate 60 years of service at various service temperatures

### 5.1.2 Development of Models for Cables with Thermal Degradation

Analytical models are used to determine the electrical properties of a cable, thereby providing an assessment of the cable's health. In addition, the models are required to determine the location of localized degradation on a cable. The development of analytical models for cables exposed to thermal aging is discussed in this section.

In order to develop an analytical model, it is important to understand the basic approach to modeling a cable. If a cable is exposed to an aging stressor uniformly along its length, it will be in a "single state" and can be represented by two frequency dependent functions; the characteristic impedance,  $Z_0(\omega)$ , and the propagation function,  $\gamma(\omega)$ . However, if a cable is exposed to different levels of an aging stressor along its length, it will have sections with different amounts of aging degradation and the cable will be in multiple states. In this case, each section will have its own characteristic impedance and propagation function, and the cable must be modeled as a complex combination of these parameters.

At low frequencies the cable's impedance is non-oscillatory and, as discussed in Section 3.2.1, the characteristic impedance and propagation function can be directly extracted from the measured impedance spectra using equations 3.2-1a and 3.2-1b. At high frequencies, where the cable's impedance oscillates, it is not possible to directly extract the characteristic impedance and propagation function. Instead, one of the following two approaches can be used:

- Extrapolative approach, or
- Physical modeling approach

The extrapolative approach is used here to model cables with thermally induced aging degradation. In this approach, the function representing the cable's characteristic impedance in the low frequency range is first determined using equation 3.2-1a. This function is then extrapolated to high frequencies ranging from 1MHz to 15MHz. By substituting the extrapolated characteristic impedance into equation 3.1-7a, the propagation function for the high frequency range can then be determined using the following equation:

$$\gamma(\omega) = \text{Coth}^{-1} \left[ \frac{Z_{open}(\omega)}{Z_{0, extrapolated}(\omega)} \right] \quad (5.1-1)$$

where  $Z_{open}$  is the measured cable impedance in the open configuration, and  $Z_{0, extrapolated}(\omega)$  is the extrapolated characteristic impedance for the cable.

#### 5.1.2.1 Extraction of Cable Properties from Measured Impedance Spectra

As discussed in Section 3.2.1, a cable's characteristic impedance and propagation function can be extracted from measured impedance data. The cable's impedance is measured in the open configuration and the shorted configuration, then equations 3.2-1a and 3.2-1b can be used to obtain the cable's characteristic impedance and propagation function. Once these functions are known, the cable's electrical properties can be determined using equations 3.2-3a to 3.2-3d. This was performed for the thermally aged cable test specimens in Table 2. Results for the cables aged to simulate 60 years of service are presented below. Similar results were obtained for the remaining cables in Table 2 and are included in Appendix A.

In Figure 19, the magnitude,  $|Z_0(\omega)|$ , and phase,  $\Psi(\omega)$ , of the characteristic impedance spectra are presented for the cables thermally aged to simulate 60 years of service (Specimens 26, 41, and 42). Examination of this figure shows that the thermal aging has only a small effect on the cable's characteristic impedance, as evidenced by the changes in magnitude of less than 5%.

Figure 20 compares the real component,  $\gamma^r$ , and imaginary component,  $\gamma^i$ , of the propagation function spectra for the cables aged to simulate 60 years of service. As shown, the real component of the propagation function increases as the aging degradation increases (higher simulated service temperature). This reflects the fact that the thermal aging process produces chemical changes in the cable's insulation.

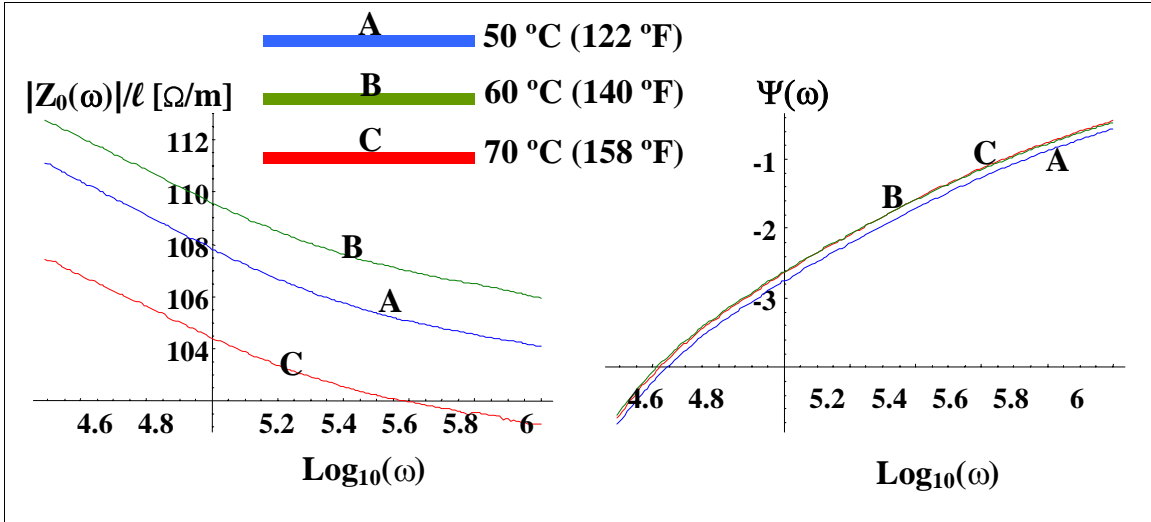


**Figure 19** Characteristic impedance magnitude per unit length and phase spectra for cables with global thermal aging to simulate 60 years of service at various temperatures

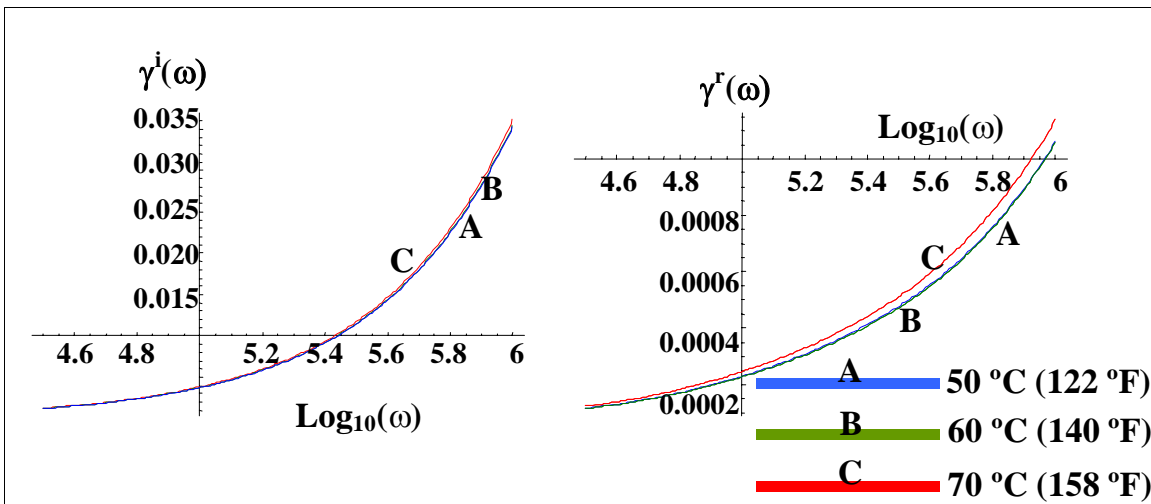


**Figure 20** Imaginary component and real component of propagation function for cables with global thermal aging to simulate 60 years of service at various temperatures

With the characteristic impedance and propagation function now known, the cable's electrical properties can be determined. First, equation 3.2-3a is used to obtain the resistance of the cables, as shown in Figure 21. The left-hand side of the figure shows the resistance per unit length of the cable in ohms/meter, while the right-hand side shows the percent change in resistance for an increase in service temperature from 50°C to 60°C, and from 50°C to 70°C. The percent change was calculated using the following equation:

$$\delta R_k(\omega) = \frac{R_k(\omega) - R_{50}(\omega)}{R_{50}(\omega)}$$

where  $R_k(\omega)$  is the resistance for service temperatures of 60°C (140°F) ( $k=60$ ) and 70°C (158°F) ( $k=70$ ), and  $R_{50}(\omega)$  is the resistance for a service temperature of 50°C (122°F).

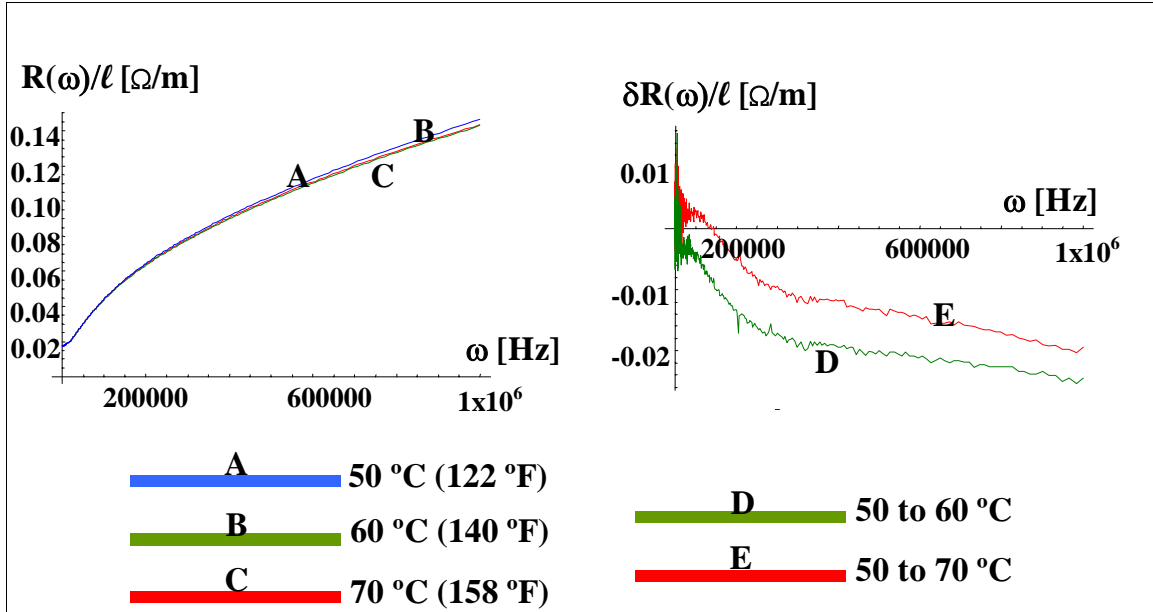


**Figure 21** Resistance per unit length and change in resistance per unit length for cables with global thermal aging to simulate 60 years of service at various temperatures

Referring to the left-hand side of Figure 21, it is seen that an increase in thermal aging (i.e., higher service temperature) results in a small but perceptible decrease in the cable's resistance. This implies that shrinkage of the insulation is greatest with the higher simulated service temperature. The right-hand side of Figure 21 shows that the resistance decreases as service temperature increases, which results in a negative percent change. Also, the percent change in resistance increases (i.e., becomes more negative) at the higher frequencies.

Using the extracted resistance, an analytical model can now be developed to represent this resistance spectra. The analytical model is based upon the knowledge that resistance is primarily governed by the skin effect, which is a function of  $\omega^{1/2}$ . Therefore, an equation of the following form was fitted to the resistance spectra presented in Figure 21:

$$R_k(\omega) = R_{0,k} \left( 1 + \sqrt{\frac{\omega}{\omega_k}} \right) \quad 5.1-3$$

where  $R_k(\omega)$  is the resistance for a cable aged to simulate service temperature  $k$ ,  $\omega_k$  is the skin

frequency for a cable aged to simulate service temperature  $k$ , and  $R_{0,k}$  is an adjustable constant. The values for the skin frequency and  $R_{0,k}$  for the cables evaluated are shown in Table 3.

**Table 3** Parameters for analytical model of resistance for cables thermally aged to simulate 60 years of service at various service temperatures <sup>1</sup>

Simulated Service Temperature	Skin Frequency ( $\omega_k$ )	Constant ( $R_{0,k}$ )
50 °C (122 °F)	12,589.3 sec <sup>-1</sup>	0.0150 Ω/m
60 °C (140 °F)	12,589.3 sec <sup>-1</sup>	0.0143 Ω/m
70 °C (158 °F)	14,125.4 sec <sup>-1</sup>	0.0150 Ω/m

1. Parameters determined by fitting equation 5.1-3 to resistance data in Figure 20

The cable resistance determined using the analytical model is compared to the extracted cable resistance in Figure 22 for the cable thermally aged to simulate 60 years of service at 50°C (122°F). As shown, the analytical model is within 5% of the extracted resistance over the frequency range from 400kHz to 1 MHz, which demonstrates reasonably good accuracy for this model. Similar results were obtained for the other cables in Table 2, which are included in Appendix A. The error in the analytical model arises from the fact that the classical relationship of the skin effect was approximated by equation 5.1-3. However, the error introduced by this approximation is acceptable for the purposes of this study.

A similar process was followed to obtain an analytical model for the cable inductance. Equation 3.2-3b was used to extract the inductance from the measured characteristic impedance and propagation function spectra. The results are presented in Figure 23. The left-hand side shows the inductance per unit length,  $L(\omega)$  Henrys/meter, for the cables aged to simulate 60 years of service. The right-hand side shows the percent change in inductance,  $\delta L(\omega)$ , for an increase in service temperature from 50°C to 60°C, and from 50°C to 70°C. The percent change was calculated using the following equation:

$$\delta L_k(\omega) = \frac{L_k(\omega) - L_{50}(\omega)}{L_{50}(\omega)} \quad 5.1-4$$

where  $L_k(\omega)$  is the inductance for cables aged to simulate service temperatures of 60°C (140°F) ( $k=60$ ) and 70°C (158°F) ( $k=70$ ), and  $L_{50}(\omega)$  is the inductance for the cable aged to simulate a service temperature of 50°C (122°F).

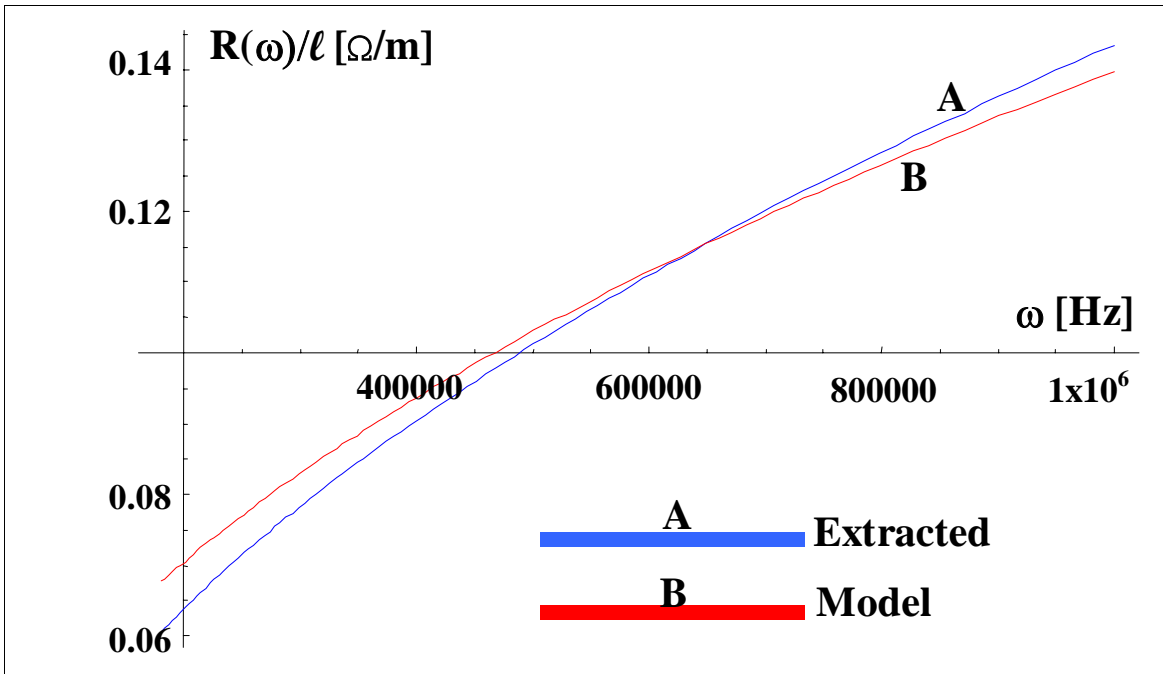


**Figure 22** Comparison of resistance per unit length predicted by analytical model to that extracted from measured impedance for cable with global thermal aging to simulate 60 years of service at 70°C

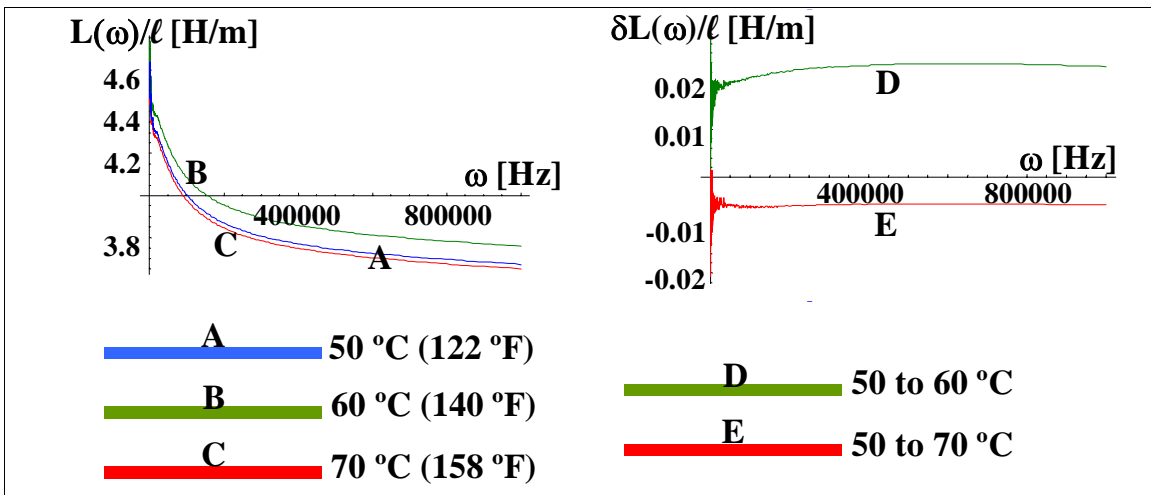


**Figure 23** Inductance per unit length and change in inductance per unit length for cables with global thermal aging to simulate 60 years of service at 70°C

Examination of the left-hand side of Figure 23 shows that the inductance tends to increase with



increasing thermal degradation, as evidenced by comparing the inductance for the 50°C (122°F) service temperature (curve A) with that for the 60°C (140°F) service temperature (curve B). This supports the notion that shrinkage of the insulation is greater with increased amounts of thermal aging. A further increase in service temperature to 70°C (158°F) (curve C) results in a decrease in inductance for this case. The reason for this decrease is not readily apparent. It is also noted that the inductance decreases with increasing frequency. This is consistent with the skin effect, although the inductance decreases with frequency as  $\omega^{-0.2}$ , whereas the skin effect predicts a  $\omega^{-0.5}$  dependence.

An analytical model of the cable's inductance is now developed based on the extracted inductance spectra. Since the inductance does not behave as the classical skin effect, the following phenomenological relation is used.

$$L_k(\omega) = L_{0,k} \left( 1 - a_k \frac{(\omega \tau_k)^{m_k}}{1 + (\omega \tau_k)^{2m_k}} \right) \quad 5.1-5$$

where  $L_{0,k}$  is the very low frequency inductance per unit length of the cable, and  $a_k$ ,  $\tau_k$ , and  $m_k$  are adjustable constants. The values for these parameters were determined for the cables aged to simulate 60 years of service by fitting equation 5.1-5 to the extracted inductance spectra presented in Figure 23 over the frequency range from 429 kHz to 1MHz. The rms error between the model prediction and extracted data was minimized to determine the parameter values, which are presented in Table 4.

**Table 4** Parameter values for analytical model of inductance for cables aged to simulate 60 years of service at various service temperatures <sup>1</sup>

Service Temperature Simulated	Very Low Frequency Inductance ( $L_{0,k}$ )	$a_k$	$\tau_k$	$m_k$
50 °C (122 °F)	4.84 $\mu$ H/m	0.612	0.10 $\mu$ sec <sup>-1</sup>	0.18
60 °C (140 °F)	4.84 $\mu$ H/m	0.612	0.10 $\mu$ sec <sup>-1</sup>	0.18
70 °C (158 °F)	5.00 $\mu$ H/m	0.675	0.10 $\mu$ sec <sup>-1</sup>	0.18

1. Parameters determined by fitting equation 5.1-5 to the inductance spectra presented in Figure 22.

Figure 24 compares the inductance extracted from the measured impedance spectra with the inductance predicted by the analytical model for the cable aged to simulate 60 years of service at 70°C (158°F). As shown, the predicted inductance is within 1% of the extracted inductance over the frequency range from 429 kHz to 1 MHz, which demonstrates good accuracy for the analytical model. Similar results were obtained for the other cables in Table 2, which are presented in Appendix A.

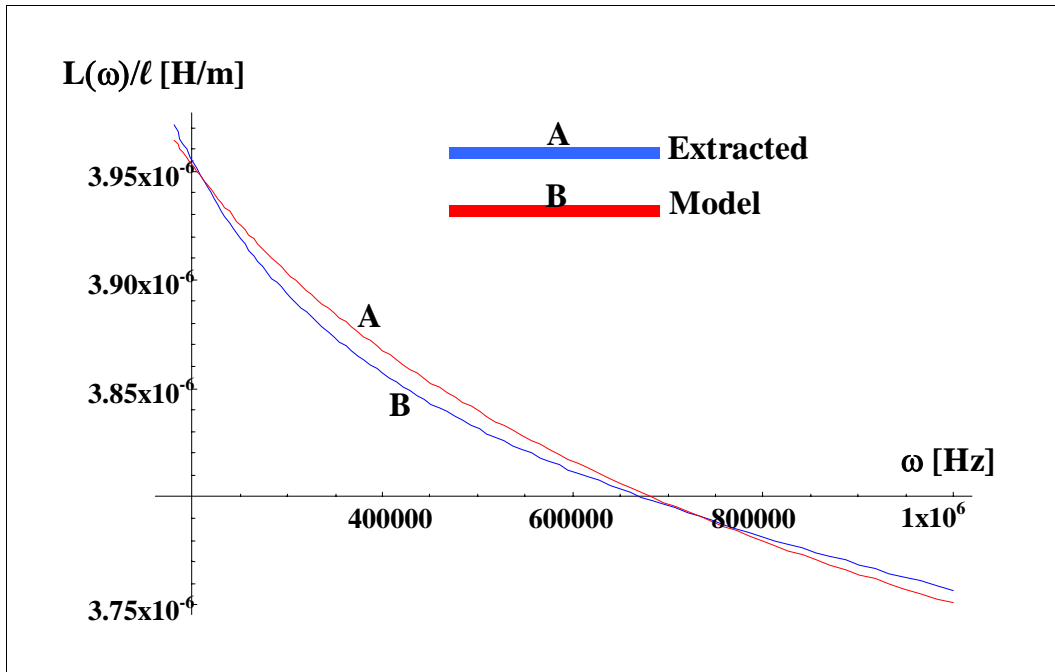


**Figure 24** Comparison of inductance per unit length predicted by analytical model to that extracted from measured impedance for cable with global thermal aging to simulate 60 years of service at 70°C

The capacitance and conductance are linked by the cable's dielectric function, which is given by equation 3.1-1. Therefore, these two electrical properties will be considered together. Using equations 3.2-3c and 3.2-3d, the real and imaginary components of the dielectric function are extracted from the characteristic impedance and propagation function. The capacitance and conductance are then determined using equation 3.1-1.

Figure 25 presents the capacitance per unit length,  $C(\omega)$  Farads/meter, for the cables aged to simulate 60 years of service. The left-hand side presents the capacitance per unit length for each of the different service temperatures simulated. The right-hand side presents the percent change in capacitance for an increase in service temperature from 50°C to 60°C (curve D), and 50°C to 70°C (158°F) (curve E). Examination of this figure shows that the capacitance, and therefore, the real component of the dielectric function,  $\epsilon_1(\omega)$ , decreases slowly with frequency and has an average value of 0.35 to 0.38 nF/m. The effect of higher simulated service temperatures is mixed; the capacitance of the cable aged to simulate a service temperature of 60°C (140°F) shows a decrease compared to the cable aged to simulate 50°C (122°F). However, an increase is noted when the capacitance for the cable aged to simulate 70°C (158°F) is compared to the cable aged to simulate 50°C (122°F). This behavior is non-intuitive and the explanation is not readily obvious.

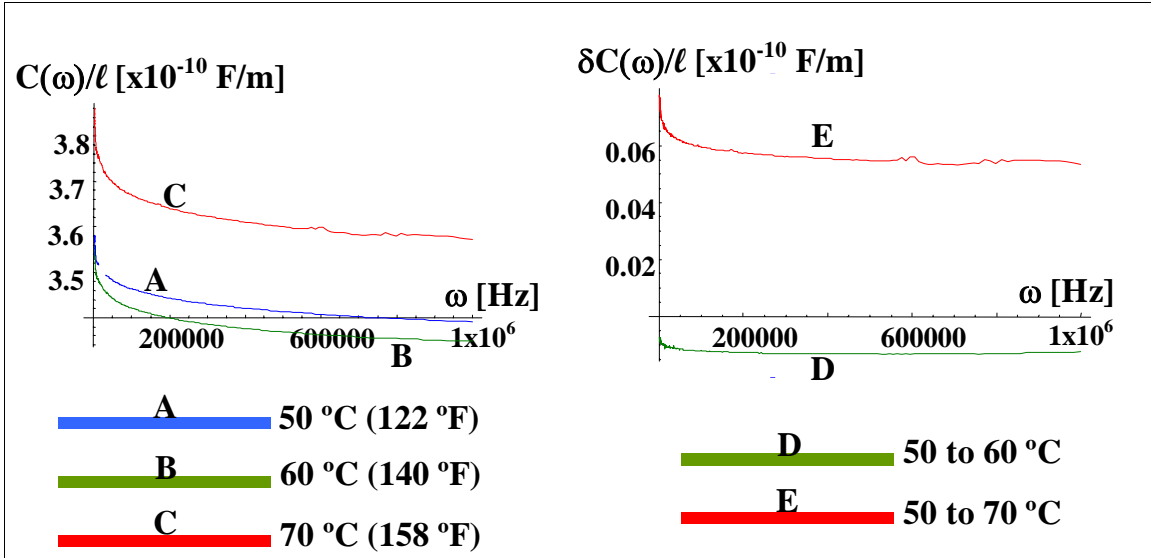


**Figure 25** Capacitance per unit length and change in capacitance per unit length for cables with global thermal aging to simulate 60 years of service at various temperatures

Figure 26 presents the conductance per unit length for the cables aged to simulate 60 years of service. The left-hand side of the figure shows the conductance per unit length normalized by the frequency,  $G(\omega)/\omega$  mho-sec/m. The right-hand side shows the change in conductance,  $\delta G(\omega)$ , for an increase in service temperature from 50° to 60°C (curve D), and from 50° to 70°C (curve E). As shown, the conductance increases with frequency and has an average value on the order of  $6 \times 10^{-3}$  mho-sec/m. Also, as the simulated service temperature increases, the conductance increases. The right-hand side of the figure shows that the conductance for the cable aged to simulate 70°C (158°F) increased by approximately 40% above that for the cable aged to 50°C (122°F). This indicates that the cable's insulation has probably passed through a glass transition phase and become more dissipative.

Using the capacitance and conductance spectra, analytical models for the cable's dielectric function are now developed. These models are based upon the fraction power law, which has been used extensively over the past two decades to model dielectric materials. The model is defined in the following equation:

$$\varepsilon = c_0 \left( 1 + \frac{A_1}{[1 + (i\omega\tau_1)^{n_1}] + \frac{A_2}{[1 + (i\omega\tau_2)^{n_2}]} \right) \quad 5.1-6$$

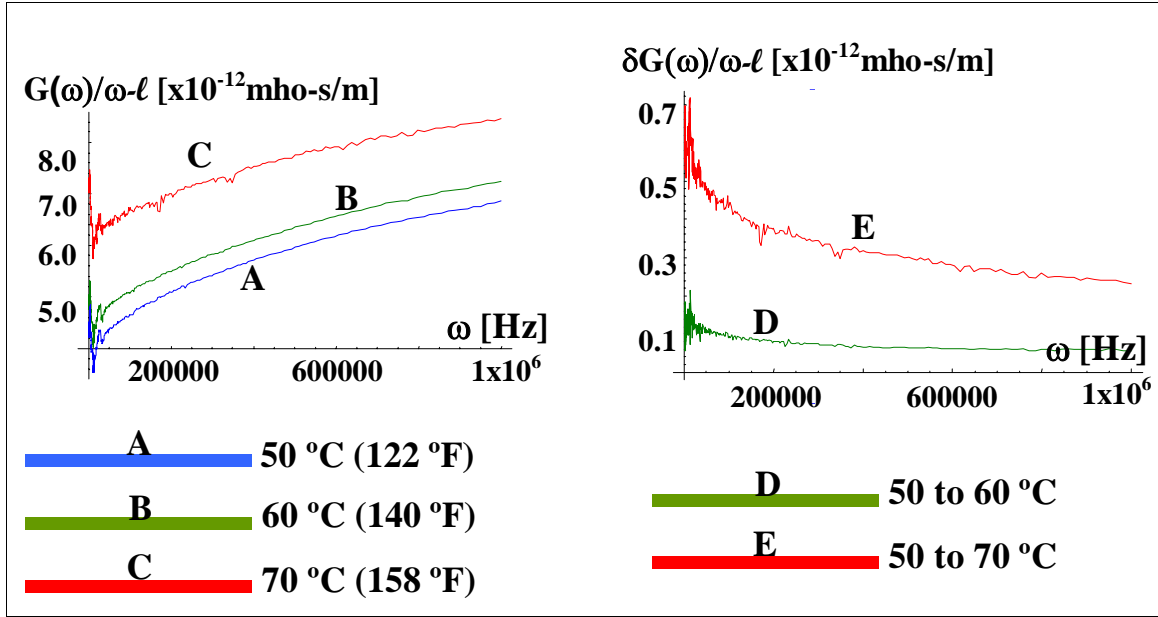


**Figure 26** Conductance-to-frequency ratio per unit length and change in conductance-to-frequency ratio per unit length for cables with global thermal aging to simulate 60 years of service at various temperatures

where the second and third terms in the equation refer to electronic processes and mixed processes that govern the insulator's dielectric response to electrical forces. The constants  $c_0$ ,  $A_1$ ,  $\tau_1$ ,  $n_1$ ,  $A_2$ ,  $\tau_2$ , and  $n_2$  are determined based upon physical considerations. For example,  $2 \leq A_2 \leq 4$  due to the fact that the electronic processes dominate the material's dielectric response to electrical forces throughout the frequency range. Furthermore, these processes are very fast ( $\tau_2 = 0.1 \mu\text{s}$ ) and nearly independent of frequency ( $0 \leq n_2 \leq 0.1$ ). On the other hand, ionic processes are not included in equation 5.1-6 since they are too slow ( $0.01 \text{s} \leq \tau_2 \leq 1 \text{s}$ ) and cannot affect the material's dielectric response to electrical forces. Also, the ionic processes are Debye in nature and are about 5% less than  $A_2$  even at low frequencies (i.e., 1kHz or less, whereas we are interested in the frequency range from 429kHz and above). Finally, the mixed processes are midway between the ionic and electronic processes. Typically, the following ranges are found for these parameters:  $0.1 \leq A_1 \leq 1.0$ ,  $0.1 \leq n_1 \leq 0.5$ , and  $10 \mu\text{s} \leq \tau_1 \leq 100 \mu\text{s}$ .

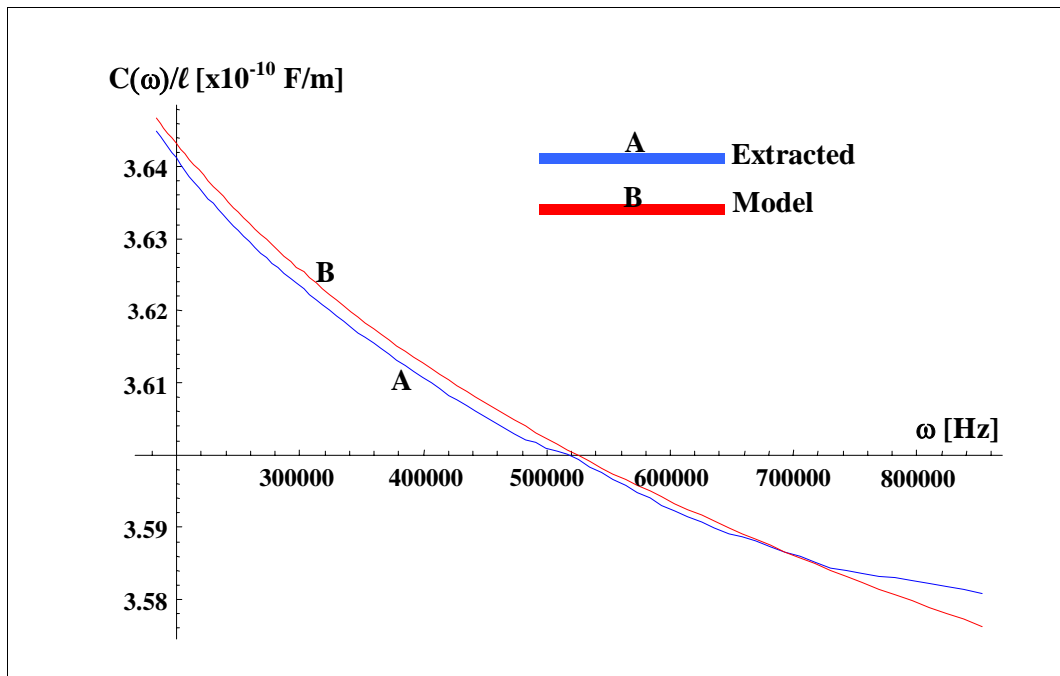
The parameter values for the dielectric function analytical model were determined by fitting equation 5.1-6 to the extracted capacitance and conductance over the frequency range from 429 kHz to 1 MHz, and minimizing the rms error between the modeled values and the extracted values. The parameter values are presented in Table 5.

**Table 5** Parameter values for dielectric function analytical model for cables thermally aged to simulate 60 years of service at various service temperatures <sup>1</sup>

Service Temperature Simulated	$c_0$	$A_1$	$\tau_1$	$n_1$	$A_2$	$\tau_2$	$n_2$
50 °C (122 °F)	0.2920	1.00	31.6	0.2500	6.00	0.10	0.010
60 °C (140 °F)	0.2874	0.85	31.6	0.2489	6.80	0.10	0.018
70 °C (158 °F)	0.2880	1.50	31.6	0.2500	5.75	0.01	0.125

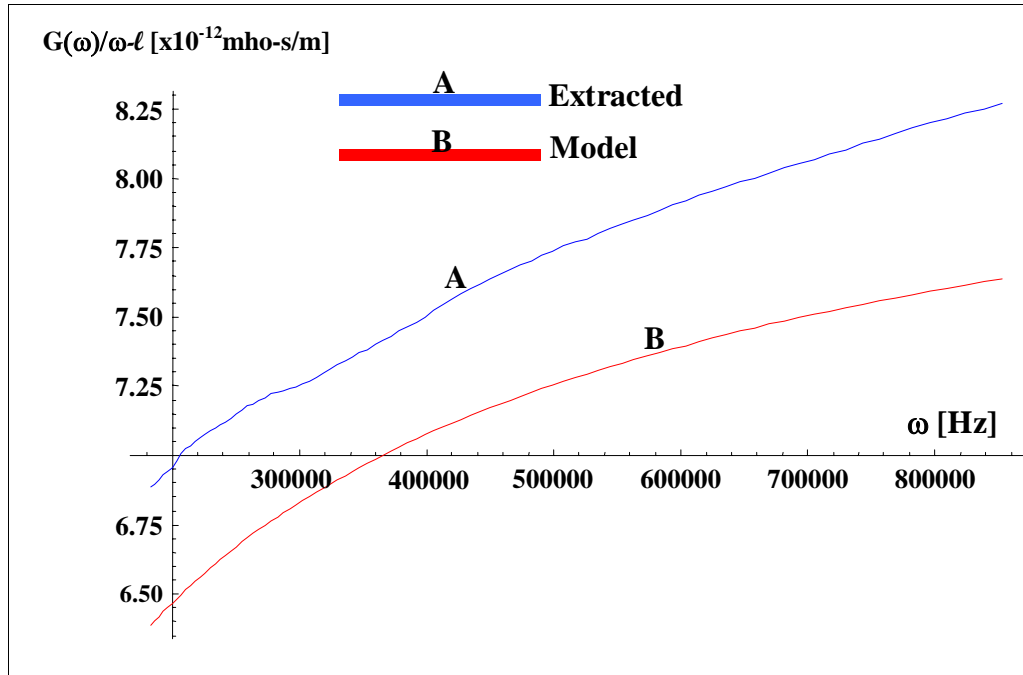
1. Parameter values determined by fitting equation 5.1-6 to the capacitance and conductance spectra presented in Figures 24 and 25, respectively.

Figure 27 compares the capacitance predicted by the model to the capacitance extracted from the measured impedance spectra for the cable aged to simulate 60 years of service at 70°C (158°F). As shown, the predicted capacitance is within 1% of the extracted capacitance over the frequency range from 429 kHz to 1MHz, which demonstrates good accuracy for the model.



**Figure 27** Comparison of capacitance per unit length predicted by analytical model to that extracted from measured impedance for cable with global thermal aging to simulate 60 years of service at 70°C

Similarly, Figure 28 compares the conductance-to-frequency ratio,  $G(\omega)/\omega$ , predicted by the model to the conductance-to-frequency ratio extracted from the measured impedance spectra for the cable aged to simulate 60 years of service at 70°C (158°F). As shown, the predicted spectra is within 10% of the extracted spectra over the frequency range from 429 kHz to 1MHz, which demonstrates good accuracy for the model.



**Figure 28** Comparison of conductance-to-frequency ratio per unit length predicted by analytical model to that extracted from measured impedance for cable with global thermal aging to simulate 60 years of service at 70°C

With the electrical properties modeled, the characteristic impedance and propagation function can now be modeled using equations 3.1-8 and 3.2-2, respectively. Figure 29 compares the characteristic impedance predicted by the analytical model to that extracted from the measured impedance spectra for the cable thermally aged to simulate 60 years of service at 70°C (158°F). As shown, the characteristic impedance predicted by the analytical model is within 1% of the extracted spectra over the frequency range from 429 kHz to 1 MHz, which demonstrates good accuracy for the model. Similarly, Figure 30 compares the propagation function predicted by the analytical model to that extracted from the measured impedance spectra for the cable thermally aged to simulate 60 years of service at 70°C (158°F). Again, good accuracy is demonstrated for the model, with predicted values within 1% for the imaginary part, and within 7% for the real part of the propagation function.

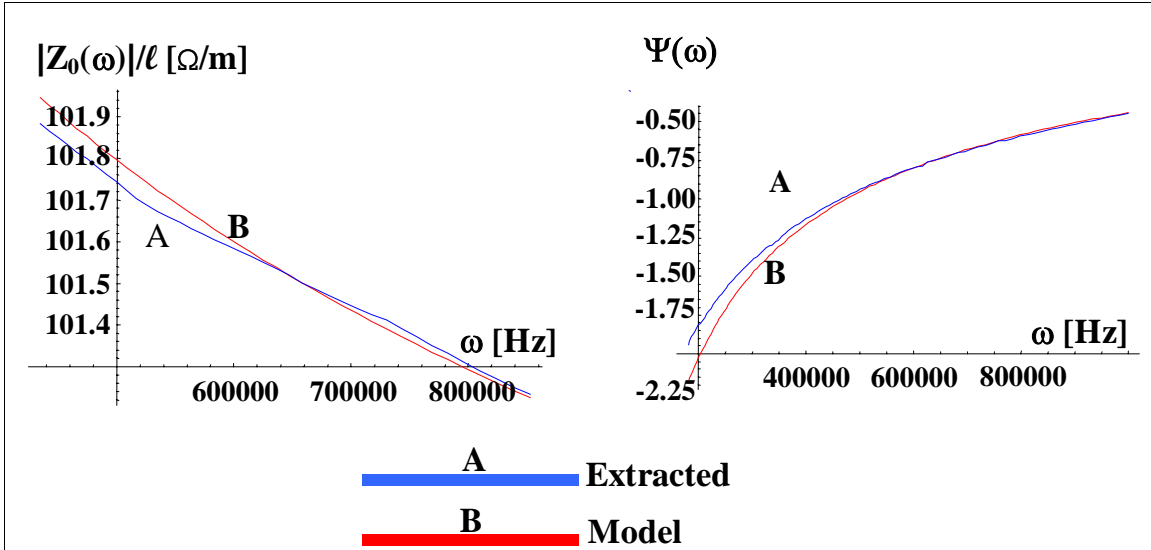


**Figure 29** Comparison of characteristic impedance magnitude per unit length and phase spectra predicted by analytical model to that extracted from measured impedance for cable with global thermal aging to simulate 60 years of service at 70°C

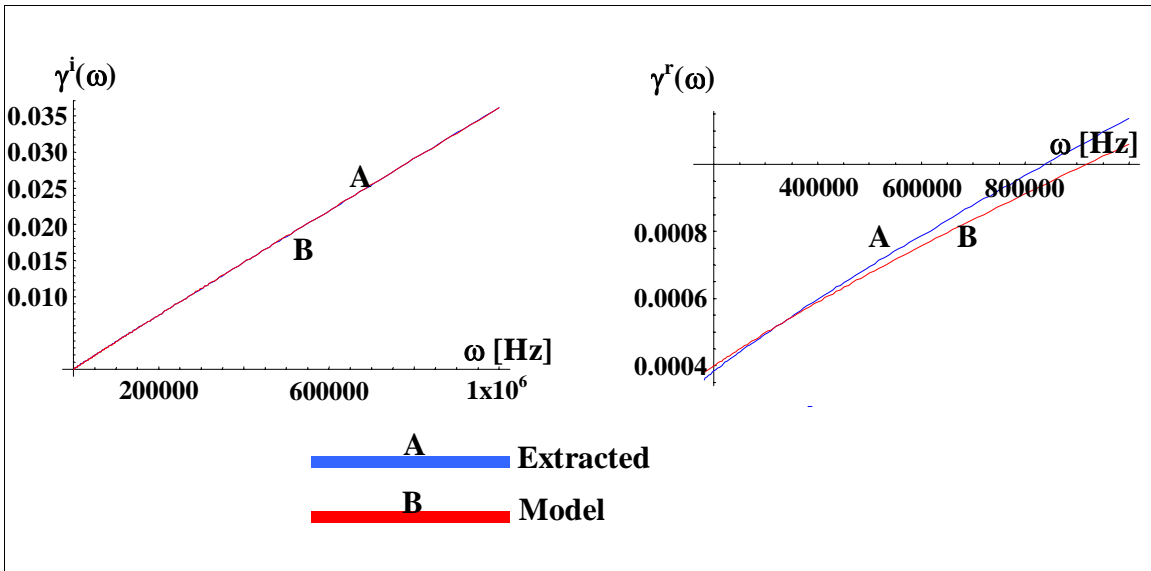


**Figure 30** Comparison of the imaginary component and real component of the propagation function predicted by analytical model to that extracted from measured impedance for cable with global thermal aging to simulate 60 years of service at 70°C

### 5.1.2.2 Extrapolation of Cable Properties to High Frequency

Next, the high frequency cable properties are determined by using the extrapolative approach, which was discussed previously. The characteristic impedance and propagation function for the cables aged to simulate 60 years of service are presented and discussed below. Similar analyses were performed for the cables aged to simulate 20 years and 40 years of service, and these results are presented in Appendix B.

The high-frequency characteristic impedance spectra were determined by extrapolating the low-frequency spectra. Figure 31 presents the extrapolated high-frequency characteristic impedance magnitude,  $|Z_0(\omega)|$ , and phase,  $\Psi(\omega)$ , spectra for cable specimens 26, 41 and 42. The limiting value of the characteristic impedance magnitude (i.e., as  $\omega \rightarrow \infty$ ) for the cables are as follows:

$$\text{Specimen 26 (50°C): } Z_0(\omega \rightarrow \infty) = 77.42 \, \Omega$$

$$\text{Specimen 41 (60°C): } Z_0(\omega \rightarrow \infty) = 79.46 \, \Omega$$

$$\text{Specimen 42 (70°C): } Z_0(\omega \rightarrow \infty) = 75.12 \, \Omega$$

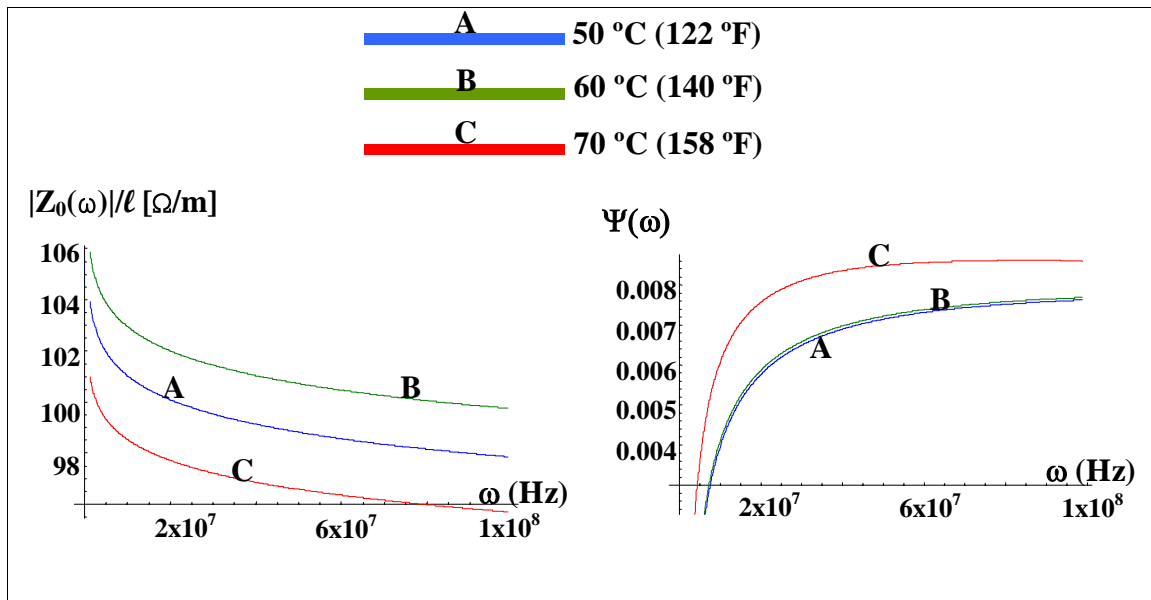


**Figure 31** High frequency characteristic impedance magnitude and phase spectra extrapolated from low frequency spectra for cables with thermal aging to simulate 60 years of service at various temperatures

Using Equation 5.1-1, each cables' propagation function at high frequency was determined, as shown in Figure 32. Examination of this figure shows that both the real and imaginary components of the propagation function exhibit a number of oscillations, starting in the vicinity of 10 MHz. These oscillations are a consequence of the extrapolative approach used, and do not represent reality. Specifically, the impedance spectra are strong functions of the frequency in the vicinity of the phase zero crossings. Thus, small differences between the actual characteristic



impedance and the extrapolated value give rise to these fictitious oscillations. Furthermore, as the frequency increases, the differences between the actual and extrapolated values also increase. To mitigate the impact of these anomalies on the evaluations performed herein, the extrapolated propagation function data used in the evaluations were restricted to values in the frequency range from 1 MHz to 10 MHz. The results in this frequency range are reliable.

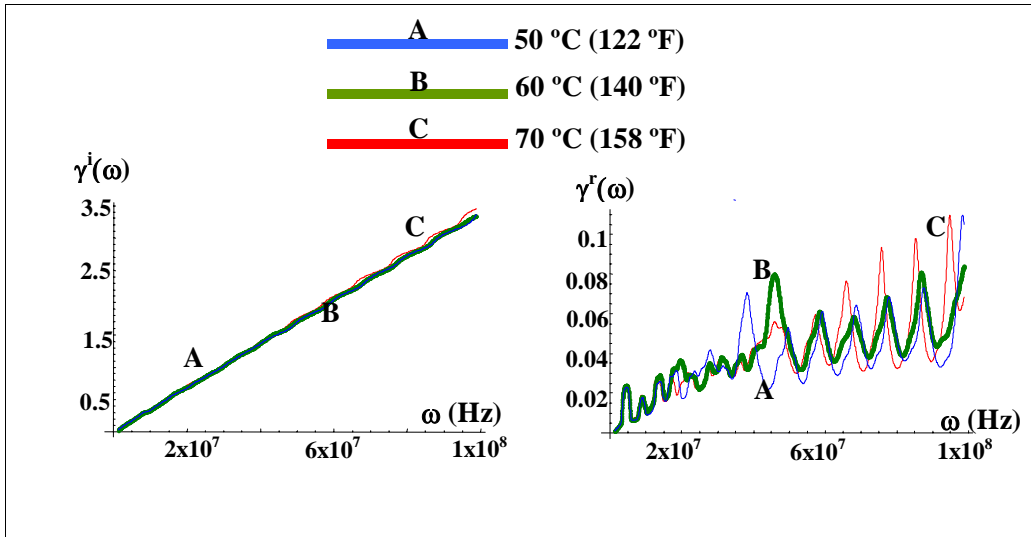


**Figure 32** Imaginary and real components of the high frequency propagation function determined from the extrapolated characteristic impedance for cables with thermal aging to simulate 60 years of service at various temperatures

### 5.1.3 Detection of Localized Degradation on Cables

In this section, the use of BIS for detecting a localized area of degradation on a cable is discussed. For purposes of this study, the localized area of degradation was simulated by exposing a small section of a cable to elevated temperature in addition to the global thermal aging applied to the cable. The cable specimens tested for this portion of the study are identified in Table 6.

First, the high frequency impedance spectra for cables with and without hot-spots are compared to demonstrate that localized damage does impact the cable’s impedance. This difference in impedance spectra can be used to detect and locate localized degradation. The data presented were obtained from BIS measurements on cables in the open configuration. Next, three tests are presented that can be used to detect localized degradation. These tests do not provide absolute values for cable properties; rather, the tests are based upon the differences between cables with and without localized degradation.

**Table 6** Specimens tested to evaluate BIS for locating localized areas of thermal aging

No.	Specimen ID	Length meters (inches)	Service Life Simulated (Global Aging)	Hot-Spot Simulated Conditions Simulated/ Location on Cable (meters from left end)
16.	PNI-79-RB-188-816	10 (393.7)	20 @ 50°C (122°F)	None
17.	PNI-79-RB-188-817	10 (393.7)	20 @ 50°C (122°F)	20 yrs. @ 60°C/8.0m to 9.0m
18.	PNI-79-RB-188-818	10 (393.7)	20 @ 50°C (122°F)	20 yrs. @ 60°C/8.0m to 8.5m
19.	PNI-79-RB-188-819	10 (393.7)	20 @ 50°C (122°F)	20 yrs. @ 70°C/8.0m to 9.0m
20.	PNI-79-RB-188-820	10 (393.7)	20 @ 50°C (122°F)	20 yrs. @ 70°C/8.0m to 8.5m
31.	PNI-79-RB-188-831	10 (393.7)	20 @ 50°C (122°F)	20 yrs. @ 90°C/8.0m to 9.0m
32.	PNI-79-RB-188-832	10 (393.7)	20 @ 50°C (122°F)	20 yrs. @ 90°C/8.0m to 9.0m
21.	PNI-79-RB-188-821	10 (393.7)	40 @ 50°C (122°F)	None
22.	PNI-79-RB-188-822	10 (393.7)	40 @ 50°C (122°F)	40 yrs. @ 60°C/1.0m to 2.0m
23.	PNI-79-RB-188-823	10 (393.7)	40 @ 50°C (122°F)	40 yrs. @ 60°C/1.5m to 2.0m
24.	PNI-79-RB-188-824	10 (393.7)	40 @ 50°C (122°F)	40 yrs. @ 70°C/1.0m to 2.0m
25.	PNI-79-RB-188-825	10 (393.7)	40 @ 50°C (122°F)	40 yrs. @ 70°C/1.5m to 2.0m
33.	PNI-79-RB-188-833	10 (393.7)	40 @ 50°C (122°F)	40 yrs. @ 90°C/1.0m to 2.0m
34.	PNI-79-RB-188-834	10 (393.7)	40 @ 50°C (122°F)	40 yrs. @ 90°C/1.5m to 2.0m
26.	PNI-79-RB-188-826	10 (393.7)	60 @ 50°C (122°F)	None
27.	PNI-79-RB-188-827	10 (393.7)	60 @ 50°C (122°F)	60 yrs. @ 60°C/7.0m to 8.0m
28.	PNI-79-RB-188-828	10 (393.7)	60 @ 50°C (122°F)	60 yrs. @ 60°C/7.0m to 7.5m
29.	PNI-79-RB-188-829	10 (393.7)	60 @ 50°C (122°F)	60 yrs. @ 70°C/7.0m to 8.0m
30.	PNI-79-RB-188-830	10 (393.7)	60 @ 50°C (122°F)	60 yrs. @ 70°C/7.0m to 7.5m
35.	PNI-79-RB-188-835	10 (393.7)	60 @ 50°C (122°F)	60 yrs. @ 90°C/7.0m to 8.0m
36.	PNI-79-RB-188-836	10 (393.7)	60 @ 50°C (122°F)	40 yrs. @ 90°C/7.0m to 7.5m

### 5.1.3.1 Comparison of Impedance Spectra With and Without Localized Degradation

In this section, the impact of localized degradation on a cable's impedance spectrum is examined. The effect of degradation severity, size, and location are evaluated.

The impact of hot-spot severity was examined by comparing cables with simulated hot-spots representing 60 years of exposure to thermal environments of 60°C and 70°C. The impedance spectra for these cables were compared to each other, and to a cable with no hot-spot. Figure 33 presents the impedance magnitude and phase spectra over the frequency range of 14MHz to 22MHz for three cables; one with no hot-spot (curve A), one with a 1-meter hot-spot representing 60 years at 60°C (curve B), and one with a 1-meter hot-spot representing 60 years at 70°C (curve C). Examination of this figure shows that the double peak structure present in the impedance magnitude spectrum for the cable with no hot-spot (curve A) disappears when a hot-spot is introduced onto the cable. Furthermore, the zero crossing of the impedance phase spectra are shifted to lower frequencies when a hot-spot is present. In this case, the increase in degradation severity from 60° (curve B) to 70°C (curve C) appears to have very little effect, as shown by the very similar impedance spectra.

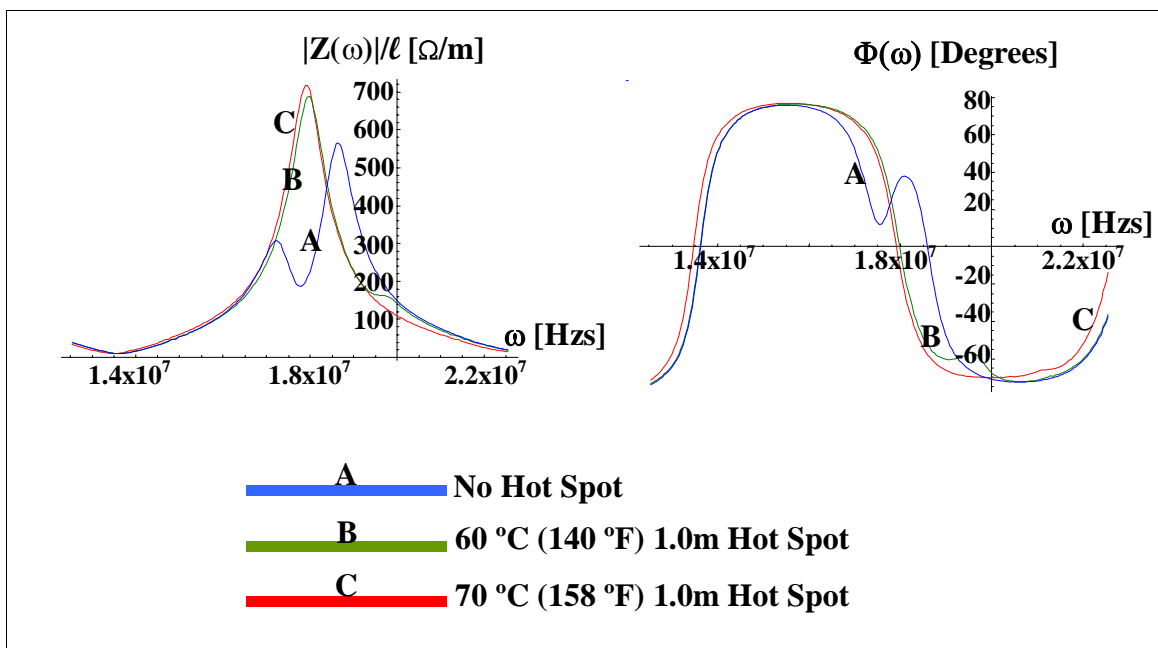


**Figure 33** Impedance magnitude and phase spectra over the frequency range of 14MHz to 22MHz for cables with global thermal aging to simulate 60 years of service at 50°C, plus additional thermal aging to simulate hot-spots of different severity

Figure 34 presents the impedance magnitude and phase spectra over the frequency range of 39MHz to 45MHz for the same three cables. As shown in this figure, a shift toward lower frequencies is noted for both the magnitude and phase spectra when a hot-spot is present. In this case, the increase in degradation severity from 60°C (curve B) to 70°C (curve C) is more pronounced with the less severe degradation resulting in an impedance spectrum that is closer to that of the baseline cable with no hot-spot (curve A). The hot-spot with more severe degradation tends to shift the impedance spectrum to lower frequencies.

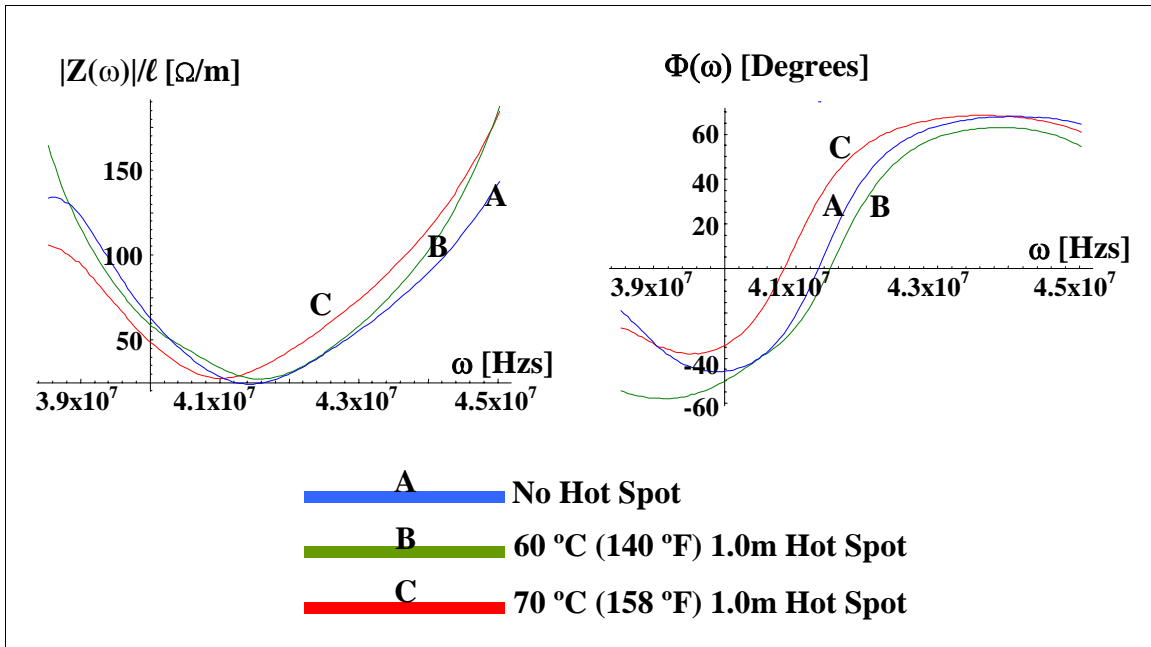


**Figure 34** Impedance magnitude and phase spectra over the frequency range of 39MHz to 45MHz for cables with global thermal aging to simulate 60 years of service at 50°C, plus additional thermal aging to simulate a hot-spot

These results demonstrate that the presence of localized degradation does impact the cable's impedance spectra. Further, the impedance spectrum appears to be sensitive to the severity of the hot-spot degradation at higher frequencies. Thus, comparison of a cables' broadband impedance spectrum to that for a cable with a known condition may be useful as an indicator of the presence and severity of a hot-spot.

The impact of hot-spot size was investigated by comparing cables with hot-spots of 0.5 meters and 1.0 meters. Again, the cables are compared to each other, as well as to a cable with no hot-spot. Figure 35 presents the impedance magnitude and phase spectra over the frequency range of 14MHz to 22MHz for three cables; one with no hot-spot (curve A), one with a 0.5-meter hot-spot representing 60 years at 70°C (curve B), and one with a 1-meter hot-spot representing 60 years at 70°C (curve C). Examination of this figure shows that the increase in degradation size from 0.5 meters (curve B) to 1.0 meters (curve C) appears to have very little effect, as shown by the very similar impedance spectra.

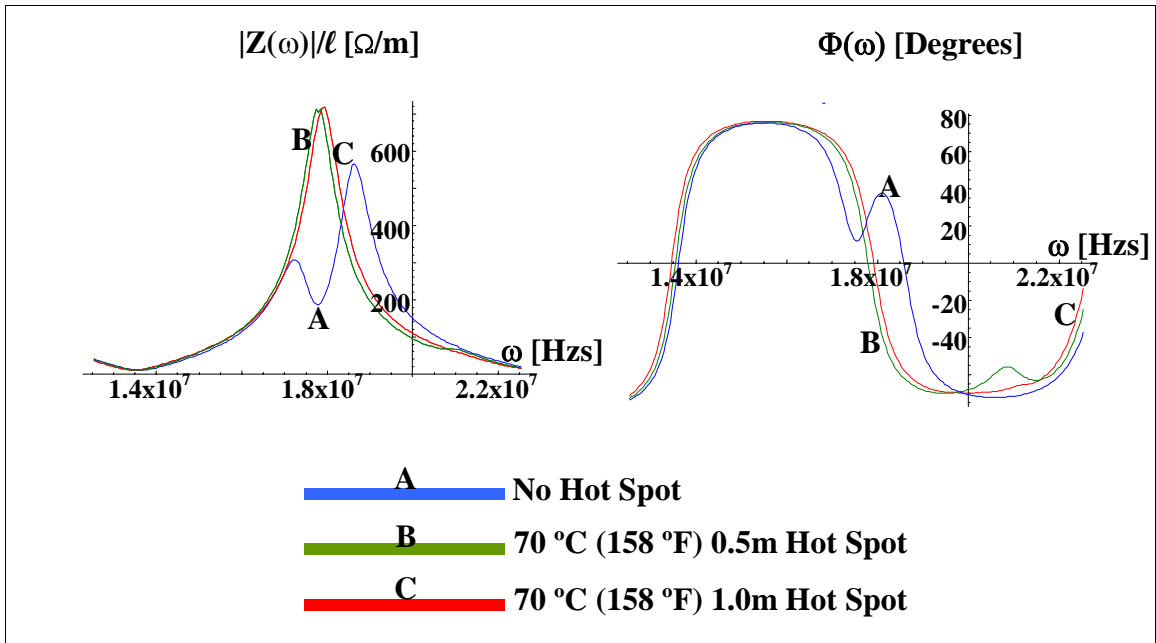


**Figure 35** Impedance magnitude and phase spectra over the frequency range from 14MHz to 22MHz for cables with global thermal aging to simulate 60 years of service at 50°C, plus additional thermal aging to simulate hot-spots of different sizes

Figure 36 presents the impedance magnitude and phase spectra over the frequency range of 39MHz to 45MHz for the same three cables. As shown in this figure, the increase in degradation size from 0.5 meters (curve B) to 1.0 meters (curve C) is more pronounced with the smaller hot-spot resulting in an impedance spectrum that is closer to that of the baseline cable with no hot-spot (curve A). The larger size hot-spot tends to shift the impedance spectrum to lower frequencies.

These results demonstrate that a cable's impedance spectrum appears to be sensitive to the size of the hot-spot at higher frequencies, as reflected by a shift to lower frequencies as the hot-spot size increases. Thus, comparison of a cables's broadband impedance spectrum to that for a cable with a known condition may be useful as an indicator of the size of a hot-spot.

Finally, the impact of hot-spot location on a cable's impedance spectrum was examined. This testing was performed using a cable with a simulated 1-meter long hot-spot representing 60 years at 70°C located from 8.0 to 9.0 meters from the left end of the cable. The cable's impedance was measured twice; once with the point of measurement (POM) at the left end of the cable, and once with the POM at the right end of the cable. This effectively yielded impedance spectra for a hot-spot located 8.0 to 9.0 meters from the POM, and for a hot-spot located 1.0 to 2.0 meters from the POM. These measurements were compared to each other, as well as to the impedance spectrum from a cable with no hot-spot.

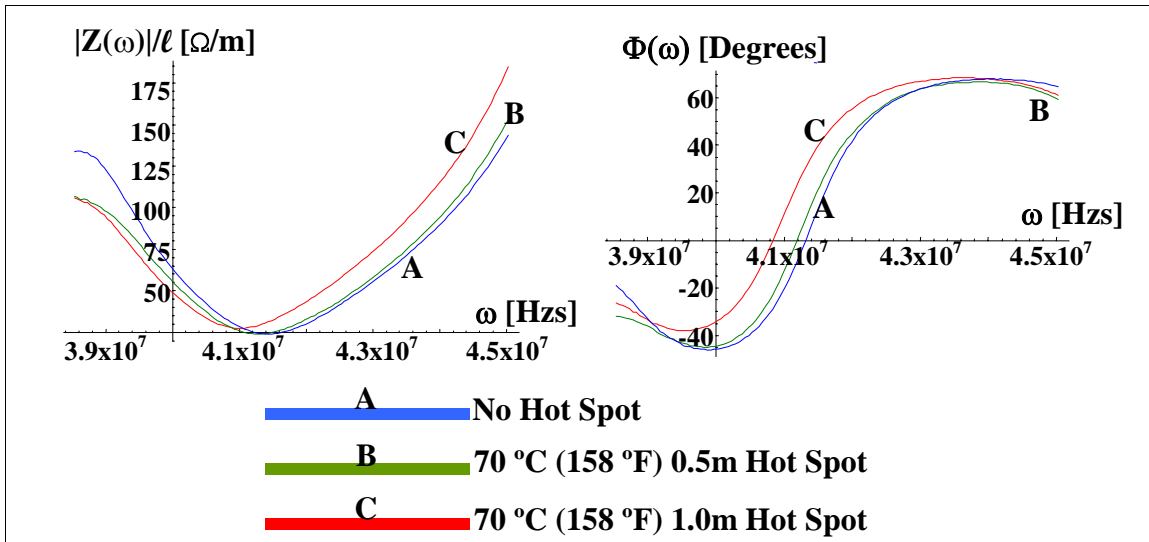
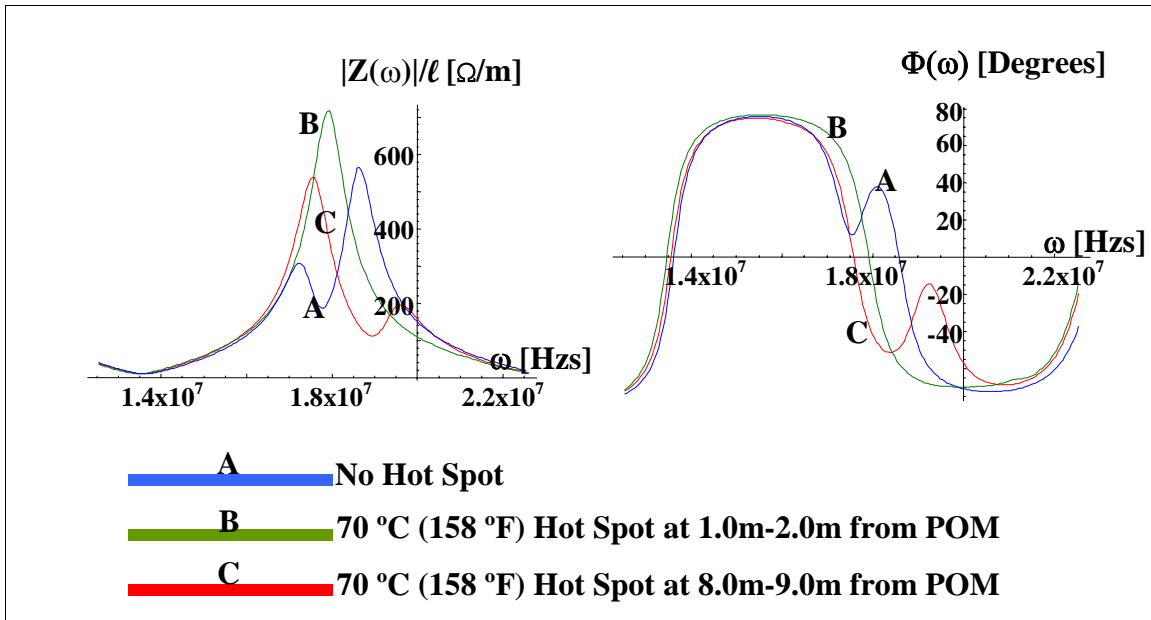


**Figure 36** Impedance magnitude and phase spectra over the frequency range of 39MHz to 45MHz for cables with global thermal aging to simulate 60 years of service at 50°C, plus additional thermal aging to simulate hot-spots of different sizes

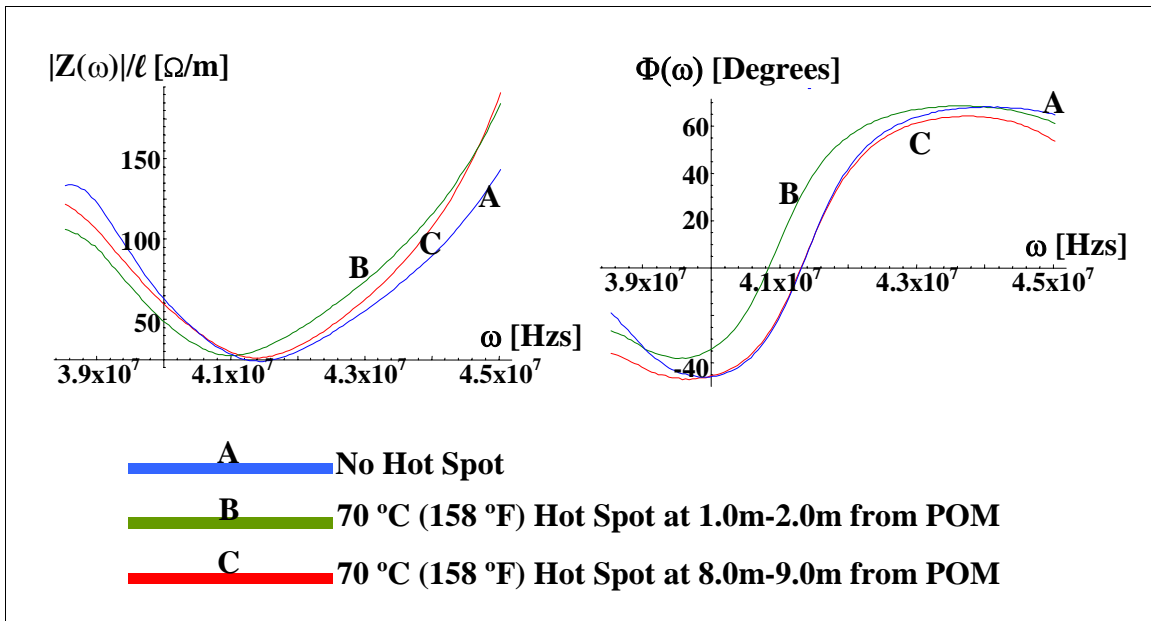
Figure 37 presents the impedance magnitude and phase spectra over the frequency range of 14MHz to 22MHz for three cases; one with no hot-spot on the cable (curve A), one with a 1.0-meter hot-spot representing 60 years at 70°C located 8.0m to 9.0 m from the POM (curve B), and one with a 1-meter hot-spot representing 60 years at 70°C located 1.0m to 2.0m from the POM (curve C). Examination of this figure shows that the location of the hot-spot does impact the impedance spectrum for the cable. With the hot-spot located close to the POM (curve B), the two peak structure observed for the cable with no hot-spot (curve A) is not present. Also, the maxima for the impedance magnitude, and the zero crossing for the impedance phase are shifted to a lower frequency. With the hot-spot farther from the POM (curve C), the two peak structure is still present; however, the impedance magnitude and phase zero crossing are also shifted to a lower frequency.

Figure 38 presents the impedance magnitude and phase spectra over the frequency range of 39MHz to 45MHz for the same three cables. As shown in this figure, a consistent trend is not readily apparent since the impedance spectra for the case in which the hot-spot is farther from the POM (curve C) is very similar to the base line cable with no hot-spot (curve A), while that for the case in which the hot-spot is close to the POM (curve B) shows a shift toward lower frequencies.

These results demonstrate that the location of a hot-spot also impacts the cable's impedance spectrum as evidenced by a shift in the spectrum to lower frequencies. The data suggest that the closer the hot-spot is to the POM, the greater is the impact on the measured impedance.



**Figure 37** Impedance magnitude and phase spectra over the frequency range from 14MHz to 22MHz for cables with global thermal aging to simulate 60 years of service at 50°C, plus additional thermal aging to simulate hot-spots at different locations



**Figure 38** Impedance magnitude and phase spectra over the frequency range from 39MHz to 45MHz for cables with global thermal aging to simulate 60 years of service at 50°C, plus additional thermal aging to simulate hot-spots at different locations

### 5.1.3.2 Numerical Tests for Detecting Localized Degradation

In this section three numerical tests that can be used to detect the presence of a hot-spot based on measured impedance spectra are presented. These tests are 1) average dissipation, 2) zero crossing location, and 3) zero crossing line spacing. Each of these tests are discussed below.

#### 5.1.3.2.1 Average Dissipation Test

As demonstrated in the previous evaluation of impedance spectra for the thermally aged cables, as the degradation on the cable increases, the cable's conductance per Hertz also increases. Therefore, cables with a higher level of degradation are expected to show more dissipation when the cable is subjected to an ac voltage. Since the presence of a hot-spot on a cable implies that some portion of the cable was degraded more than the remainder of the cable, a cable containing a hot-spot is expected to show more dissipation than a cable without a hot-spot. The phase spectrum for the cable should reflect this increased dissipation by forcing the phase spectrum further away from  $\pm 90^\circ$ . This should be the case throughout the frequency range used to probe the cable. However, since cable physics in the oscillatory region is dominated by wave phenomena, the impedance phase is not expected to decrease at every discrete frequency when a hot-spot is present on the cable. Rather, the average value of the absolute phase magnitude,  $\langle |\Phi(\omega)| \rangle$ , should exhibit the aforementioned behavior and can be used as an indicator of the presence of a hot-spot. This is defined by the following equation

$$\langle |\Phi(\omega)| \rangle \equiv \frac{\int_{\omega_1}^{\omega_2} \Phi(\omega) d\omega}{\int_{\omega_1}^{\omega_2} d\omega} \quad 5.1-7$$

In Equation 5.1-7, the integration is performed over the frequency range from  $\omega_1=1\text{MHz}$  to  $\omega_2=100\text{MHz}$  since this is the range of frequencies over which the impedance is measured.

#### 5.1.3.2.2 Phase Zero Crossing Frequency Test

Changes in the zero crossing frequencies of the impedance phase spectra are useful as indicators of cable degradation. At high frequencies, the impedance phase is a strong function of the propagation function phase since the characteristic impedance phase is essentially zero. Consequently, the frequencies at which the impedance phase zero crossings occur can be determined by the following equation:

$$\gamma^i(\omega) \approx \frac{1}{\sqrt{L(\omega) C(\omega)}} \approx \frac{n\pi}{l} \quad 5.1-8$$



From the low frequency impedance data presented previously, it was shown that the cable inductance and capacitance increase with increasing degradation of the cable. Although that data are restricted to the non-oscillatory region of the impedance spectrum, it is reasonable to assume that this behavior extends to higher frequencies. Based on this assumption, it is expected that the zero crossings of the impedance phase spectrum will exhibit a shift to lower frequencies when the spectrum for a cable containing a hot-spot is compared to that for a cable without a hot-spot.

The impedance data presented previously showed that, in some cases, the cable's impedance spectra contain a double peak structure. Also, in some cases additional zero crossings occur. To compare the various zero crossings between different spectra, it is desirable to average the spectra over a range of frequencies as follows:

$$\langle \Phi(\omega) \rangle = \frac{\int_{\omega-\Delta\omega}^{\omega+\Delta\omega} \Phi(\varpi) d\varpi}{\int_{\omega-\Delta\omega}^{\omega+\Delta\omega} d\varpi} \quad 5.1-9$$

where  $\varpi = \omega \pm \Delta\omega$ , and  $\Delta\omega = 1.30\text{MHz}$ .

#### 5.1.3.2.3 Phase Zero Crossing Line Spacing Test

In the phase zero crossing line spacing test the sum of the spacing between zero crossings is compared. The line spacing of the zero crossings is defined by the following equation:

$$\mathcal{G}_n = \frac{\sum_{n=2}^k (\omega_n - \omega_{n-1})}{\Delta\omega_{meas}} \quad 5.1-10$$

where  $n$  is the zero crossing being evaluated,  $k$  is the total number of zero crossings in the frequency interval of interest,  $\omega_n$  is the frequency of the  $n^{\text{th}}$  zero crossing, and  $\Delta\omega_{meas}$  is the frequency spacing between measured data points. For this study, measurements were taken at 2000 equally spaced data points over the frequency range from 100kHz to 100MHz; therefore,  $\Delta\omega_{meas} = (100 \times 10^6 - 0.1 \times 10^6) / 2000 = 49,950$ .

Figure 39 shows an example of the averaged impedance phase spectrum,  $\langle |\Phi(\omega)| \rangle$ , over the frequency range from 100kHz to 100MHz. Examination of this figure shows that the frequency increments between the individual zero crossings can be viewed as line spacings.

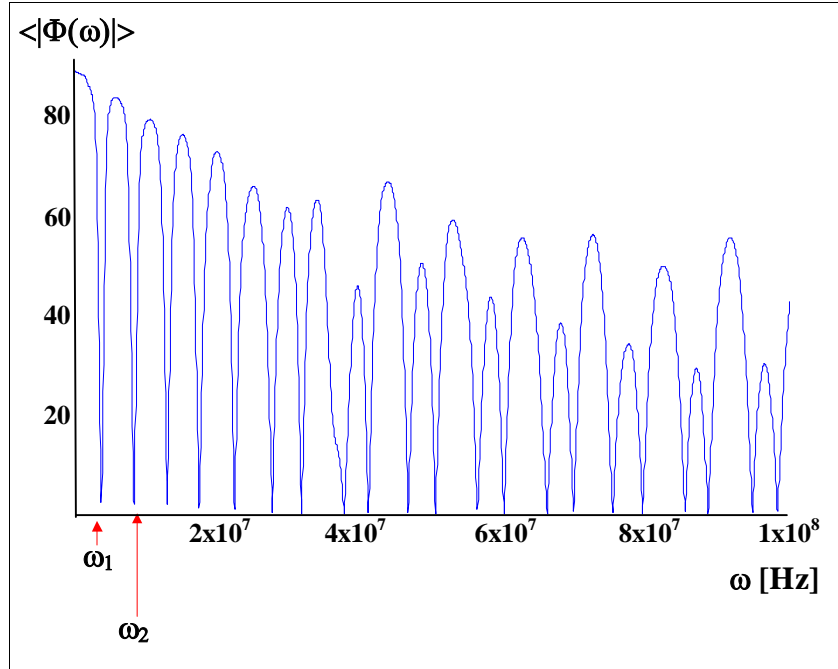


**Figure 39** Example of average impedance phase spectrum over the frequency range from 100kHz to 100MHz for cable with global thermal aging

#### 5.1.3.2.4 Results of the Numerical Tests

Each of the three tests discussed above were applied to the cable test samples to determine their effectiveness for detecting a hot-spot on a cable. Results for the cables with global thermal aging to simulate 60 years of service are discussed below. Results for the cables with thermal aging to simulate 20 years and 40 years of service are included in Appendix B.

First, the average of the phase magnitude was determined for each of the cables. Table 7 presents the results of this test, which compares the values for each of the cables aged to simulate 60 years of service, both with and without hot-spots. For this test, the frequency range was restricted and included data from 7MHz to 100MHz since data measurements below 7MHz were found to be unreliable. In the table the change in average impedance phase magnitude,  $\delta \langle |\Phi(\omega)| \rangle$ , is determined by the following equation:

$$\delta \langle \phi(\omega) \rangle = \frac{|\langle |\phi(\omega)| \rangle_B - \langle |\phi(\omega)| \rangle|}{\langle |\phi(\omega)| \rangle_B} \quad 5.1-11$$

where  $\langle |\Phi(\omega)| \rangle_B$  represents the average impedance phase magnitude for the baseline cable and  $\langle |\Phi(\omega)| \rangle$  represents the average impedance phase magnitude of the cable being tested.

Examination of Table 7 shows that 7 of the 8 cables with hot-spots had an average impedance phase magnitude lower than that for the baseline cable without a hot-spot. These results support the finding that the average dissipation of the cable decreases with increased degradation, thus suggesting that the average dissipation test may be a useful indicator for detecting hot-spots.

**Table 7** Average impedance phase magnitude for cables with global thermal aging to simulate 60 years of service at 50°C, plus additional thermal aging to simulate hot-spots

Cable	Hot-spot Temperature	Hot-spot Size	Hot-spot Location	$\langle  \phi(\omega)  \rangle$	$\delta \langle  \phi(\omega)  \rangle$
26.	None	None	None	37.0340	-
27A.	60°C (140°F)	1.0m	1.0m to 2.0m	36.7463	+ 0.78%
27B.	60°C (140°F)	1.0m	8.0m to 9.0m	36.5958	+ 1.18%
28A.	60°C (140°F)	0.5m	1.5m to 2.0m	36.1382	+ 2.42%
28B.	60°C (140°F)	0.5m	8.5m to 9.0m	35.6967	+ 3.61%
29A.	70°C (158°F)	1.0m	1.0m to 2.0m	36.7463	+ 0.78%
29B.	70°C (158°F)	1.0m	8.0m to 9.0m	35.5958	+ 3.88%
30A.	70°C (158°F)	0.5m	1.5m to 2.0m	36.8930	+ 0.38%
30B.	70°C (158°F)	0.5m	8.5m to 9.0m	37.2820	- 0.67%

Next, the zero crossing frequencies are compared between the baseline cable with no hot-spot (cable 26) and each of the cables with a hot-spot (cables 27 to 30). To make this comparison, a matrix of zero crossing frequency differences is created using the following relationship:

$$\Delta\omega_{zc,n,x} = \frac{\omega_{zc,n,26} - \omega_{zc,n,x}}{\Delta\omega_{meas}} \quad 5.1-12$$

where  $\omega_{zc,n,26}$  is the zero crossing frequency for the  $n^{\text{th}}$  impedance phase zero crossing for cable 26 (baseline),  $\omega_{zc,n,x}$  is the zero crossing frequency for the  $n^{\text{th}}$  impedance phase zero crossing for cable  $x$  ( $x = 27, 28$ , etc. for cables with hot-spots), and  $\Delta\omega_{meas}$  is the frequency spacing between measured data points, which for this study is 49,950Hz, as discussed previously. Positive

differences would indicate a downshift in frequency for the zero crossing for the cables with hot-spots. The results are presented in Table 8.

**Table 8** Differences in zero crossing frequencies between cable with no hot-spot (cable 26) and cables with hot-spots (cables 27 to 30) at odd number zero crossings

Cable	Frequency Difference for Zero Crossing No.										
	1	3	5	7	9	11	13	15	17	19	21
27A	0	0	0	+ 2	- 4	- 4	- 2	- 2	- 7	+ 4	0
27B	+ 1	+ 1	+ 1	0	- 2	- 2	+ 1	+ 1	0	- 7	+ 10
28A	+ 1	+ 4	+ 7	+ 4	0	+ 3	+ 2	+ 6	+ 4	+ 10	+ 20
28B	+ 1	0	+ 1	+ 5	- 1	0	+ 2	+ 1	- 2	0	+ 12
29A	0	0	0	+ 2	- 4	- 4	- 2	- 2	- 7	+ 4	0
29B	+ 1	+ 1	+ 1	0	- 2	- 1	+ 1	+ 1	0	- 7	+ 10
30A	+ 1	+ 2	+ 3	+ 6	+ 2	+ 1	+ 7	+ 5	+ 7	+ 1	+ 19
30B	+ 2	+ 3	+ 6	+ 5	+ 7	+ 7	+ 8	+ 11	+ 4	+ 22	+ 25

Examination of Table 8 shows that there is no clear trend in the zero crossing frequencies. For zero crossings 1, 3, 5, and 7 on the cables with hot-spots, each is either the same or downshifted to a lower frequency relative to the baseline cable. For the higher zero crossings the results are mixed with some showing a downshift and others showing a shift toward higher frequencies. These results suggest that this test may not be effective at detecting hot-spots.

Finally, the phase zero crossing line spacing test is applied to the cables with global thermal aging to simulate 60 years of service. Again, each cable with a hot-spot is compared to the baseline cable without a hot-spot. The results are presented in Table 9.

Examination of Table 9 shows that the line spacing for most of the cables with hot-spots is smaller (positive change) than that for the baseline cable. These results support the finding that the zero crossings occur closer together for cables with hot-spots. Therefore, the line spacing test may be a useful indicator of the presence of hot-spots on cables.

**Table 9** Impedance phase zero crossing line spacing for cables with global thermal aging to simulate 60 years of service, with and without hot-spots

<b>Cable</b>	<b>Line Spacing</b>	<b>Percent Change from Baseline Cable</b>
26 (Baseline)	93.60	-
27A	93.60	0
27B	93.15	+ 0.48%
28A	92.65	+ 1.01%
28B	93.05	+ 0.59%
29A	93.60	0
29B	93.15	+ 0.48%
30A	92.70	+ 0.96%
30B	92.45	+ 1.23%

#### 5.1.4 Locating Localized Degradation on Cables

This section presents the results of research on the use of BIS to locate localized areas of degradation, or hot-spots, on a cable. The cables shown in Table 6 were also used for this portion of the research. First, the theory behind hot-spot location is discussed. Subsequently, results from the application of this theory are presented.

##### 5.1.4.1 Theory Behind Hot-spot Location in Thermally Aged Cables

The formation of a hot-spot in a thermally aged cable occurs when a segment of the cable is exposed to higher temperatures than the other portions of the cable. This could occur, for example, if the cable is routed near a hot steam line in the plant. Figure 40 presents a schematic depicting a model for a two-conductor cable with a hot-spot. In this figure, “H” represents the healthy portion of the cable exposed to normal operating conditions, and “D” represents the damaged portion of the cable exposed to elevated temperature conditions (i.e., hot-spot). The total length of the cable is denoted by  $\ell$ , and the length of the hot-spot is indicated by  $\ell_a$  to  $\ell_b$ . The cable has a frequency dependent voltage applied to the two conductors represented by  $V(\omega)$ .

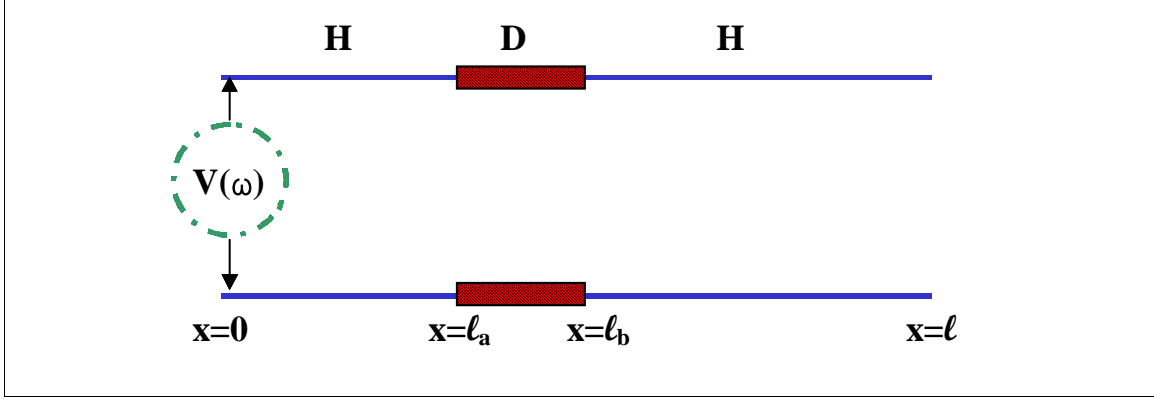


**Figure 40** Schematic model of a cable with a hot-spot

In Section 5.1, it was shown that aging degradation will alter the cable's electrical properties. Furthermore, the cable's characteristic impedance and propagation function depend upon the severity of the degradation. To model this dependence, the following equation can be used:

$$Z_{MODEL}(\omega) = Z_{0,H}(\omega) \left\{ \frac{Z_{0,H}(\omega) \coth[\gamma_H(l - l_a)] + Z_{0,D}(\omega) \coth[\gamma_D(l_b - l_a)]}{Z_{0,D}(\omega) + Z_{0,H}(\omega) \coth[\gamma_H(l - l_b)] \tanh[\gamma_D(l_b - l_a)]} \right\} \quad 5.1-13$$

where  $Z_{0,H}(\omega)$  and  $\gamma_H(\omega)$  represent the cable's characteristic impedance and propagation function in the healthy portion of the cable, and  $Z_{0,D}(\omega)$  and  $\gamma_D(\omega)$  represent the cable's characteristic impedance and propagation function in the damaged (hot-spot) portion of the cable.

In Section 5.1.2 of this report, models for the thermally aged cables were developed that can be used to approximate the cable's actual electrical properties. Specifically, models were developed based on low frequency impedance data and were extrapolated to high frequencies. Equation 5.1-1 was then used to obtain the cable's high frequency propagation function. Although the model has the correct cable impedance, since it is built into the model, the extrapolated characteristic impedance is an approximation of the real function; therefore, the propagation function is also an approximation of the real function. To minimize the introduction of modeling error into the evaluation, the modeling is limited to the frequency range from 1MHz to 10MHz. This is sufficient since the first three or four zero crossings of the impedance phase occur within this frequency range.

The most direct method of determining a hot-spot location would be to invert equation 5.1-13 and solve for  $l_a$  and  $l_b$ . However, inverting the equation yields a transcendental equation that includes  $l_a$  and  $l_b$  in a non-linear way. An easier method of locating a hot-spot is to calculate the cable's impedance using equation 5.1-13 based on assumed values of  $l_a$  and  $l_b$  and compare the result to the measured impedance. Based on the root mean square (rms) error between the value predicted by the model and the measured value, new values of  $l_a$  and  $l_b$  are chosen and the process is repeated. The final hot-spot location is determined by minimizing the rms error.

The following process is used to determine a hot-spot location:

1. Measure the cable impedance
2. Calculate the cable impedance using equation 5.1-13 using an assumed hot-spot location
3. Compare the impedance predicted by the model with the measured value and calculate a rms error
4. Based on the rms error, assume a new hot-spot location and repeat steps 2 and 3.
5. Repeat steps 2 through 4 until the rms error is minimized

In comparing the modeled impedance to the measured impedance, four different parameters are calculated. These are defined by the following equations:

$$\langle \delta\phi(\omega) \rangle \equiv \sum_{\omega_n=1\text{ MHz}}^{\omega_n=10\text{ MHz}} \frac{|\phi_{MODEL}(\omega_n) - \phi_{MEASURED}(\omega_n)|}{|\phi_{MEASURED}(\omega_n)|} \quad 5.1-14$$

$$\langle \delta|Z(\omega)| \rangle \equiv \sum_{\omega_n=1\text{ MHz}}^{\omega_n=10\text{ MHz}} \frac{|Z_{MODEL}(\omega_n) - Z_{MEASURED}(\omega_n)|}{|Z_{MEASURED}(\omega_n)|} \quad 5.1-15$$

$$\langle \delta\Theta(\omega) \rangle \equiv \sqrt{\langle \delta\phi(\omega) \rangle^2 + \langle |Z(\omega)| \rangle^2} \quad 5.1-16$$

$$\langle \delta\Omega \rangle \equiv \sum_{\omega_n=1\text{ MHz}}^{\omega_n=10\text{ MHz}} \frac{|v_{n,MODEL} - v_{n,MEASURED}|}{|v_{n,MEASURED}|} \quad 5.1-17$$

where  $\phi_{MODEL}(\omega)$  and  $\phi_{MEASURED}(\omega)$  are the predicted and measured values of the cable impedance phase,  $Z_{MODEL}(\omega)$  and  $Z_{MEASURED}(\omega)$  are the predicted and measured cable impedance magnitude, and  $v_{n,MODEL}$  and  $v_{n,MEASURED}$  are the predicted and measured frequency of the  $n^{\text{th}}$  impedance phase zero crossing, and  $\Theta$  and  $\Omega$  are parameters developed specifically to represent the model accuracy.

The relationships defined by equations 5.1-14 to 5.1-17 are referred to as the “error functions” since they represent the error between the cable’s properties predicted by the model to the actual measured value. Each of the error functions is evaluated in making a determination as to the correct location of a hot-spot.

The process for locating a hot-spot is demonstrated below for cable 29. This cable has a 1 meter

hot-spot representing 60 years of service at 70°C (158°F). The hot-spot is located 7.0 to 8.0 meters from the left end of the cable. In this demonstration, the cable impedance point of measurement is first taken at the left end of the cable (29A), then at the right end of the cable (29B). Thus, one cable is used to demonstrate two hot-spot locations; namely, 7.0 to 8.0 meters from the POM and 2.0 to 3.0 meters from the POM. In each case, a hot-spot location is assumed and the error functions are calculated. The results are plotted as a function of length along the cable to facilitate the identification of maxima and minima.

Figures 41 presents the results of the impedance phase error function calculations,  $\langle \delta\Phi(\omega) \rangle$ , and impedance magnitude,  $\langle \delta|Z(\omega)| \rangle$ , for cable 29A as a function of distance along the cable. Examination of this figure shows that the impedance phase error has an absolute minimum at 6.0 meters, while the impedance magnitude also has an absolute minimum at 6.0 meters. These minima are relatively close to the actual hot-spot location of 7.0 to 8.0 meters from the POM.

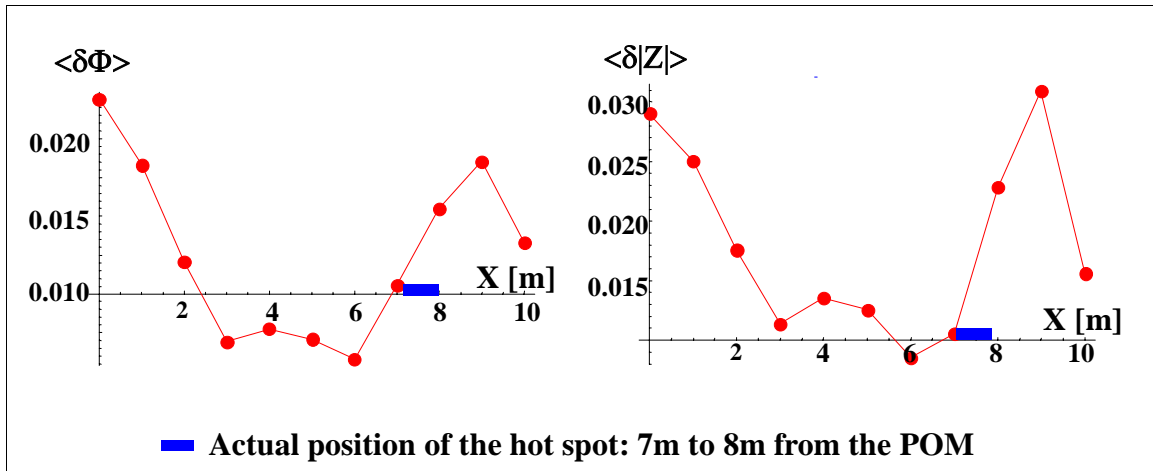


**Figure 41** Impedance phase and magnitude error functions for cable with thermal aging to simulate a 1 meter hot-spot located 7.0 to 8.0 meters from the cable end representing 60 years of service at 70°C

Figures 42 presents the results of the error function calculations,  $\langle \delta\Theta(\omega) \rangle$ , and zero crossing frequency change,  $\langle \delta\Omega \rangle$ , for cable 29A as a function of distance along the cable. Examination of this figure shows that  $\langle \delta\Theta(\omega) \rangle$  has an absolute minimum at 6.0 meters, while the zero crossing frequency change,  $\langle \delta\Omega \rangle$ , has an absolute minimum at 5.0 to 7.0 meters. Again, these minima are relatively close to the actual hot-spot location of 7.0 to 8.0 meters from the POM.



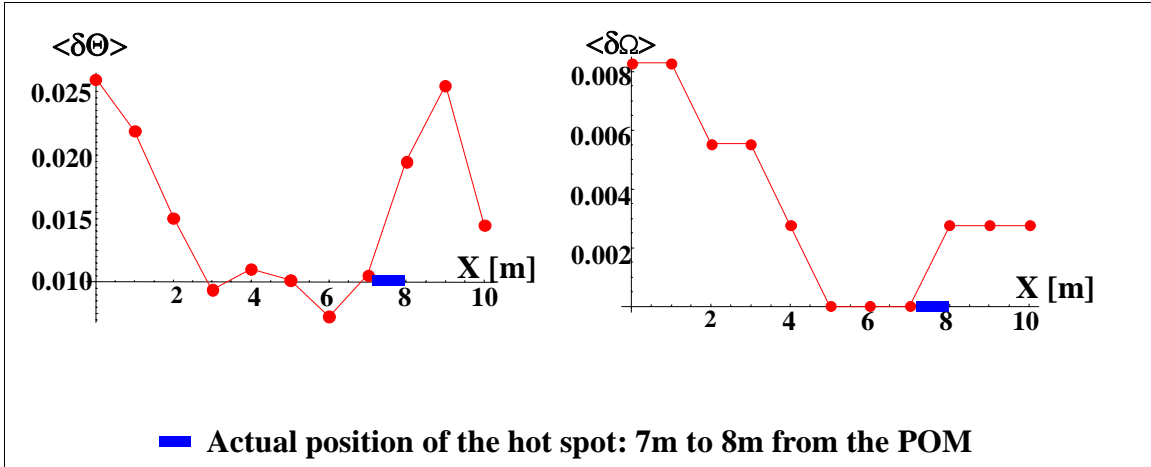


**Figure 42** Impedance phase zero crossing error functions for cable with thermal aging to simulate a 1.0 meter hot-spot located 7.0 to 8.0 from the cable end representing 60 years of service at 70°C

From an evaluation of the four error functions obtained for this cable, a hot-spot location of 5.0 to 7.0 meters from the POM would be predicted. This is in excellent agreement with the actual hot-spot location of 7.0 to 8.0 meters from the POM.

Figures 43 presents the results of the impedance phase error function calculations,  $\langle \delta\Phi(\omega) \rangle$ , and impedance magnitude,  $\langle \delta|Z(\omega)| \rangle$ , for cable 29B as a function of distance along the cable. Examination of this figure shows that the impedance phase error has an absolute minimum at 4.0 meters, while the impedance magnitude has an absolute minimum at 3.0 meters. These minima are relatively close to the actual hot-spot location of 2.0 to 3.0 meters from the POM.

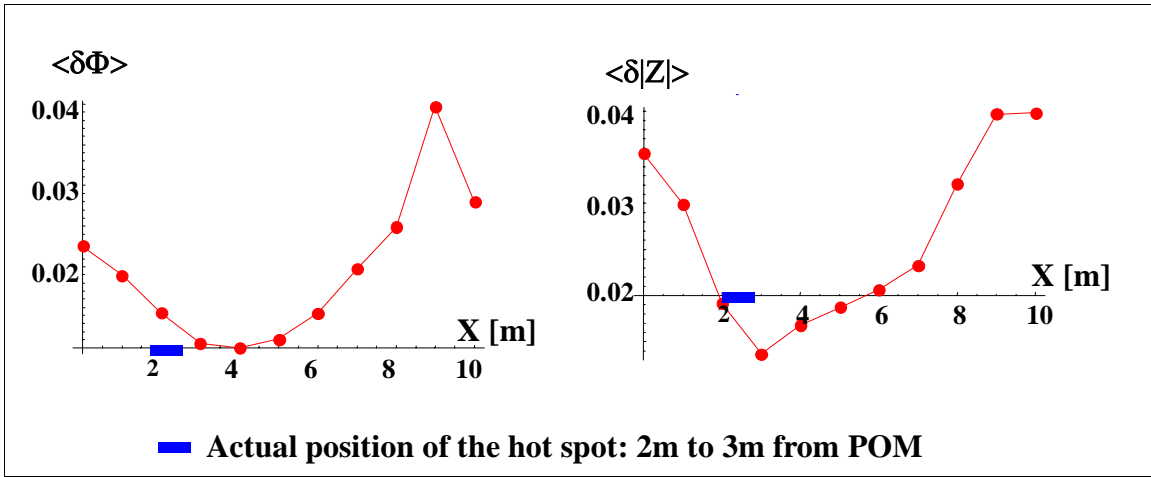


**Figure 43** Impedance phase and magnitude error functions for cable with thermal aging to simulate a 1 meter hot-spot 2.0 to 3.0 meters from the end of the cable representing 60 years of service at 70°C

Figure 44 presents the results of the error function calculations,  $\langle \delta\Theta(\omega) \rangle$ , and zero crossing frequency change,  $\langle \delta\Omega \rangle$ , for cable 29B as a function of distance along the cable. Examination of this figure shows that  $\langle \delta\Theta(\omega) \rangle$  has an absolute minimum at 3.0 meters, while the zero crossing frequency change,  $\langle \delta\Omega \rangle$ , has an absolute minimum at 2.0 meters. Again, these minima are relatively close to the actual hot-spot location of 2.0 to 3.0 meters from the POM. It is also noted that  $\langle \delta\Omega \rangle$  has a second minima at 7.0 meters; however, based on the other error function minima, this one is seen to be inconsistent and can be eliminated.

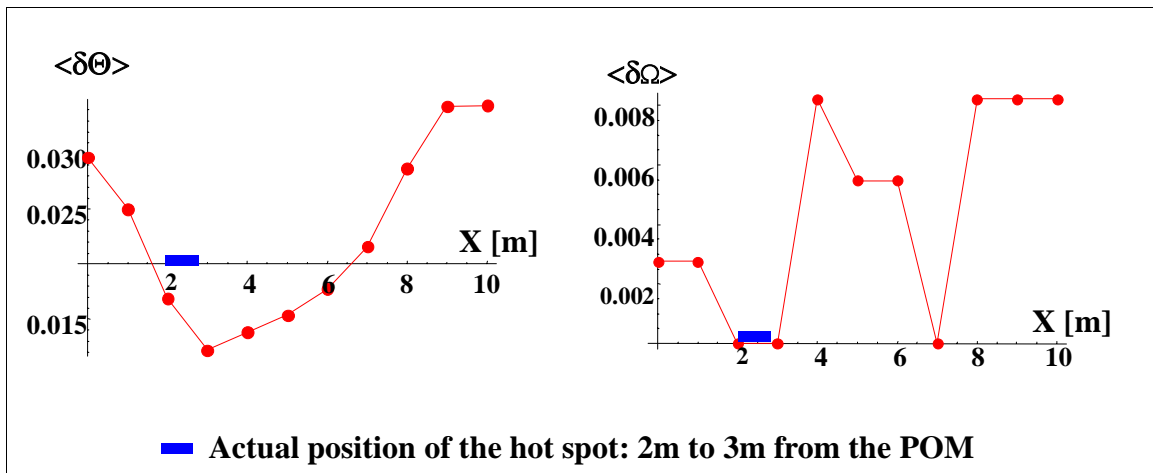


**Figure 44** Impedance phase zero crossing error functions for cable with thermal aging to simulate a 1 meter hot-spot located 2.0 to 3.0 meters from the end representing 60 years of service at 70°C

From an evaluation of the four error functions obtained for this cable, a hot-spot location of 2.0 to 4.0 meters from the POM would be predicted. Again, excellent agreement with the actual hot-spot location of 2.0 to 3.0 meters from the POM is obtained. Additional examples of hot-spot location are included in Appendix B.

## 5.2 Application of BIS to Cables with Attached Loads

When cables are monitored in a nuclear power plant environment it is very likely that they will be connected to a piece of equipment. Rather than disconnect the cable from the equipment, it would be desirable to monitor the cable as installed. To determine the impact of attached loads on the BIS method, tests were performed with a load attached to the test cables to determine if degradation can be detected and located without disconnecting the cable. The results are reported in this section.

### 5.2.1 Test Specimens Used for Testing with Attached Loads

For this portion of the research the cable test specimens presented in Table 10 were used.

**Table 10** Specimens tested to evaluate BIS for testing cables with attached loads

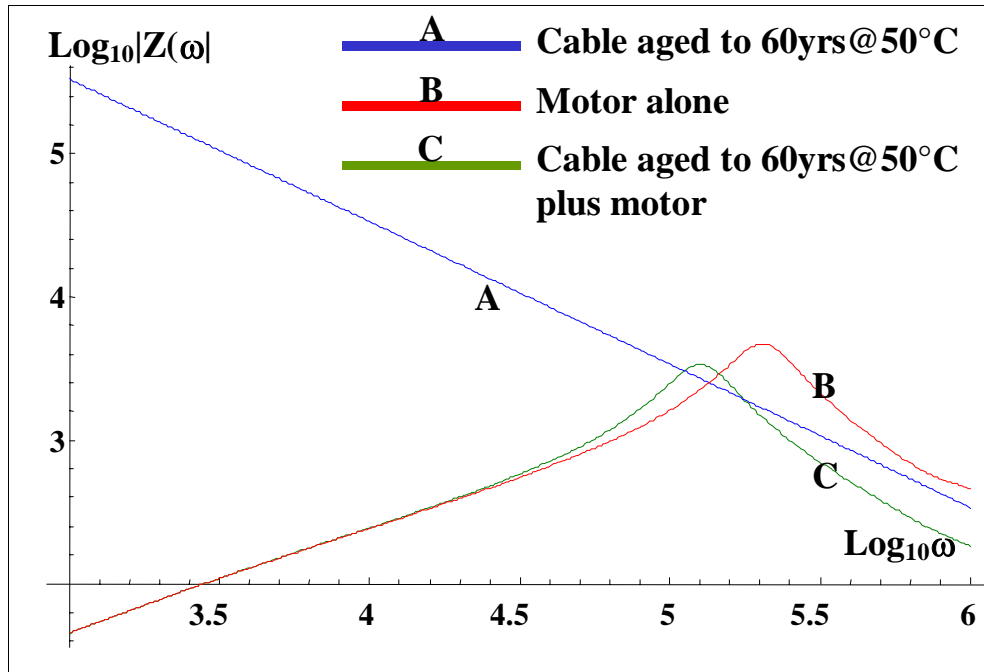
No.	Specimen ID	Length meters (inches)	Service Life Simulated	Hot-Spot Simulated
26.	PNI-79-RB-188-826	10 (393.7)	60yrs. @ 50°C	None
27.	PNI-79-RB-188-827	10 (393.7)	60yrs. @ 50°C	60yrs. @ 60°C
29.	PNI-79-RB-188-829	10 (393.7)	60yrs. @ 50°C	60yrs. @ 70°C

Two different loads were used for these tests; 1) a small induction motor, and 2) a solenoid coil. Both loads have very broad impedance spectra and produced very similar results. Therefore, most of the testing was focused on the motor and those results are reported herein. The results apply equally well to the coil or any load that has a capacitance and inductance in parallel. The combination of test cable with load attached is referred to as the “cable system” in the following discussion.

### 5.2.2 Low Frequency BIS Tests for Cables with Attached Loads

Impedance measurements were made on the cables alone in the open circuit configuration, and with the load attached to determine their frequency response. The load used was a 1 Hp, 3-phase ac induction motor. Figure 45 compares the low frequency impedance magnitudes for the cable specimen with no hot-spot (Specimen 26), the load, and the cable system (cable connected to the load). As shown, the impedance magnitude of the motor is less than that of the cable for frequencies less than the crossing frequency,  $\omega_c$ , which is the point at which the impedance curves cross (approximately 126kHz). As a result, most of the current will flow through the motor and not through the cable’s capacitance. As the cable’s length increases, the crossing frequency decreases.

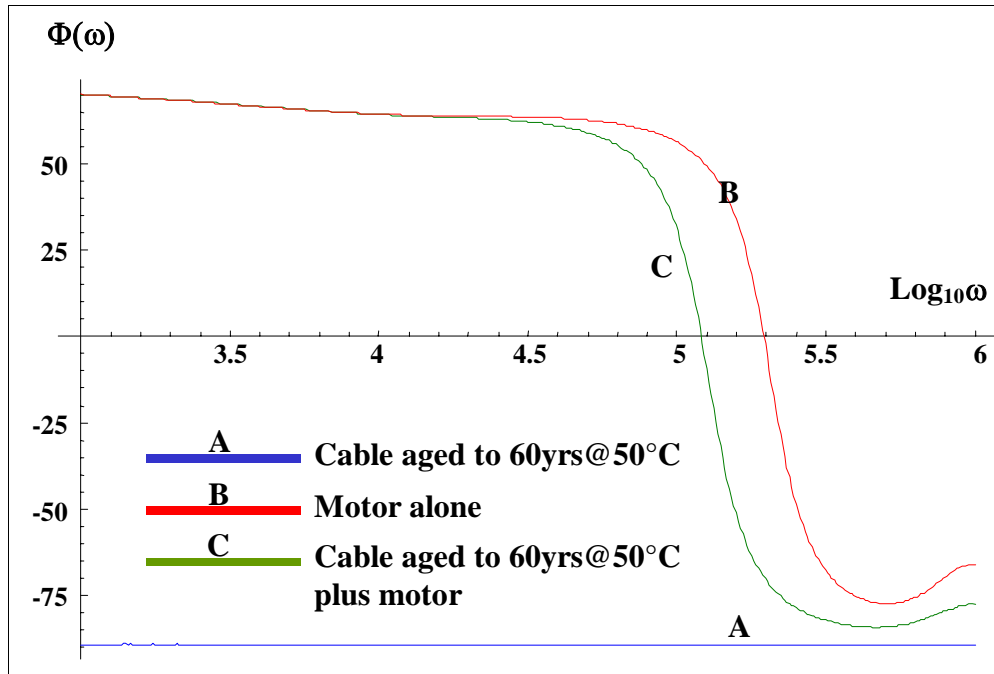
Figure 45 also shows that as the frequency increases, the magnitude of the cable’s impedance continues to decrease as  $1/\omega$ , whereas the cable system’s impedance magnitude decreases as  $1/(\omega - \omega_c)^2$ . Once the load’s impedance is greater than the cable’s impedance, less current flows through the motor and more flows through the cable’s capacitance. As a result, the cable system’s impedance will be dominated by the physics of the cable.



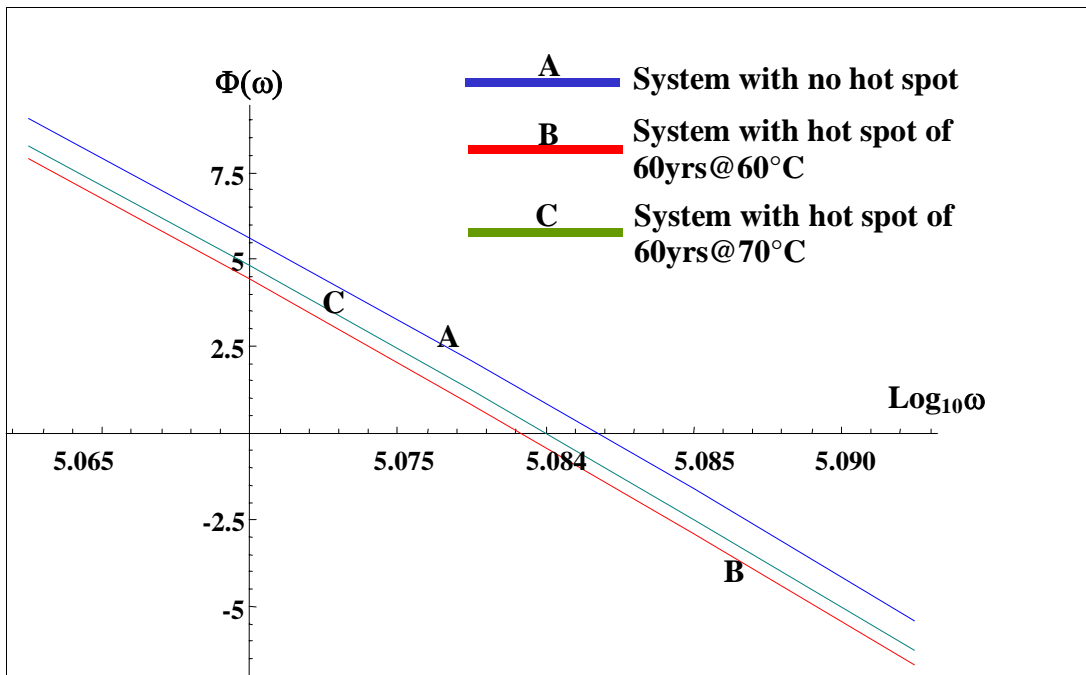
**Figure 45** Comparison of measured impedance magnitude for cable with and without an attached load

Figure 46 compares the impedance phase spectra for the cable, load, and cable system. As shown, the motor's impedance phase is nearly 90 degrees at 100Hz and gradually decreases until 100kHz, at which point it drops below 0 degrees. This behavior implies that the motor can be viewed as a simple L-C circuit with the inductance and capacitance in parallel. It is noted that the motor's impedance phase has a zero crossing at 200kHz and that the cable system itself has a zero crossing at 120kHz. Thus, at low frequencies the cable system's impedance is heavily dominated by the motor. However, the zero crossing of the impedance phase does react to the presence of a hot-spot.

Figure 47 compares the impedance phase spectra of a cable system consisting of an aged cable without a hot-spot connected to a load to that of a system consisting of an aged cable with a hot-spot connected to a load. The severity of the hot-spot is varied. As shown, the presence of a hot-spot does affect the system's impedance in the region of the zero crossing, although the effect is small. Specifically, the hot-spot decreases the frequency at which the cable system's impedance phase has a zero crossing. The more severe the hot-spot, the greater the downshift in zero crossing frequency.



**Figure 46** Comparison of the impedance phase spectra for cables with and without a load attached



**Figure 47** Comparison of impedance phase in the frequency range from 116kHz to 123kHz for cables with and without a load attached

Figure 48 presents the difference in the impedance phase between the cable system with the hot-spot and the cable system without the hot-spot. As shown, the differences are localized to the vicinity of the impedance phase zero crossing. Also, as the severity of the hot-spot increases, the difference also increases. Therefore, an accurate model of the cable system impedance can be used to examine the behavior of the impedance phase in the vicinity of the low frequency zero crossings and this can be used as an indicator for the presence of a hot-spot on the cable's insulation.

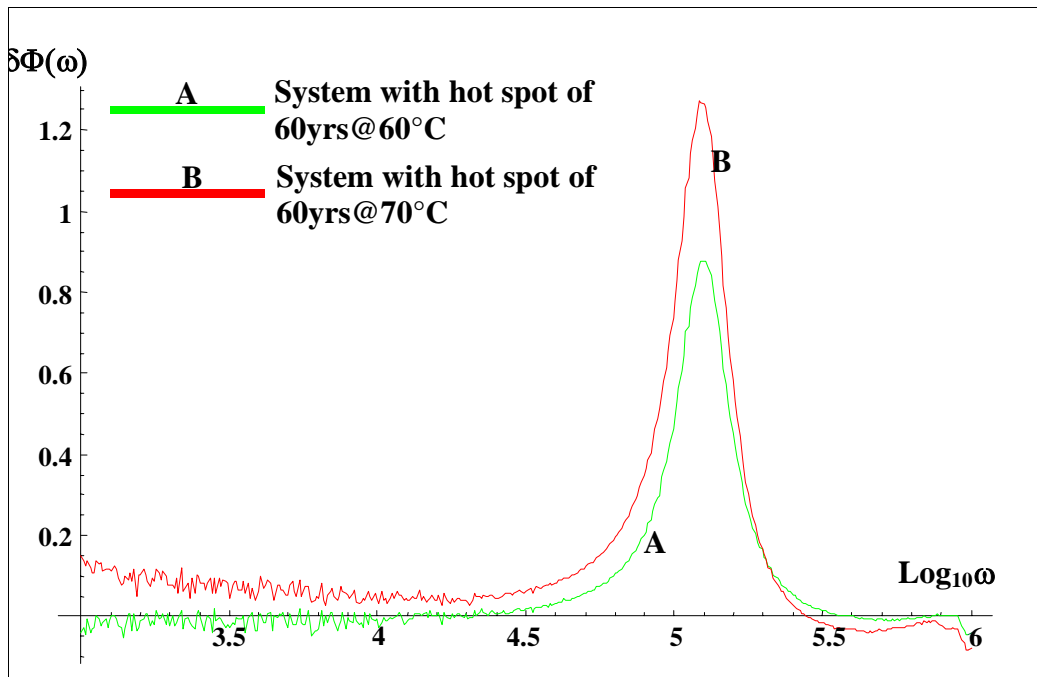


**Figure 48** Change in impedance phase for cable system with a hot-spot from cable system without a hot-spot

### 5.2.3 High Frequency BIS Tests for Cables with Attached Loads

In evaluating the high frequency BIS measurements, the frequency averaged second derivative of the impedance phase spectra was found to provide useful information for detecting hot-spots on a cable connected to a load. Specifically, the zero crossings of this parameter were found to be downshifted when the cable's insulation contains a hot-spot.

The second derivative of the impedance phase,  $\Pi(\omega)$ , is developed as follows. At each frequency  $\omega_n$  at which a measurement is taken,  $\Phi(\omega_n)$  is the measured impedance phase. This phase value is averaged over a frequency range of  $\omega_n \pm n_0$ , where  $n_0 = 0.749625\text{MHz}$  (15 frequency steps) for this parameter. This averaged impedance phase is represented by the following equation:

$$\langle \Phi(\omega_n) \rangle = \frac{\sum_{m=-n_0}^{m=n_0} \Phi(\omega_{n+m})}{2 n_0} \quad 5.2-1$$

The second derivative of the impedance phase can then be developed as follows:

$$\langle \Omega(\omega_n) \rangle = \langle \Phi(\omega_{n+10}) \rangle - 2 \langle \Phi(\omega_n) \rangle + \langle \Phi(\omega_{n-10}) \rangle \quad 5.2-2$$

This is then averaged over a frequency range of  $\omega_n \pm s_0$ , where  $s_0 = 1.22429\text{MHz}$  (25 frequency steps) for this parameter to form the second derivative parameter as follows:

$$\Pi(\omega_n) = \frac{\sum_{m=-s_0}^{m=s_0} \langle \Omega(\omega_{n+m}) \rangle}{2 s_0} \quad 5.2-3$$

The parameter  $\Pi(\omega)$  is the second derivative in frequency of the cable's phase impedance. It is observed that attached loads downshift the zero crossings of  $\Pi(\omega)$ . These zero crossings are referred to herein as the "Detection Zero Crossings" (DZC). For a 10 meter cable, there are 14 DZCs between 1MHz and 100MHz.

The  $\Pi(\omega)$  parameter was compared for the cable systems with and without a hot-spot. An examination of the  $\Pi(\omega)$  spectra showed that a frequency downshift occurs at all of the 14 DZCs when a hot-spot is present on the cable. Figure 49 presents an example in which the  $\Pi(\omega)$  parameter is compared for the cable systems with and without a hot-spot in the vicinity of the first DZC, which occurs at 11.4MHz. It is observed that a frequency downshift occurs when the hot-spot is present. Similar results were found for the remaining DZCs.

Figure 49 also shows that the location of the hot-spot relative to the point of measurement also affects the zero crossing frequency. As shown, the farther the hot-spot is from the POM, the greater the downshift in frequency of the zero crossing. Thus, in principle, a cable system's impedance phase spectra are sensitive to the location of the hot-spot.

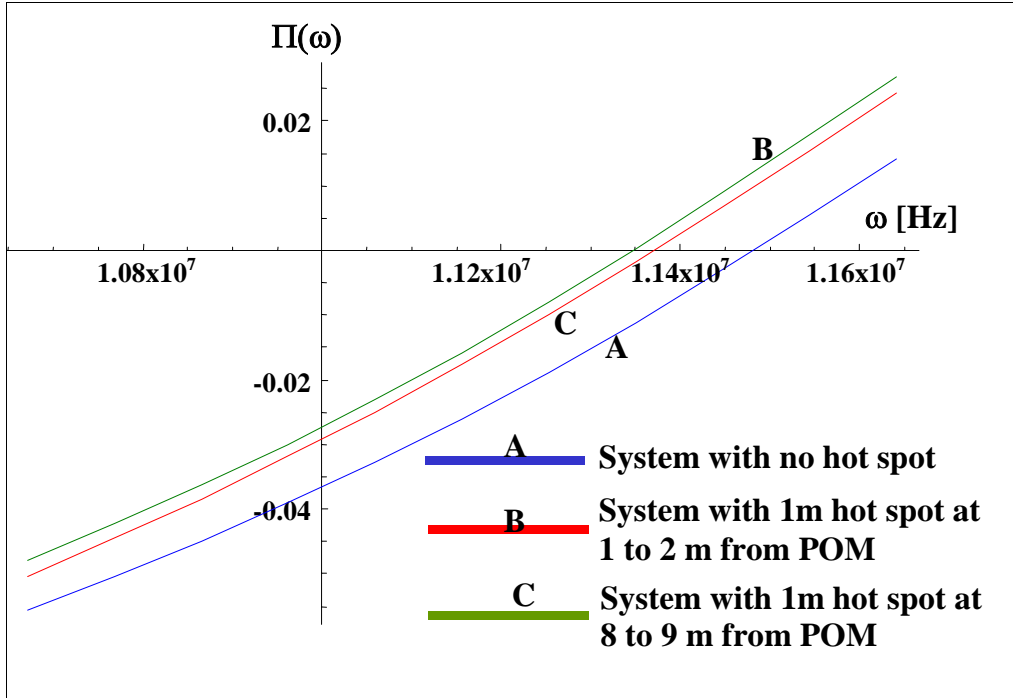


**Figure 49** Comparison of  $\Pi(\omega)$  parameter in the vicinity of the first zero crossing for cable systems with and without a hot-spot

#### 5.2.4 Phenomenological Models of Cables with Attached Loads

In this section a model for predicting the properties of a thermally aged cable with an attached load is developed. The model is based on the phenomenological approach and, therefore, is valid in the frequency range from 10Hz to 1MHz. Models are developed for the following two cases:

- Thermally aged cable with no hot-spots and a load attached
- Thermally aged cable with a 1 meter hot-spot and a load attached

The first scenario modeled is shown schematically in Figure 50. The cable is 10 meters long and has been thermally aged to simulate 60 years of service at 50°C (specimen 26). No hot-spots are present on the cable, and a load is attached to the far end of the cable, represented by an impedance,  $Z_L(\omega)$ . The cable system's impedance,  $Z_{\text{model}}(\omega)$ , is given by the following equation:

$$Z_{\text{Model}}(\omega) = Z_0(\omega) \frac{Z_L(\omega) + Z_0(\omega) \tanh[\gamma(\omega)l]}{Z_0(\omega) + Z_L(\omega) \tanh[\gamma(\omega)l]} \quad 5.2-4$$



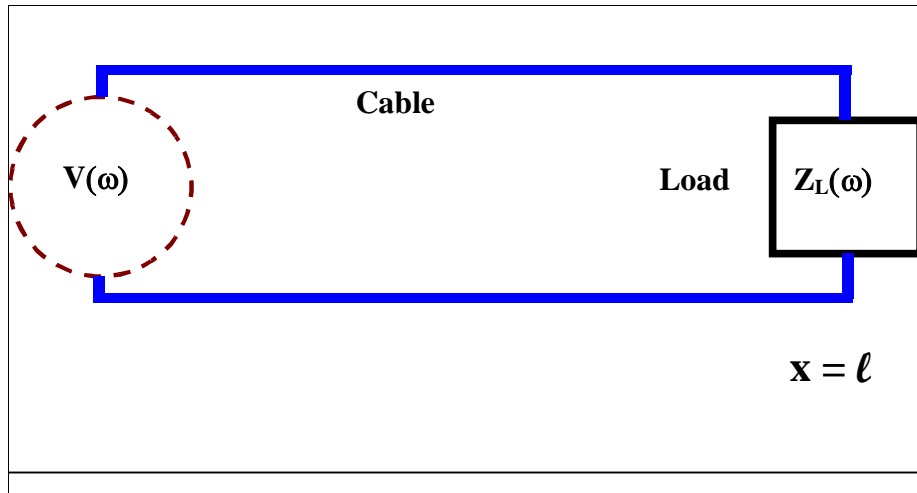


**Figure 50** Schematic of model for thermally aged cable with a load attached

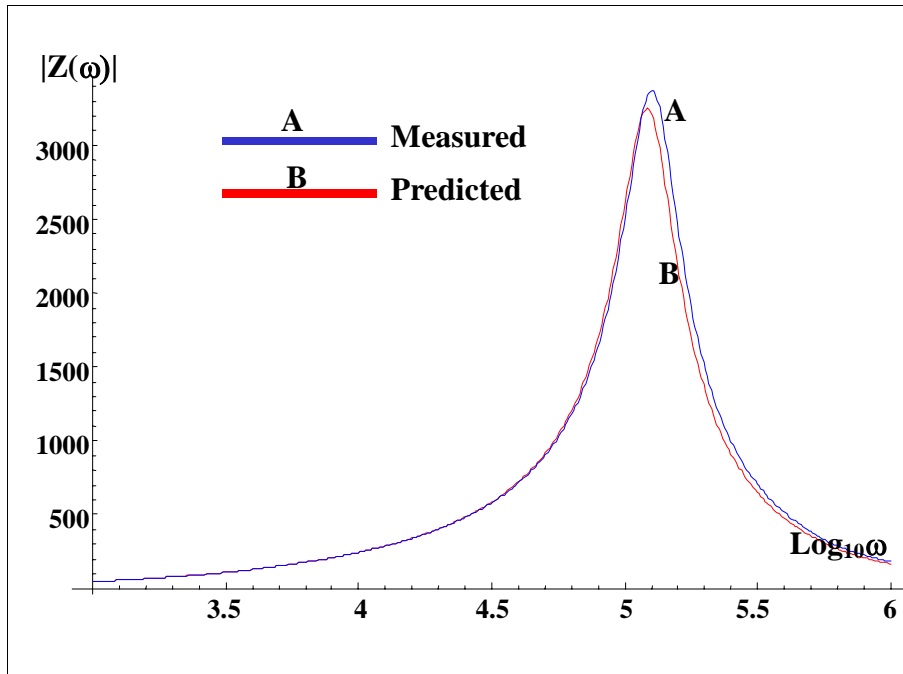
In Equation 5.2-4  $Z_0(\omega)$  and  $\gamma(\omega)$  are the cable's characteristic impedance and propagation function, and  $Z_L(\omega)$  is the impedance of the load.

In Section 5.1 phenomenological models were developed for thermally aged cables and the characteristic impedance and propagation function were extracted from measured impedance spectra using Equations 3.2-1a and 3.2-1b. Using that information and the measured impedance of the load, the modeled impedance of the cable system can be constructed. The results are shown in Figures 51 and 52, which compare the modeled versus measured impedance magnitude and phase, respectively.

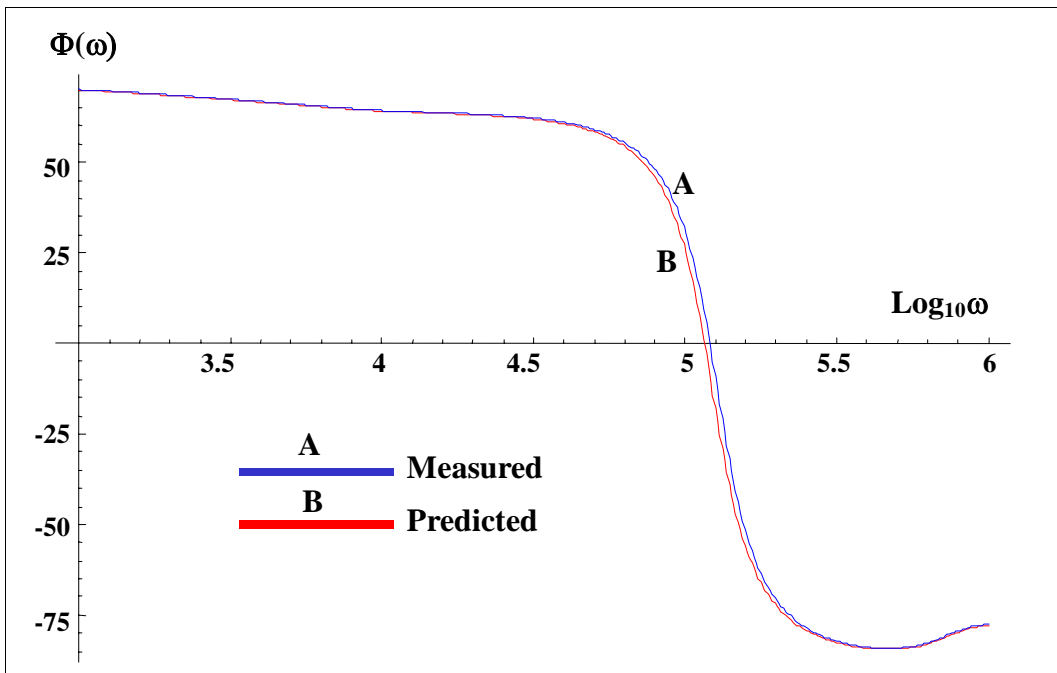
Figure 51 shows that in the frequency range from 100Hz to 1MHz, the modeled impedance magnitude is within approximately 3% of the measured impedance magnitude. The error is concentrated in the vicinity of the spectrum's peak at approximately 126MHz. The model's peak is slightly downshifted relative to the measured peak.

Figure 52 shows that in the frequency range from 100Hz to 1MHz, the modeled impedance phase spectra is within approximately 6% of the measured impedance phase. The error is concentrated in the vicinity of the spectrum's zero crossing at approximately 126MHz. The model's zero crossing is slightly downshifted relative to the measured zero crossing.

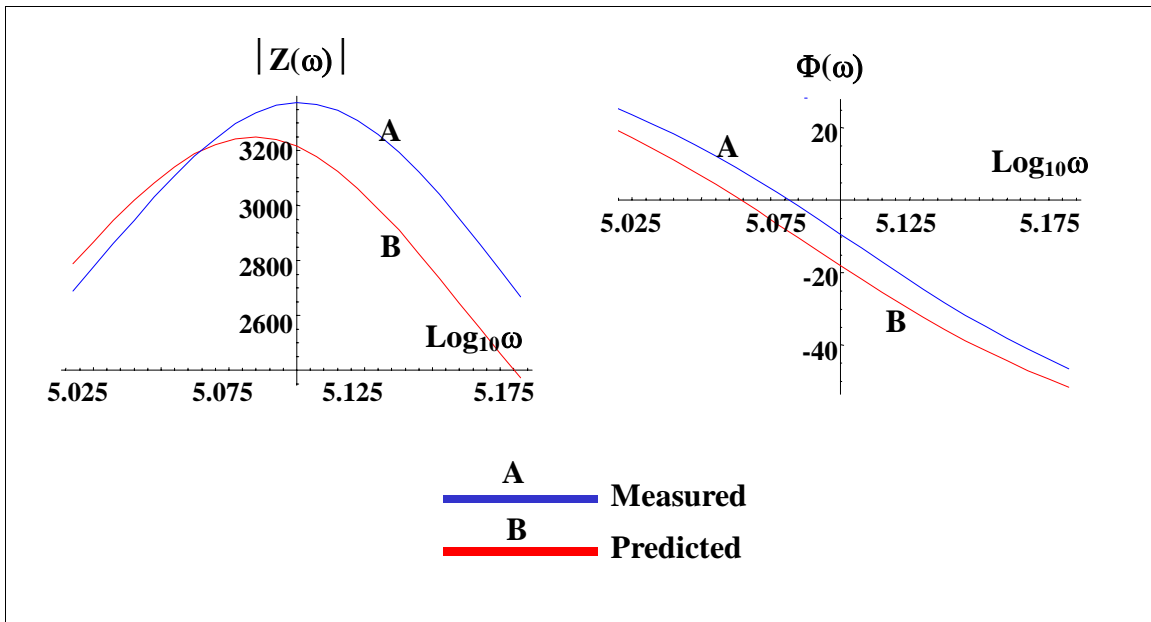
Figure 53 provides a comparison of the modeled and measured impedance magnitude and phase for the cable system without a hot-spot.



**Figure 51** Comparison of low frequency measured and predicted impedance magnitude for a cable system with no hot-spots and an attached load

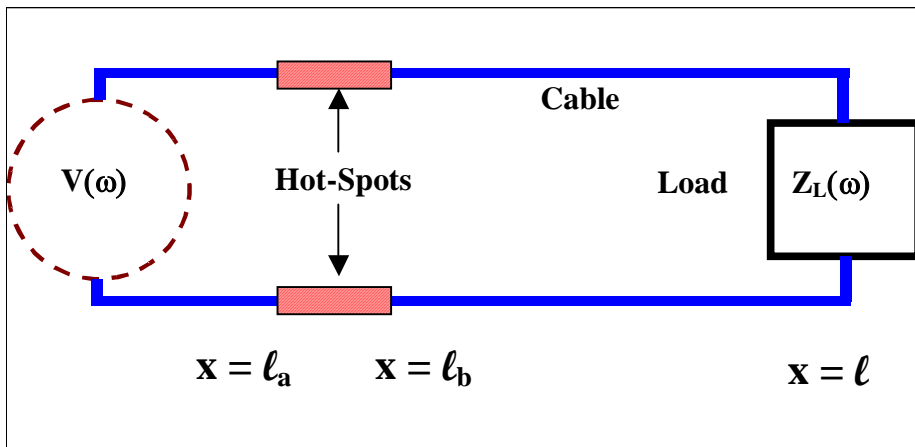


**Figure 52** Comparison of low frequency measured and predicted impedance phase spectra for a cable system with no hot-spots and an attached load



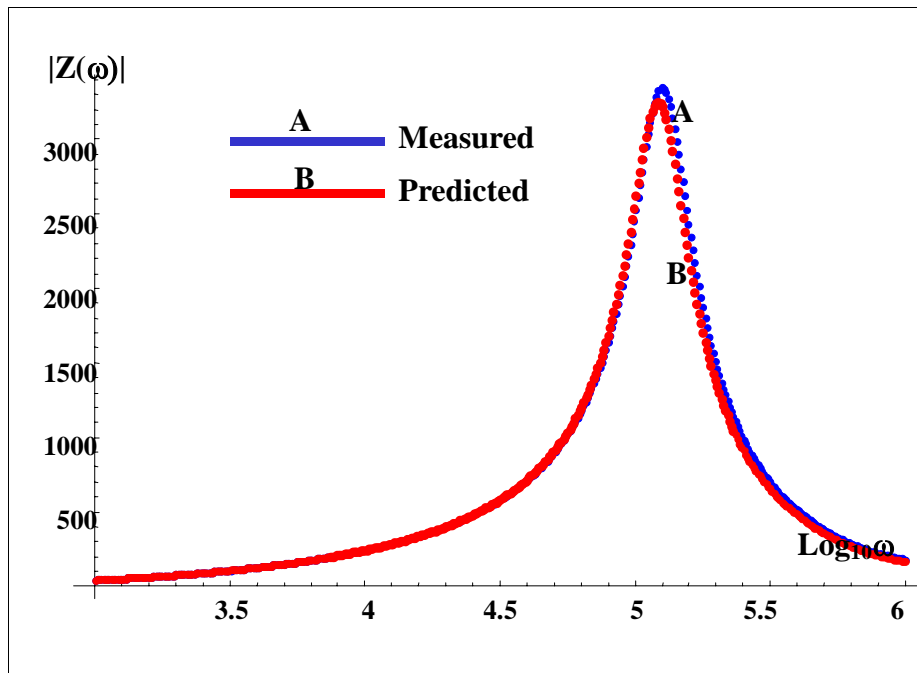
**Figure 53** Comparison of high frequency measured and predicted impedance magnitude and phase for a cable system with a hot-spot and an attached load

Next, the model for a cable system with a hot-spot is developed. This case is shown schematically in Figure 54. The cable is 10 meters long and has been thermally aged to simulate 60 years of service at 50°C (specimen 29). A 1 meter hot-spot representing 60 years at 70°C is present on the cable, and a load is attached to the far end of the cable, represented by an impedance,  $Z_L(\omega)$ .



**Figure 54** Schematic of a cable system with a hot-spot and an attached load

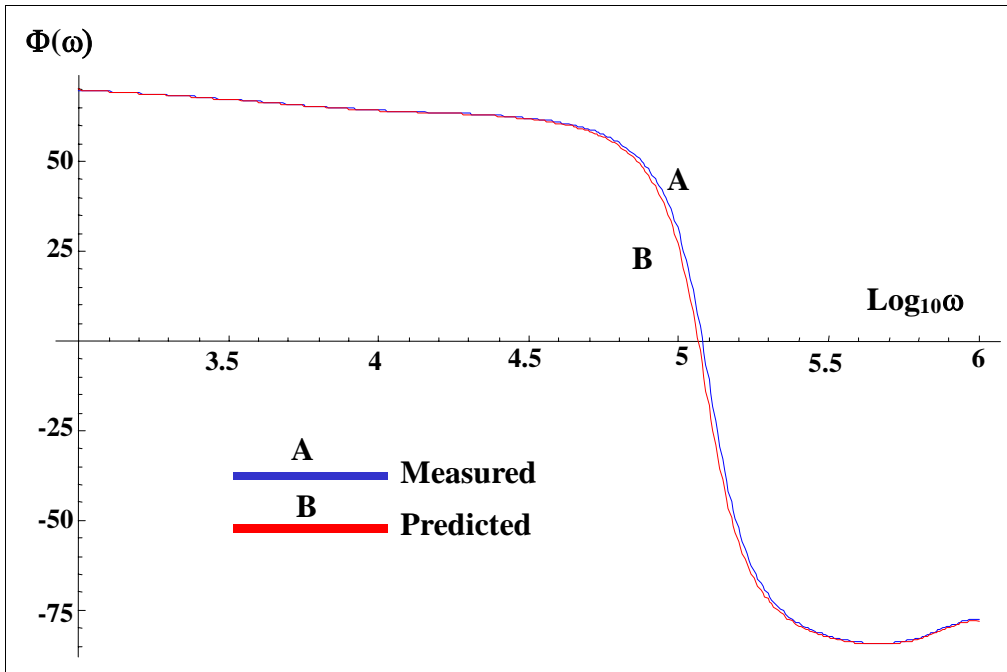
Figure 55 compares the measured and modeled impedance magnitude for the cable system in the frequency range from 1kHz to 1MHz. As shown, the model is within approximately 1% of the measured impedance magnitude, indicating good agreement.



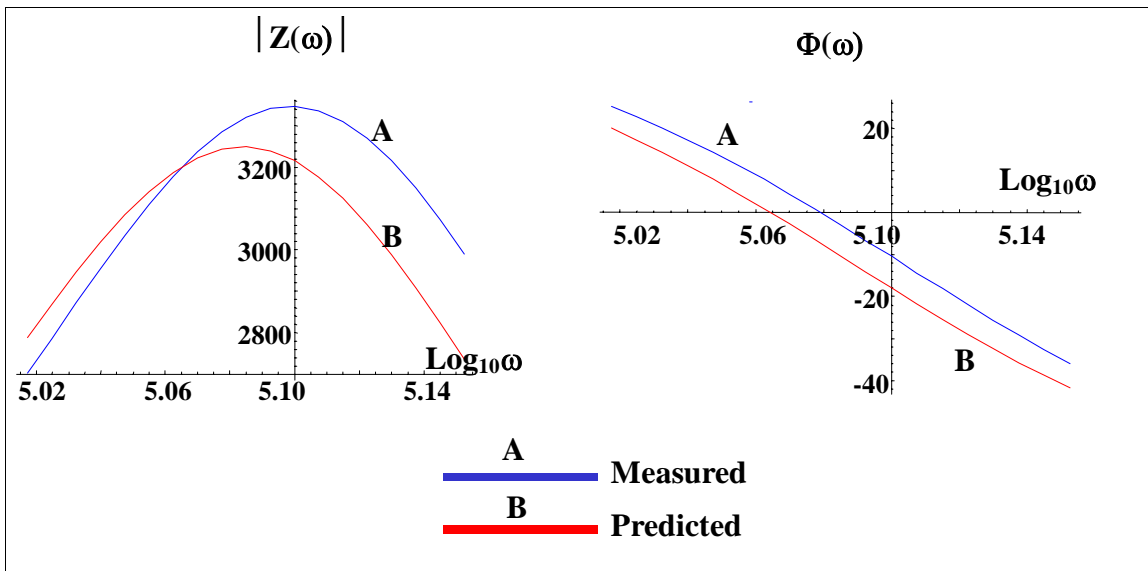
**Figure 55** Comparison of measured and modeled impedance magnitude for cable system with a hot-spot and an attached load

Figure 56 compares the measured and modeled impedance phase for the cable system in the frequency range from 1kHz to 1MHz. As shown, the model is within approximately 1% of the measured impedance phase, indicating good agreement. It is also observed that the modeled impedance phase in the vicinity of the zero crossing is slightly larger than the measured peak and is downshifted relative to the measured value.

Figure 57 provides a comparison of the modeled and measured impedance magnitude and phase for the cable system with a hot-spot.



**Figure 56** Comparison of low frequency measured and modeled impedance phase spectra for a cable system with a hot-spot and an attached load



**Figure 57** Comparison of high frequency impedance magnitude and phase spectra for cable system with a hot-spot and an attached load

### 5.2.5 Locating a Hot-Spot on a Cable with an Attached Load

Here, an approach is developed to locate the position of a hot-spot on a cable with an attached load using the low frequency impedance spectrum. This work is based on the models developed in the previous sections for a cable with an attached load. As a demonstration of the approach, specimen 29 is used, which is thermally aged to simulate 60 years of service @ 50°C, and has a 1 meter hot-spot representing 60 years @ 70°C.

For this demonstration, the impedance phase spectrum in the vicinity of the zero crossing at 120kHz is focused on. The cable system's impedance in the frequency range from 110kHz to 142kHz is calculated based on an assumed location of the hot-spot, and the relative difference between the modeled phase and measured phase is calculated. Using an iterative procedure, the assumed hot-spot location is incremented and the difference between measured and modeled phase values is again calculated. The predicted hot-spot location is obtained when this difference is a minimum. Figure 58 presents the results of the difference calculations as a function of assumed hot-spot location. As shown, the hot-spot location is correctly predicted.

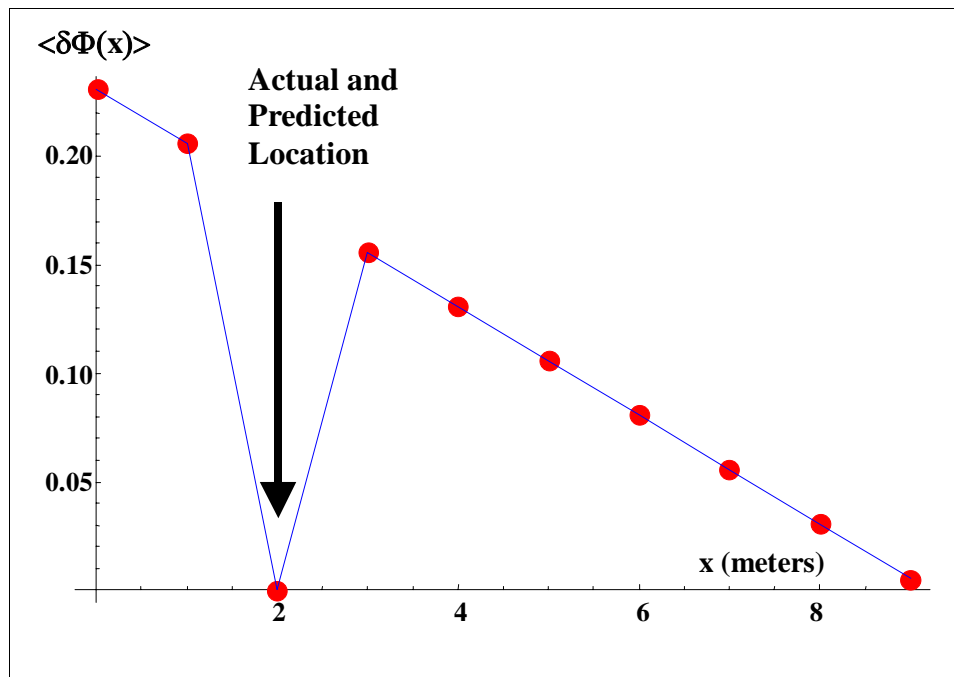


**Figure 58** Prediction of hot-spot location for a cable system with a load attached

These results demonstrate that the low frequency BIS can be used to predict the location of a hot-spot on a cable that has a load attached. Relatively good accuracy was demonstrated in the example presented.

### 5.3 Application of BIS to Cables with Abrasion Damage

This section presents the results of testing performed to evaluate the use of the BIS method for

detecting and locating abrasion damage on cables. First, a discussion of the cables tested is presented. Subsequently, results of tests performed at low frequency are discussed followed by the results of tests performed at high frequency.

### 5.3.1 Abrasion Test Specimens

In this portion of the research, the cable test specimens shown in Table 11 were used.

**Table 11** Specimens tested to evaluate BIS for detecting abrasion

No.	Specimen ID	Length meters (inches)	Service Life Simulated	Hot-Spot Simulated
15.	PNI-79-RB-188-815	10 (393.7)	None	None
22.	PNI-79-RB-188-822	10 (393.7)	40yrs. @ 50°C	40yrs. @ 60°C
29.	PNI-79-RB-188-829	10 (393.7)	60yrs. @ 50°C	60yrs. @ 70°C
30.	PNI-79-RB-188-830	10 (393.7)	60yrs. @ 50°C	60yrs. @ 70°C

Specimen 15 was used as the baseline representing a healthy cable with no aging or abrasion. On specimen 22, one of the conductors was abraded using a Dremel tool to grind the cable’s insulation down to the bare metal conductor over a length of 2mm (0.08in.). On specimens 29 and 30, both conductors were abraded as previously described. A conductive contaminant was applied to the abraded portion of specimen 30. In all cases, the abrasion was located in the middle of the cable at 5m (196.85in.) from the end. The following four cases were studied:

- Case A: Unabraded cable
- Case B: Cable with one conductor abraded
- Case C: Cable with two conductors abraded
- Case D Cable with two conductors abraded and a conductive contaminant applied to the abraded portion of the cable

Case D represents a typical scenario expected in a power plant since a number of contaminants are commonly found on cables that have not been touched in many years. These contaminants can absorb moisture and hold it near the cables resulting in a conductive pathway between cables and ground. For this study, the contaminant used was a mixture of 85% Skydrol hydraulic fluid, 11% iron filings, and 4% carbon black powder. This mixture had as a jelly-like consistency and was applied directly to the cables in the location of the abrasion. Figure 59 presents a schematic of the four cases studied.

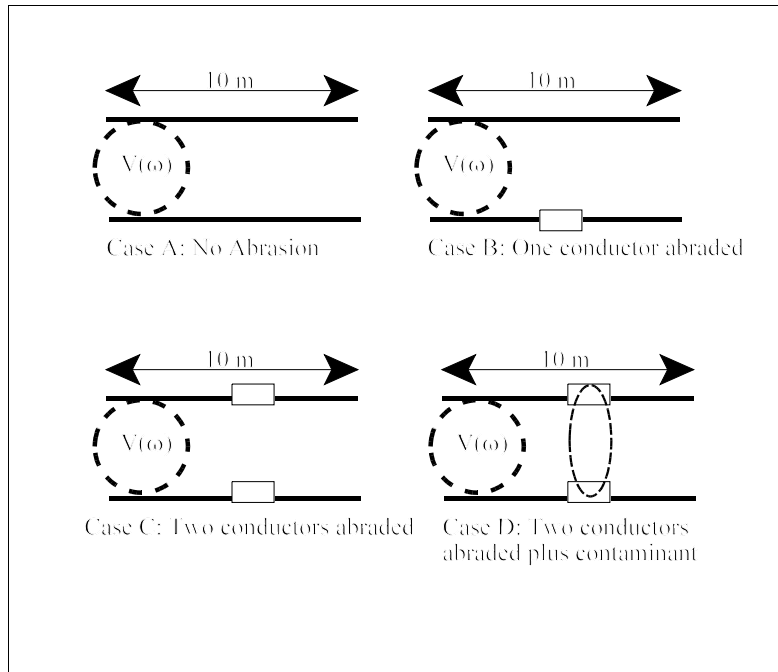


**Figure 59** Schematic of four cases studied to evaluate BIS for detecting and locating abrasion

BIS measurements were made by placing the test specimen in a humidity chamber so that the temperature and humidity surrounding the cable could be controlled. Test leads were connected to the cables by extending the cable ends through ports in the wall of the humidity chamber. Measurements were taken at various humidity levels while holding the temperature at 30°C (86°F).

The BIS measurements were performed over two frequency ranges: 1) the low frequency or non-oscillatory range, which was 1kHz to 1MHz, and 2) the high frequency or oscillatory range, which was 1MHz to 100MHz. In the non-oscillatory range, the measurements were performed with the HP-5094 device, which provided data points at 401 discrete frequencies equally spaced over the range. In the oscillatory region the measurements were made with the Eclipse instrument, which provided data points at 2000 discrete frequencies equally spaced over the range.

### 5.3.2 Evaluation of Low Frequency BIS Results on Cables with Abrasion

The impedance response of abraded cables in the low frequency range is evaluated in the following sections.

#### 5.3.2.1 Low Frequency Impedance Measurements on Abraded Cables



Figure 60 compares the measured impedance phase spectra for cables with and without abrasion exposed to an environment of 20% relative humidity (RH). As shown, the abrasion does not affect the cables' impedance phase in the non-oscillatory frequency range.

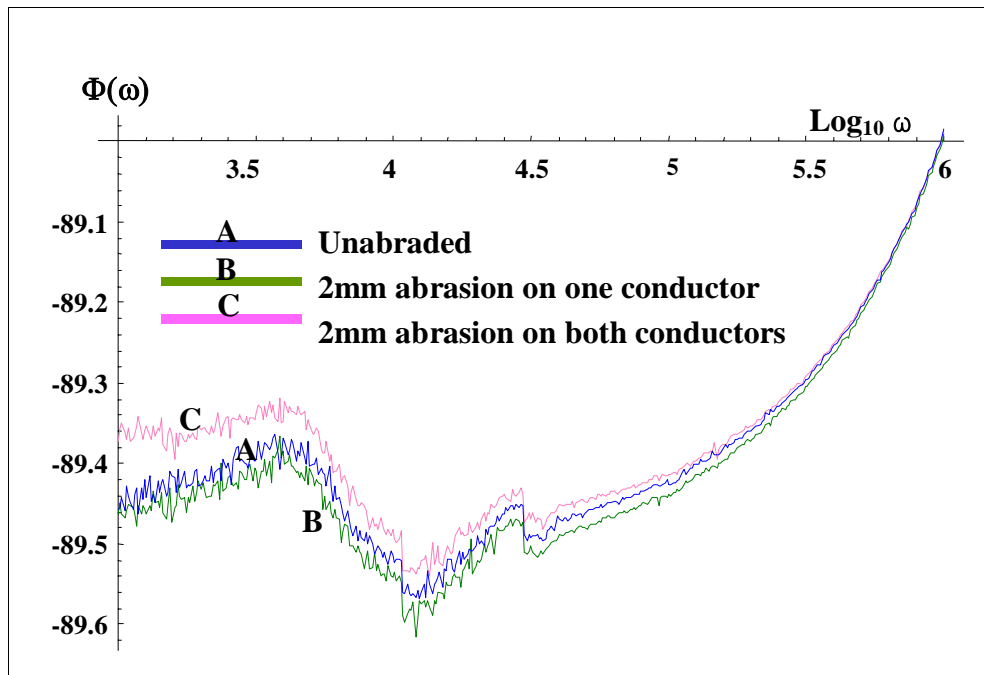


**Figure 60** Low frequency impedance phase spectra for cables with and without abrasion exposed to an environment of 20% Relative Humidity

Figure 61 compares the impedance phase spectra for cables with and without abrasion exposed to an environment of 85% RH. As shown, when a higher level of humidity is present, all of the phase spectra have a new structure; i.e., a peak in the vicinity of 5kHz to 10kHz. This structure arises from the increased humidity level, which provides a conductive pathway for leakage currents. It is also observed that the abraded cable's peak is shifted to higher frequencies relative to the unabraded cable. This frequency shift may be attributable to the fact that the averaged dielectric function of the abraded cable is smaller than that for the unabraded cable. As a result, any structures must occur at higher frequencies. It is further observed that there is no readily observable difference between the phase spectra of the cables with one and two conductors abraded.

It should be noted that, while the change in the low frequency impedance phase spectra can be used to detect abrasion under high humidity levels, this may not be practical in a nuclear power plant environment since the humidity levels may not be high enough to observe these changes. For example, the peaks previously discussed were not observed when BIS measurements were made under conditions of 70% RH.

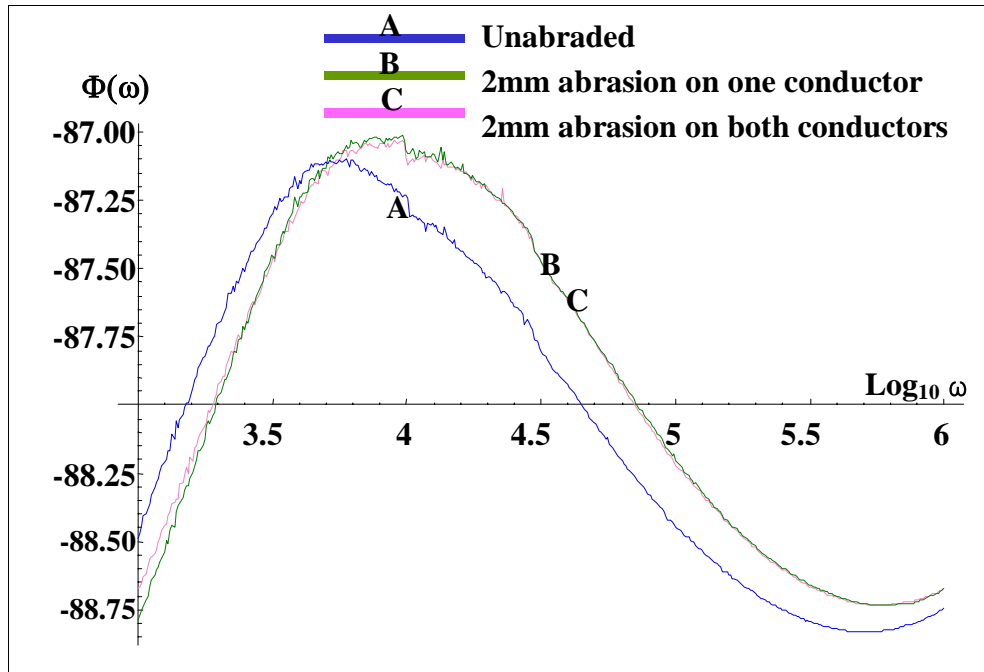


**Figure 61** Low frequency impedance phase spectra for cables with and without abrasion exposed to an environment of 85% Relative Humidity

Next, the case in which a conductivity path is present in the vicinity of the abraded portion of the cables is evaluated (Case D). Figure 62 compares the measured impedance magnitude for cables with and without abrasion, including cables with abrasion and a conductive contaminant applied to the cables. The environment was 85% RH for these measurements. As shown, at the low end of the frequency range (1kHz) the impedance decreases from approximately 245Ω to 7000Ω when the conductive contaminant is present. This is consistent with the loss of insulation, which degrades the cable’s insulating capability.

Figure 63 presents the impedance phase spectra for the cables with and without abrasion and a conductive contaminant. Again the environment is 85% RH. As shown, the impedance phase near the low end of the frequency range increases from approximately -89.5 degrees to -16.7 degrees when the conductive contaminant is placed on the abraded portion of the cable. This supports the concept that there is a conductivity path between the abraded conductors since the impedance phase behaves more like a resistor (which has zero degree phase) than a capacitor (which has a 90 degree phase).

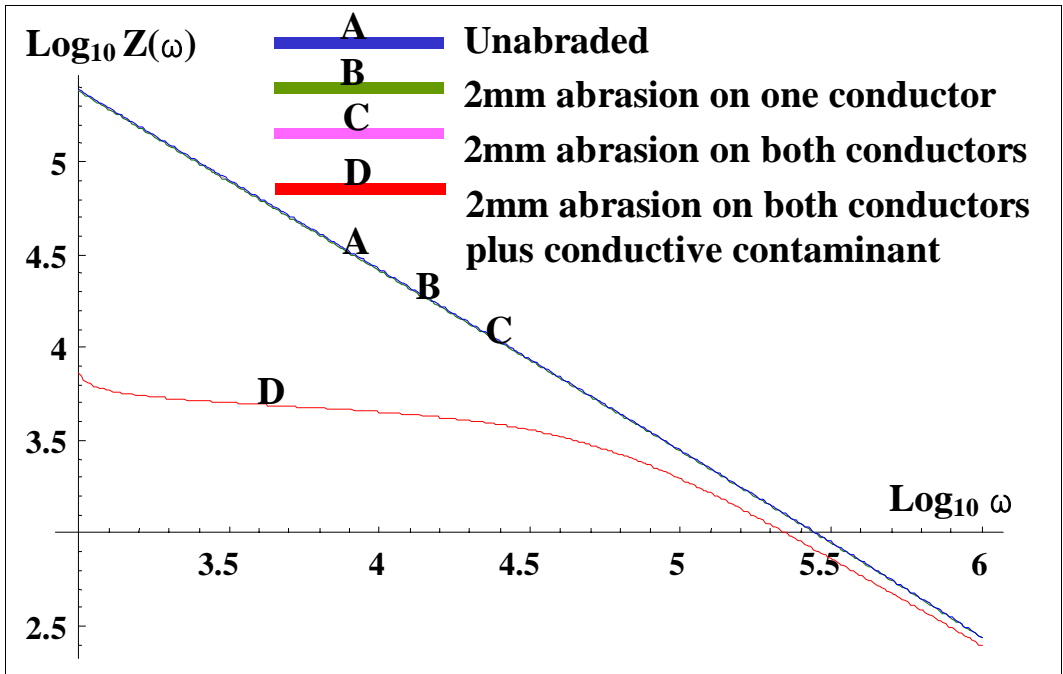


**Figure 62** Impedance magnitude for cables with and without abrasion plus a conductive contaminant exposed to an environment of 85% RH

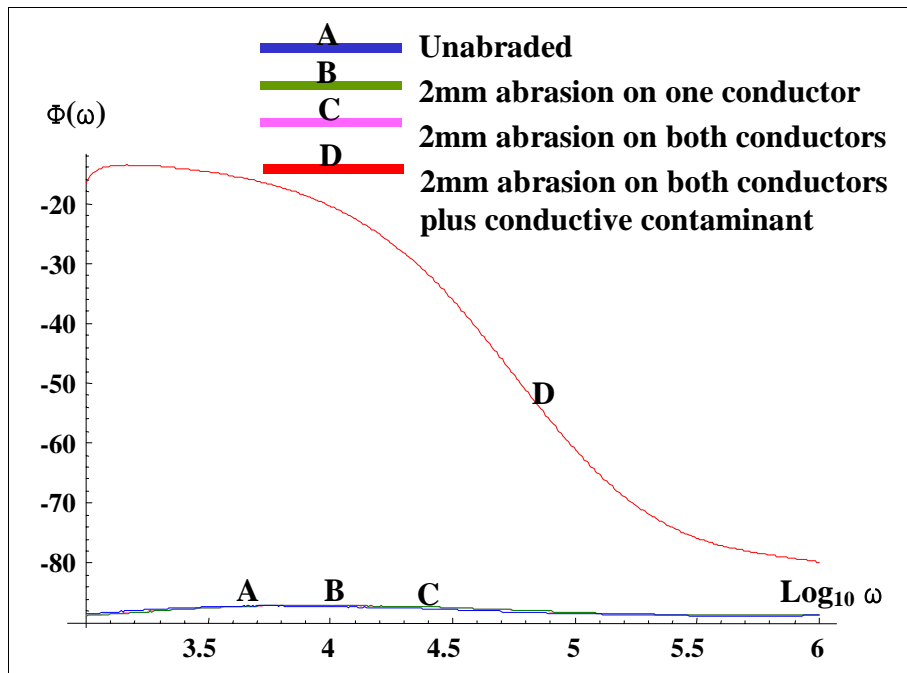


**Figure 63** Impedance phase spectra for cables with and without abrasion plus a conductive contaminant exposed to an environment of 85% RH.

Further examination of the previous two figures shows that, as the frequency increases, the effect of the conductivity path on the cable's properties decreases to the point where all of the impedance spectra converge. This implies that the micro-processes taking place are slow; i.e., on the order of milli-seconds, which is reasonable since the contaminant used contained iron particles.

### 5.3.2.2 Low Frequency Models of Abraded Cables

A phenomenological approach was used to model the characteristic impedance and propagation function for abraded cables. First, the characteristic impedance and propagation function for cables with abrasion only were extracted from the low frequency impedance measurements made at 85% RH. Figure 64 presents the magnitude of the characteristic impedance for each of the cables with and without abrasion. The difference from the unabraded case is also presented for each abraded cable. As shown, the differences are very small (on the order of  $1\Omega$  to  $2\Omega$  or less).

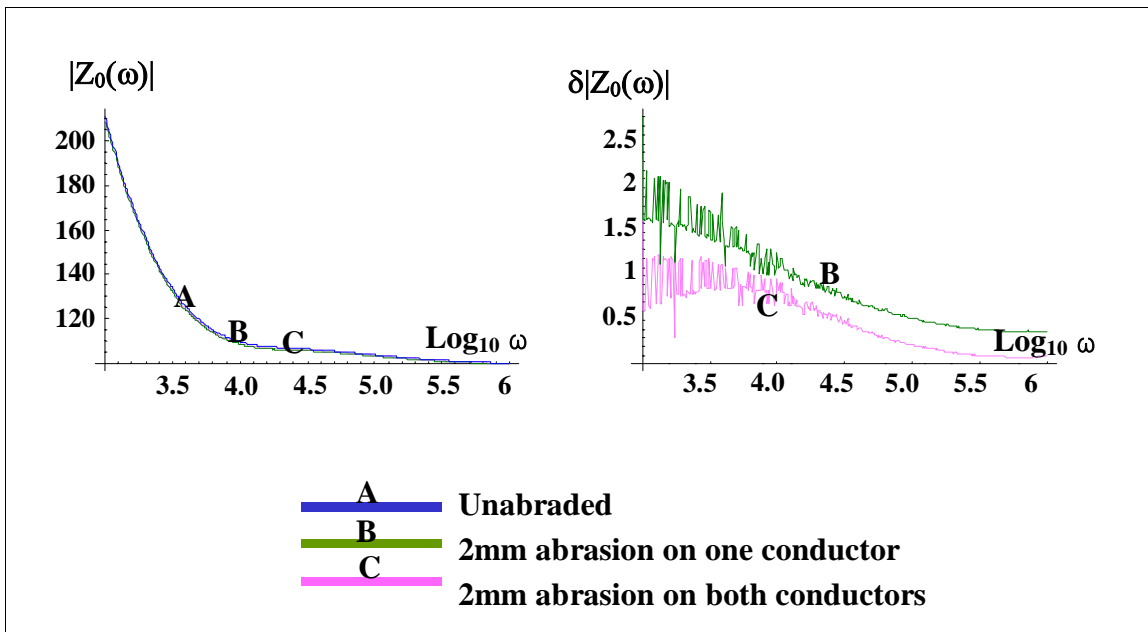


**Figure 64** Low frequency characteristic impedance magnitude for cables with and without abrasion exposed to an environment of 85% RH

Figure 65 presents the characteristic impedance phase spectra for cables with and without abrasion exposed to an environment of 85% RH. The change from the baseline (unabraded) case is also presented. Again, the changes are very small ( on the order of  $\pm 2$  degrees or less).

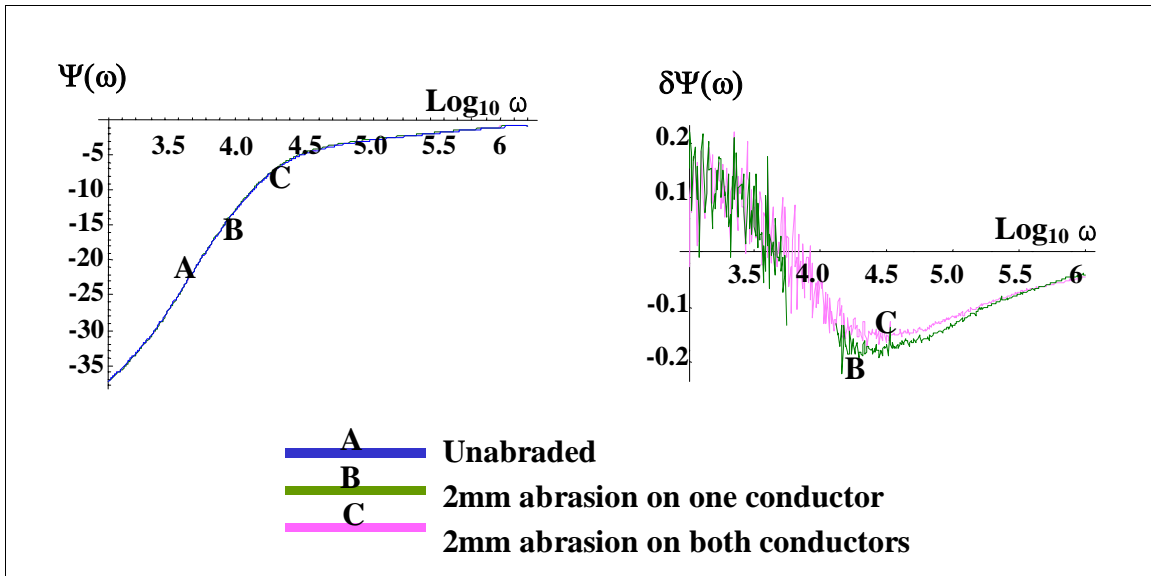


**Figure 65** Low frequency characteristic impedance phase spectra for cables with and without abrasion exposed to an environment of 85% RH

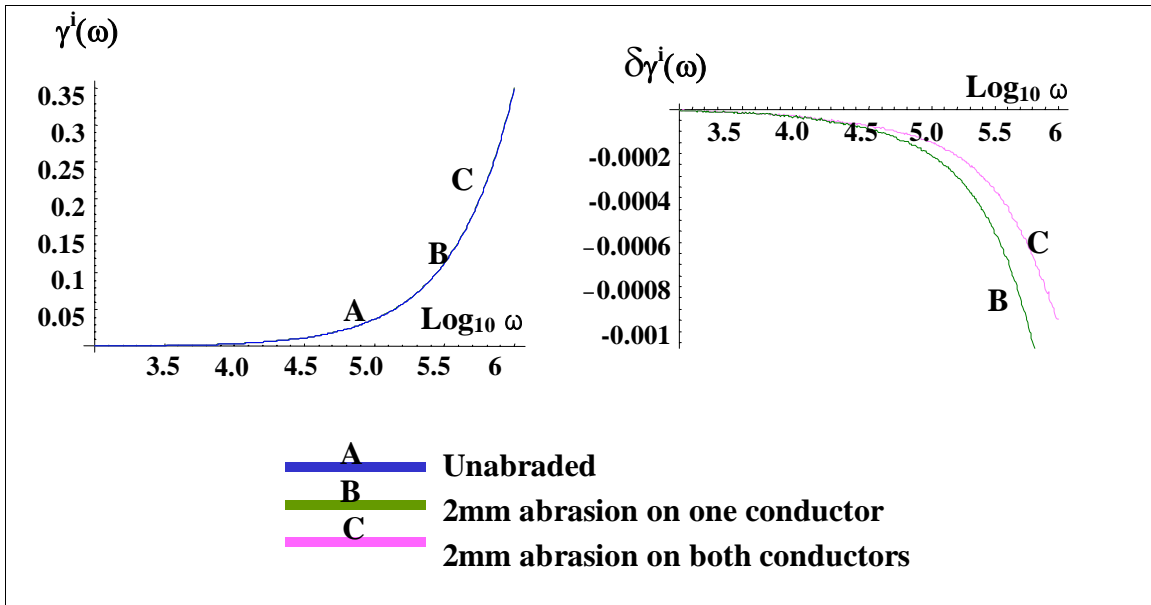
Figures 66 and 67 present the imaginary and real components of the propagation function for each of the cables with and without abrasion. The difference from the unabraded case is also presented for each abraded cable. As shown, the differences are very small (on the order of 1% to 2% or less).

It should be noted that, while the parameter changes are on the order of 1% to 2%, only 0.02% of the cable’s insulation was removed in these tests. Thus, the measured changes are two orders of magnitude greater than the amount of insulation removed.

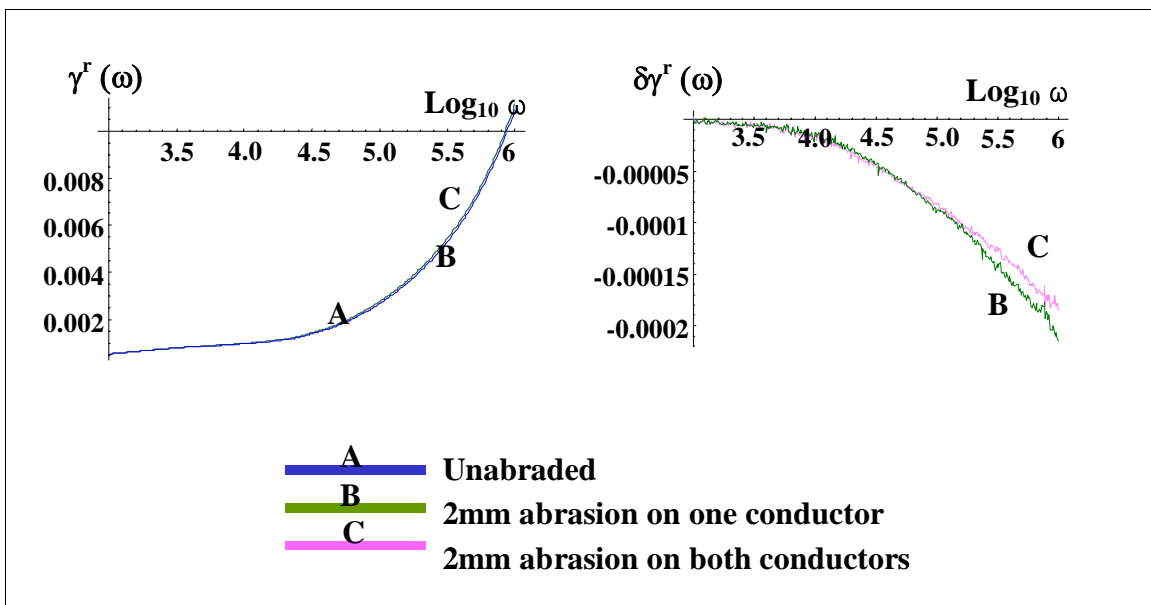
Next, the cables’ electrical properties were extracted from the measured low frequency impedance spectra. Figure 68 compares the cables’ capacitance with and without abrasion exposed to an environment of 85% RH. The relative change from the baseline (unabraded) case is also presented. It is observed that the changes are on the order of 2%.

Figure 69 compares the cables’ conductance with and without abrasion exposed to an environment of 85% RH. The relative change from the baseline (unabraded) case is also presented. It is observed that the changes are relatively large; on the order of 15%.

It is noted that abrasion of a small portion of a cable’s insulation cannot by itself change the cable’s electrical and material properties. However, abrasion down to the metallic conductor of a cable allows the environment to enter the cable’s insulation and degrade its insulating capabilities. Specifically, humidity can moisten the insulation and increase its dielectric function. Also, humidity can form a weak conductivity path between the conductor and ground. This behavior would not occur when the humidity is low.



**Figure 66** Imaginary component of the low frequency propagation function for cables with and without abrasion exposed to an environment of 85% RH



**Figure 67** Real component of the low frequency propagation function for cables with and without abrasion exposed to an environment of 85% RH

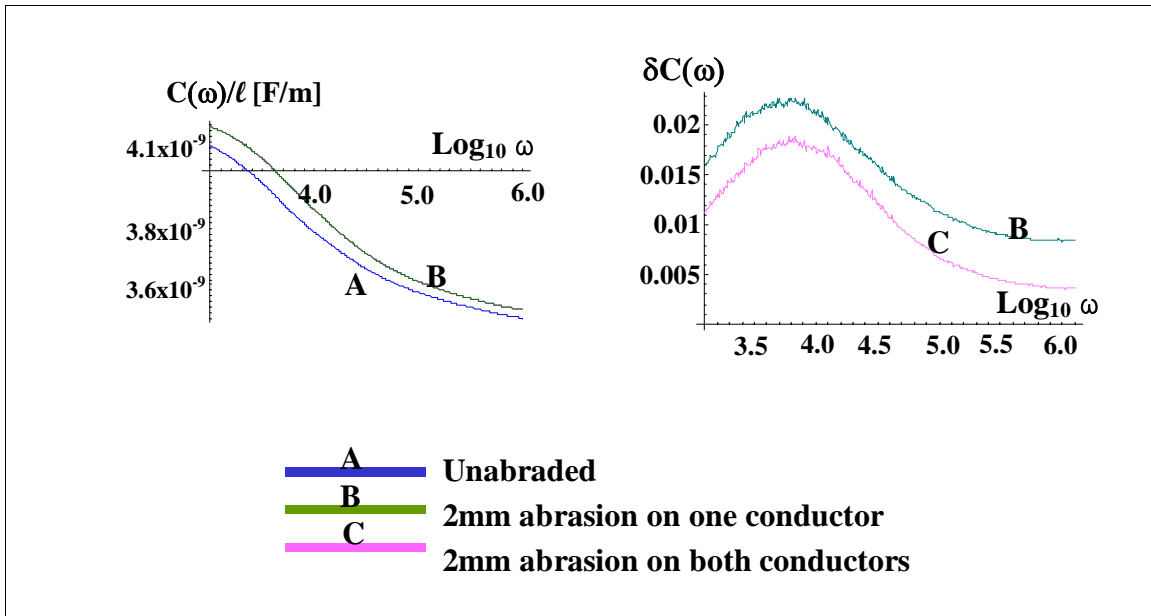


**Figure 68** Capacitance per unit length extracted from measured low frequency impedance spectra for cables with and without abrasion exposed to an environment of 85% RH

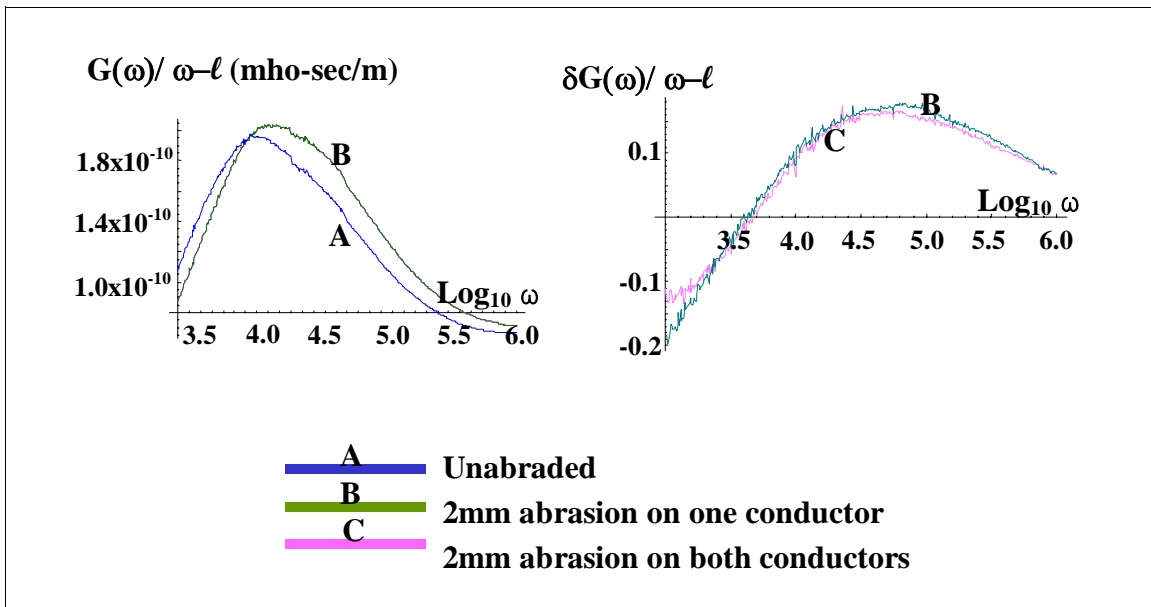


**Figure 69** Conductance per unit length extracted from measured low frequency impedance spectra for cables with and without abrasion exposed to an environment of 85% RH

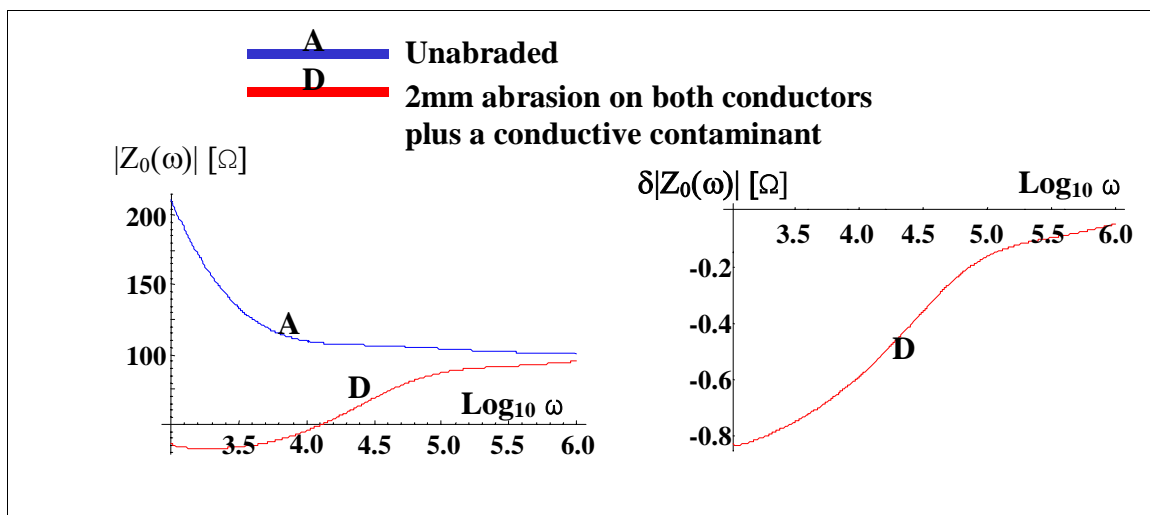
Next, models for cables with both abrasion and a conductive contaminant are developed. The characteristic impedance, propagation function, and electrical properties can be calculated based on two scenarios, as follows:

1. Assume the cable is degraded uniformly along its entire length
2. Assume an interaction between the abraded cable conductors, localized at the point where the conductive contaminant was placed

Since the actual phenomena can best be described as a composite of the above two scenarios, two models were developed; 1) a spatially averaged degradation model, and 2) a localized cable interaction model. These models are presented below.

For the spatially averaged cable degradation model, a phenomenological approach is used to extract the cable's characteristic impedance, propagation function, and electrical properties from measured impedance data. Here, the extracted cable parameters represent the quantities spatially averaged over the length of the cable.

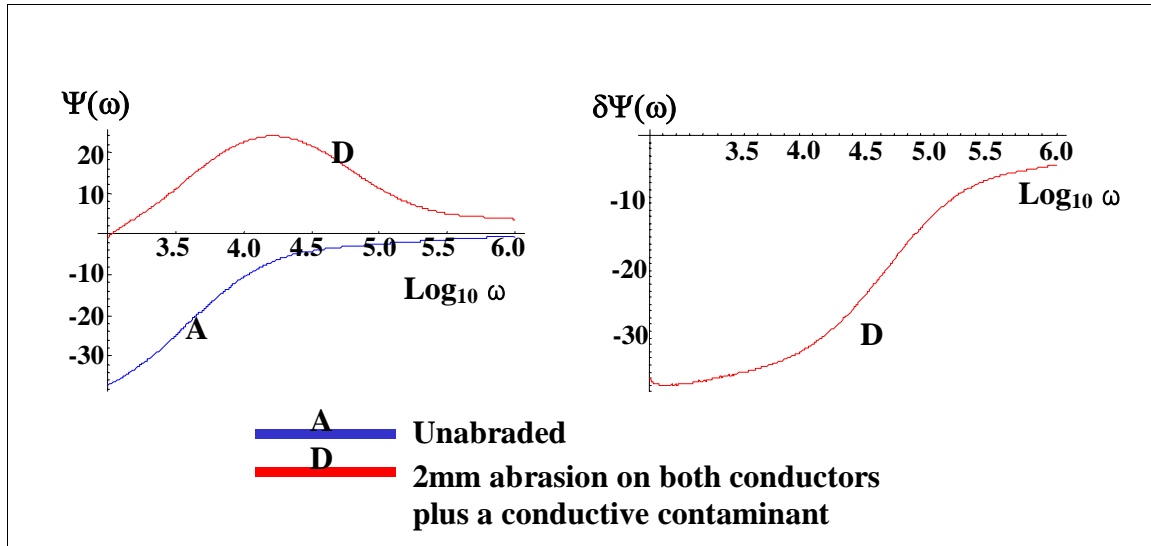
Figure 70 presents the magnitude of the characteristic impedance for each of the cables with and without abrasion plus a conductive contaminant. The difference from the unabraded case is also presented for each abraded cable. As shown, the addition of a conductive contaminant greatly decreases the magnitude of the cable's characteristic impedance at low frequencies (on the order of 80%). As the frequency approaches 1MHz, the magnitude of the characteristic impedance for the cables with and without abrasion merge, as expected.



**Figure 70** Low frequency characteristic impedance magnitude for cables with and without abrasion plus a conductive contaminant exposed to an environment of 85% RH



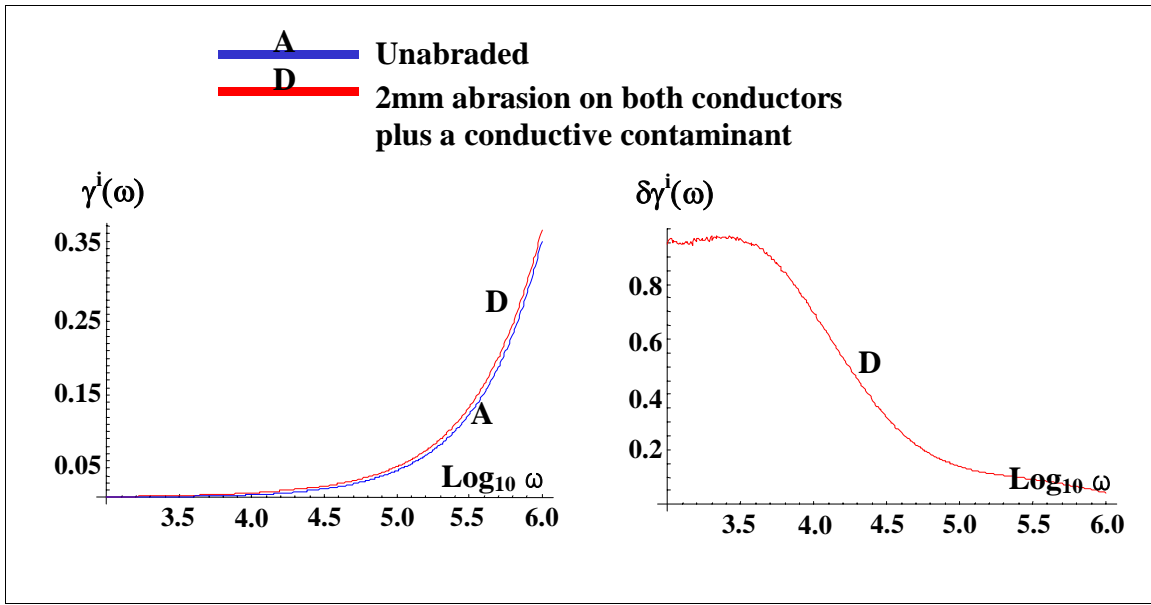
Figure 71 presents the characteristic impedance phase spectra for cables with and without abrasion plus a conductive contaminant exposed to an environment of 85% RH. The difference from the baseline (unabraded) case is also presented. As shown, the characteristic impedance phase is significantly changed by the presence of a conductivity path. Specifically, the change in phase,  $\delta\Psi(\omega)$ , approaches zero as the frequency approaches 1MHz.



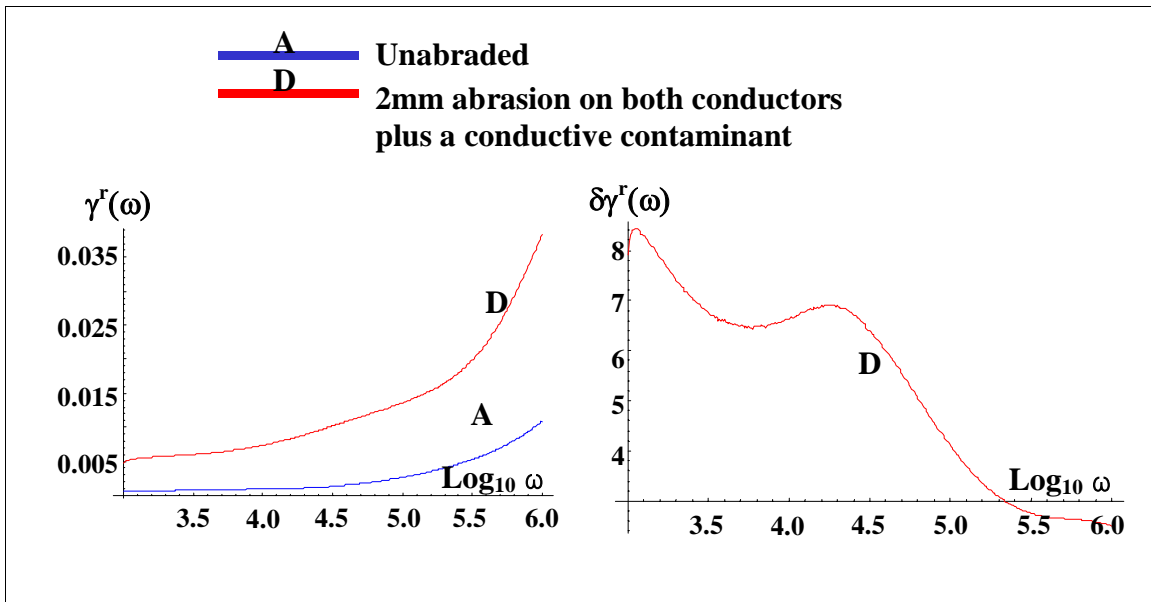
**Figure 71** Low frequency characteristic impedance phase spectra for cables with and without abrasion plus a conductive contaminant exposed to an environment of 85% RH

Figures 72 and 73 present the imaginary and real components of the propagation function for each of the cables with and without abrasion plus a conductive contaminant. The difference from the unabraded case is also presented for each abraded cable. As shown, the imaginary component of the propagation function increases when a conductive path is present. Again, the larger changes occur at the very low frequencies (1kHz) and as the frequency increases the change approaches zero. Similarly, the real component increases by a factor as large as eight at the low frequencies when the conductive path is present. These results clearly show that the cable is very dissipative and is on the verge of shorting out.

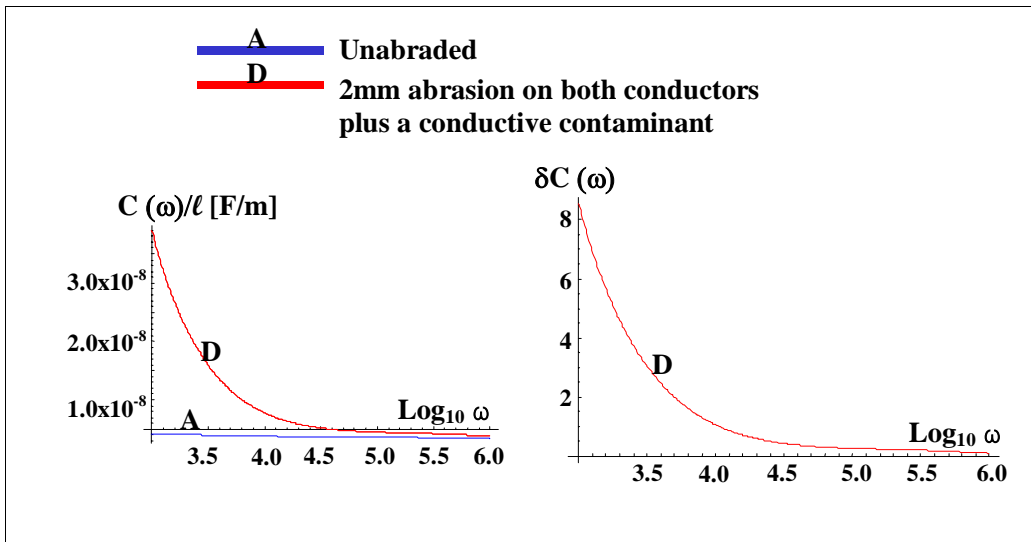
An examination of the cables resistance and inductance show that these properties show little or no change in the presence of a conductive path. However, the cable insulation's dielectric function (averaged over the length of the cable) is greatly changed by the conductive path. Figure 74 compares the cables' capacitance per unit length with and without abrasion plus a conductive contaminant exposed to an environment of 85% RH. The relative change from the baseline (unabraded) case is also presented. It is observed that at low frequencies, the cable's capacitance per unit length increases by a factor of approximately eight when the conductive path is present. This difference approaches zero as the frequency approaches 1MHz.



**Figure 72** Imaginary component of the low frequency propagation function for cables with and without abrasion plus a conductive contaminant exposed to an environment of 85% RH



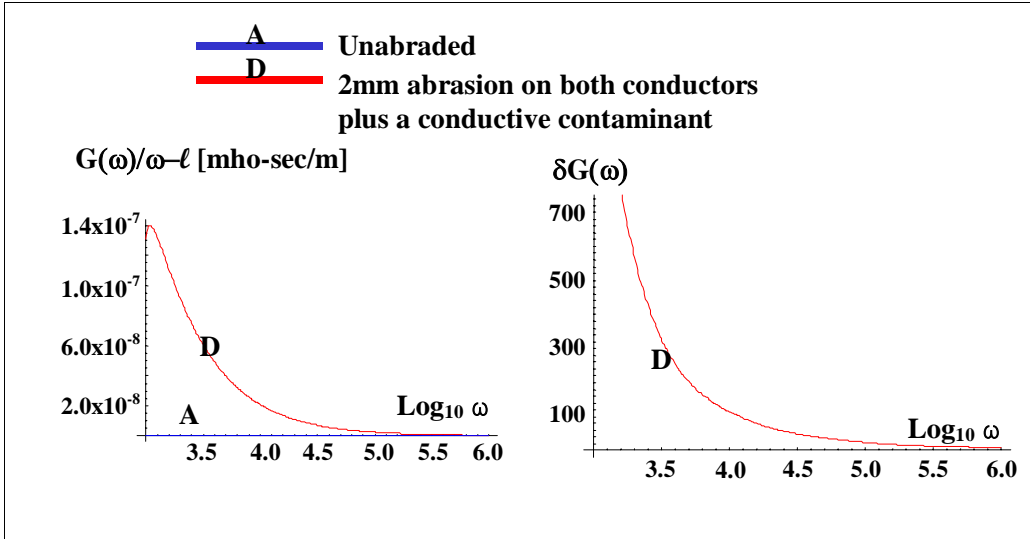
**Figure 73** Real component of the low frequency propagation function for cables with and without abrasion plus a conductive contaminant exposed to an environment of 85% RH



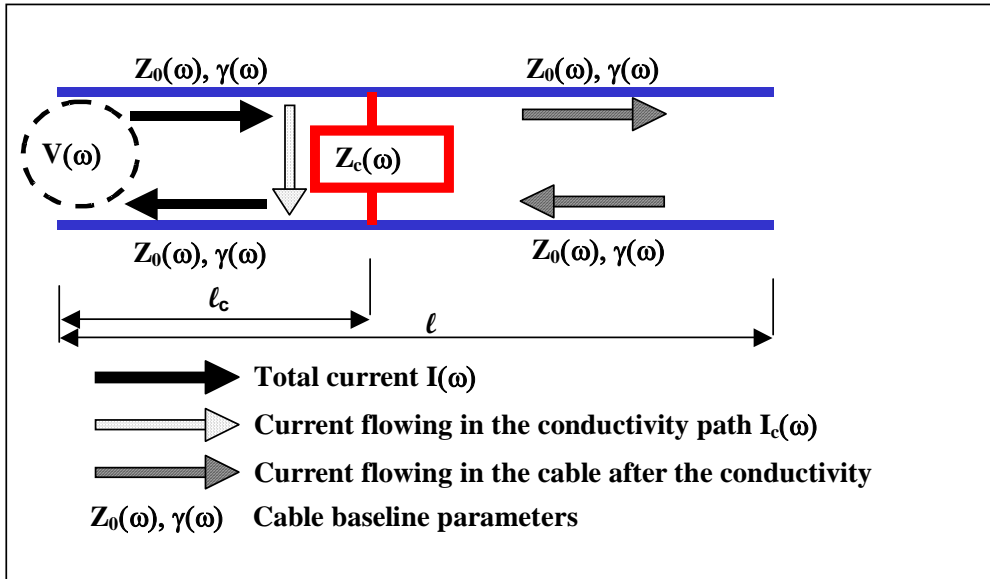
**Figure 74** Capacitance per unit length extracted from measured low frequency impedance spectra for cables with and without abrasion plus a conductive contaminant exposed to an environment of 85% RH

Figure 75 compares the cables' conductance per unit length with and without abrasion plus a conductive contaminant exposed to an environment of 85% RH. The relative change from the baseline (unabraded) case is also presented. It is observed that at low frequencies, the cable's conductance increases by a factor of approximately 1,000 or more when the conductive path is present. This difference approaches a factor of eight as the frequency approaches 1MHz.

For the localized cable interaction model, the conductivity path is viewed as a point structure in which current can flow from one conductor to the other at a specified point located in the area of the abrasion. Thus, it is assumed that the cable is not degraded throughout its entire length; only a small region is degraded and this is approximated by a point at the location of the conductive contaminant. Furthermore, it is assumed that the cable interaction that arises from the conductive contaminant can be represented by a localized impedance,  $Z_c(\omega)$ , located at a point in the cable where the conductive contaminant was placed. This model is depicted in Figure 76.



**Figure 75** Conductance per unit length extracted from measured low frequency impedance spectra for cables with and without abrasion plus a conductive contaminant exposed to an environment of 85% RH



**Figure 76** Schematic of the localized cable interaction model for abraded cables plus a conductive contaminant

In this model, the current flowing in the cable is separated into two different components, as follows:

$$I(\omega) = I_{\text{cable}}(\omega) + I_C(\omega) \quad 5.3-1$$

where  $I(\omega)$  is the total current flowing in the cable,  $I_C(\omega)$  is the current that flows through the localized impedance  $Z_C(\omega)$ , and  $I_{\text{cable}}$  is the remaining current that continues to flow in the cable after the localized area of abrasion. Therefore, the impedances due to the localized interaction,  $Z_C(\omega)$ , and the cable length after the abraded point,  $Z_{\text{cable}}(\omega)$ , are in parallel with each other. This can be modeled by treating the portion of cable after the conductivity path as a load, as shown in Figure 77. Here,  $\ell_c$  is the distance from the cable end to the abraded portion of the cable, and the load represents the portion of cable after the conductivity path. The impedance of the portion of the cable represented by the load,  $Z_{\text{cable}}(\omega)$ , is determined by the following equation:

$$Z_{\text{cable}}(\omega) = Z_0(\omega) \text{Coth}[\gamma(\omega)(\ell - \ell_c)] \quad 5.3-2$$

where  $\ell$  represents the length of the whole cable. In this equation it is assumed that the system is in the open configuration. It should be noted that, if the impedance of the conductive path is less than that for the remainder of the cable, the current will short through the conductive path.

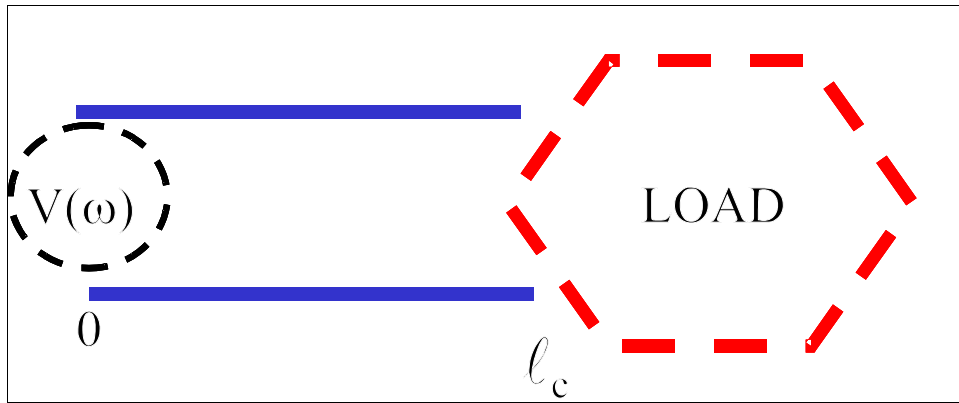


**Figure 77** Schematic representation of abraded cable with a conductive path between conductors

The total impedance for the load is represented by the following equation:

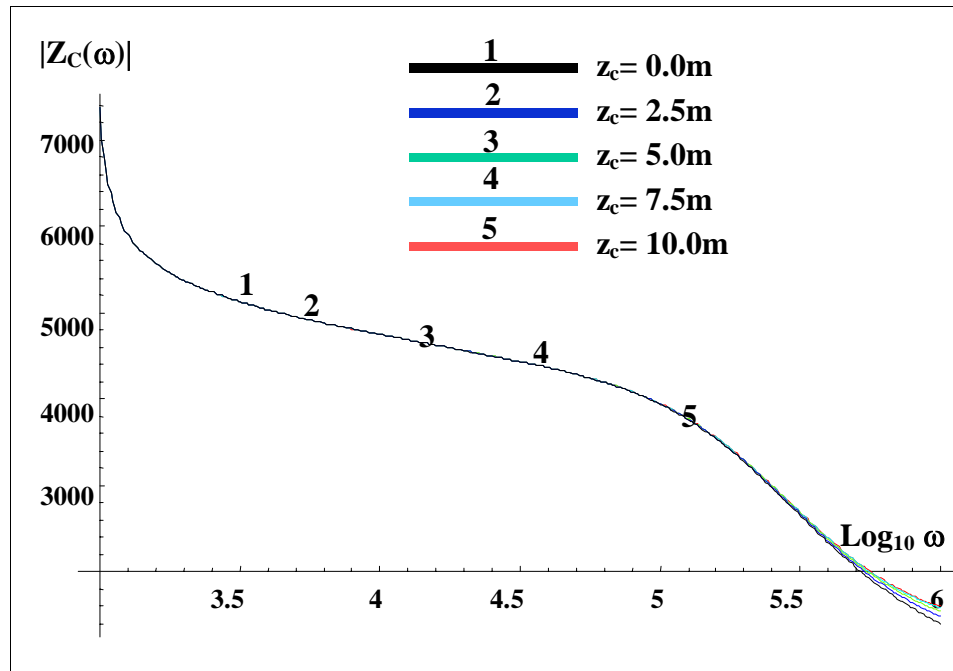
$$Z_{\text{Load}}(\omega) = \frac{Z_{\text{cable}}(\omega)Z_C(\omega)}{Z_{\text{cable}}(\omega) + Z_C(\omega)} \quad 5.3-3$$

The impedance for a system consisting of a cable connected to a load is represented by the following equation:

$$Z_{\text{Model}}(\omega) = Z_0(\omega) \frac{Z_{\text{Load}}(\omega) + Z_0(\omega) \tanh[\gamma(\omega)\ell]}{Z_0(\omega) + Z_{\text{Load}}(\omega) \tanh[\gamma(\omega)\ell]} \quad 5.3-4$$

Thus, using the measured impedance for  $Z_{\text{model}}(\omega)$ , and the above equations, the impedance of the conductive path,  $Z_c(\omega)$ , can be determined. Figure 78 presents the frequency dependence of the magnitude of  $Z_c(\omega)$  in the frequency range from 1kHz to 1MHz for cables with abrasion and various locations of a conductive path between conductors. As shown, there is no significant difference in the impedance for the different locations. Therefore, in the non-oscillatory region, the modeled impedance,  $Z_{\text{model}}(\omega)$ , is essentially independent of the point at which the conductive path is located, and it decreases with increasing frequency.

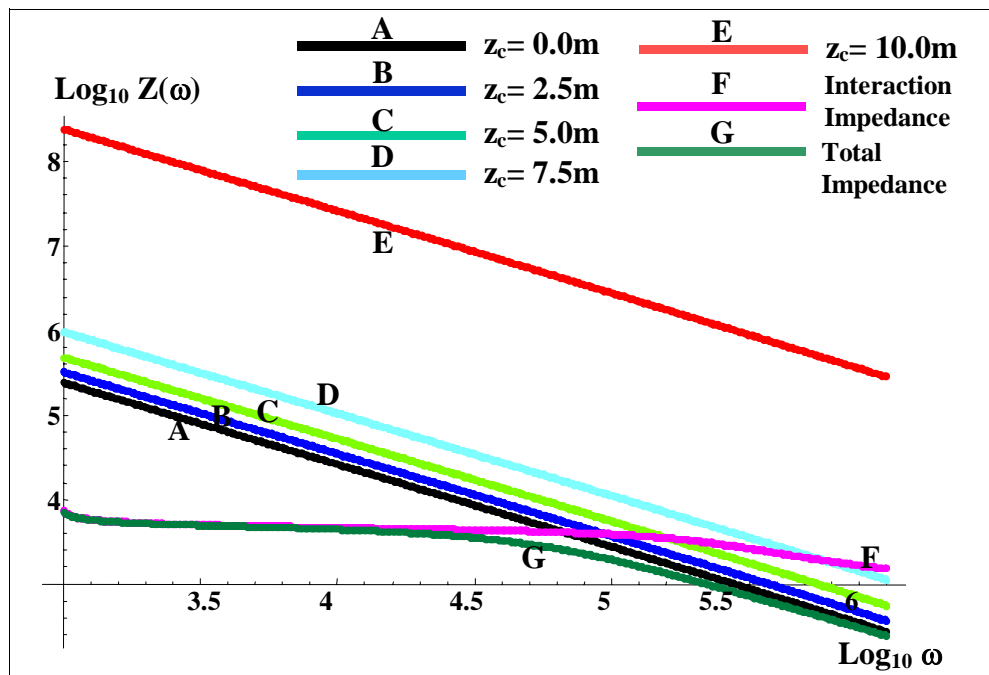
It is noted from equations 5.3-2 that  $Z_{\text{cable}}(\omega)$  depends on its location on the cable,  $(\ell - \ell_c)$ . This is physically reasonable since, in this region of the frequency spectrum, the electrical waves that are used to probe the cable's impedance have wavelengths that are much larger than the cable's length. However, the currents that flow in the cable and the conductivity path depend upon the relative size of the impedances of these two paths. Furthermore, the cable's total impedance should react to the location of the conductivity path. This is discussed below.



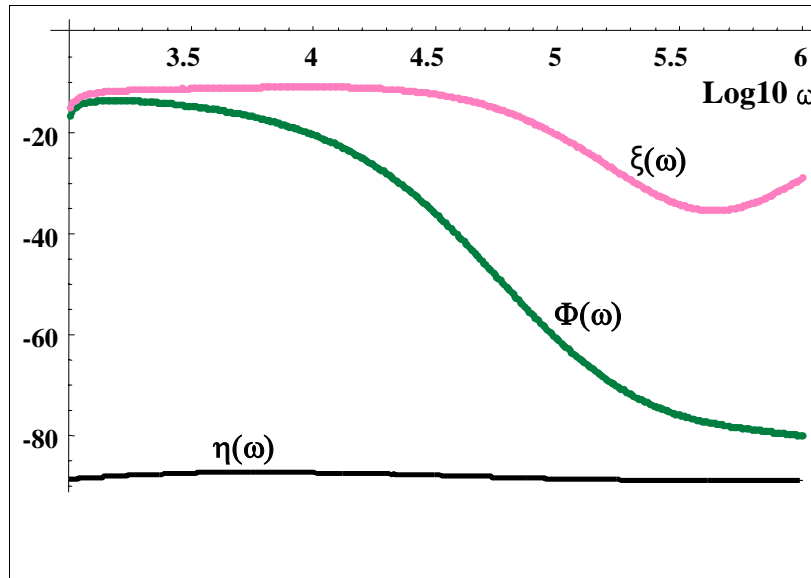
**Figure 78** Impedance magnitude of conductivity path for abraded cable with conductive path between conductors at various locations

Figure 79 compares the impedances of the conductivity path and the cable as a function of frequency for the case in which the location of the conductivity path varies. As shown, at very low frequencies, the magnitude of  $Z_{\text{cable}}(\omega)$  is two to three orders of magnitude larger than  $Z_C(\omega)$  for all locations on the cable. Thus, for frequencies below 1kHz, most of the current flows through the conductivity path and the total impedance is the same as  $Z_C(\omega)$ . At higher frequencies  $Z_C(\omega)$  approaches  $Z_{\text{cable}}(\omega)$ , depending upon the frequency and location of the conductivity path; therefore, more current flows through the cable and less through the conductivity path. In this region, the total impedance approaches  $Z_{\text{cable}}(\omega)$ . At frequencies near 1MHz,  $Z_C(\omega)$  becomes larger than  $Z_{\text{cable}}(\omega)$ , and little current flows through the conductivity path; therefore, the total impedance merges with the impedance  $Z_{\text{cable}}(\omega)$ .

Figure 80 presents the frequency dependence of the impedance phase for the conductivity path,  $\xi(\omega)$ , in the frequency range from 1kHz to 1MHz, along with the impedance phase for the total impedance,  $\Phi(\omega)$ , and the impedance phase of  $Z_{\text{cable}}(\omega)$ ,  $\eta(\omega)$ . As shown, at low frequencies where most of the current flows through the conductivity path,  $\Phi(\omega)$  is approximately equal to  $\xi(\omega)$ . As the frequency increases,  $\Phi(\omega)$  approaches  $\eta(\omega)$ . This is to be expected since the ion particles cannot follow the probe frequency and, therefore, less current flows in the conductivity path. Also, if  $Z_C(\omega_o) \leq Z_{\text{cable}}(\omega_o)$ , where  $\omega_o$  is the operating frequency of the system, a significant portion of the current will flow through the conductivity path and the cable will short.



**Figure 79** Comparison of magnitude for total impedance, interaction impedance, and conductivity path impedance for abraded cable with a conductivity path at various locations



**Figure 80** Comparison of conductivity path impedance phase,  $\xi(\omega)$ , cable impedance phase,  $\eta(\omega)$ , and total impedance phase,  $\Phi(\omega)$ , for abraded cable with a conductivity path

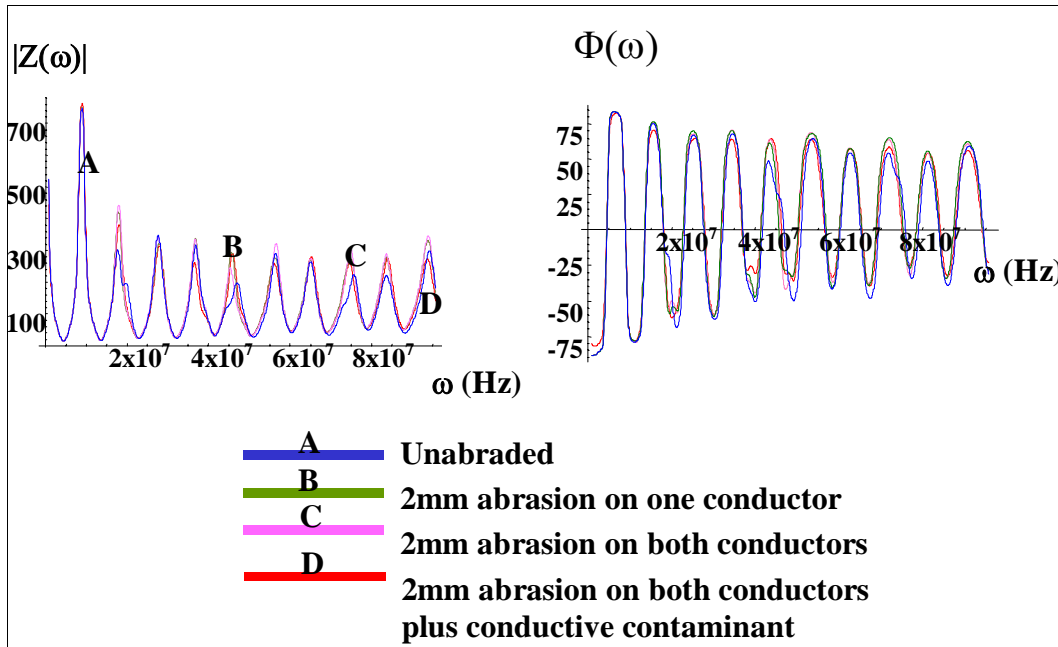
### 5.3.3 Evaluation of High Frequency BIS Results on Cables with Abrasion

This section presents the results of BIS testing in the high frequency range (1MHz to 100MHz) for abraded cables. The same cable test specimens used for the low frequency testing were used for this portion of the research. Phenomenological models of the abraded cables are presented that can be used at high frequency, and are the basis for detecting abrasion on cables. An approach for locating abrasion on cables is also presented.

#### 5.3.3.1 High Frequency Impedance Measurements on Abraded Cables

The open configuration impedance was measured for each of the cables using the Eclipse instrument, as discussed previously. Figure 81 presents the averaged high frequency impedance magnitude and phase spectra for cables with and without abrasion exposed to an environment of 85% RH. The impedance spectra were averaged over a frequency range of  $\pm 800$  MHz to remove small structures in the spectra associated with additional zero crossings. These small structures would prevent an accurate analysis of the spectra. As shown, small but significant changes occur in the impedance spectra when abrasion is present on the cable.

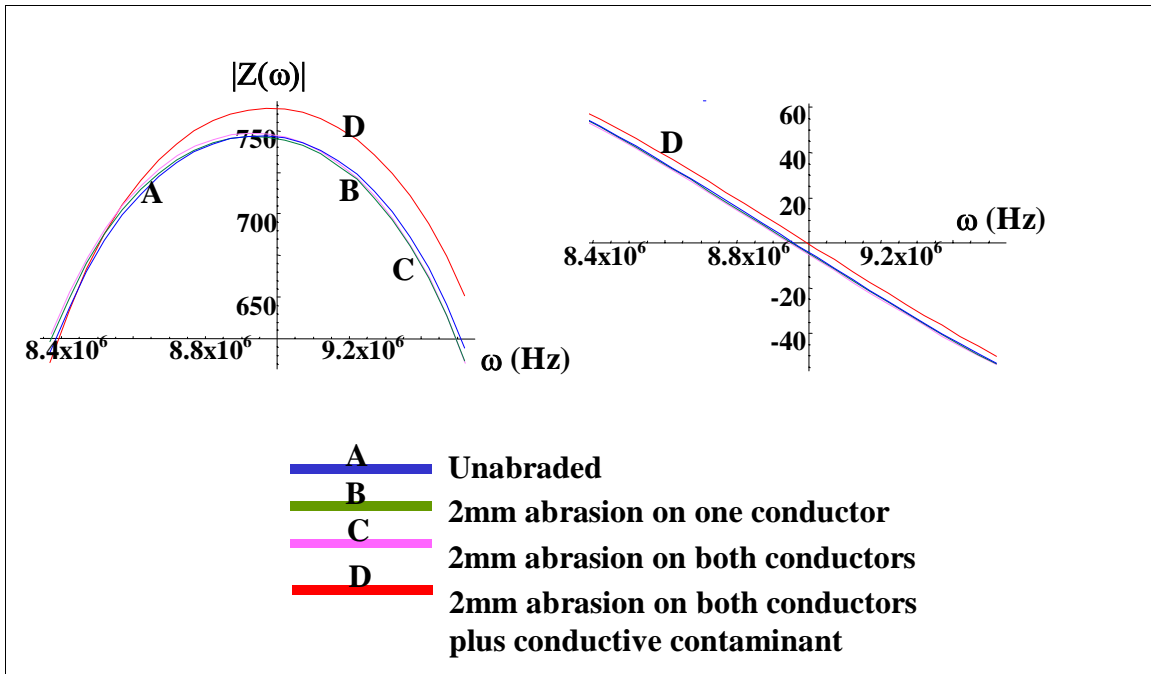




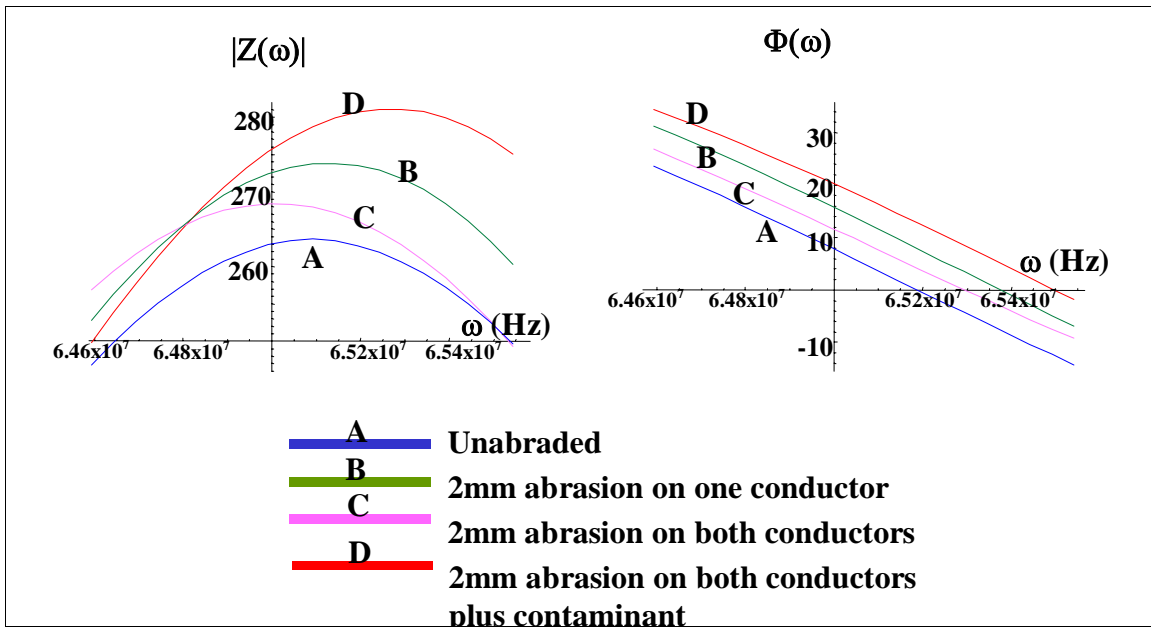
**Figure 81** Comparison of high frequency impedance magnitude and phase spectra for cables with and without abrasion

Figure 82 shows an expanded view of the high frequency impedance magnitude and phase for the frequency range from 8.4 MHz to 9.6 MHz, in the vicinity of the first zero crossing. As shown, the phase zero crossing and the first maxima of the impedance magnitude are shifted to a higher frequency when the cable is abraded. The largest change is observed for the case in which the abrasion is covered by a conductive contaminant, thus establishing a conductivity path.

Figure 83 shows an expanded view of the high frequency impedance magnitude and phase for the frequency range from 64 MHz to 65.5 MHz. As shown, the phase zero crossing and the maxima of the impedance magnitude are again shifted to a higher frequency when the cable is abraded. The changes in this region of the spectra are larger than those in the vicinity of the first zero crossing. This implies that a small portion of the process remains that is due to the iron particles in the contaminant. It is noted that the frequency shift in the zero crossing of the cable with one conductor abraded is larger than that for the cable with both conductors abraded. Thus, there is no simple pattern in these spectra.



**Figure 82** Comparison of high frequency impedance magnitude and phase spectra for the frequency range from 8.4 MHz to 9.6MHz for cables with and without abrasion



**Figure 83** Comparison of high frequency impedance magnitude and phase spectra in the frequency range from 64MHz to 65.5MHz for cables with and without abrasion

### 5.3.3.2 High Frequency Phenomenological Models of Abraded Cables

In Section 5.2 the propagation function for thermally degraded cables was extracted from the high frequency portion of the cable's measured impedance by extrapolating the low frequency characteristic impedance to higher frequencies. However, the extrapolated characteristic impedance exhibited incorrect behavior due to its strong dependence on frequency in the vicinity of 1MHz. While the extracted characteristic impedance is correct, its form does not lend itself to extrapolation.

To model the high frequency response of abraded cables, the high frequency portion of the characteristic impedance is approximated by a constant,  $z_0$ , which is equal to the value of the characteristic impedance at a frequency of 1MHz,  $Z_0(\omega=10^6)$ . The resulting propagation function is given by the following equation:

$$\gamma(\omega) = \frac{1}{l} \text{Coth}^{-1} \left[ \frac{Z_{open}(\omega)}{z_0} \right] \quad 5.3-5$$

Figure 84 presents the extracted imaginary component of the propagation function for the cables with and without abrasion. As shown, only small differences are noted when abrasion is present.

Examination of the real component of the propagation function reveals that, similar to the results for cables with thermal degradation discussed in Section 5.2, the real component of the propagation function exhibits large oscillations that are unphysical in nature and arise from the approximation of the characteristic impedance. To overcome this anomalous behavior, the real component of the propagation function is fitted to the following function:

$$\gamma^r(\omega) = \beta + \delta\sqrt{\omega} \quad 5.3-6$$

where  $\beta$  and  $\kappa$  are fitting constants with the values shown in Table 12.

Figure 85 presents the real component of the propagation function for the cables based on equation 5.3-6. As shown, the abraded cables are similar to the unabraded cables in terms of dissipation; however, when the conductive contaminant is applied, the cable becomes much more dissipative.

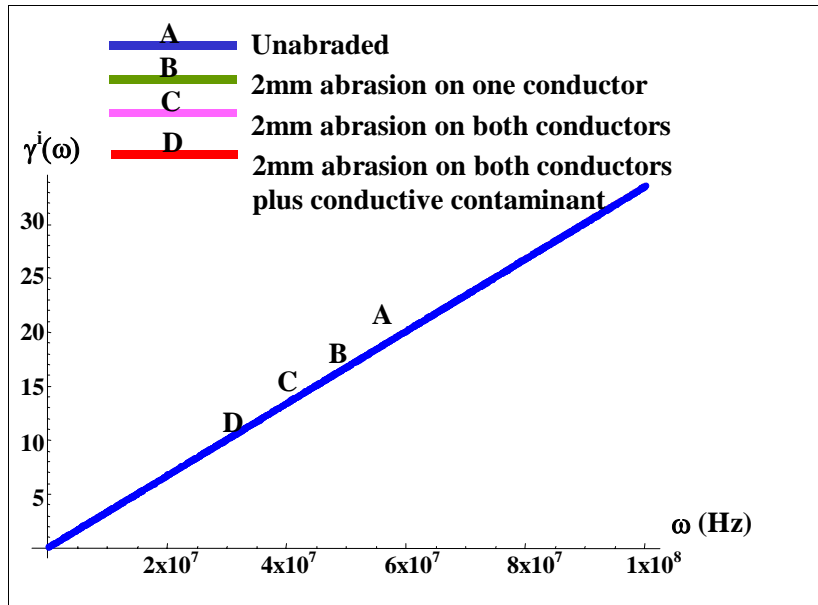


**Figure 84** Imaginary component of the high frequency propagation function for cables with abrasion plus a conductive contaminant

**Table 12** Fitting constants for equation representing the real component of the high frequency propagation function for cables with abrasion plus a conductive contaminant

Case	$\beta$	$\kappa$
A: Unabraded	-0.00380219	0.0115745
B: One Conductor Abraded	-0.00518014	0.0115005
C: Two Conductors Abraded	-0.00552897	0.0116347
D: Two Conductors Abraded Plus Conductive Contaminant	-0.00398439	0.0123597

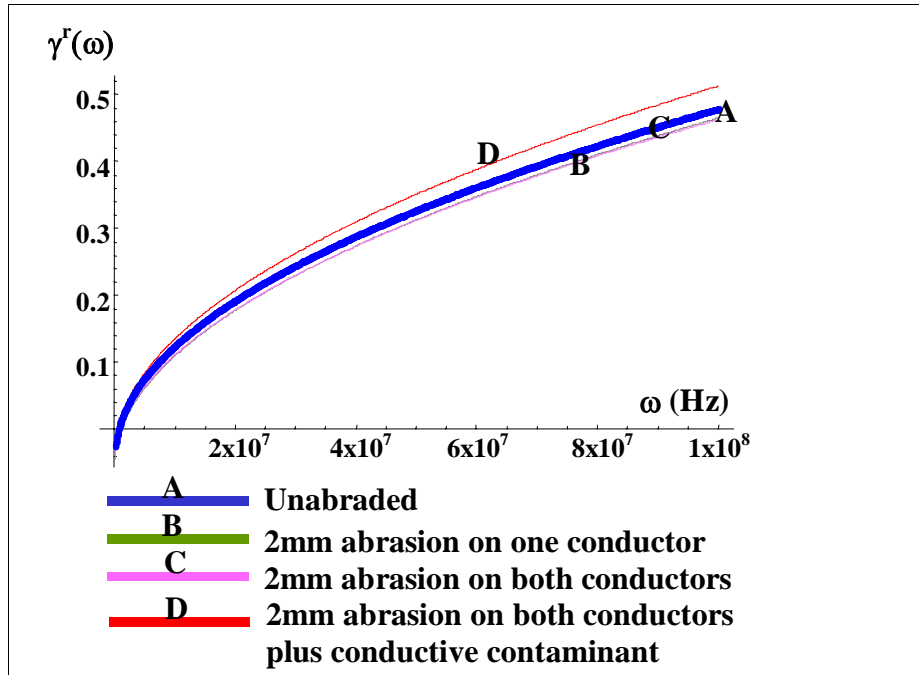


**Figure 85** Real component of the high frequency propagation function for cables with abrasion plus a conductive contaminant

A similar approach is used to model the electrical properties of the abraded cables at high frequencies. The following equations are used:

$$\text{Resistance: } R(\omega) = \beta + \delta\sqrt{\omega} \quad 5.3-7$$

$$\text{Inductance: } L(\omega) = \beta + \frac{\delta}{\omega^{0.05}} \quad 5.3-8$$

$$\text{Capacitance: } C(\omega) = \beta + \frac{\delta}{\omega^{0.05}} + \frac{\alpha}{\omega^{0.5}} \quad 5.3-9$$

$$\text{Conductance: } G(\omega) = \beta + \frac{\delta}{\omega^{0.05}} + \frac{\alpha}{\omega^{0.5}} \quad 5.3-10$$

The values of the fitting constants are presented in Table 13.

**Table 13** Fitting constants for equations representing the high frequency electrical properties of abraded cables

Case	Fitting Constant		
	$\beta$	$\kappa$	$\alpha$
<b><i>Resistance</i></b>			
Case A: Unabraded Cable	0.2	0.005955662	0
Case B: One Conductor Abraded	0.2	0.005955662	0
Case C: Two Conductors Abraded	0.2	0.005955662	0
<b><i>Inductance</i></b>			
Case A: Unabraded Cable	$4.0 \times 10^{-6}$	1.11936	0
Case B: One Conductor Abraded	$4.0 \times 10^{-6}$	1.11936	0
Case C: Two Conductors Abraded	$4.0 \times 10^{-6}$	1.11936	0
<b><i>Capacitance</i></b>			
Case A: Unabraded Cable	$1.86 \times 10^{-10}$	$2.97289 \times 10^{-8}$	$1.04147 \times 10^{-9}$
Case B: One Conductor Abraded	$1.86 \times 10^{-10}$	$1.48645 \times 10^{-8}$	$0.52073 \times 10^{-9}$
Case C: Two Conductors Abraded	$1.86 \times 10^{-10}$	0	0
<b><i>Conductance</i></b>			
Case A: Unabraded Cable	0	$2.97289 \times 10^{-8}$	$3.60049 \times 10^{-11}$
Case B: One Conductor Abraded	0	$1.48645 \times 10^{-8}$	$1.80024 \times 10^{-11}$
Case C: Two Conductors Abraded	0	0	0

The following figures present the electrical properties of the abraded cables as represented by Equations 5.3-7 to 5.3-10.

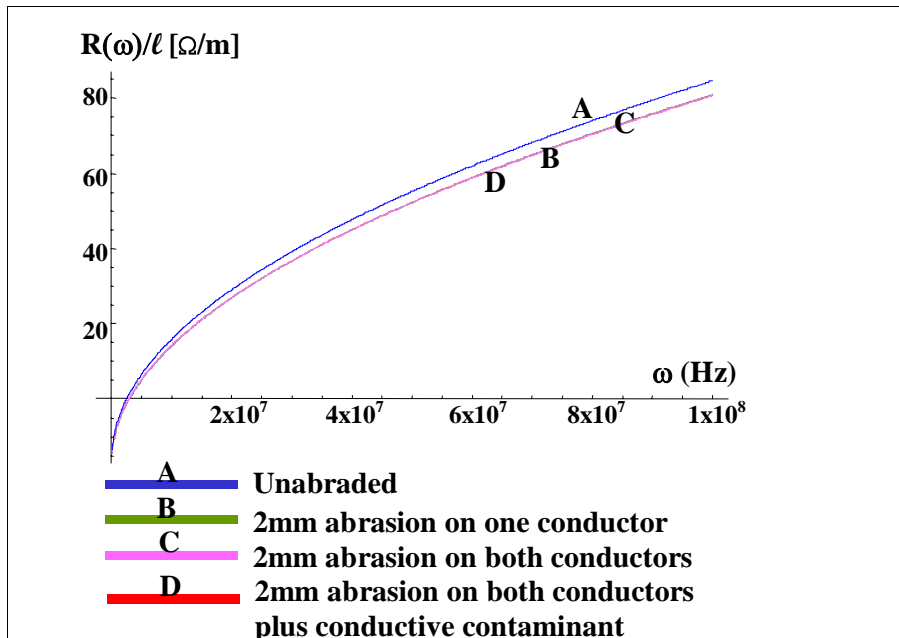


**Figure 86** Resistance spectra for abraded cables in the high frequency range from phenomenological model

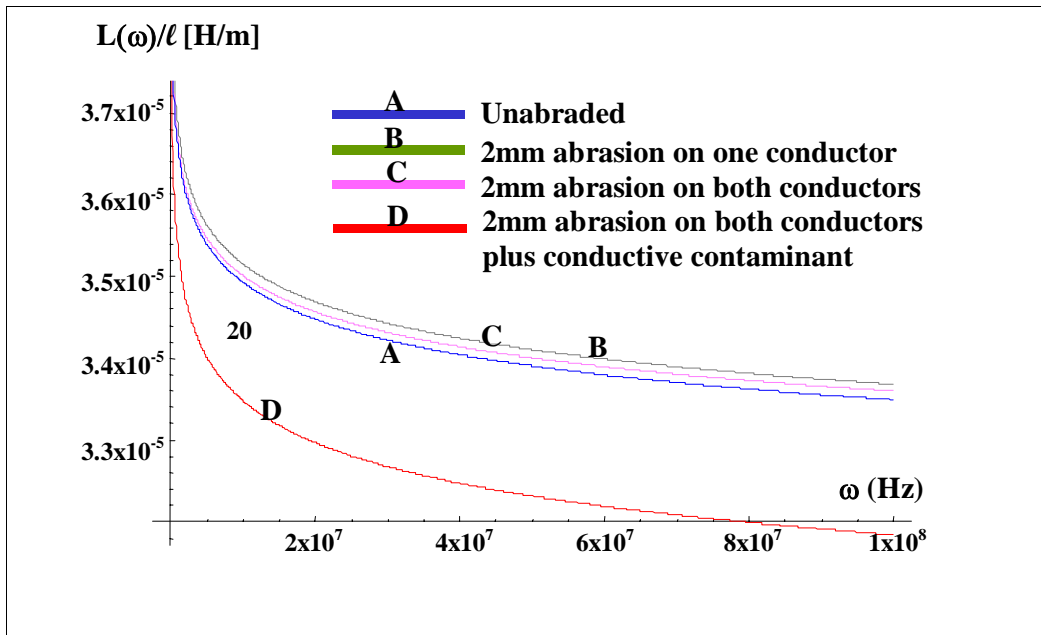


**Figure 87** Inductance spectra for abraded cables in the high frequency range from phenomenological models

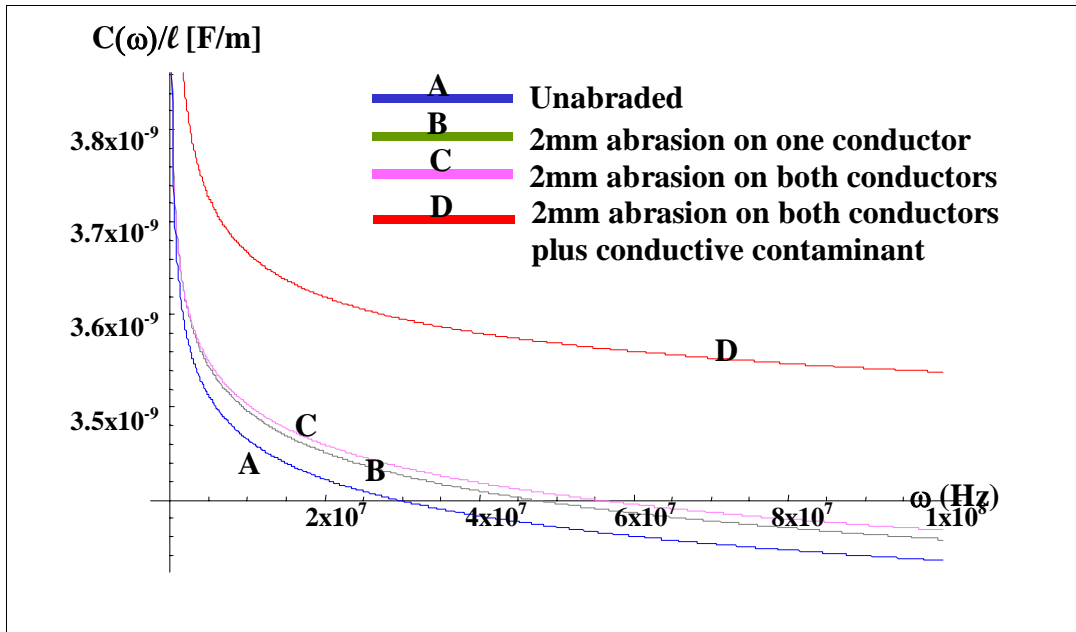


**Figure 88** Capacitance spectra for abraded cables in the high frequency range from phenomenological models

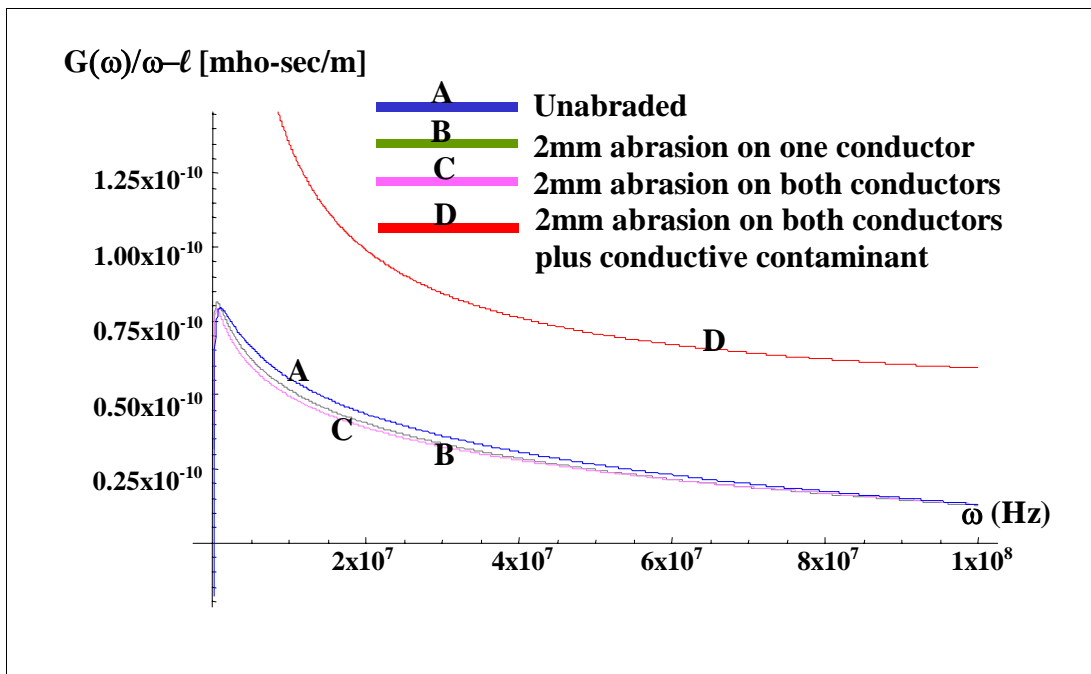


**Figure 89** Conductance spectra for abraded cables in the high frequency range from phenomenological models

### 5.3.4 Detection of Abrasion Damage Using BIS



Two different approaches were developed for the detection of abrasion on cables using BIS. The first involves the properties of the propagation function; specifically the inverse of the velocity of propagation of electrical signals that propagate on the cable,  $v_p^{-1}(\omega)$ , which is defined by the following equation:

$$v_p^{-1}(\omega) \equiv \frac{d\gamma^i(\omega)}{d\omega} \quad 5.3-11$$

The second approach is phenomenological in nature and involves the zero crossings of the second derivative of the impedance phase,  $\Pi(\omega)$ , which is defined by the following equation:

$$\Pi(\omega) \equiv \left\langle \frac{d^2\langle\Phi\rangle}{d\omega^2} \right\rangle \quad 5.3-12$$

In Equation 5.3-12,  $\langle\Phi\rangle$  implies an average of the impedance phase over a frequency range of  $\pm 600\text{kHz}$ .

It can be shown that the slope of  $v_p^{-1}(\omega)$  increases whenever the cable's insulation is abraded. From Equation 5.3-11 the imaginary component of the propagation function is required in the oscillatory region of the frequency spectrum. However, the slope of the extracted parameter exhibits large oscillations that are unphysical in nature. This behavior arises from the approximation used for the cable's characteristic impedance. To overcome this anomalous behavior, the imaginary component of the propagation function is fitted to a linear function, as follows:

$$\gamma^i(x) = \alpha + x \zeta \quad 5.3-13$$

In this equation, discrete  $x$  values from 1 to 2000 replace the continuous frequency spectra,  $\omega$ , over the range from 1MHz to 100MHz. Recall that the impedance measurements were made at 2000 discrete frequencies in the high frequency range. These individual data points correspond to the  $x$  values from 1 to 2000. This approximation ignores the propagation velocity's dispersion. Figure 90 presents the slope of this equation,  $\zeta$ . As shown, the slope for the unabraded cable is smaller than that for any of the abraded cables. As a result the slope for each abraded cable can be compared to the baseline (unabraded) cable as an indicator for the presence of abrasion on the cable. These results imply that the velocity of propagation for electrical signals traveling on the cable decreases when the insulation is abraded.

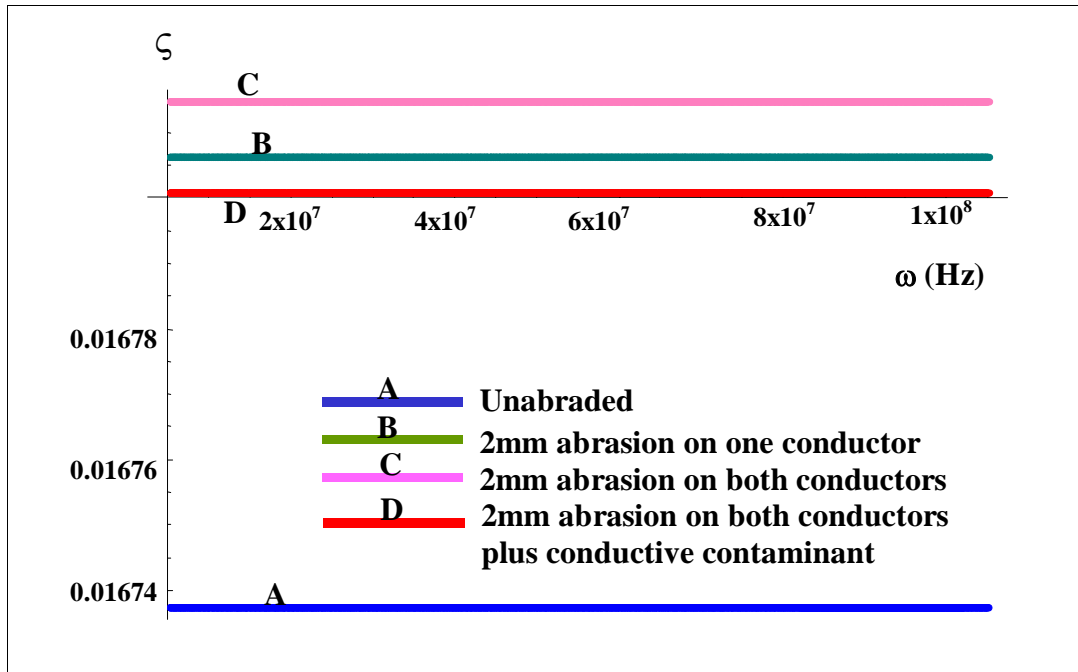


**Figure 90** Slope of the equation representing the imaginary component of the high frequency propagation function for abraded cables

The approach using the zero crossings of the second derivative of the impedance phase,  $\Pi(\omega)$ , to detect abrasion is now discussed. Figure 91 compares the zero crossings of  $\Pi(\omega)$  for the cables with and without abrasion. It is observed that the zero crossings are downshifted to lower frequencies when abrasion is present on the cables. The reason for this behavior is not understood. This behavior is not observed for the impedance phase spectra. In general, the zero crossing of the impedance phase depends upon the product  $[L(\omega) C(\omega)]^{-1/2}$ , and this is true for  $\Pi(\omega)$  as well. However, in the oscillatory region of the frequency spectrum the impedance is dominated by wave phenomena, especially interference. As a result, the behavior of the zero crossings when the cable's properties are changed is complex and cannot easily be explained.

Figure 92 presents  $\Pi(\omega)$  in the frequency range from 4.2MHz to 5.2MHz. As shown the zero crossing of the abraded cables is downshifted relative to the unabraded cable. It is noted that the zero crossing of the abraded cables are the same, despite the differences in the cable's insulation.

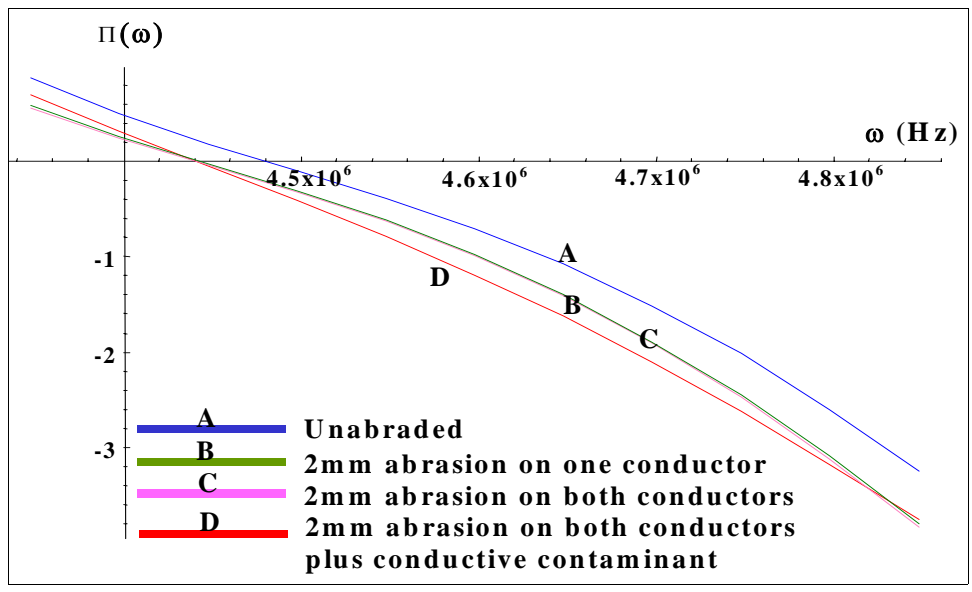


**Figure 91** Comparison of zero crossings in the frequency range 4.4MHz to 4.8MHz for the second derivative of the impedance phase,  $\Pi(\omega)$ , for cables with and without abrasion

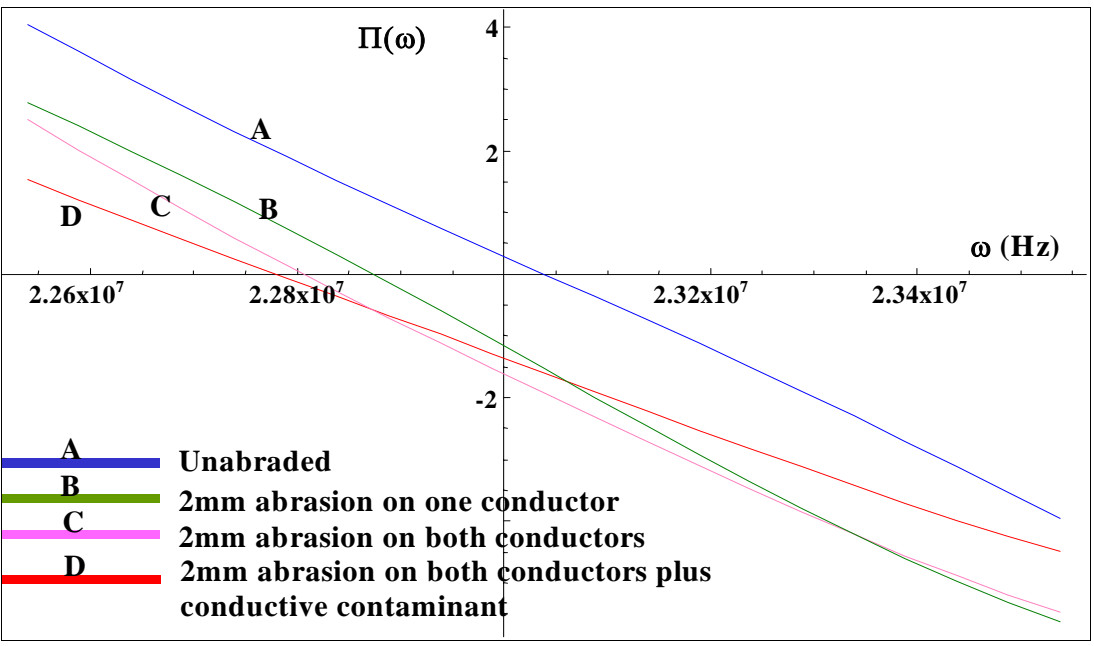


**Figure 92** Comparison of the zero crossings of the second derivative of the impedance phase,  $\Pi(\omega)$ , in the frequency range from 22.4MHz to 23.8MHz for cables with and without abrasion

Similar results were found for other zero crossings examined. These results show that a select number of zero crossings of  $\Pi(\omega)$  can be used to determine if the cable's insulation is abraded. When abrasion is present, the zero crossings for  $\Pi(\omega)$  are downshifted in frequency. For the tests performed in this study, 28 out of 29 zero crossings examined followed this rule.

### 5.3.5 Location of Abrasion Damage Using BIS

The high frequency phenomenological models developed previously for abraded cables are not useful for locating this damage. This is due to the following observation. The cable insulation's dielectric function follows the fractional power law for dielectric materials, which is:

$$\varepsilon(\omega) = \varepsilon_0 \left( 1 + \frac{A_1}{(1 + (i\omega\tau_1)^{n_1})} + \frac{A_2}{(1 + (i\omega\tau_2)^{n_2})} + \frac{A_3}{(1 + (i\omega\tau_3)^{n_3})} \right) \quad 5.3-14$$

The first term in the above equation refers to ionic processes, while the second and third terms refer to electronic processes that contribute to the cable insulation dielectric function. Here,  $\varepsilon_0$  is the dielectric function of vacuum, and  $A_1$ ,  $A_2$  and  $A_3$  refer to various micro processes that dominate the insulation's dielectric function. When a portion of the insulation is abraded down to the metallic conductor, the parameters  $A_1 = A_2 = A_3 = 0$ , and  $\varepsilon(\omega) = \varepsilon_0$ . The phenomenological models developed previously deal with the capacitance between two conductors in a cable via the structure factor,  $\Lambda$ , and knowledge of this structure factor is imprecise. Therefore, a model is required that includes knowledge of all the parameters contained in the cable's capacitance. Also, if only one of the wires is abraded, then the capacitance per unit length and conductance per unit length are given by the following equation:

$$G(\omega) + i\omega C(\omega) = \Lambda \varepsilon_0 \left( 1 + \frac{\frac{1}{2}A_1}{(1 + (i\omega\tau_1)^{n_1})} + \frac{\frac{1}{2}A_2}{(1 + (i\omega\tau_2)^{n_2})} + \frac{\frac{1}{2}A_3}{(1 + (i\omega\tau_3)^{n_3})} \right) \quad 5.3-15$$

If both of the conductors are abraded to the metallic conductor (thus there is no insulation present), the capacitance per unit length and conductance per unit length are given by the following equation:

$$G(\omega) + i\omega C(\omega) = \Lambda \varepsilon_0 \quad 5.3-16$$

The phenomenological models developed previously cannot accurately represent this scenario.

As such, at high frequencies the following models for resistance per unit length and inductance per unit length can be used:

$$R(\omega) = R_0 \left( 1 + \sqrt{\frac{\omega}{\omega_s}} \right) \quad 5.3-17$$

$$L(\omega) = L_0 \left( 1 - 0.5 \frac{(\omega/\omega_1)^{n_1}}{1 + (\omega/\omega_1)^{2n_1}} \right) \quad 5.3-18$$

At high frequencies the inoic portion of  $\epsilon(\omega)$  can be ignored since the ions are too slow to react to the high frequency fields, and the fractional power law for the insulation's dielectric function reduces to the following equation:

$$\epsilon(\omega) = \Lambda \epsilon_0 \left( 1 + \frac{A_2}{(1 + (i \omega \tau_2)^{n_2})} + \frac{A_3}{(1 + (i \omega \tau_3)^{n_3})} \right) \quad 5.3-19$$

For a cable with a twisted pair of conductors, the structure factor becomes:

$$\Lambda = \frac{\pi}{\text{Arc Coth}\left(\frac{s}{d}\right)} \quad 5.3-20$$

Here “s” is the distance between the centers of the conductors and “d” is their diameter. The various constants in the above equations arise from various physical processes. At high frequencies the cable's resistance is dominated by the skin effect and Equation 5.3-17 is the asymptotic form of the skin effect, with  $\omega_s$  being the skin frequency. The various constants can be determined by obtaining the cable's characteristic impedance and propagation function from the measured impedance spectra, and then calculating the open configuration impedance using assumed values for the constants. The measured impedance can then be compared to the calculated impedance and the error calculated. Using an iterative process, the final value of the constants can be determined by minimizing the rms error between the calculated impedance and the measured impedance.

For the unabraded cable (Specimen 15) the best fit values for the constants are the following:

Resistance per unit length:  $R_0 = 0.02\Omega/\text{m}$   
 $\omega_s = 28.183\text{kHz}$

Inductance per unit length  $L_0 = 4.1\mu\text{H}/\text{m}$   
 $\omega_1 = 10\text{MHz}$   
 $n_1 = 0.275$

Dielectric Function  $\Lambda\epsilon_0 = 0.185\text{nF}/\text{m}$

$$A_2 = 1.2, \tau_2 = 2.82\mu\text{s}, n_2 = 0.5$$

$$A_3 = 3.94, \tau_3 = 0.1\mu\text{s}, n_3 = 0.022$$

The characteristic impedance and propagation function are then calculated using Equations 3.2-1a and 3.2-1b. The open configuration impedance is then calculated using Equation 3.2-7a.

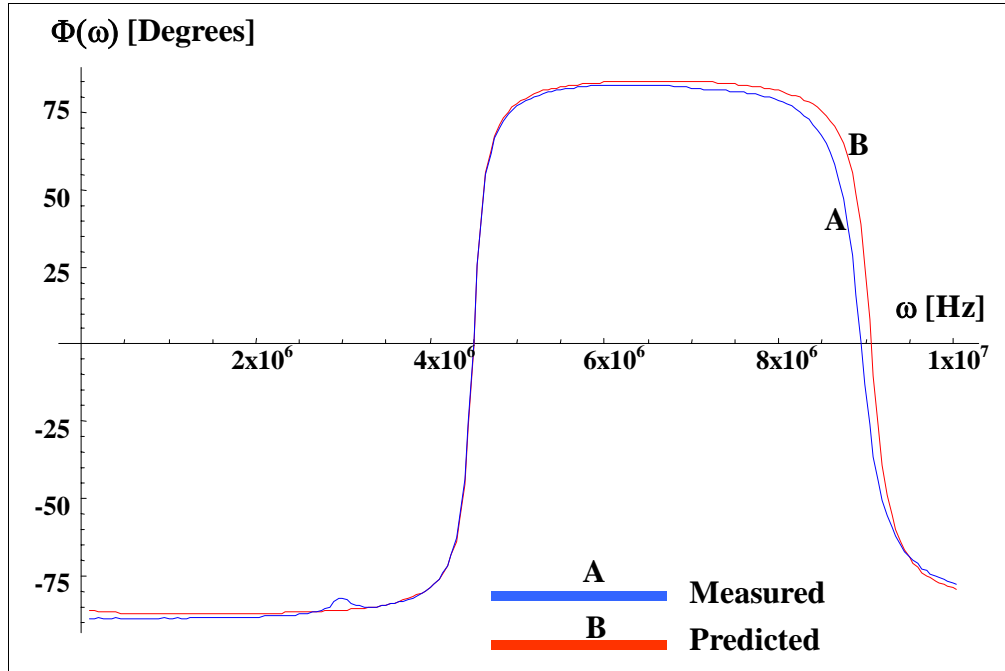


**Figure 93** Comparison of predicted and measured impedance phase in the range from 2.55MHz to 10.04MHz for unabraded cable (Specimen 15)

Figure 94 compares the cable impedance phase predicted by the model to the measured impedance. The rms error of the impedance phase is 4.76%, indicating good agreement between the predicted and measured values. As shown, the impedance phase predicted by the model deviates slightly from the measured impedance after the first zero crossing. Also, there is a small deviation between the model and the measured values in the vicinity of 1MHz to 2MHz. Since the model was developed in the frequency range from 2.55MHz to 10.04MHz it is not surprising that deviations appear outside this range.

Figure 94 compares the cable impedance magnitude predicted by the model to the measured impedance. Again, good agreement is observed between the predicted and measured values.

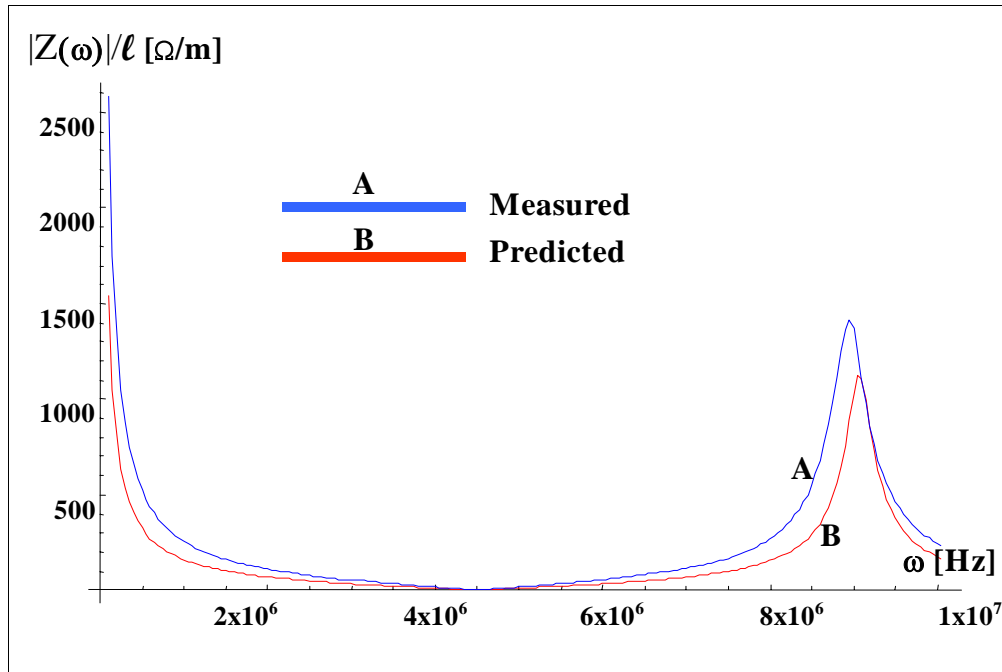


**Figure 94** Comparison of predicted and measured impedance magnitude in the range from 2.55MHz to 10.04MHz for unabraded cable (Specimen 15)

Next, the characteristic impedance and propagation function for cables with one or both conductors abraded is determined. This is useful since the abraded cable is modeled as if it is in two states; 1) the conductor has all of its insulation (i.e., unabraded), and 2) the conductor is bare.

Figures 95 and 96 present the characteristic impedance magnitude and phase in the frequency range from 2.55MHz to 10.04MHz for the cables with and without abrasion. As shown, the characteristic impedance magnitude increases when the insulation is abraded. The characteristic impedance phase decreases when the insulation is abraded.

Figures 97 and 98 present the imaginary and real components of the propagation function in the frequency range from 2.55MHz to 10.04MHz for the cables with and without abrasion. In all cases the behavior of the propagation function is as expected in light of the fact that the cable's capacitance and conductance decrease when the insulation is abraded.

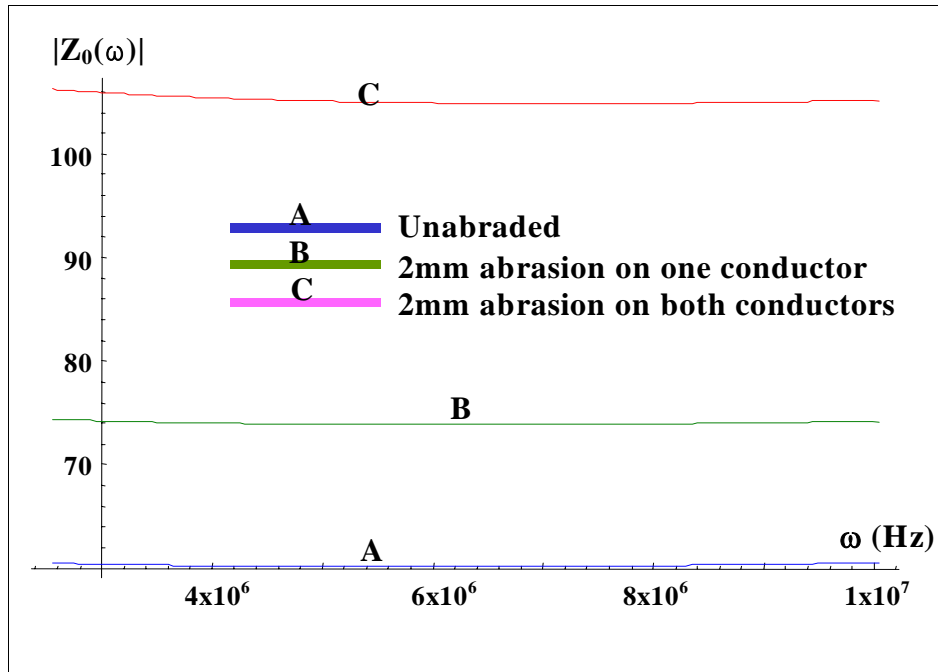


**Figure 95** Characteristic impedance magnitude in the frequency range from 2.55MHz to 10.04MHz for cables with and without abrasion

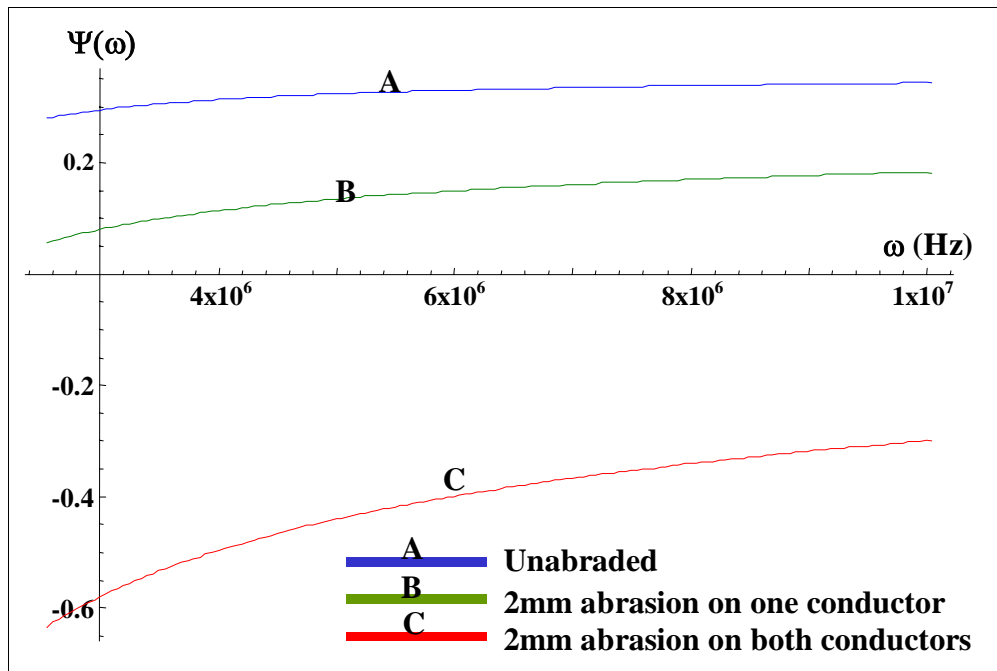


**Figure 96** Characteristic impedance phase spectra in the frequency range from 2.55MHz to 10.04MHz for cables with and without abrasion



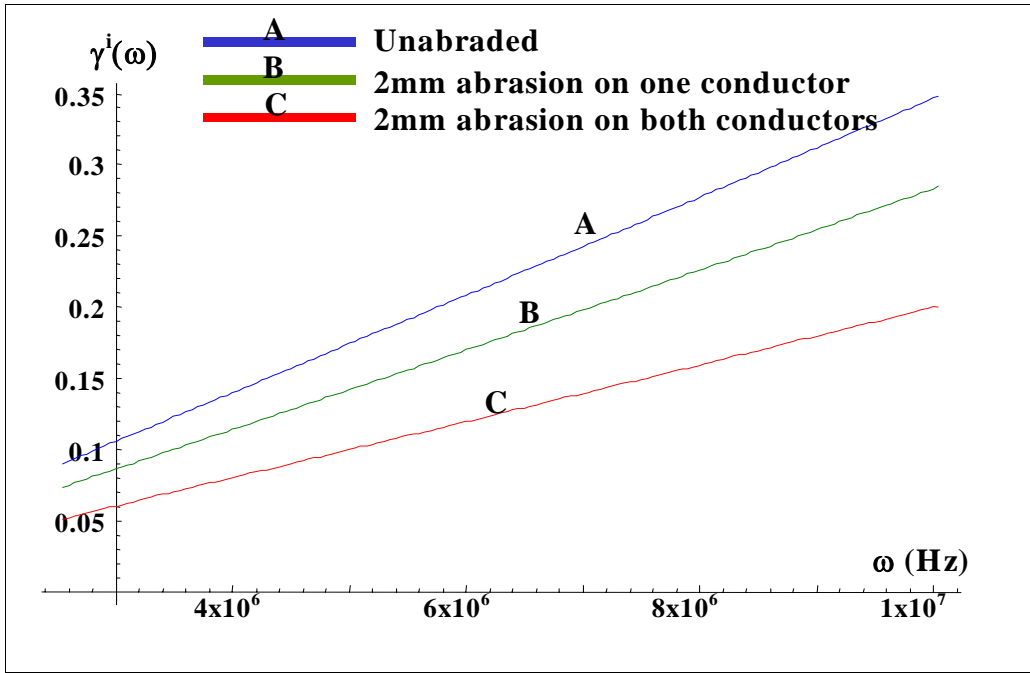


**Figure 97** Imaginary component of the propagation function in the frequency range from 2.55MHz to 10.04MHz for cables with and without abrasion

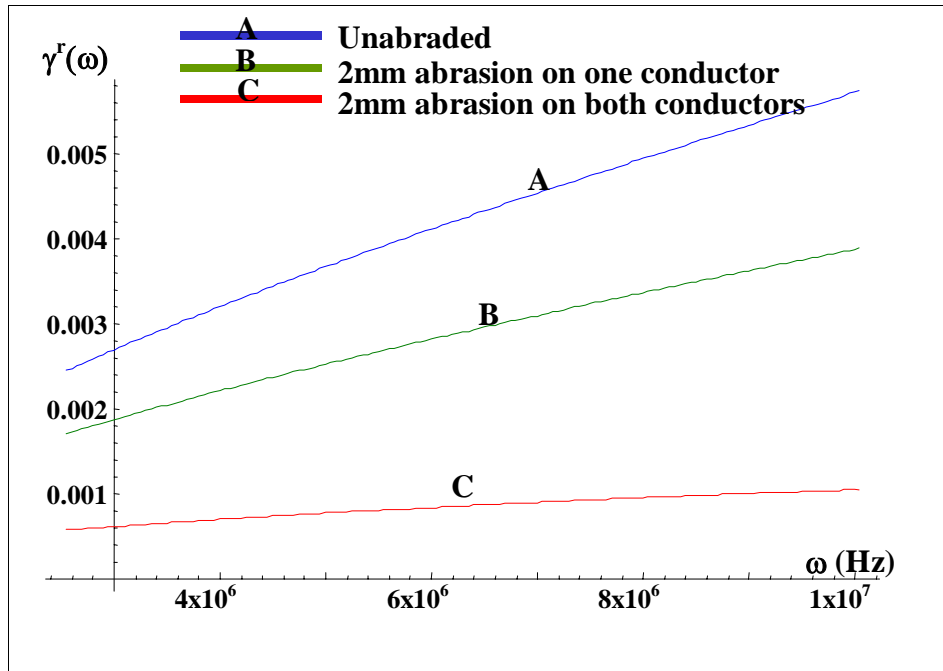


**Figure 98** Real component of the propagation function in the frequency range from 2.55MHz to 10.04MHz for cables with and without abrasion

In this section, an approach for locating abrasion damage is presented using the cable models developed in the previous section. Specifically, two cases are evaluated; 1) a cable with the insulation abraded on one conductor, and 2) a cable with the insulation abraded on both conductors. In both cases, the models are able to predict the location of the abrasion within 10%.

The approach used is the same as that used to locate insulation damage when the cable is thermally aged, which is discussed in Section 5.2. As such, different models are developed for each of the two cases being studied.

### 5.3.5.1 Model for Cable with One Conductor Abraded

The scenario evaluated here is depicted in Figure 44 as Case B. A 2mm (0.08in.) length of insulation is abraded from one conductor in the middle of the cable. The total cable length is 10m (393.7in.) and the start and end points of the abraded section are labeled  $l_a$  and  $l_b$ , respectively. The cable is not shorted at the point of abrasion.

For this case, the abraded cable is in two states; the abraded portion is in a “damaged” state, and the unabraded portion is in a “healthy” state. The model for the impedance of the cable is represented by the following equation:

$$Z_{model}(\omega) = Z_{0,h}(\omega) \frac{Z_{0,h}(\omega) \text{Coth}[\gamma_h(\omega)(l - l_a)] + Z_{0,d}(\omega) \text{Tanh}[\gamma_d(\omega)(l_b - l_a)]}{Z_{0,d}(\omega) + Z_{0,h}(\omega) \text{Coth}[\gamma_h(\omega)(l - l_b)] \text{Tanh}[\gamma_d(\omega)(l_b - l_a)]} \quad 5.3-21$$

In Equation 5.3-21, the subscript “d” refers to the cable property in the damaged state, and the subscript “h” refers to the cable property in the healthy state. The parameter “ $l$ ” is the total length of the cable. This model will be used together with the measured impedance to locate the abrasion damage on the cable.

Figure 99 presents the measured impedance phase spectra in the frequency range from 4.048MHz to 15.04MHz for the cables with and without abrasion. As shown, the cables are very similar with small differences in the spectra after the first zero crossing. These differences are on the order of the deviations observed between the models presented in the previous section.

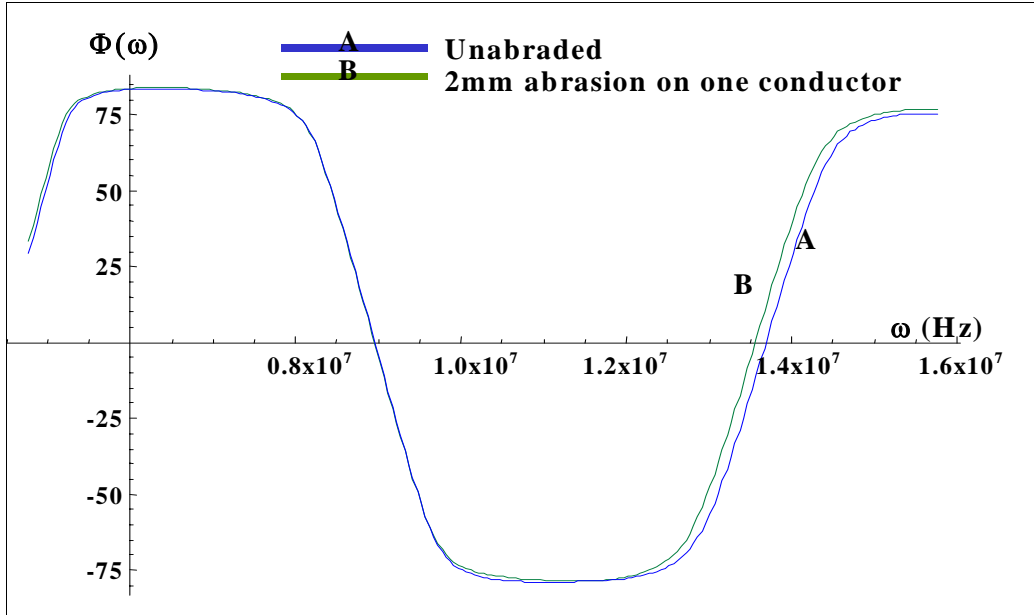


**Figure 99** Measured impedance phase spectra in the frequency range from 4.048MHz to 15.04MHz for cables with and without abrasion on one conductor

To locate the abrasion damage on the cable, the following procedure is used:

- Calculate the impedance of the cable using Equation 5.3-21 and an assumed location for the abrasion
- Compare the calculated impedance to the measured impedance and compute the rms error in the values at each data point
- Using an iterative process, assume new locations for the abrasion along the cable and compute the rms error between the predicted and measured impedance for each location
- The location that minimizes the rms error is the predicted location of the abrasion

For this example, abrasion locations were assumed every 1 meter (39.37in.) along the cable. The impedance phase values were compared at discrete frequencies in the range from 4.048MHz to 15.04MHz. The error in the predicted phase values was computed using the following equation:

$$\langle \delta \Phi \rangle = \frac{\sum_{\omega_n=4.048\text{MHz}}^{\omega_n=15.04\text{MHz}} |\Phi_{\text{Model}}(\omega_n, \ell_b) - \Phi_{\text{Measured}}(\omega)|}{\sum_{\omega_n=4.048\text{MHz}}^{\omega_n=15.04\text{MHz}} |\Phi_{\text{Measured}}(\omega)|} \quad 5.3-22$$

In this example, the model predicts that the abrasion is located at 6 meters from the end of the cable and the correct location is 5 meters. Figure 100 presents the results of the error calculations showing the minima at 6 meters, which represents the predicted damage location. It is noted that the error at this predicted location is 8.55%.

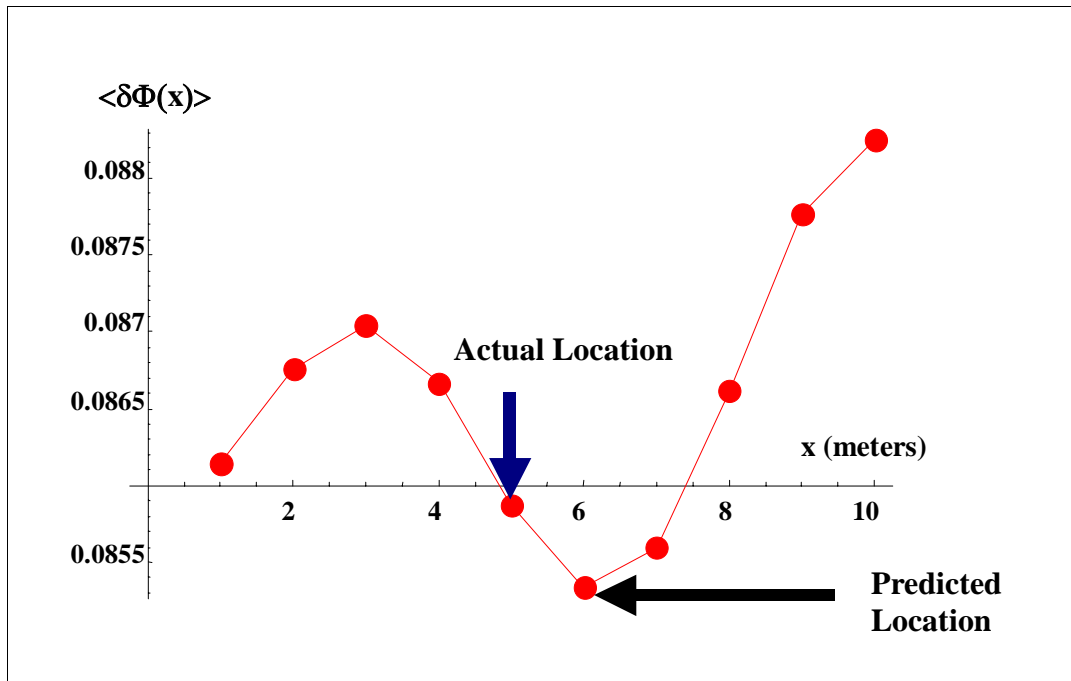


**Figure 100** Predicted location of abrasion damage for cable with one conductor abraded

### 5.3.5.2 Model for Cable with Two Conductors Abraded

The scenario evaluated here is depicted in Figure 44 as Case C. A 2mm (0.08in.) length of insulation is abraded from both conductors in the middle of the cable. The total cable length is 10m (393.7in.) and the start and end points of the abraded section are labeled  $\ell_a$  and  $\ell_b$ , respectively. The cable is not shorted at the point of abrasion.

Figure 101 presents the measured impedance phase spectra in the frequency range from 4.048MHz to 15.04MHz for the cables with and without abrasion. As shown, the cables are very similar with small differences in the spectra before the first zero crossing and in the region before and after the third zero crossing. Again, these differences are on the order of the deviations observed between the models presented previously.

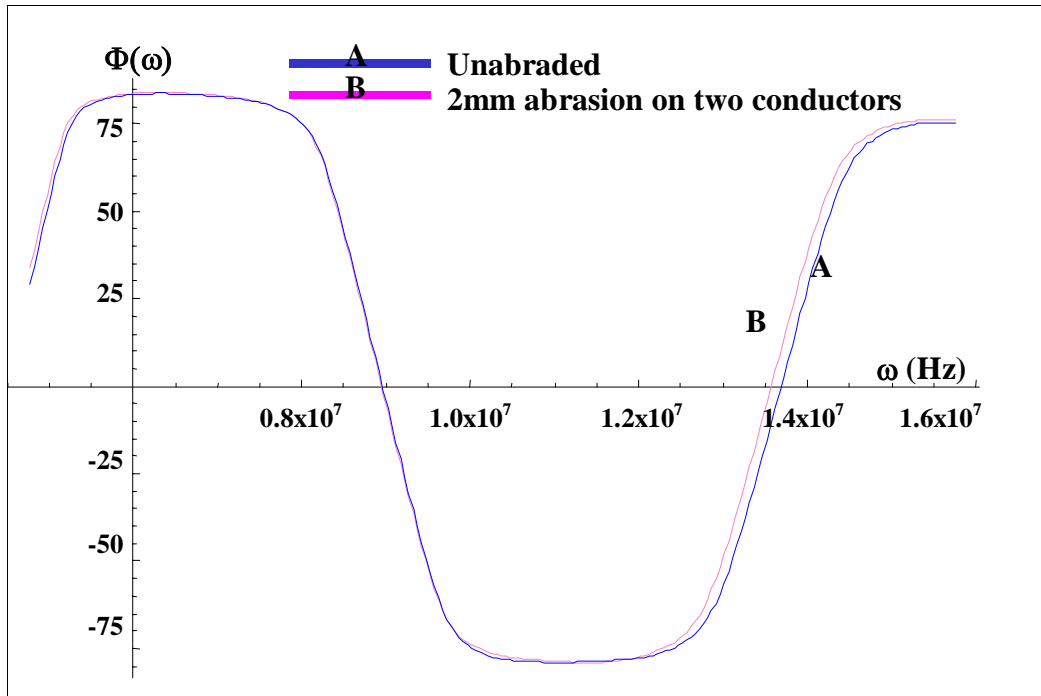


**Figure 101** Measured impedance phase spectra in the frequency range from 4.048MHz to 15.04MHz for cables with and without abrasion on both conductors

Using the appropriate characteristic impedance and propagation function, the iterative process described previously in this section was used to predict the location of the abrasion. The results predict a location of 6 meters, while the correct location is 5 meters. Figure 102 presents the error calculations and the predicted versus actual location of the abrasion.

These results demonstrate the BIS method can be used to predict the location of abrasion damage with relatively good accuracy.

#### 5.4 Application of BIS to Cables with Cracking Damage

Cracking of the insulation on aged cables is a potential problem in nuclear power plants since it can lead to leakage currents that may cause the system to fail. This is particularly true under humid or wet conditions, during which moisture can enter the crack and create a conductive path between the cable conductor and ground. Therefore, it is desirable for a condition monitoring technique to be able to detect and locate cracking in cables.

In this section, the BIS method is evaluated for its ability to detect and locate cracking damage on cables.

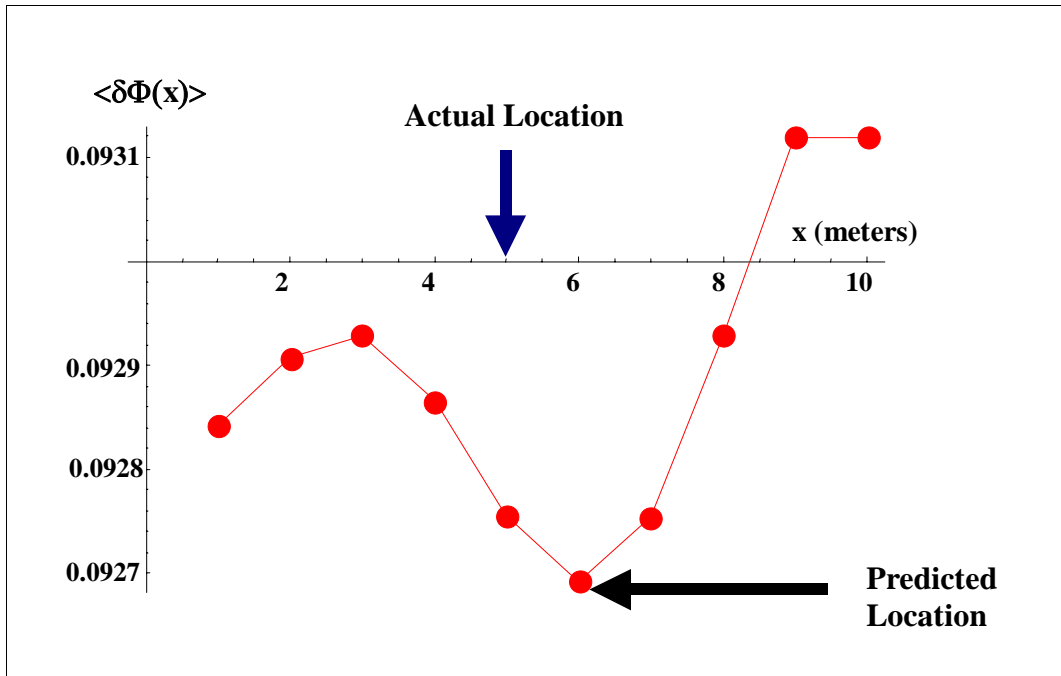


**Figure 102** Predicted location of abrasion damage on cable with both conductors abraded

#### 5.4.1 Test Specimens Used for Testing of Cables with Cracking

For this portion of the research, unaged cables were used. To simulate the cracking damage a knife was used to slice the insulation on both conductors of the cable. A total of 12 simulated cracks were placed on the cable over a length of 2.54 cm (1in.). The crack location was 4 meters from the left end of the cable. Figure 103 shows a schematic of the scenario evaluated.

Baseline impedance measurements were obtained using the Eclipse instrument and the HP instrument. Measurement parameters used were a 1-Volt oscillation level, medium integration time, and 4-samples of averaging. High frequency measurements were collected at 2000 discrete frequency points between 1MHz and 100MHz. Low frequency measurements were collected at logarithmically spaced points over the frequency range from 1kHz to 1MHz. Measurements were made with the conductors in both the open and the shorted configuration, and from both ends of the cable. The cable was coiled and placed in a humidity chamber that was maintained at 60%RH and 30°C for all measurements.

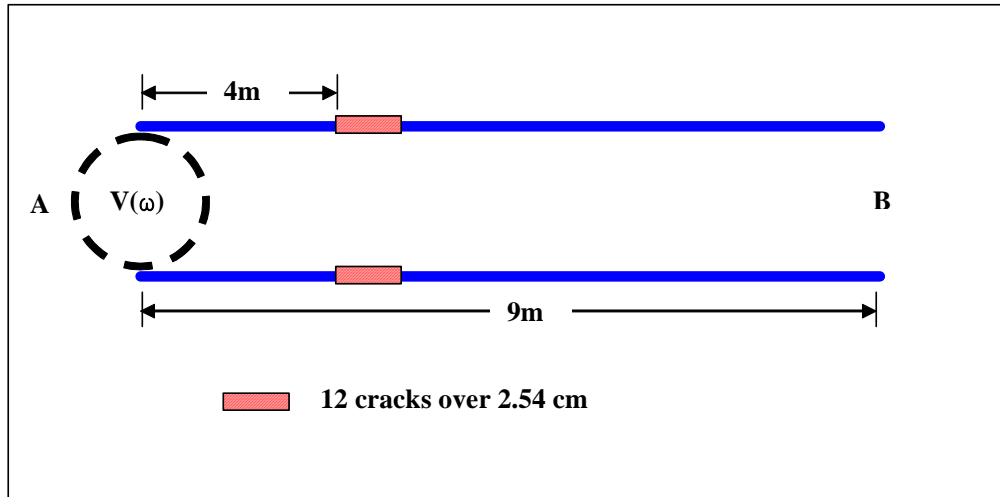


**Figure 103** Schematic of cable with cracking damage

After baseline impedance measurements were made, the cable was removed from the environmental chamber and 12 cracks were simulated on each conductor of the cable. Each simulated crack was equally spaced at 0.21mm, with a width of 0.1mm. The cracks were first made to a depth of 50% of the insulation thickness and measurements were made. A conductive contaminant consisting of 85% Skydrol hydraulic fluid, 11% iron particles, and 4% carbon black powder was applied to the cracked portion of the cable and the impedance measurements were repeated. The cracks were then extended completely through the insulation (100%) and additional conductive contaminant was applied, after which the impedance measurements were again performed. Thus, four sets of impedance measurements were made on the cable.

#### **5.4.2 Low Frequency BIS Measurements of Cables with Cracking**

Figure 104 compares the impedance phase spectra in the low frequency range from 1kHz to 1MHz for cables with and without cracking. As shown, there is only a small difference between the uncracked cable and the cable with cracks. Even the conductive path does not appear to impact the impedance phase. This can be attributed to the lack of a conductivity path between the conductors, even with the conductive contaminant applied. A possible reason for this is the size of the iron filings used, which were on the order of 100 $\mu$ . This is approximately the same dimension as the crack width. Thus, it is believed that the iron particles could not enter the crack and make a connection with the cable conductor.

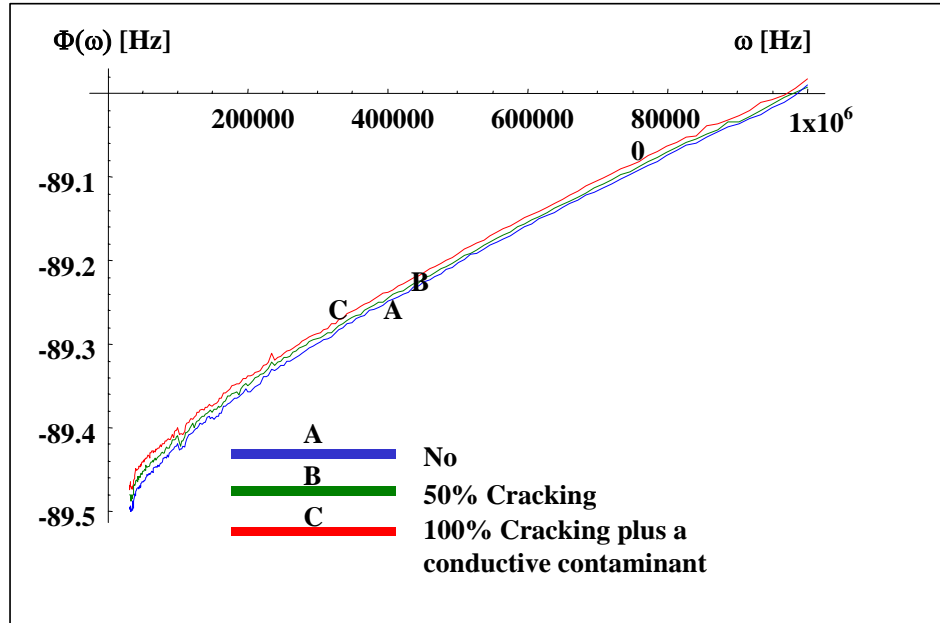


**Figure 104** Comparison of impedance phase for cables with and without cracking

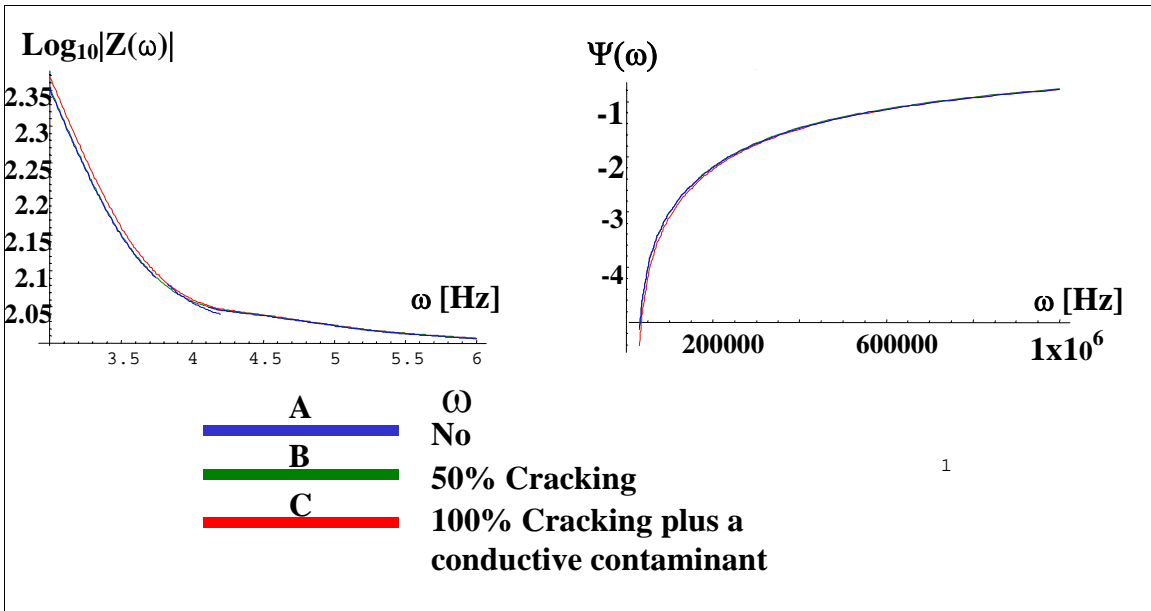
Although the differences in the impedance spectra are very small, the data were analyzed to determine the spatially averaged electrical properties of the cable. Figures 105 and 106 present the characteristic impedance magnitude and phase spectra, and the propagation function, respectively, for the cable with and without cracking. As shown, only small differences are observed between the cable with no cracking and the cable with cracking.

Figure 107 compares the resistance per unit length for the cable with and without cracking. As shown the resistance per unit length does not change when the cable contains cracks, even when a conductive contaminant is applied to the cracks.

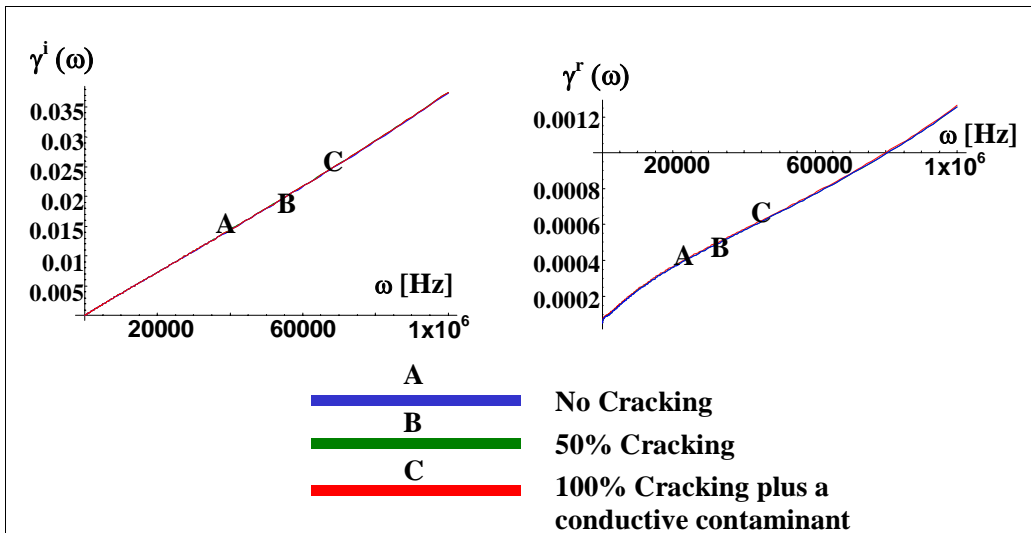
Figure 107 compares the inductance per unit length for the cable with and without cracking. As shown the inductance per unit length increases slightly when the cable contains cracks and a conductive contaminant is applied to the cracks. This change is more apparent near the upper end of the low frequency region.

Figure 108 compares the capacitance per unit length for the cable with and without cracking. As shown the capacitance per unit length increases slightly when the cable contains cracks and a conductive contaminant is applied to the cracks. This change is also more apparent near the upper end of the low frequency region. It is observed that the capacitance per unit length for the cable with cracking but no conductive contaminant was higher than the baseline cable with no cracking, and the cable with cracking plus a conductive contaminant.





**Figure 105** Characteristic impedance log magnitude and phase for cables with and without cracking



**Figure 106** Imaginary and real components of the propagation function for cables with and without cracking

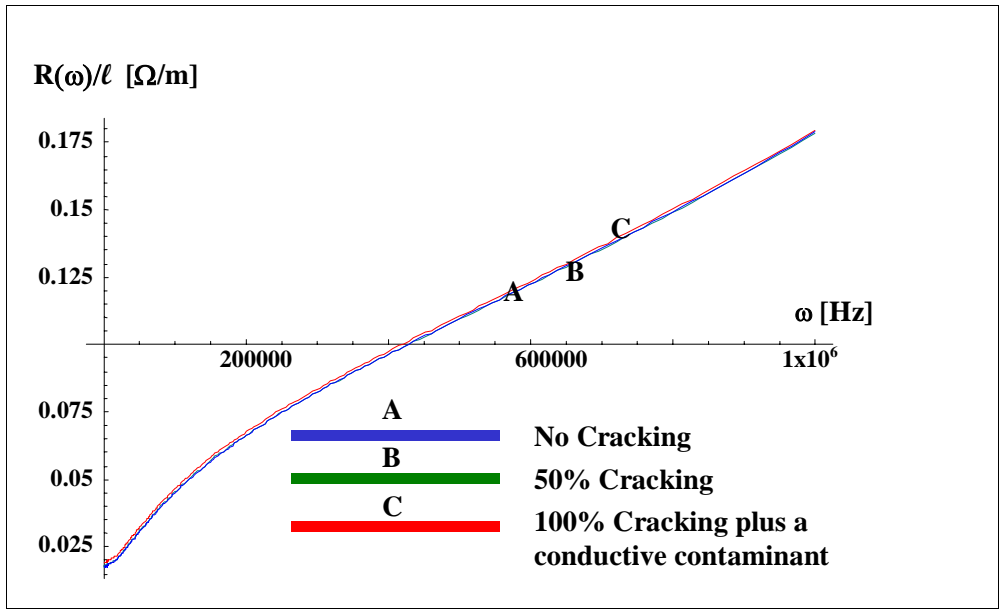


**Figure 107** Resistance per unit length for cables with and without cracking

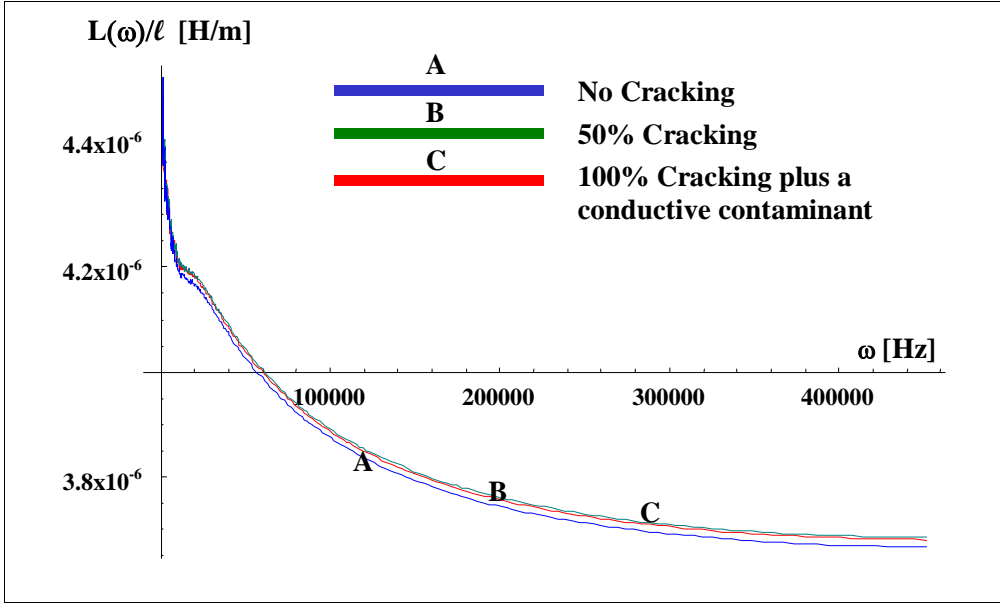


**Figure 108** Inductance per unit length for cables with and without cracking

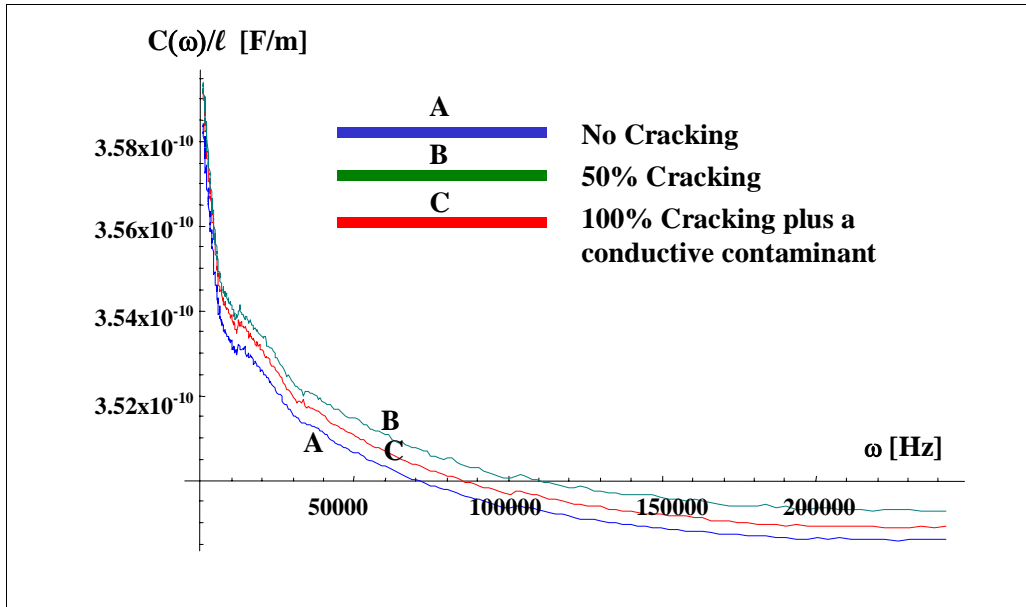


**Figure 109** Comparison of capacitance per unit length for cable with and without cracks

Figure 110 compares the conductance per frequency per unit length for the cable with and without cracking. As shown the conductance per unit length increases slightly when the cable contains cracks and a conductive contaminant is applied to the cracks. This change is also more apparent near the upper end of the low frequency region. It is observed that the capacitance per unit length for the cable with cracking but no conductive contaminant was higher than the baseline cable with no cracking, and the cable with cracking plus a conductive contaminant.

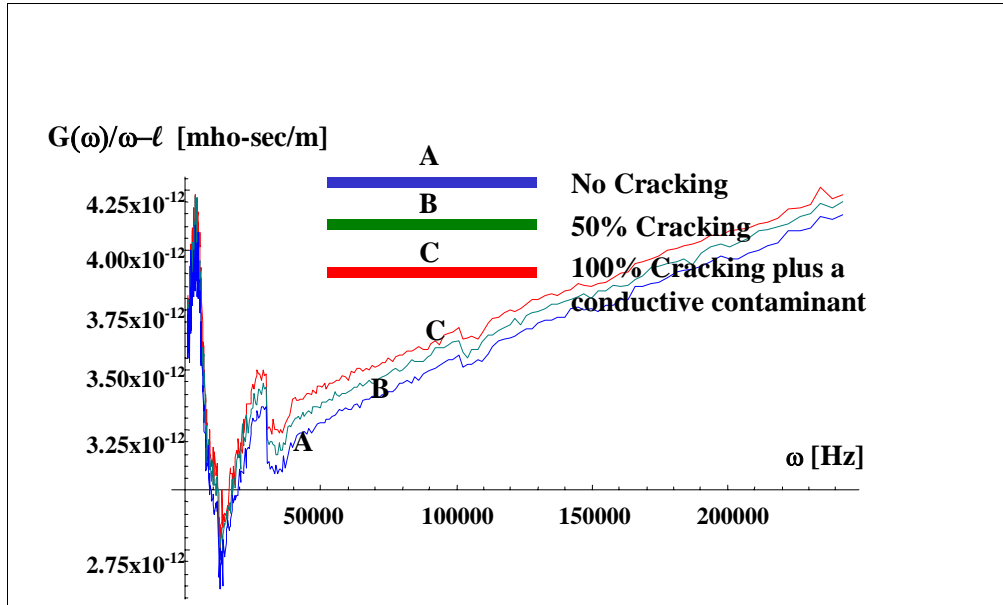
### 5.4.3 High Frequency BIS Measurements of Cables with Cracking

In this section the high frequency impedance spectra of the cable test specimens is analyzed to develop an approach for detecting cracking on cables. Specifically, a similar approach to that used in Section 5.2 for evaluating attached loads is used here in which the zero crossings of the second derivative of the impedance phase spectra,  $\Pi(\omega)$ , are examined for differences. These differences are then used as indicators for the presence of cracking. The development and definition of the parameter  $\Pi(\omega)$  was presented previously in Equations 5.2-1 through 5.2-3.

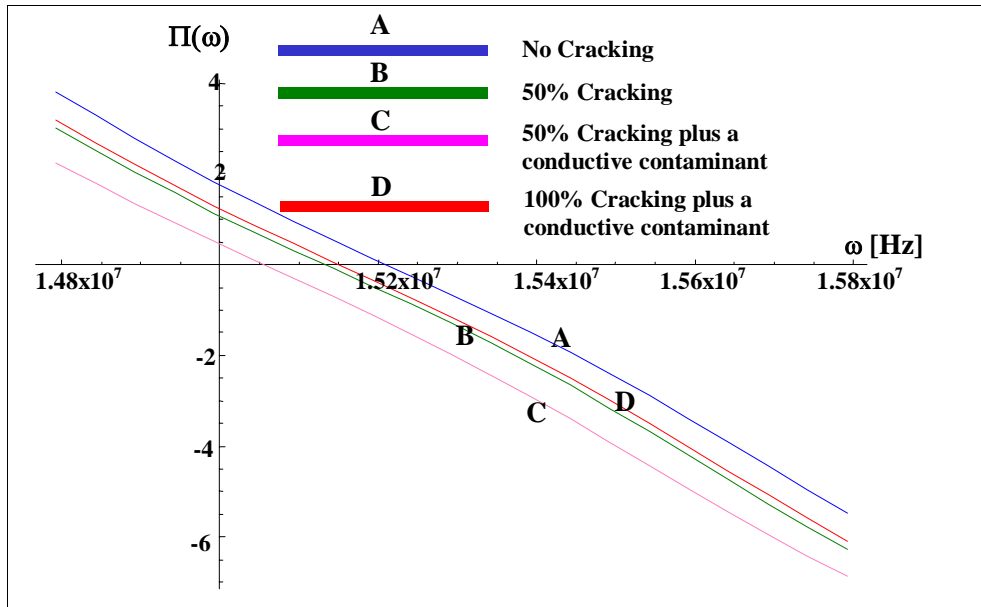
It is observed from the test results that, for a 9-meter cable, there are eight detection zero crossings (DZCs) in the high frequency range used for the cracking tests (i.e., 1MHz to 100MHz).

Figure 111 compares the first DZC for  $\Pi(\omega)$  for the cables with and without cracking. As shown, the DZC is downshifted to lower frequencies when cracking is present on the cables.

Similar results were observed for the other seven DZCs. These results suggest that monitoring the zeros crossings of the parameter  $\Pi(\omega)$  may be an effective indicator for the presence of cracking on a cable.



**Figure 110** Conductance per frequency per unit length for cable with and without cracks



**Figure 111** Comparison of second derivative of the impedance spectra,  $\Pi(\omega)$ , for cables with and without cracking

It should be noted that cracking of a cable's insulation arises when a cable that has been embrittled by long-term exposure to environmental stresses is physically stressed. For example, bending or crushing of an embrittled cable can lead to cracking of the insulation. In the experiments performed as part of this research, cracking was simulated by slicing the cable's insulation using a knife. This approach was selected since it was an efficient method of simulating the physical characteristics of a crack; however, the approach does not accurately capture the physics or the chemistry of the cracking. As a result, the results demonstrate the potential for detecting cracking using the BIS method; however, accurate models for real world cracking are not currently available, thus, a model for locating cracking could not be developed as part of this study. Additional research using more realistically simulated cracking is recommended to further evaluate the BIS method for detecting this type of degradation. Continuous BIS measurement during the aging process would be beneficial to understanding and modeling the cracking process. Chemical analysis of the cable's insulation would also be useful.

## 5.5 Application of BIS to Cables with Varying Environments

Electric cables in nuclear power plants can be very long and can traverse several different areas of the plant. Thus, the environment along the length of the cable may vary. In order to apply a condition monitoring technique to cables in their installed configuration, the impact of this varying environment on the measurements must be evaluated. To investigate the impact of

varying environments, long runs of cable were tested. Several different environments were imposed on sections of the cable during the tests to determine the impact on the test results.

### 5.5.1 Specimens Tested to Evaluate BIS for Cables with a Varying Environment

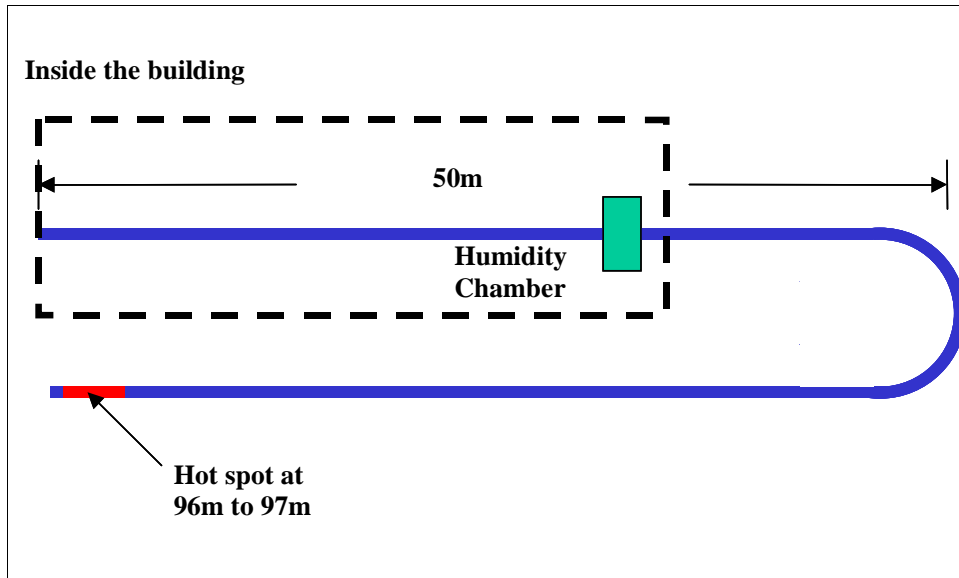
For this portion of the research, the cable test specimens shown in Table 14 were tested. The 10 meter cables were used to provide data for developing the phenomenological models for the 100 meter cables. The 100 meter cables were tested with constant temperature and humidity on the external surface of the cables, and with a varying environment along their length. Comparisons were made between the test results not only for the different environments, but also for the cables with and without the hot-spot.

BIS tests were performed over the frequency range from 1kHz to 1MHz using the HP instrument. Due to the length of test specimens 47 and 48, these cables were tested with the first 10 meters inside the test facility building, and the remainder outside the building. As a result, the cables were exposed to two different environments. Inside the building, the temperature was maintained at approximately 20°C (68°F) with low humidity. The portion of cable inside the building was also placed in a humidity chamber for several tests. The temperature outside the building varied several degrees as a function of location, and as a function of time of day.

**Table 14** Specimens tested to evaluate BIS for testing cables with a varying environment

No.	Specimen ID	Length meters (inches)	Service Life Simulated	Hot-Spot Simulated
26.	PNI-79-RB-188-826	10 (393.7)	60yrs. @ 50°C	None
43.	PNI-79-RB-188-843	10 (393.7)	60yrs. @ 90°C	None
47.	PNI-79-RB-188-847	100 (3,937)	None	60yrs. @ 90°C
48.	PNI-79-RB-188-848	100 (3,937)	None	None

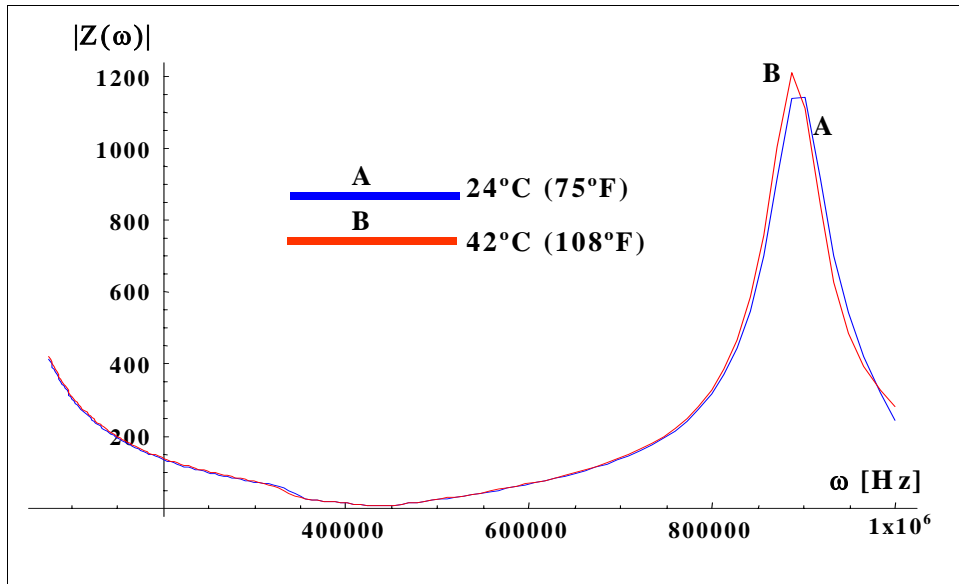
Figure 112 depicts the test setup schematically.



**Figure 112** Schematic of test setup for cables with varying environment

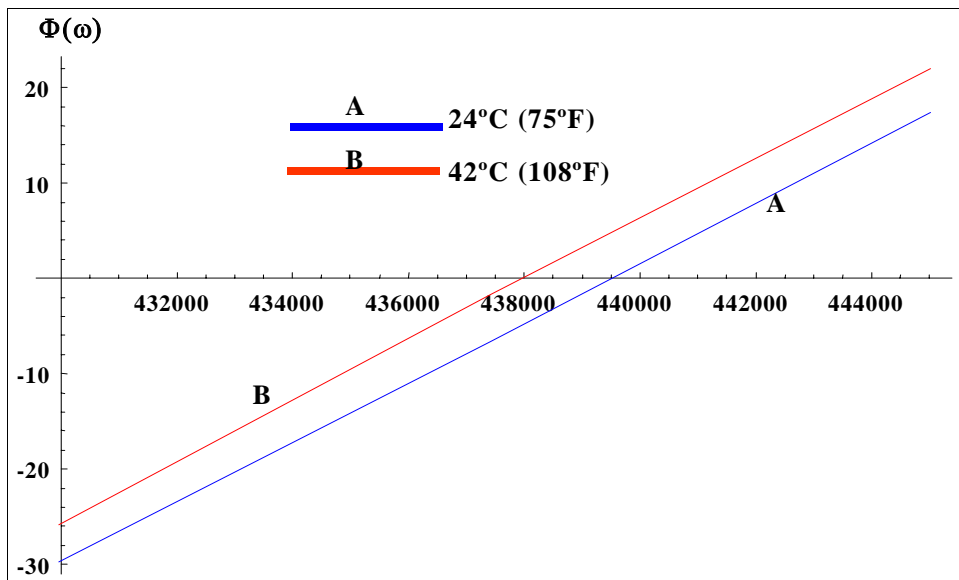
### 5.5.2 Low Frequency BIS Results

Figure 113 compares the measured impedance magnitude for the 100 meter cable without any aging or hot-spot (specimen 47) using external temperatures of 24°C (75°F), and 42°C (107.6°F) along the entire length of the cable. The results presented cover a frequency range of 400kHz to 1MHz. As shown, the impedance magnitude peak value is downshifted slightly for the case in which the higher external temperature was used.



**Figure 113** Impedance magnitude for 100 meter cable with no aging or hot-spot and external temperatures of 24°C (75°F), and 42°C (107.6°F)

Figure 114 compares the impedance phase spectra for the 100 meter cable with no aging or hot-spots (specimen 48) and external temperatures of 24°C (75°F), and 42°C (107.6°F). As shown, the higher external temperature causes a downshift in the first zero crossing of the impedance phase.



**Figure 114** Impedance phase spectra for 100 meter cable with no aging or hot-spot and external temperatures of 24°C (75°F), and 42°C (107.6°F)



Figure 115 compares the impedance phase spectra for the 100 meter cable with no aging or hot-spot and varying humidity levels over the first 10 meters of cable. For this test, the first 10 meters of the cable were placed in a humidity chamber and the conditions were maintained at 29°C (85°F) and 85% RH. As shown, the higher external humidity causes a downshift in the first zero crossing of the impedance phase, similar to that observed for the elevated temperature case.

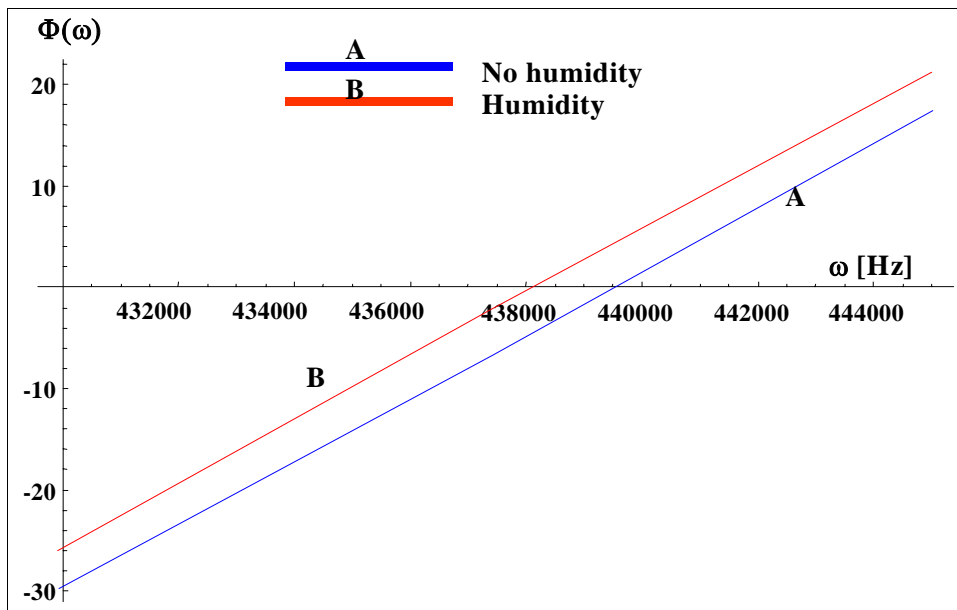
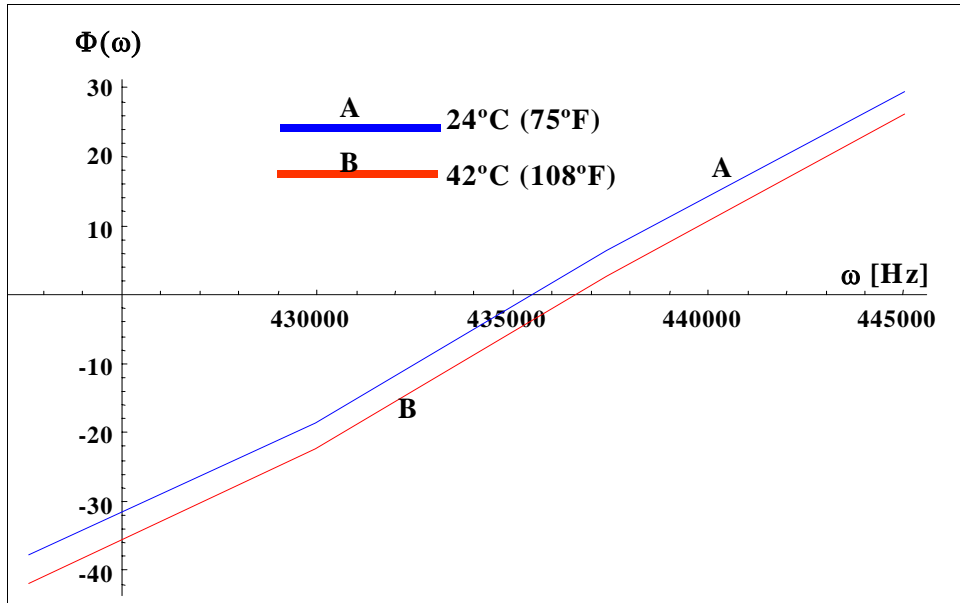


**Figure 115** Impedance phase spectra for 100 meter cable with no aging or hot-spot and external temperatures of 24°C (75°F) low humidity, and 29°C (85°F) and 85% RH.

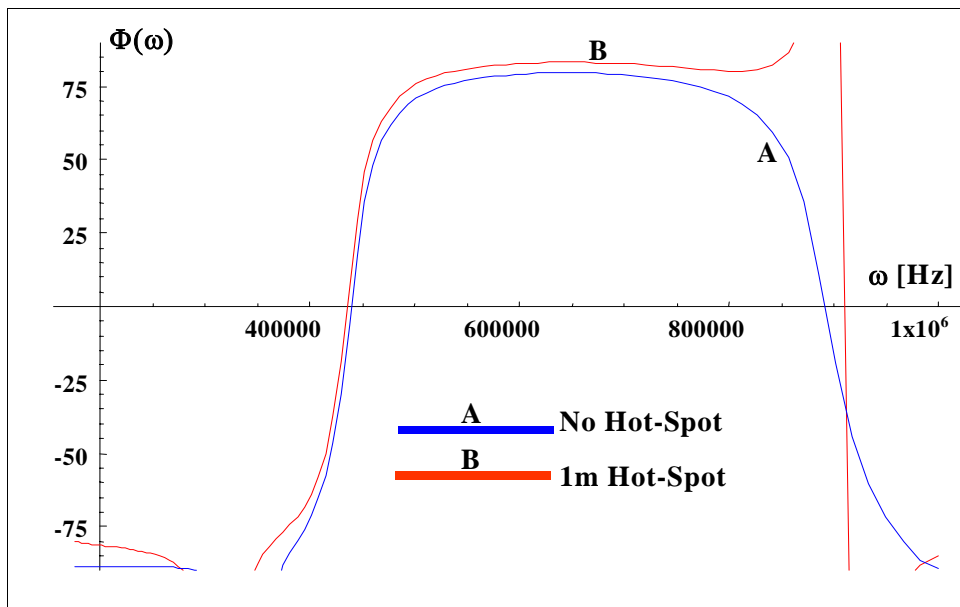
Next, the impact of a varying external temperature on a cable with a 1 meter hot-spot (specimen 47) was examined. Figure 116 compares the measured impedance phase spectra for the 100 meter cable with a 1 meter hot-spot and external temperatures of 24°C (75°F), and 42°C (107.6°F). As shown, the higher external temperature causes an upshift in the zero crossing of the impedance phase. This is contrary to previous observations and the reason for this behavior is not readily apparent.

Finally, a comparison of the two 100 meter cables was made to examine the impact of the hot-spot on the cables properties, particularly in the vicinity of the zero crossings. Figure 117 compares the measured impedance phase spectra for the two 100 meter cables. For this measurement, the external temperature was maintained at 24°C (75°F). As shown, the zero crossing of the impedance phase is downshifted by the presence of the 1 meter hot-spot. It should be noted that for this figure, the impedance phase is limited to the range from -90 to +90, since this is the physical range of the impedance phase. Measured values outside this range are

unphysical in nature and arise from instrument error, therefore, they are eliminated from the figure. However, the zero crossing frequencies presented are correct.

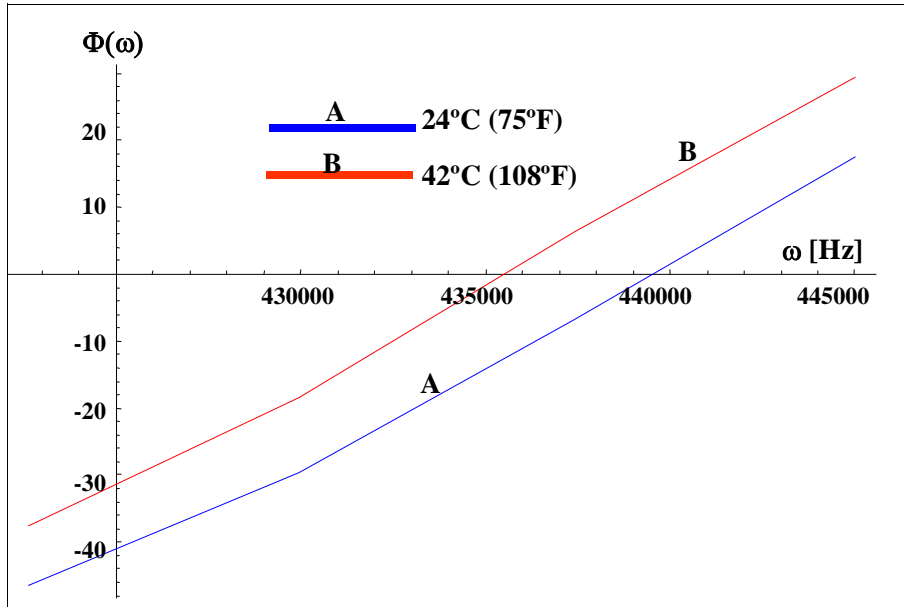


**Figure 116** Impedance phase spectra for 100 meter cable with 1 meter hot-spot and external temperatures of 24°C (75°F), and 42°C (107.6°F)



**Figure 117** Impedance phase spectra for 100 meter cables with and without a 1 meter hot-spot, and an external temperature of 24°C (75°F)

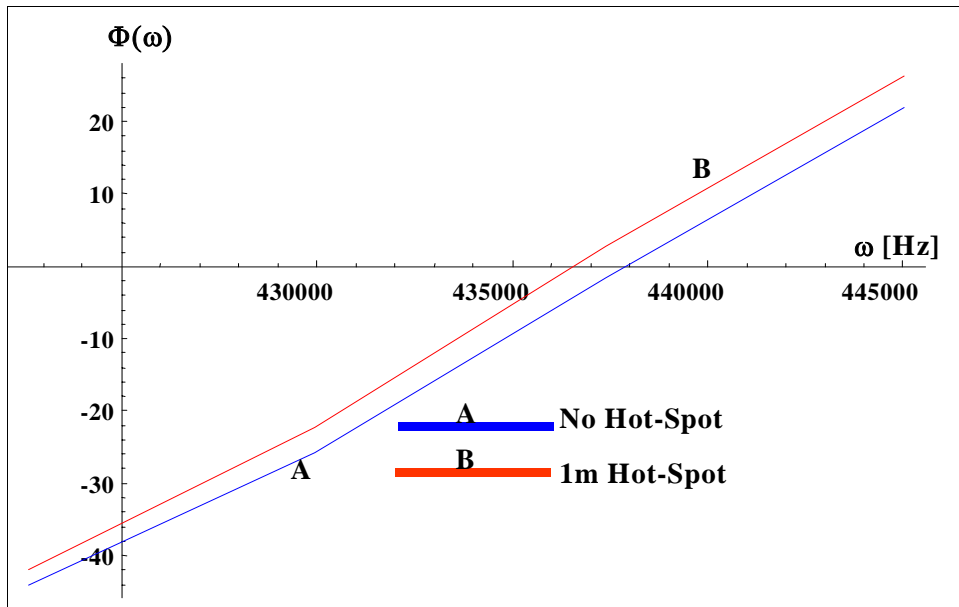
Figure 118 shows an expanded view of the measured impedance phase spectra for the two 100 meter cables in the vicinity of the first zero crossing with an external temperature of 24°C (75°F). The downshift in the zero crossing of the impedance phase is clearly visible with the presence of the 1 meter hot-spot.



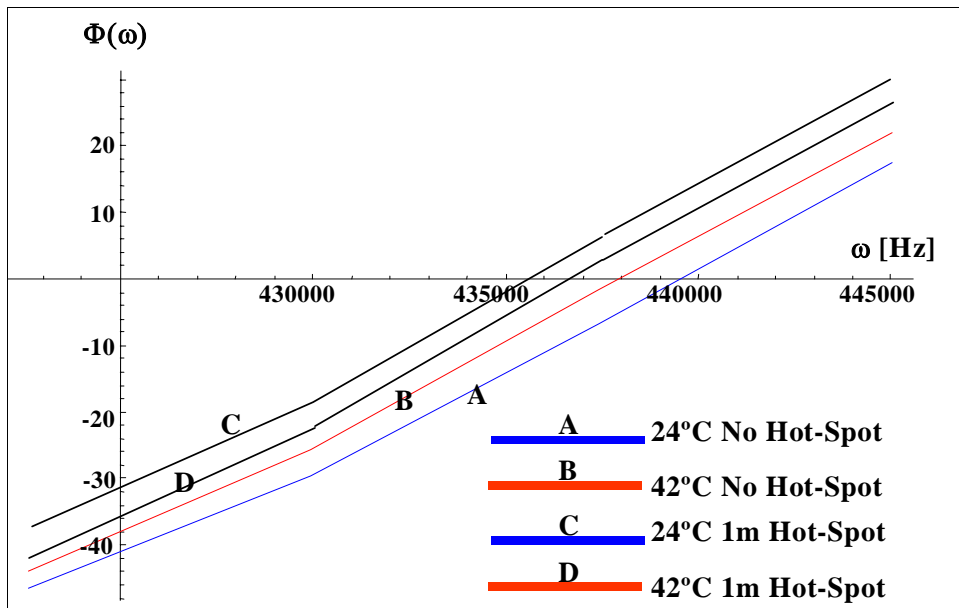
**Figure 118** Expanded view of the impedance phase spectra in the frequency range from 425kHz to 445kHz for 100 meter cables with and without a 1 meter hot-spot, and an external temperature of 24°C (75°F)

Figure 119 shows an expanded view of the measured impedance phase spectra for the two 100 meter cables in the vicinity of the first zero crossing with an external temperature of 42°C (107.6°F). Again, a downshift in the zero crossing of the impedance phase is observed with the presence of the 1 meter hot-spot.

Figure 120 summarizes the comparison of the impedance phase spectra for the various cases examined above; namely, 100 meter cables with and without a hot-spot, and external temperature of 24°C (75°F) and 42°C (107.6°F). This figure shows the different behavior that these two cables exhibit when the mean outside temperature changes. For the cable without a hot-spot, increasing the external temperature results in a downshift in the impedance phase zero crossing, while the reverse is true for the cable with the 1-meter hot-spot. This reverse behavior is attributed to the presence of the hot-spot.



**Figure 119** Expanded view of the impedance phase spectra in the frequency range from 425kHz to 445kHz for 100 meter cables with and without a 1 meter hot-spot, and an external temperature of 42°C (107.6°F)



**Figure 120** Summary comparison of impedance phase spectra for 100 meter cables with and without a 1-meter hot-spot and external temperatures of 24°C (75°F) and 42°C (107.6°F)

### 5.5.3 Phenomenological Models of Cables with Varying Environment

In this section a phenomenological model for a cable containing a hot-spot with a varying external environment is developed. The approach taken is to consider the cable to be in two states; namely a healthy state with no hot-spots, and a degraded state with the hot-spot. Each state is then modeled separately accounting for a varying environment, then the models are combined to represent the cable with a hot-spot. To develop the separate models, impedance results from test specimen 43, which was thermally aged to simulate 60 yrs @ 90°C, and specimen 26, which was thermally aged to simulate 60 yrs @ 50°C were used.

Figure 121 compares the measured impedance magnitude for the two 10 meter cables in the frequency range from 1kHz to 1MHz. As shown, the impedance magnitude for the cable with the more severe aging is lower. Thus, the more severe aging has made the cable's insulation more conductive.

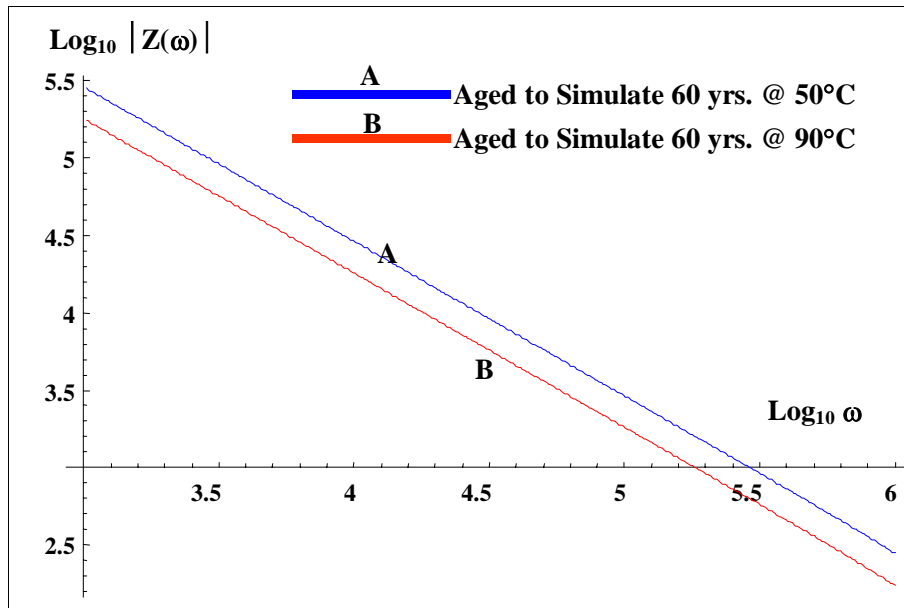


**Figure 121** Comparison of impedance magnitude in the frequency range from 1kHz to 1MHz for cables aged to simulate 60 yrs @ 50°C and 60 yrs @ 90°C

Figure 122 compares the measured impedance phase spectra for the two 10 meter cables in the frequency range from 1kHz to 1MHz. As shown, the impedance phase for the cable with the more severe aging is higher than that for the cable with less aging for frequencies less than approximately 400kHz. Again, this indicates that the more severe aging has made the cable's

insulation more conductive. It is observed that the impedance phase for specimen 43 drops significantly over 0.5MHz. The reason for this is not clear.

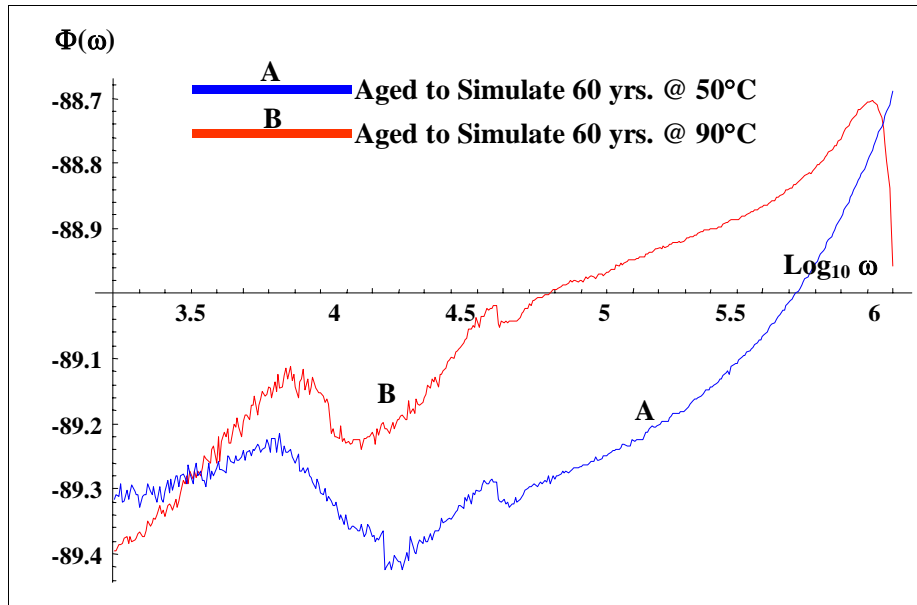
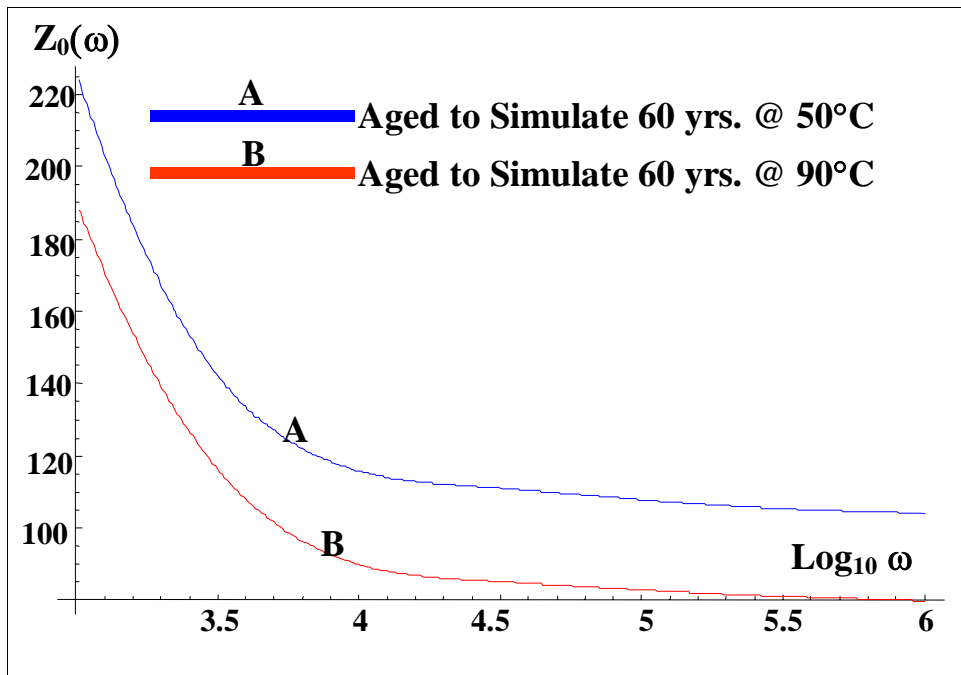


**Figure 122** Comparison of impedance phase spectra for 10 meter cables aged to simulate 60 yrs @ 50°C and 60 yrs @ 90°C

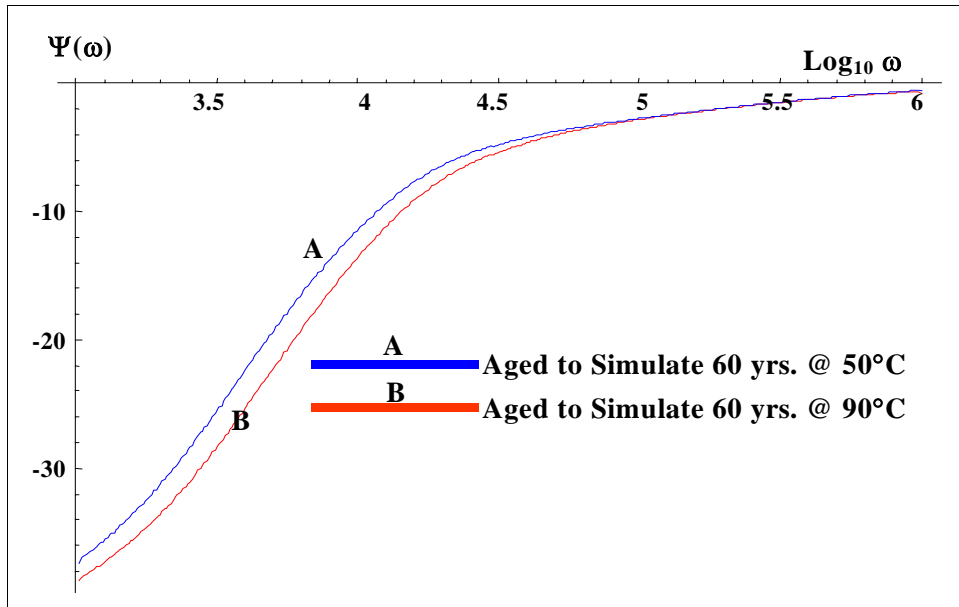
The cables characteristic impedance and propagation function are now extracted from the measured impedance in the frequency range from 1kHz to 1MHz. Figure 123 compares the extracted characteristic impedance magnitude for the 10-meter cables. As shown, the more severe aging results in a decrease in the characteristic impedance magnitude.

Figure 124 compares the extracted characteristic impedance phase spectra for the 10-meter cables. As shown, the more severe aging results in a decrease in the characteristic impedance phase. The largest difference occurs at the lowest frequencies in this range, i.e., 1kHz. This behavior arises from the fact that more severe aging degrades the cable's electrical properties.

Figures 125 and 126 compare the extracted imaginary and real components, respectively, of the propagation function for the 10-meter cables. As shown, the more severe aging results in an increase in these parameters.



**Figure 123** Comparison of extracted characteristic impedance magnitude for 10 meter cables aged to simulate 60 yrs. @ 50°C and 60 yrs @ 90°C



**Figure 124** Comparison of extracted characteristic impedance phase spectra for 10 m cables aged to simulate 60 yrs. @ 50°C and 60 yrs @ 90°C

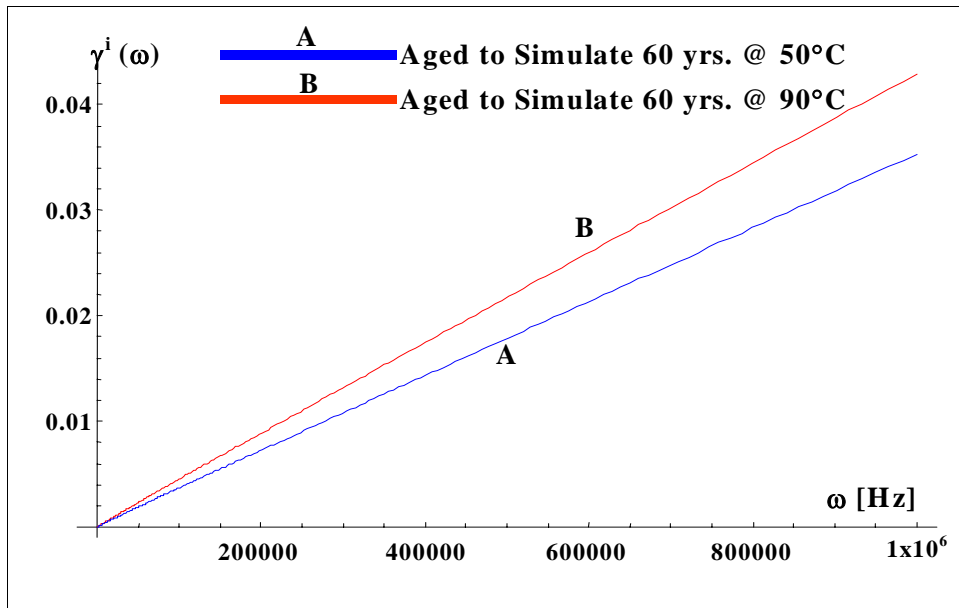


**Figure 125** Comparison of imaginary component of the propagation function for 10 m cables aged to simulate 60 yrs. @ 50°C and 60 yrs @ 90°C



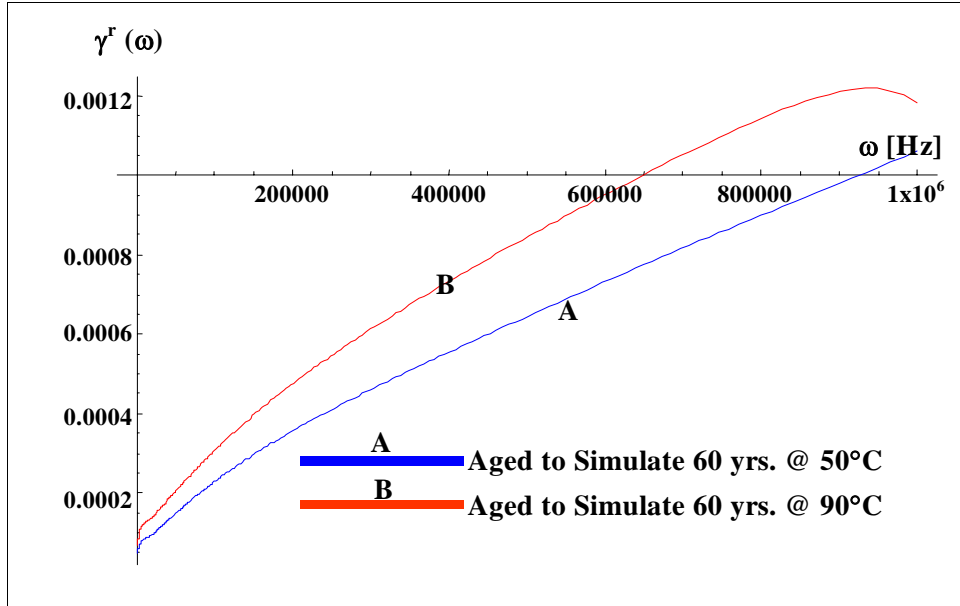


**Figure 126** Comparison of the real component of the propagation function for 10 meter cables aged to simulate 60 yrs. @ 50°C and 60 yrs @ 90°C

The electrical properties of the cables are now determined for the 10-meter cables aged to simulate 60 yrs. @ 50°C and 60 yrs @ 90°C. Figure 127 compares the resistance per unit length for the cables, along with the relative difference in resistance per unit length. It is observed that both resistance curves follow the square root frequency dependence due to the skin effect. As shown, at very low frequencies, the resistance for the cable with the more severe aging is larger. For direct currents, the resistance per unit length depends on the geometry of the twisted conductor pair according to the following equation:

$$R_{dc} = \frac{2 R_s}{\pi d} \left[ \frac{s/d}{\sqrt{(s/d)^2 - 1}} \right] \quad 5.5-1$$

where “s” is the distance between the cable conductor centers, “d” is the wire insulation’s diameter, and  $R_s$  is the skin resistance of a single conductor. Thus, the smaller the diameter of the conductor insulation, the larger the resistance at direct current. These results imply that the insulation shrinkage increases when the aging becomes more severe, which is consistent with intuition. It is observed that for frequencies above 100kHz, the relative difference in resistance per unit length is negative, which implies that the resistance for the cable with the more severe aging becomes smaller than the cable with less aging. This behavior is an anomaly for which no readily apparent explanation is available.

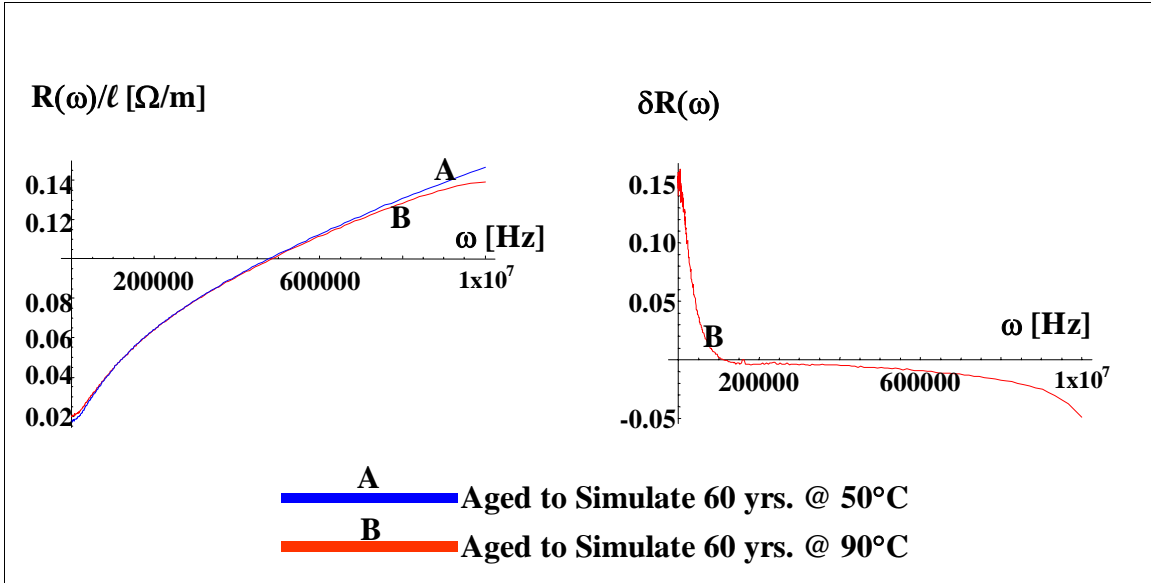


**Figure 127** Comparison of resistance per unit length and relative difference in resistance per unit length for 10-meter cables aged to simulate 60 yrs. @ 50°C and 60 yrs @ 90°C

Figure 128 compares the inductance per unit length for the cables, along with the relative difference in inductance per unit length. As shown, the inductance is smaller when the aging severity is increased. This behavior does not reflect the standard formula for the dc inductance per unit length dependence on the cable geometry, which is defined by the following equation:

$$L = \frac{\mu}{\pi} \text{Cosh}^{-1} \left( \frac{s}{d} \right) \quad 5.5-2$$

This behavior is not currently understood; however, cables have a very complicated structure that involves a number of wire strands that form the conductor. Each strand creates its own magnetic field and it is possible that the individual contributions from each strand to the cable's magnetic field may interfere with each other. In that case, Equation 5.5-2 would not describe the cable's inductance.

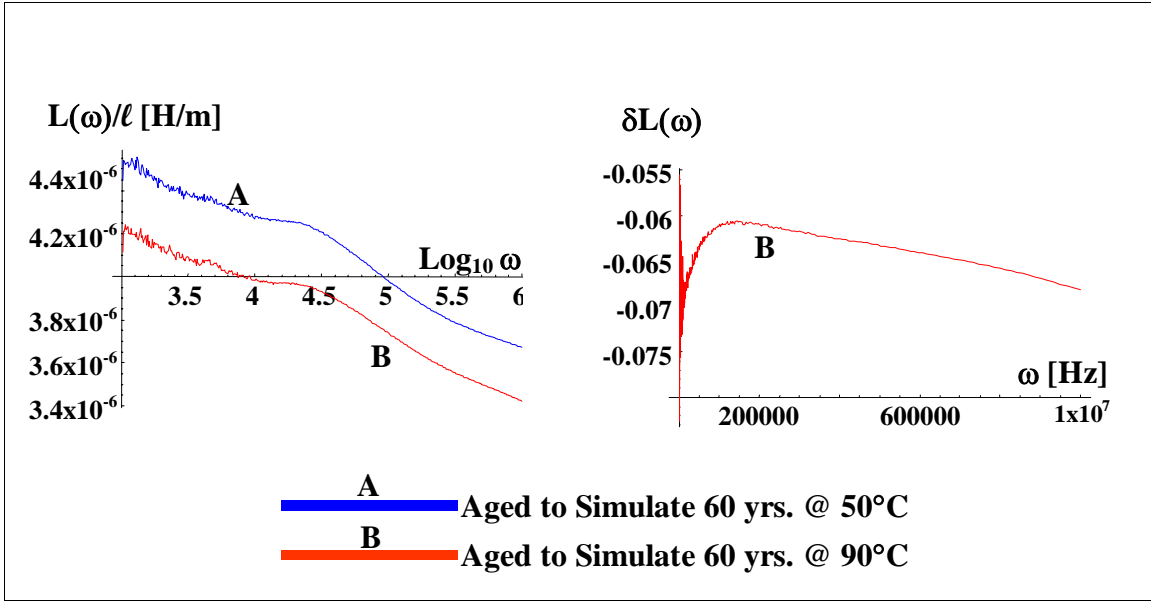


**Figure 128** Comparison of inductance per unit length and relative difference in inductance per unit length for 10m cables aged to simulate 60yrs.@50°C and 60yrs@90°C

Figure 129 compares the capacitance per unit length for the cables, along with the relative difference in capacitance per unit length. As shown, the capacitance is increased when the aging severity is increased. This behavior does not reflect the dc capacitance per unit length dependence on the cable's geometry, as defined by the following equation:

$$C(\omega) = \frac{\pi \epsilon_1(\omega)}{\text{Cosh}^{-1}\left(\frac{s}{d}\right)} \quad 5.5-3$$

In the above equation,  $\epsilon_1(\omega)$  refers to the real component of the insulation's dielectric function. However, the thermal aging can change the insulation's chemistry. Throughout this frequency range, the thermally degraded cable's insulation has a capacitance that is larger than for the less degraded cable. Furthermore, the capacitance exhibits a weak dependence on frequency. That implies that the more severe aging degradation affected all of the microprocesses that control the insulation's dielectric function.

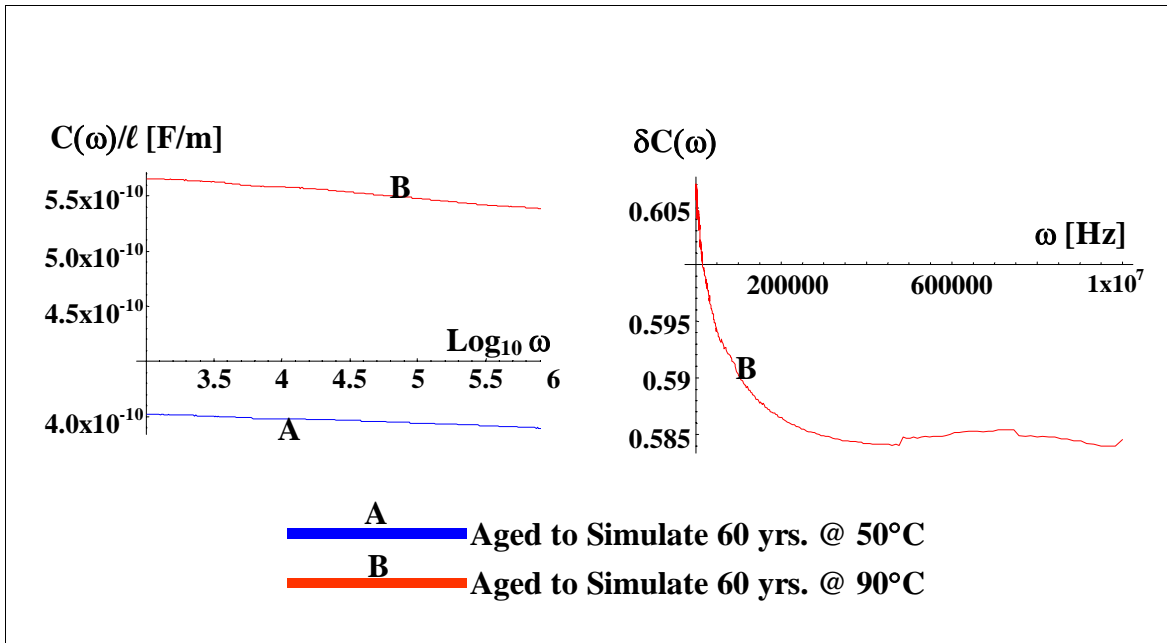


**Figure 129** Comparison of capacitance per unit length and relative difference in capacitance per unit length for 10m cables aged to simulate 60 yrs@50°C and 60 yrs@90°C

Figure 130 compares the conductance per unit length for the cables, along with the relative difference in conductance per unit length. As shown, the conductance is increased when the aging severity is increased. This behavior does not reflect the dc conductance per unit length dependence on the cable's geometry, as defined by the following equation:

$$G(\omega) = \frac{\pi \omega \varepsilon_2(\omega)}{\text{Cosh}^{-1}\left(\frac{s}{d}\right)} \quad 5.5-4$$

In the above equation,  $\varepsilon_2(\omega)$  refers to the imaginary component of the insulation's dielectric function. However, the thermal aging can change the insulation's chemistry. Throughout this frequency range, the degraded cable's insulation has a capacitance that is larger than for the cable that is less severely degraded.

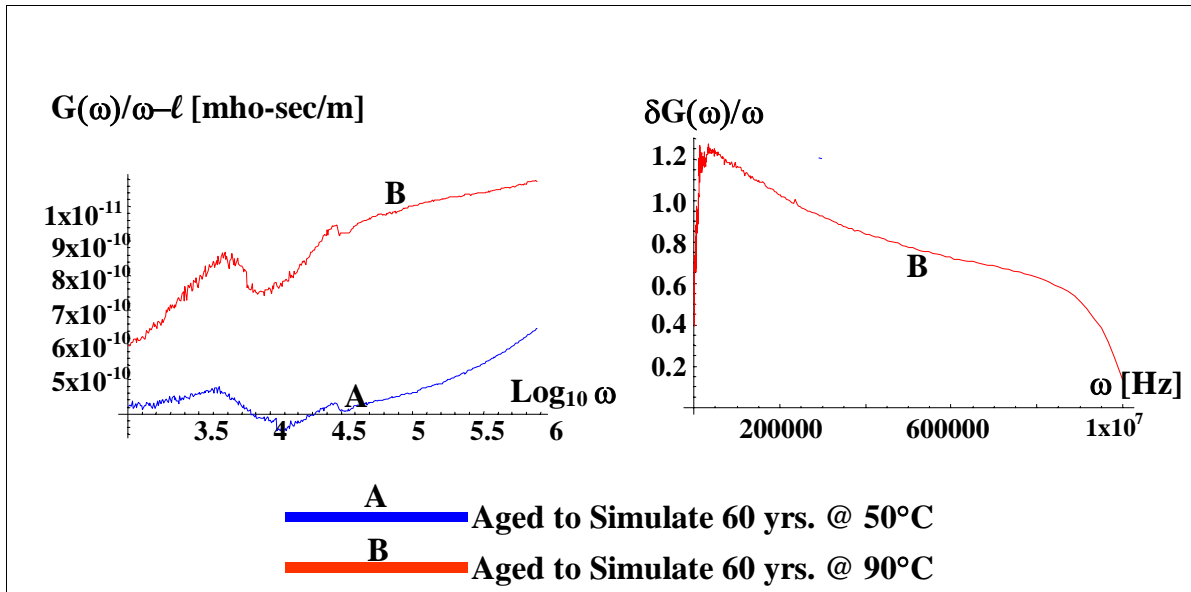


**Figure 130** Comparison of conductance per unit length and relative difference in conductance per unit length for 10m cables aged to simulate 60 yrs@50°C and 60 yrs@90°C

With the electrical properties of the individual 10-meter cables modeled, a model can be developed for the 100 meter cable with a hot-spot. The model is then applied to the impedance measurements made on the cables shown schematically in Figure 1. The geometry of the model is shown schematically in Figure 131.

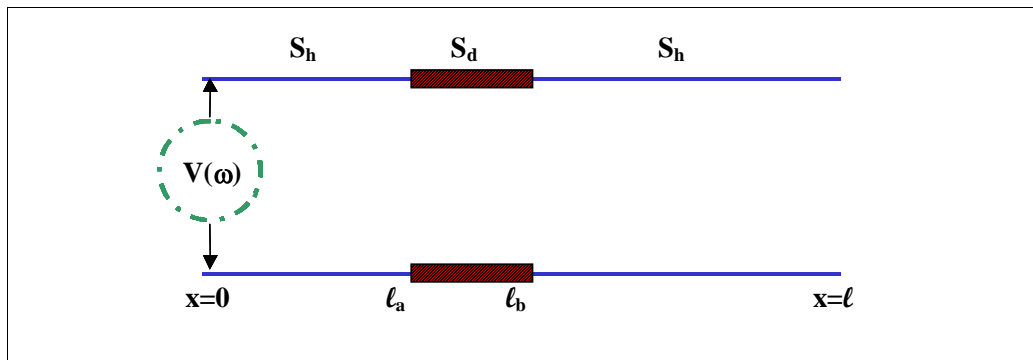


**Figure 131** Schematic of model for 100-meter cable containing a hot-spot

Referring to the above figure,  $S_h$  refers to the healthy section of cable with no aging, and  $S_d$  refers to the damaged section of cable thermally aged to simulate a hot-spot. Also,  $l_a$  and  $l_b$  refer to the start and end location, respectively, of the damaged hot-spot section of cable.

The modeled impedance for this configuration is represented by the following equation:

$$Z_{\text{model}}(\omega) = Z_{0,h}(\omega) \left( \frac{Z_{0,h}(\omega) \coth [\gamma_h(\ell - \ell_a)] + Z_{0,d}(\omega) \coth [\gamma_d(\ell_b - \ell_a)]}{Z_{0,d}(\omega) + Z_{0,h}(\omega) \coth [\gamma_h(\ell - \ell_b)] \tanh [\gamma_d(\ell_b - \ell_a)]} \right) \quad 5.5-5$$

where  $Z_{0,h}(\omega)$  and  $Z_{0,d}(\omega)$  are the characteristic impedances, and  $\gamma_h(\omega)$  and  $\gamma_d(\omega)$  are the propagation functions for the healthy and damaged sections of cable, respectively. In applying this model, the impedance data from the 10-meter cable aged to simulate 60yrs @ 50°C are used to represent the healthy section, and the impedance data from the 10-meter cable aged to simulate 60yrs @ 90°C are used to represent the damaged section. It should be noted that the impedance measurements for the 10-meter cables were performed with the cables in a humidity chamber and the conditions maintained at 30°C (85°F) and 20% RH. Thus, there is some error introduced in using impedance data from these cables to model the 100 meter cables, which were measured under slightly different conditions of 24°C (75°F) and low humidity.

To determine the hot-spot location relative to the point of measurement, it is first assumed that  $\ell_a$  is zero. The model is used to calculate the impedance and the results are compared to the measured impedance. In the frequency range from 1kHz to 1MHz. The assumed hot-spot location is then changed and the impedance calculation is repeated. This process is continued until the hot-spot location is varied over the entire length of the cable. For each calculation, the error in the impedance phase is calculated using the following equation:

$$\delta\Theta(\ell_a) \equiv \frac{\sum_{m=n_0-n}^{m=n_0+n} |\Phi_{\text{Measurement}}(\omega_m) - \Phi_{\text{Model}}(\omega_m, \ell_a)|}{\sum_{m=n_0-n}^{m=n_0+n} |\Phi(\omega_m)|} \quad 5.5-6$$

where  $\Phi_{\text{Measurement}}(\omega_m)$  is the measured impedance phase at the frequency  $\omega_m$  and  $\Phi_{\text{Model}}(\omega_m, \ell_a)$  is the model's impedance phase at the frequency  $\omega_m$  based on the assumption that the hot-spot location is  $\ell_a$ . In addition,  $\omega_{n_0}=437,419\text{Hz}$  and the lower and upper frequencies were 429, 949Hz and 445, 020Hz, respectively. The results are shown in Figure 132.

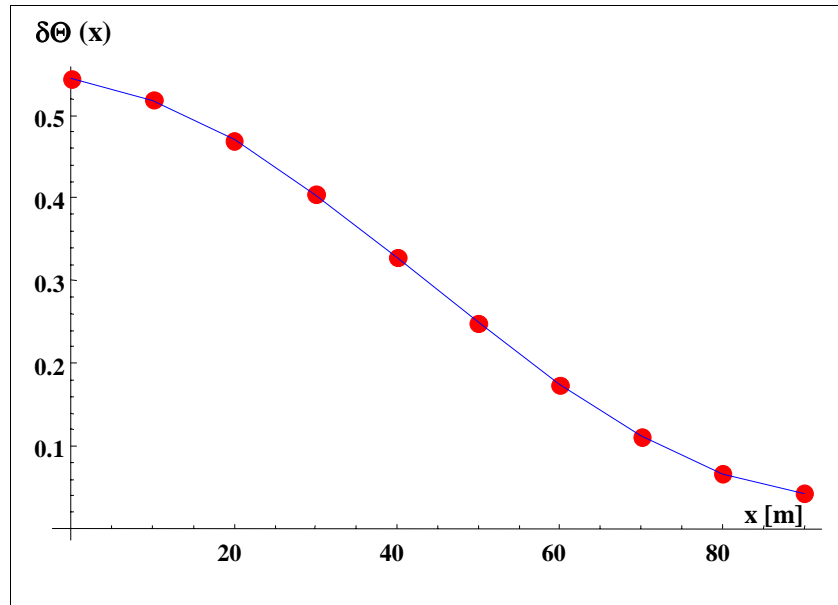


**Figure 132** Error in predicted impedance phase as a function of assumed hot-spot location

Examination of the above figure shows that the model predicted the hot-spot location to be within 90 meters to 99 meters from the point of measurement. The error varies from approximately 56% down to approximately 5% near the correct location. To more accurately locate the hot-spot, the calculations were repeated in the region from 90 meters to 99 meters using refined assumptions for the hot-spot location. The predicted location is then found to be 99 meters from the point of measurement. This is in good agreement with the correct location of 96 meters. Thus, the model's prediction is within 3% of the correct location. Figure 133 presents the results of this calculation. As shown, the model is within 4.2% of the correct location.

These results demonstrate that BIS can be used to locate hot-spots on cables even when the environment is variable along the external surface of the cable. For the example presented herein, the model's prediction of hot-spot location is within a few percent of the correct position. This is particularly interesting in light of the fact that parameters from the 10 meter cables aged at slightly different conditions were used to represent the 100 meter cable being modeled. In addition, 90% of the 100 meter cable was outside the building during testing, which resulted in a dynamic external environment. In spite of these adverse factors, the model was able to predict the hot-spot location with good accuracy.

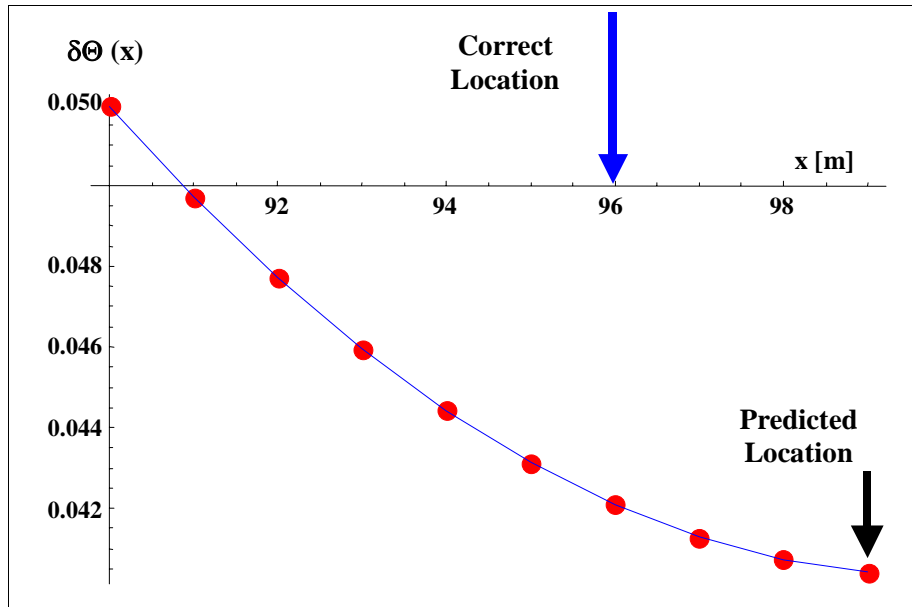


**Figure 133** Error in predicted impedance phase as a function of assumed hot-spot location over the cable length from 90 meters to 99 meters



(This page intentionally left blank)

## 6. EVALUATION OF THE BIS METHOD FOR NUCLEAR PLANT CABLES

The goal of this research program was to evaluate the effectiveness of the BIS method for detecting and locating degradation in electric cables in nuclear power plant applications. To achieve this goal, a commonly used low-voltage instrumentation and control (I&C) cable was selected to prepare cable test specimens, which were exposed to accelerated aging to simulate various types of service conditions in a typical nuclear power plant application. Specific types of degradation were inflicted on the cable after which the cable test specimens were tested using the BIS method. The types of degradation evaluated are the following;

- Global thermal aging of the cable
- Global plus localized thermal aging of the cable (i.e., hot-spots)
- Thermal degradation with cracking, and
- Abrasion damage to the cable

In testing the cables, the following three different cable configurations were evaluated to provide a representative sampling of the applications commonly expected in a nuclear power plant setting:

- Constant temperature and humidity along the cable with no load attached
- Constant temperature and humidity along the cable with a load attached
- Varying environments along the length of the cable with no load attached

For each configuration, BIS measurements were made and the data were analyzed to determine if the degradation could be detected and located. Detection and location of the degradation is based on the use of the measured impedance data, the governing equations for the electrical properties of an electric cable, and models developed to analytically represent the cable properties. The results for each of the different configurations are discussed below.

### 6.1 Results for Global Thermal Aging

The test results on the cables with global thermal aging clearly show that the BIS method is capable of detecting thermal degradation of a cable. In the low frequency range, comparison of the measured impedance phase spectra show an increase in the impedance phase angle when thermal aging is present on the cable. This increase in impedance phase indicates that the cable is more dissipative, and can be used as an indicator of aging degradation on the cable.

The high frequency BIS data show that, as thermal aging is applied to the cable, the impedance magnitude and phase spectra are downshifted to lower frequencies. Therefore, by measuring the

impedance of a cable and comparing it to a baseline for a known cable in good condition, this downshift in frequency can also be used as an indicator of thermal degradation on the cable.

Analytical models were developed to predict the electrical properties of a degraded cable based on measured impedance data. The approach used is based upon the fact that, at low frequencies the cable's impedance is non-oscillatory and the characteristic impedance and propagation function can be directly extracted from the measured impedance spectra. At high frequencies, where the cable's impedance oscillates, it is not possible to directly extract the characteristic impedance and propagation function. Instead, the cable's characteristic impedance in the low frequency range is first determined. This function is then extrapolated to the high frequency range. The propagation function for the high frequency range can then be determined. Once the characteristic impedance and propagation function are known, the models developed for the cable's electrical properties can be used to predict the electrical properties of the cable. Results showed relatively good accuracy for the models developed.

These results demonstrate that the BIS method can detect thermal degradation and predict the electrical properties of the degraded cable with relatively good accuracy for the type of cable tested in this study. It should be noted that this testing was performed in a laboratory environment. Testing in a actual plant environment is recommended to verify the effectiveness of the BIS method for detecting this type of degradation.

## **6.2 Results for Global Plus Localized Thermal Aging (Hot-Spot)**

The results from the testing of cables with global thermal aging were used as the basis for detecting and locating localized thermal aging (i.e., hot-spots) in cables. The high frequency impedance spectra for cables with and without hot-spots were compared and they demonstrated that localized damage does impact the cables impedance characteristics. The presence of a hot-spot tends to downshift the frequency of the impedance spectra. This difference in impedance spectra can be used to detect and locate localized degradation.

The impact of hot-spot severity, size, and location were also investigated in this study. Tests were performed to compare the impedance response of cables with a hot-spot representing 60 years of service at 60°C (140°F) and 60 years of service at 70°C (158°F). The results indicate that the difference in hot-spot severity was not significant enough for the low frequency impedance spectra to show a measurable difference. However, the high frequency spectra did show a downshift in frequency. This change is useful for estimating the size of a hot-spot. Cables with hot-spots 1.0 meters in length and 0.5 meters in length were also compared to evaluate the impact of hot-spot size, and similar results were obtained.

To determine the sensitivity of the BIS method to hot-spot location, test cables were measured from both ends. This effectively provided data for a hot-spot at two different distances from the point of measurement. Results demonstrated that the location of the hot-spot does impact the

impedance spectra, and this difference can be used to locate the degradation. The closer the hot-spot is to the point of measurement, the greater is the change in the impedance spectra.

A method for locating a hot-spot was developed based on the models for the cable's properties. Specifically, the cable's impedance is calculated using equation 5.1-13 based on assumed values of the hot-spot location. This calculated value is compared to the measured impedance. Based on the root mean square (rms) error between the value predicted by the model and the measured value, new values of hot-spot location are chosen and the process is repeated. The final hot-spot location is determined by minimizing the rms error.

In comparing the modeled impedance to the measured impedance, four different parameters are used, which are based on the impedance magnitude and the impedance phase zero crossings. Results show that this approach can be used to predict hot-spot location with an accuracy of 10%.

It should be noted that this testing was performed in a laboratory environment with a known, well defined hot-spot on the test specimen. Also, only one hot-spot was present on the cable. Therefore, generalization of these results to cables with multiple hot-spots would not be appropriate. However, these results do show promise that the BIS method is a powerful tool for locating localized damage in an installed cable system.

### **6.3 Results for Global Thermal Aging with an Attached Load**

Impedance measurements were made on cables with localized thermal aging both with and without a load attached to the cable. The goal was to determine the impact of the load on the ability of the BIS method to detect and locate a hot-spot. The results showed that, at low frequencies, the cable system's impedance is heavily dominated by the load. However, the zero crossing of the impedance phase does react to the presence of a hot-spot. Therefore, an accurate model of the cable system impedance can be used to examine the behavior of the impedance phase in the vicinity of the low frequency zero crossings. This can be used as an indicator for the presence of a hot-spot on the cable's insulation even with a load attached to the cable.

In evaluating the high frequency BIS measurements for cables with an attached load, the frequency averaged second derivative of the impedance phase spectra was found to provide useful information for detecting hot-spots. Specifically, the zero crossings of this parameter were found to be downshifted when the cable's insulation contains a hot-spot. An examination of the  $\Pi(\omega)$  spectra showed that a frequency downshift occurs at all of the 14 DZCs when a hot-spot is present on the cable. Thus, detection of a hot-spot appears to be feasible for cables with a load attached.

Models were also developed to predict the electrical properties for cables with hot-spots and an attached load. Using these models and an approach similar to that used for the detection of hot-spots without an attached load, the location of a hot-spot was correctly predicted. These results

demonstrate that the BIS method is capable of detecting and locating localized degradation on cables even if there is a load attached to the cable. Some knowledge of the impedance response of the load is useful.

#### **6.4 Results for Global Plus Localized Abrasion Damage**

The testing on cables with simulated abrasion damage showed that the low frequency impedance spectra do not respond to the presence of abrasion unless a high humidity level is present to create a conductivity path. When a higher level of humidity is present, all of the phase spectra have a new structure (i.e., a peak) in the vicinity of 5kHz to 10Khz. This structure arises from the increased humidity level, which provides a conductive pathway for leakage currents.

It is also observed that the abraded cable's impedance peak is shifted to higher frequencies relative to the unabraded cable. This frequency shift may be attributable to the fact that the averaged dielectric function of the abraded cable is smaller than that for the unabraded cable. As a result, any changes to the spectra must occur at higher frequencies. It is further observed that there is no readily observable difference between the phase spectra of the cables with one and two conductors abraded.

It should be noted that, while the change in the low frequency impedance phase spectra can be used to detect abrasion under high humidity levels, this may not be practical in a nuclear power plant environment since the humidity levels may not be high enough to observe these changes. For example, the peaks previously discussed were not observed when BIS measurements were made under conditions of 70% RH.

An evaluation of the high frequency data shows that the phase zero crossing and the first maxima of the impedance magnitude are shifted to a higher frequency when the cable is abraded. The largest change is observed for the case in which the abrasion is covered by a conductive contaminant, thus establishing a conductivity path.

Models were developed to represent the electrical properties of the abraded cable. Using these models together with the measured impedance spectra, abrasion damage was located on a test specimen with an accuracy of 15%. An iterative approach similar to that used for detecting hot-spots was used in which an assumed damage location is used to calculate the cable impedance. This is compared to a measured value and an iterative process is used to minimize the rms error between predicted and measured values. These results demonstrate that the BIS method is potentially useful for detecting and locating abrasion damage on a cable.

#### **6.5 Results for Global Thermal Aging with Cracking Damage**

Testing of cables with simulated cracking was performed to evaluate the effectiveness of the BIS method for detecting and locating this type of degradation. The impedance phase spectra in the low frequency range from 1kHz to 1MHz for cables with and without cracking show that there is only a small difference between the uncracked cable and the cable with cracks. Even a conductive contaminant applied to the cable does not appear to impact the impedance phase. This can be attributed to the lack of a conductivity path between the conductors, even with the conductive contaminant applied. A possible reason for this is the size of the iron filings used, which were on the order of 100 $\mu$ . This is approximately the same dimension as the crack width. Thus, it is believed that the iron particles could not enter the crack and make a connection with the cable conductor.

The high frequency impedance spectra of the cable test specimens showed that the zero crossings of the second derivative of the impedance phase spectra,  $\Pi(\omega)$ , did show differences that may be useful as indicators for the presence of cracking. Monitoring the zero crossings of the parameter  $\Pi(\omega)$  may be an effective indicator for the presence of cracking on a cable.

In the experiments performed herein, cracking was simulated by slicing the cable's insulation using a knife. This approach was selected since it was an efficient method of simulating the physical characteristics of a crack; however, the approach does not accurately capture the physics or the chemistry of cracking that would occur in real plant environments. As a result, the results demonstrate the potential for detecting cracking using the BIS method; however, accurate models for real world cracking are not currently available. Additional research using more realistically simulated cracking is recommended to further evaluate the BIS method for detecting this type of degradation. Continuous BIS measurement during the aging process would be beneficial to understanding and modeling the cracking process. Chemical analysis of the cable's insulation would also be useful.

## **6.6 Results for Global Thermal Aging with a Varying Environment**

Testing of long cables (100 meters) was performed to evaluate the impact of varying environments along the external surface of the cables on BIS measurements. One of the cables contained a 1-meter hot-spot that simulated 60 years of service at 90°C. The hot-spot was located at 96 meters from the end of the cable. Two different environments were simulated during the testing process.

The predicted location using BIS was 99 meters from the point of measurement. This is in good agreement with the correct location of 96 meters. Thus, the model's prediction is within 3% of the correct location. The results demonstrate that the BIS method can be used to locate hot-spots on cables even with varied environments along the external surface of the cable. For the example presented herein, the model's prediction of hot-spot location is within a few percent of the correct position.

(This page intentionally left blank)

## 7. CONCLUSIONS AND CONSIDERATIONS FOR FOLLOW-ON RESEARCH

### 7.1 Conclusions on the Effectiveness of the BIS Method

The research program reported herein evaluated the BIS method as a prognostic and diagnostic tool for monitoring installed electric cable systems in nuclear power plants. The results demonstrated that this method is effective for nuclear plant cables, and that it is capable of detecting and locating localized degradation within a cable in its incipient stage prior to failure. Various degradation scenarios were evaluated, including the following:

- global thermal aging damage,
- localized thermal aging damage,
- abrasion damage, and
- cracking damage

The following conclusions are drawn based on the results of this research:

- The BIS method was clearly able to detect the presence of thermal degradation on the cables used in this study. Specifically, the impedance phase spectra of the cables tested were observed to increase as the amount of thermal degradation on the cable increased. This increase can be used as an indicator of global thermal degradation.
- The BIS method was able to detect the presence of localized thermal degradation, or hot-spots on the cables. Specifically, a shift in the zero crossings of the impedance phase spectra were observed when a hot-spot was present on the cable.
- An approach was developed for locating hot-spots on a cable using models of the cables electrical properties. The models were able to predict the hot-spot location with an accuracy of 10%.
- The BIS method was not sensitive enough to distinguish between the different severities and sizes of hot-spots simulated in the low frequency range; however, measurements in the high frequency range did detect the differences. Additional research is warranted to establish the sensitivity limits for this technique
- The BIS method was able to detect and locate the presence of abrasion damage on a cable. The models and approach used are similar to that for detecting and locating thermal hot-spots.
- The BIS method was demonstrated to be effective for detecting and locating degradation on cables with an attached load. This is important since it is desirable to have a technique that can test cables in their installed configuration, without having to disconnect them from attached equipment.



- The BIS method was able to detect the simulated cracking damage on cables. However, the simulation method used in this study was determined not to accurately represent the cracking phenomena. Additional research should be considered to more accurately evaluate the BIS method on actual cable cracking.
- The BIS method was able to detect the presence of localized thermal degradation, or hot-spots on the cables even with a varying environment along the external surface of the cables. For the example presented herein, the model's prediction of hot-spot location is within a few percent of the correct position.

The results from this study suggest that the technology that makes use of BIS may represent a breakthrough in the condition monitoring of installed electric cables. In a laboratory setting, this technique was able to detect and locate the various forms of aging degradation commonly found in nuclear power plant applications. This technique has the capability to provide a means of scanning an entire cable system to determine its acceptability for continued service. The technique can be applied in situ with low voltage signals that will not damage the cable under test, and can detect aging damage in an incipient state prior to a failure occurring.

## **7.2 Considerations for Follow-On Research to Demonstrate the Effectiveness of the BIS Method in Nuclear Plant Environment**

While the BIS method shows great promise as a prognostic and diagnostic technique for installed cable systems, additional research is desirable before it can be applied in the field. Specifically, the following additional items should be considered during future research, preferably in a collaborative manner:

- Research on the detection and location of cracking damage in cables using more realistic simulation of the cracking damage,
- The technique should be demonstrated on additional types of cable to determine its usefulness for other materials and cable configurations
- The technique should be evaluated with different types of loads attached to the cables to determine the impact of loads encountered in a plant environment
- The technique should be demonstrated in an actual plant environment to determine the impact of the various environmental factors that may impact the BIS measurements
- The technique should be demonstrated on blind test samples in which the type, severity, size, and location of the degradation are unknown

Based upon the promising results obtained from this phase of the research effort, the Office of Nuclear Regulatory Research (RES) is considering a follow-on research effort. The primary focus of the next phase of the research should be on the demonstration of the BIS method for installed cable systems in operating nuclear power plant environment.

## 8. REFERENCES

Durney, C. and Johnson, C., "Introduction to Modern Electromagnetics," McGraw-Hill, 1969.

Grayson, S.J., et al., "*Fire Performance of Electric Cables*," Interscience Communications, Ltd., United Kingdom, 2000.

Lofaro, R.J., "Proceedings of the International Conference on Wire System Aging," NUREG/CP-0179, Brookhaven National Laboratory, November 2002.

Lofaro, R.J., et al., "Assessment of Environmental Qualification Practices and Condition Monitoring Techniques for Low-voltage Electric Cables," NUREG/CR-6704, Brookhaven National Laboratory, Upton, NY, USA, February 2001.

Moore, G.F., "*Electric Cables Handbook*," Blackwell Science, Inc., Malden, MA, USA, 3<sup>rd</sup> Edition, 1997.

National Science and Technology Council, Committee on Technology, United States White House, "Review of Federal Programs for Wire System Safety," Wire System Safety Interagency Working Group, November 2000.

Rogovin, D. and Kendig, M., "Diagnostic/Prognostics of Aged Wiring Using Broadband Frequency Impedance," 6<sup>th</sup> Joint FAA/DOD NASA Conference on Aging Aircraft, San Francisco, 2002.

Thue, W.A., "*Electric Power Cable Engineering*," Marcel Dekker, Inc., New York, NY, USA, 1999.

Vaughan, W., "Dielectric Properties and Molecular Behavior," Chap. 2, Van Nostrand, 1969.

Villaran, M. and Lofaro, R.J., "*Evaluation of Aging and Environmental Qualification Practices for Power Cables Used in Nuclear Power Plants*" NUREG/CR-6794, Brookhaven National Laboratory, Upton, NY, USA, January 2003.

(This page intentionally left blank)

## **Appendix A**

### **BIS Test Results for Cables with Global Thermal Aging Simulating 20 years and 40 years of Service**

(This page intentionally left blank)

## List of Figures

	<u>Page No.</u>
<b>Figure A-1</b> Low frequency impedance phase spectra for cables globally aged to simulate 20 years of service at various service temperatures . . . . .	168
<b>Figure A-2</b> High frequency impedance phase spectra for cables with global thermal aging to simulate 20 years of service at various service temperatures . . . . .	169
<b>Figure A-3</b> Expanded view of impedance phase and magnitude per unit length spectra for the frequency range from 78 MHz to 86 MHz for cables with global thermal aging to simulate 20 years of service at various service temperatures . . . . .	169
<b>Figure A-4</b> Characteristic impedance magnitude per unit length and phase spectra for cables with global thermal aging to simulate 20 years of service at various service temperatures . . . . .	170
<b>Figure A-5</b> Imaginary and real components of the propagation function spectra for cables with global thermal aging to simulate 20 years of service at various service temperatures . . . . .	170
<b>Figure A-6</b> Resistance per unit length and change in resistance per unit length for cables with global thermal aging to simulate 20 years of service at various service temperatures . . . . .	171
<b>Figure A-7</b> Comparison of resistance per unit length predicted by analytical model to resistance extracted from measured impedance for cable with global thermal aging to simulate 20 years of service at 60°C . . . . .	171
<b>Figure A-8</b> Comparison of resistance per unit length predicted by analytical model to resistance extracted from measured impedance for cable with global thermal aging to simulate 20 years of service at 70°C . . . . .	172
<b>Figure A-9</b> Comparison of resistance per unit length predicted by analytical model to resistance extracted from measured impedance for cable with global thermal aging to simulate 20 years of service at 50°C . . . . .	172
<b>Figure A-10</b> Inductance per unit length and change in inductance for cables with global thermal aging to simulate 20 years of service at various service temperatures .	173
<b>Figure A-11</b> Comparison of inductance per unit length predicted by analytical model to inductance per unit length extracted from measured impedance for cable with global thermal aging to simulate 20 years of service at 50°C . . . . .	173

<b>Figure A-12</b>	Comparison of inductance per unit length predicted by analytical model to inductance per unit length extracted from measured impedance for cable with global thermal aging to simulate 20 years of service at 60°C .....	174
<b>Figure A-13</b>	Comparison of inductance per unit length predicted by analytical model to inductance per unit length extracted from measured impedance for cable with global thermal aging to simulate 20 years of service at 70°C .....	174
<b>Figure A-14</b>	Capacitance per unit length and change in capacitance per unit length for cables with global thermal aging to simulate 20 years of service at various service temperatures .....	175
<b>Figure A-15</b>	Comparison of capacitance per unit length predicted by analytical model to capacitance per unit length extracted from measured impedance for cable with global thermal aging to simulate 20 years of service at 50°C .....	175
<b>Figure A-16</b>	Comparison of capacitance per unit length predicted by analytical model to capacitance per unit length extracted from measured impedance for cable with global thermal aging to simulate 20 years of service at 70°C .....	176
<b>Figure A-17</b>	Conductance-to-frequency ratio per unit length and change in conductance-to-frequency ratio per unit length for cables with global thermal aging to simulate 20 years of service at various service temperatures .....	176
<b>Figure A-18</b>	Comparison of capacitance per unit length predicted by analytical model to capacitance per unit length extracted from measured impedance for cable with global thermal aging to simulate 20 years of service at 60°C .....	177
<b>Figure A-19</b>	Comparison of conductance-to-frequency ratio per unit length predicted by analytical model to that extracted from measured impedance for cable with global thermal aging to simulate 20 years of service at 50°C .....	177
<b>Figure A-20</b>	Comparison of conductance-to-frequency ratio per unit length predicted by analytical model to that extracted from measured impedance for cable with global thermal aging to simulate 20 years of service at 60°C .....	178
<b>Figure A-21</b>	Comparison of conductance-to-frequency ratio per unit length predicted by analytical model to that extracted from measured impedance for cable with global thermal aging to simulate 20 years of service at 70°C .....	178
<b>Figure A-22</b>	Comparison of characteristic impedance magnitude per unit length and phase spectra predicted by analytical model to that extracted from measured impedance for cables with global thermal aging to simulate 20 years of service at 50°C ..	179

<b>Figure A-23</b>	Comparison of imaginary and real components of the propagation function predicted by analytical model to that extracted from measured impedance for cable with global thermal aging to simulate 20 years of service at 50°C . . . . .	179
<b>Figure A-24</b>	Comparison of characteristic impedance magnitude and phase spectra predicted by analytical model to that extracted from measured impedance for cable with global thermal aging to simulate 20 years of service at 60°C . . . . .	180
<b>Figure A-25</b>	Comparison of imaginary and real components of the propagation function predicted by analytical model to that extracted from measured impedance for cable with global thermal aging to simulate 20 years of service at 60°C . . . . .	180
<b>Figure A-26</b>	Comparison of characteristic impedance magnitude per unit length and phase spectra predicted by analytical model to that extracted from measured impedance for cable with global thermal aging to simulate 20 years of service at 70°C . . .	181
<b>Figure A-27</b>	Comparison of imaginary component and real component of the propagation function for cable with global thermal aging to simulate 20 years of service at 70°C . . . . .	181
<b>Figure A-28</b>	Low frequency impedance phase spectra for cables with global thermal aging to simulate 40 years of service at various service temperatures . . . . .	182
<b>Figure A-29</b>	High frequency impedance phase spectra for cables with global thermal aging to simulate 40 years of service at various service temperatures . . . . .	183
<b>Figure A-30</b>	Expanded view of impedance phase and magnitude per unit length spectra over the frequency range from 78 MHz to 86 MHz for cables with global thermal aging to simulate 40 years of service at various service temperatures . . . . .	183
<b>Figure A-31</b>	Characteristic impedance magnitude and phase spectra for cables with global thermal aging to simulate 40 years of service at various service temperatures .	184
<b>Figure A-32</b>	Imaginary and real components of the propagation function for cables with global thermal aging to simulate 40 years of service at various service temperatures .	184
<b>Figure A-33</b>	Resistance per unit length and change in resistance per unit length for cables with global thermal aging to simulate 40 years of service at various service temperatures . . . . .	185
<b>Figure A-34</b>	Comparison of resistance per unit length predicted by analytical model to that extracted from measured impedance for cable with global thermal aging to simulate 40 years of service at 50°C . . . . .	185



<b>Figure A-35</b>	Comparison of resistance per unit length predicted by analytical model to that extracted from measured impedance for cable with global thermal aging to simulate 40 years of service at 60°C .....	186
<b>Figure A-36</b>	Comparison of resistance per unit length predicted by analytical model to that extracted from measured impedance for cable with global thermal aging to simulate 40 years of service at 70°C .....	186
<b>Figure A-37</b>	Inductance per unit length and change in inductance per unit length for cables with global thermal aging to simulate 40 years of service at various service temperatures .....	187
<b>Figure A-38</b>	Comparison of inductance per unit length predicted by analytical model to that extracted from measured impedance for cable with global thermal aging to simulate 40 years of service at 50°C .....	187
<b>Figure A-39</b>	Comparison of inductance per unit length predicted by analytical model to that extracted from measured impedance for cable with global thermal aging to simulate 40 years of service at 60°C .....	188
<b>Figure A-40</b>	Comparison of inductance per unit length predicted by analytical model to that extracted from measured impedance for cable with global thermal aging to simulate 40 years of service at 70°C .....	188
<b>Figure A-41</b>	Capacitance per unit length and change in capacitance per unit length for cables with global thermal aging to simulate 40 years of service at various service temperatures .....	189
<b>Figure A-42</b>	Comparison of capacitance per unit length predicted by analytical model to that extracted from measured impedance for cable with global thermal aging to simulate 40 years at 50°C .....	189
<b>Figure A-43</b>	Comparison of capacitance per unit length predicted by analytical model to that extracted from measured impedance for cable with global thermal aging to simulate 40 years of service at 60°C .....	190
<b>Figure A-44</b>	Comparison of capacitance per unit length predicted by analytical model to that extracted from measured impedance for cable with global thermal aging to simulate 40 years of service at 70°C .....	190
<b>Figure A-45</b>	Conductance-to-frequency ratio per unit length and change in conductance-to-frequency ratio per unit length for cables with global thermal aging to simulate 40 years of service at various service temperatures .....	191

<b>Figure A-46</b>	Comparison of conductance-to-frequency ratio per unit length predicted by analytical model to that extracted from measured impedance for cable with global thermal aging to simulate 40 years of service at 50°C .....	191
<b>Figure A-47</b>	Comparison of conductance-to-frequency ratio per unit length predicted by analytical model to that extracted from measured impedance for cable with global thermal aging to simulate 40 years of service at 60°C .....	192
<b>Figure A-48</b>	Comparison of conductance-to-frequency ratio per unit length predicted by analytical model to that extracted from measured impedance for cable with global thermal aging to simulate 40 years of service at 70°C .....	192
<b>Figure A-49</b>	Comparison of characteristic impedance magnitude per unit length and phase spectra predicted by analytical model to that extracted from measured impedance for cable with global thermal aging to simulate 40 years of service at 50°C ..	193
<b>Figure A-50</b>	Comparison of characteristic impedance magnitude per unit length and phase spectra predicted by analytical model to that extracted from measured impedance for cable with global thermal aging to simulate 40 years of service at 60°C ..	193
<b>Figure A-51</b>	Comparison of characteristic impedance magnitude per unit length and phase spectra predicted by analytical model to that extracted from measured impedance for cable with global thermal aging to simulate 40 years of service at 70°C ..	194
<b>Figure A-52</b>	Comparison of the imaginary component and real component of the propagation function predicted by analytical model to that extracted from measured impedance for cable with global thermal aging to simulate 40 years of service at 50°C .....	194
<b>Figure A-53</b>	Comparison of the imaginary component and real component of the propagation function predicted by analytical model to that extracted from measured impedance for cable with global thermal aging to simulate 40 years of service at 60°C .....	195
<b>Figure A-54</b>	Comparison of the imaginary component and real component of the propagation function predicted by analytical model to that extracted from measured impedance for cable with global thermal aging to simulate 40 years of service at 70°C .....	195
<b>Figure A-55</b>	Comparison of resistance per unit length predicted by analytical model to that extracted from measured impedance for cable with global thermal aging to simulate 60 years of service at 50°C .....	196

<b>Figure A-56</b>	Comparison of resistance per unit length predicted by analytical model to that extracted from measured impedance for cable with global thermal aging to simulate 60 years of service at 60°C .....	197
<b>Figure A-57</b>	Comparison of inductance per unit length predicted by analytical model to that extracted from measured impedance for cable with global thermal aging to simulate 60 years of service at 50°C .....	197
<b>Figure A-58</b>	Comparison of inductance per unit length predicted by analytical model to that extracted from measured impedance for cable with global thermal aging to simulate 60 years of service at 60°C .....	198
<b>Figure A-59</b>	Comparison of capacitance per unit length predicted by analytical model to that extracted from measured impedance for cable with global thermal aging to simulate 60 years of service at 50°C .....	198
<b>Figure A-60</b>	Comparison of capacitance per unit length predicted by analytical model to that extracted from measured impedance for cable with global thermal aging to simulate 60 years of service at 60°C .....	199
<b>Figure A-61</b>	Comparison of conductance-to-frequency ratio per unit length predicted by analytical model to that extracted from measured impedance for cable with global thermal aging to simulate 60 years of service at 50°C .....	199
<b>Figure A-62</b>	Comparison of conductance-to-frequency ratio per unit length predicted by analytical model to that extracted from measured impedance for cable with global thermal aging to simulate 60 years of service at 60°C .....	200
<b>Figure A-63</b>	Comparison of characteristic impedance magnitude per unit length and phase spectra predicted by analytical model to that extracted from measured impedance for cable with global thermal aging to simulate 60 years of service at 50°C ..	200
<b>Figure A-64</b>	Comparison of characteristic impedance magnitude per unit length and phase spectra predicted by analytical model to that extracted from measured impedance for cable with global thermal aging to simulate 60 years of service at 60°C ..	201
<b>Figure A-65</b>	Comparison of the imaginary component and real component of the propagation function predicted by analytical model to that extracted from measured impedance for cable with global thermal aging to simulate 60 years of service at 50°C .....	201
<b>Figure A-66</b>	Comparison of the imaginary component and real component of the propagation function predicted by analytical model to that extracted from measured	

impedance for cable with global thermal aging to simulate 60 years of service at  
60°C ..... 202

## A.1 Test Results for Cables with Global Thermal Aging to Simulate 20 Years of Service

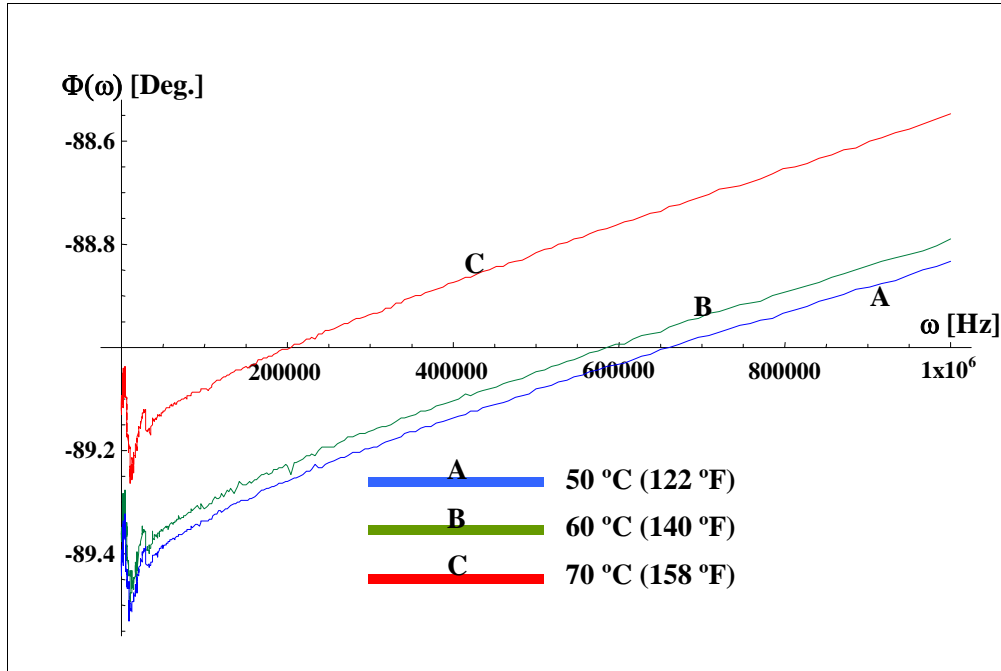


**Figure A-1** Low frequency impedance phase spectra for cables globally aged to simulate 20 years of service at various service temperatures

The following figures present the results of broadband impedance tests performed on cables with global thermal aging to simulate 20 years of service in a nuclear power plant at service temperatures of 50°C (122°F), 60°C (140°F), and 70°C (158°F). These results supplement the data presented in Section 5 of this report.

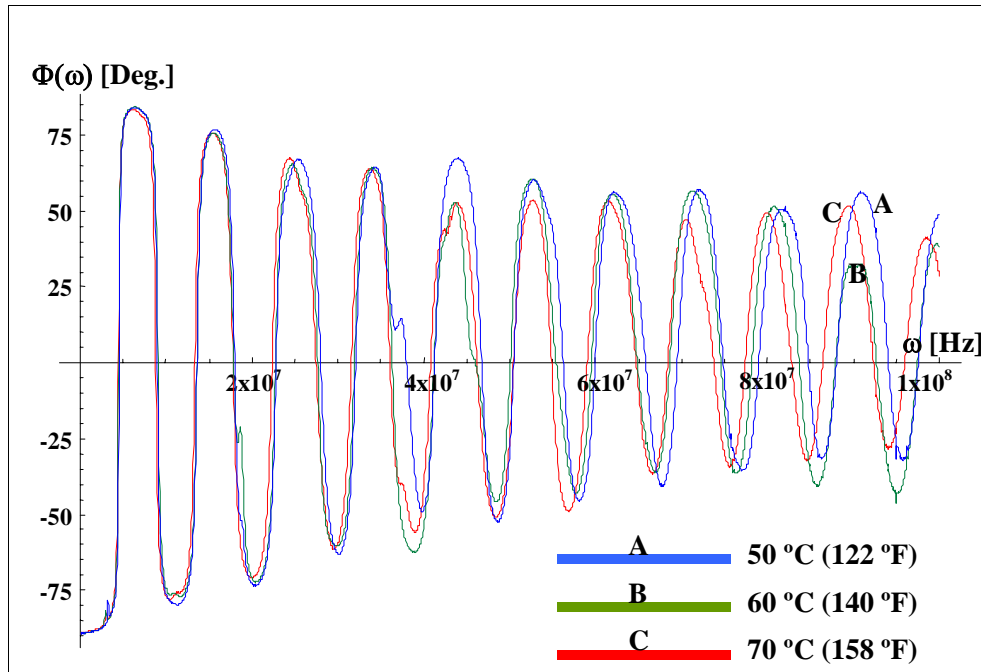


**Figure A-2** High frequency impedance phase spectra for cables with global thermal aging to simulate 20 years of service at various service temperatures

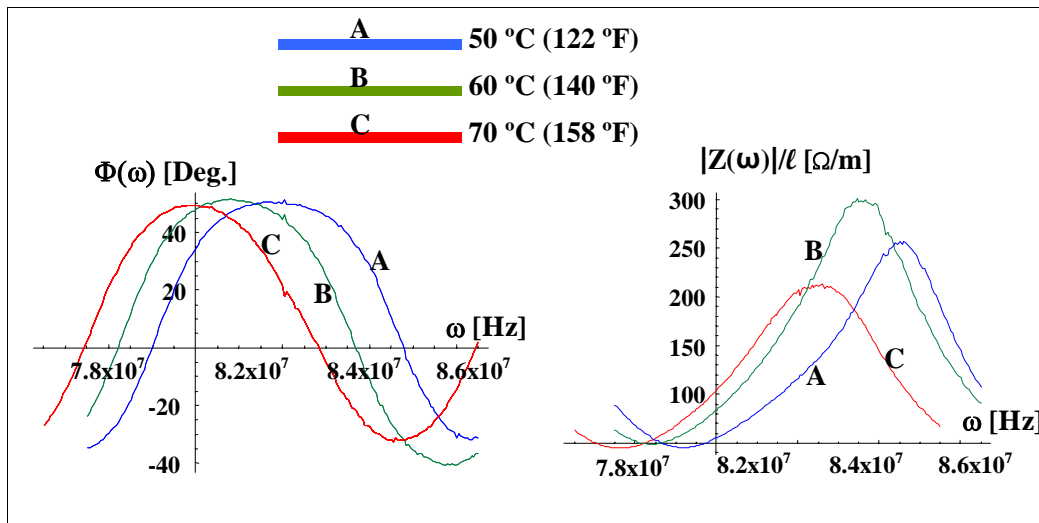


**Figure A-3** Expanded view of impedance phase and magnitude per unit length spectra for the frequency range from 78 MHz to 86 MHz for cables with global thermal aging to simulate 20 years of service at various service temperatures

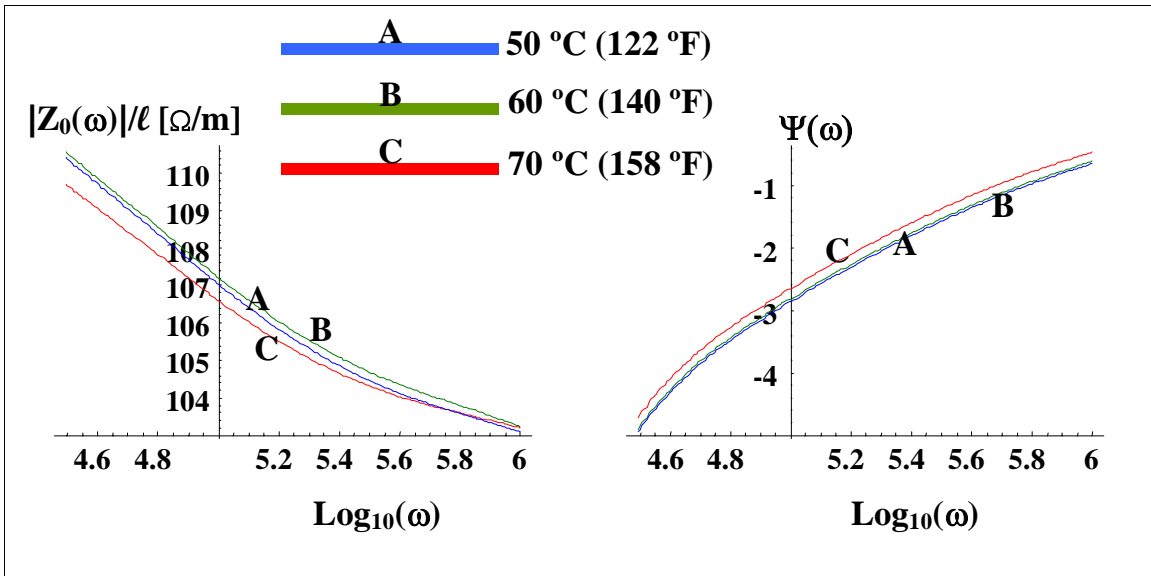


**Figure A-4** Characteristic impedance magnitude per unit length and phase spectra for cables with global thermal aging to simulate 20 years of service at various service temperatures

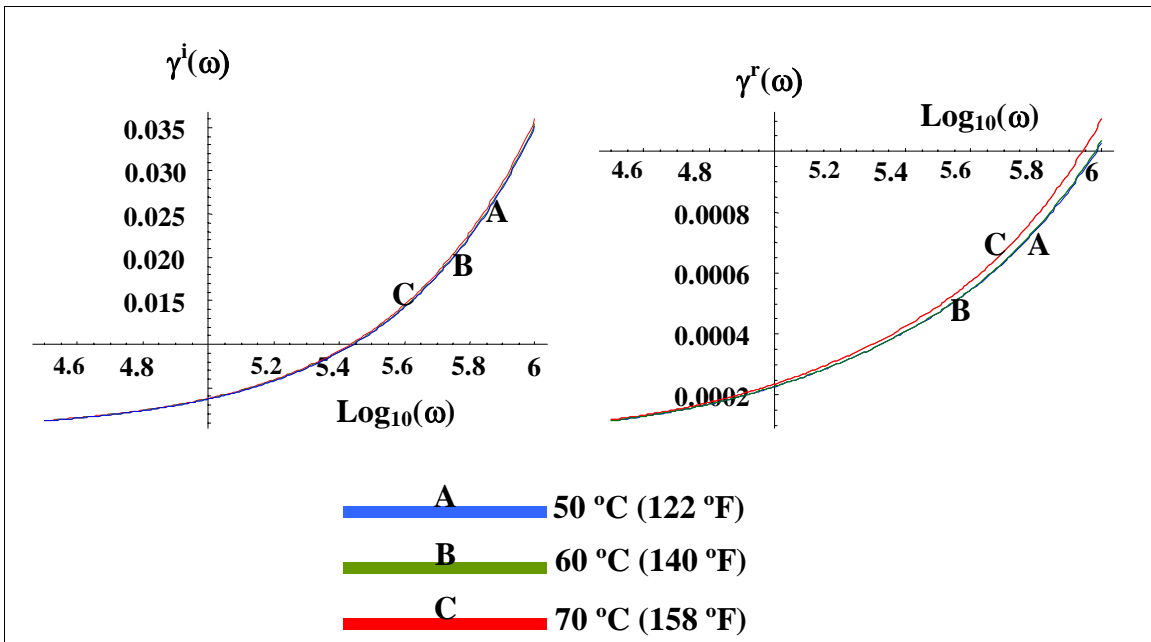


**Figure A-5** Imaginary and real components of the propagation function spectra for cables with global thermal aging to simulate 20 years of service at various service temperatures

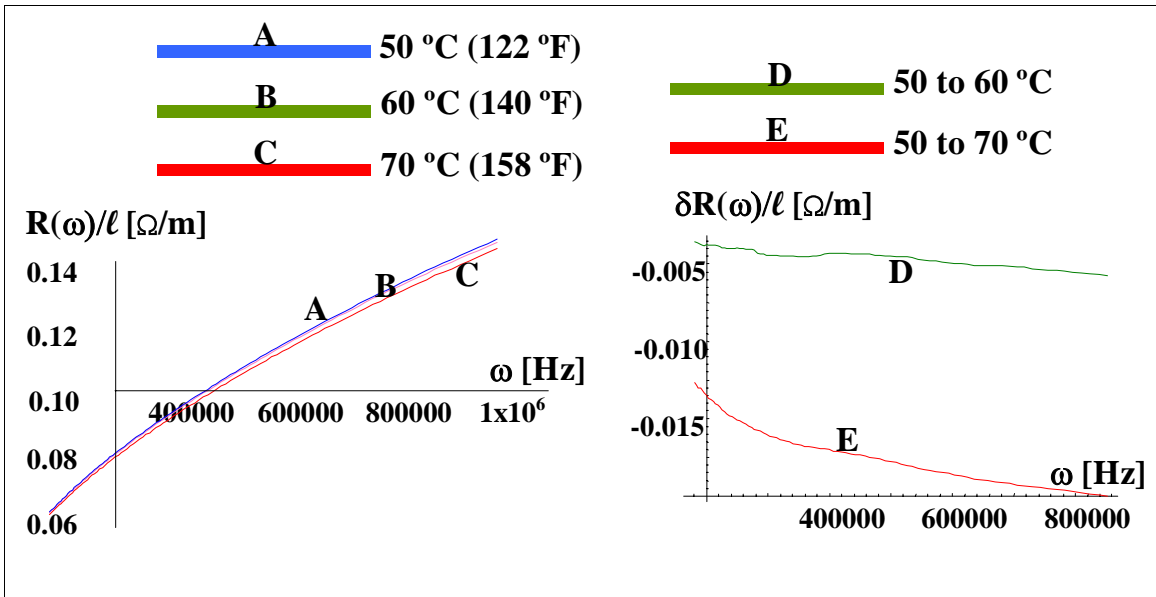


**Figure A-6** Resistance per unit length and change in resistance per unit length for cables with global thermal aging to simulate 20 years of service at various service temperatures

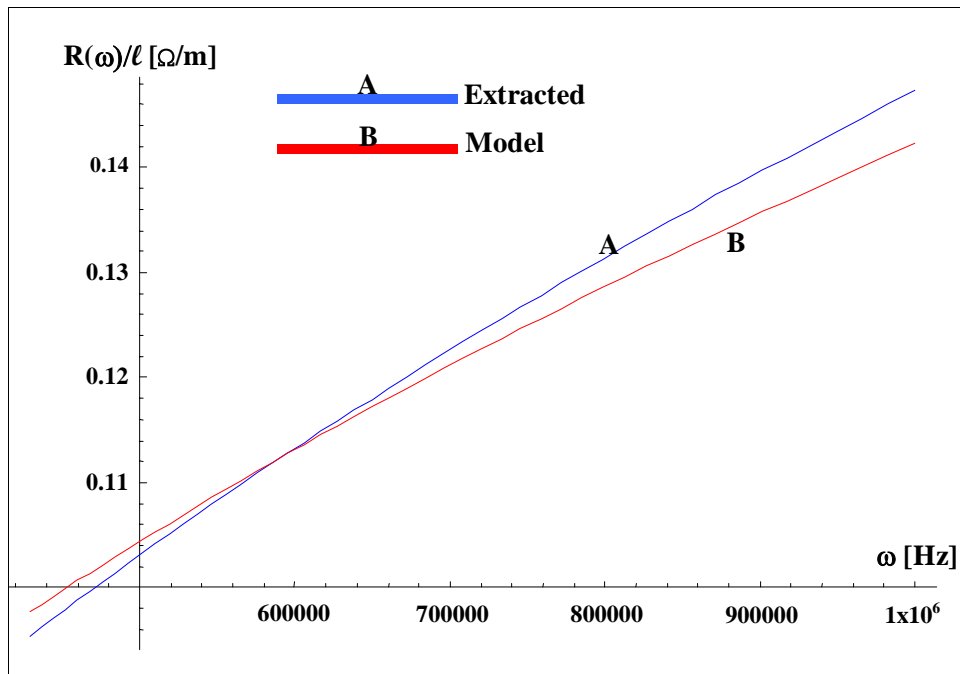


**Figure A-7** Comparison of resistance per unit length predicted by analytical model to resistance extracted from measured impedance for cable with global thermal aging to simulate 20 years of service at 60°C



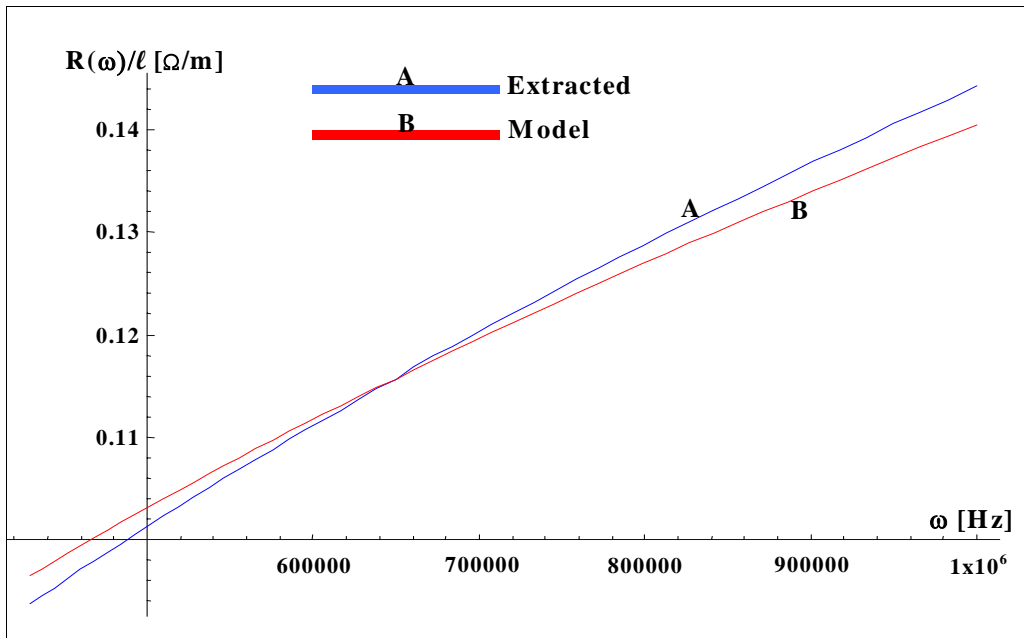


**Figure A-8** Comparison of resistance per unit length predicted by analytical model to resistance extracted from measured impedance for cable with global thermal aging to simulate 20 years of service at 70°C

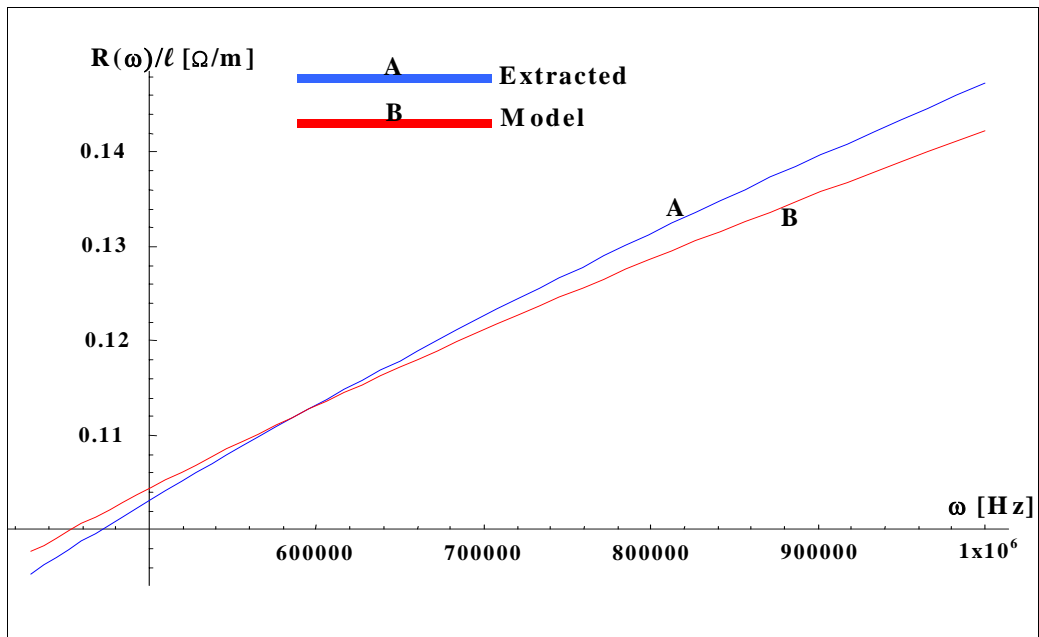


**Figure A-9** Comparison of resistance per unit length predicted by analytical model to resistance extracted from measured impedance for cable with global thermal aging to simulate 20 years of service at 50°C

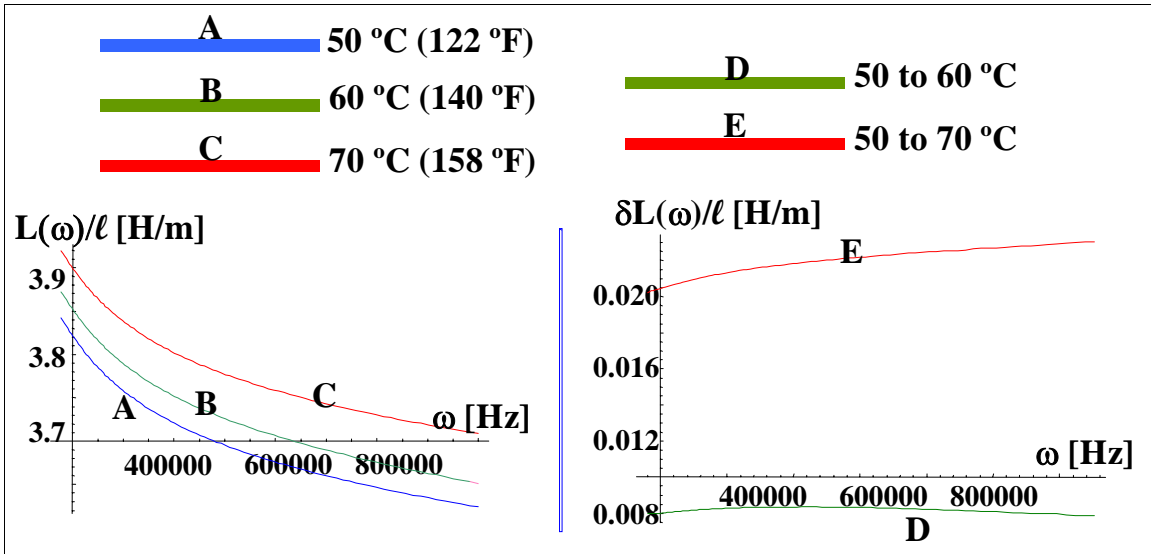


**Figure A-10** Inductance per unit length and change in inductance for cables with global thermal aging to simulate 20 years of service at various service temperatures

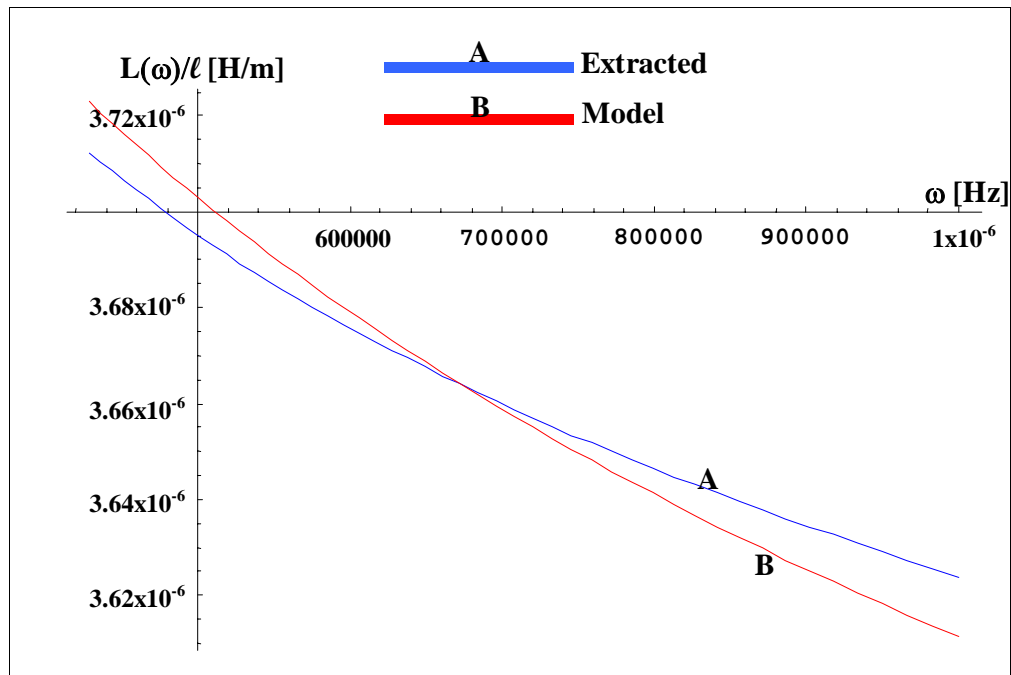


**Figure A-11** Comparison of inductance per unit length predicted by analytical model to inductance per unit length extracted from measured impedance for cable with global thermal aging to simulate 20 years of service at 50°C

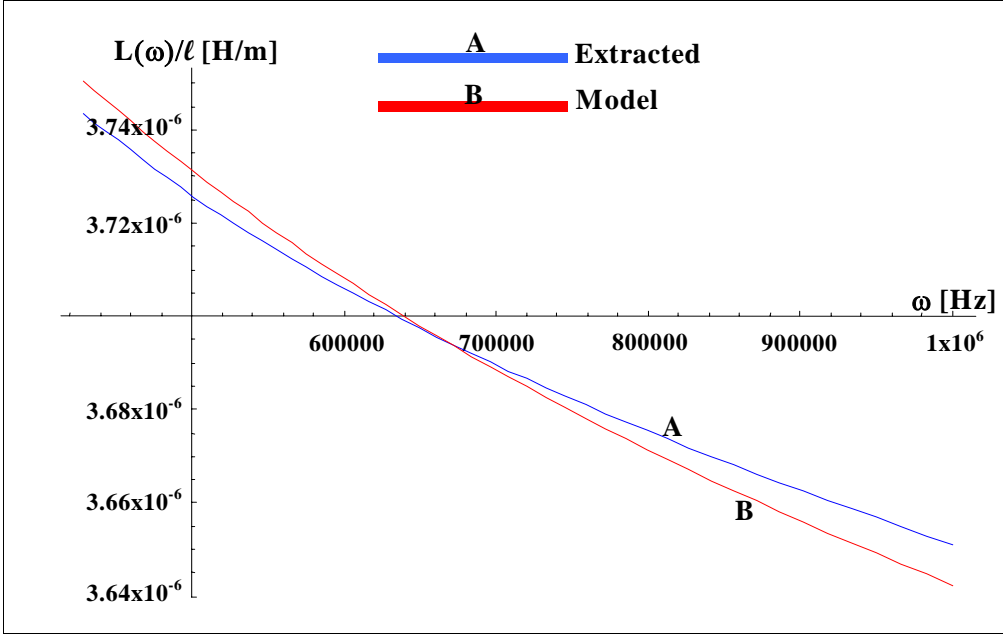


**Figure A-12** Comparison of inductance per unit length predicted by analytical model to inductance per unit length extracted from measured impedance for cable with global thermal aging to simulate 20 years of service at 60°C

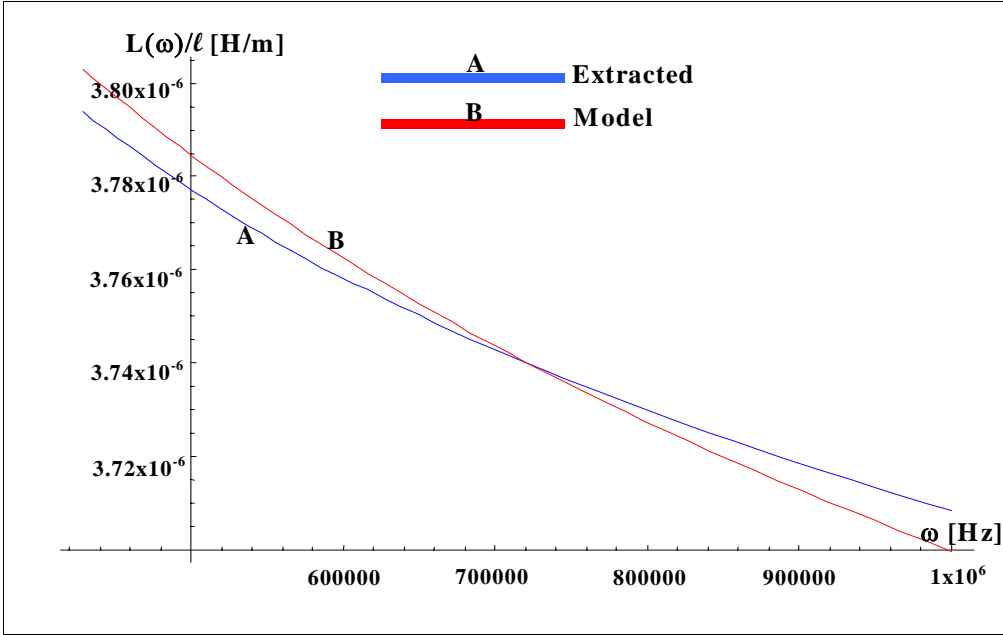


**Figure A-13** Comparison of inductance per unit length predicted by analytical model to inductance per unit length extracted from measured impedance for cable with global thermal aging to simulate 20 years of service at 70°C

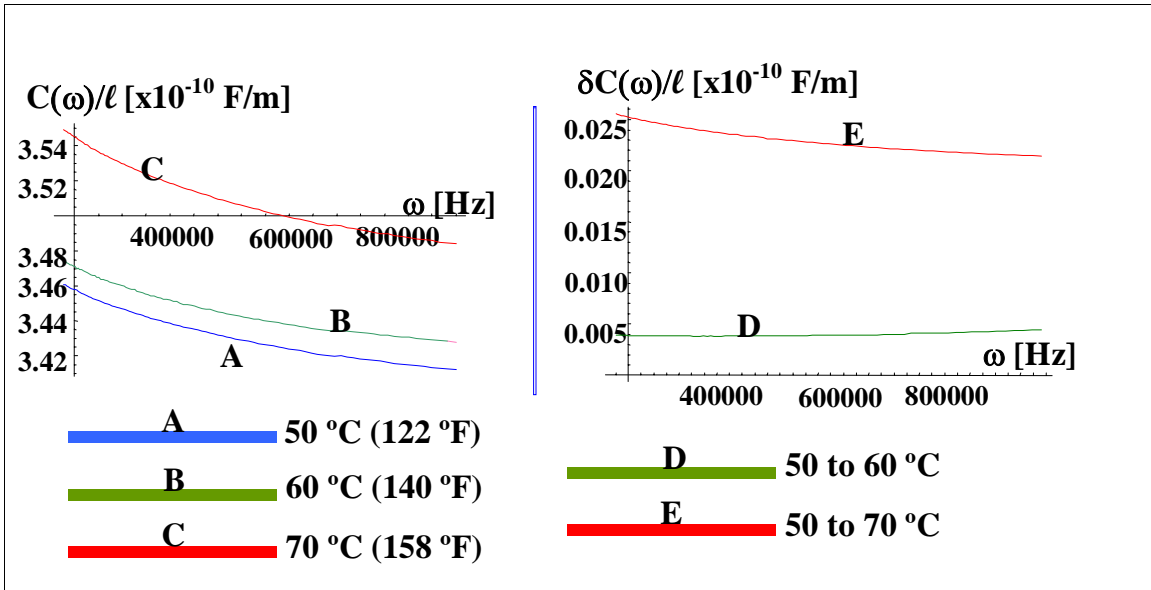


**Figure A-14** Capacitance per unit length and change in capacitance per unit length for cables with global thermal aging to simulate 20 years of service at various service temperatures

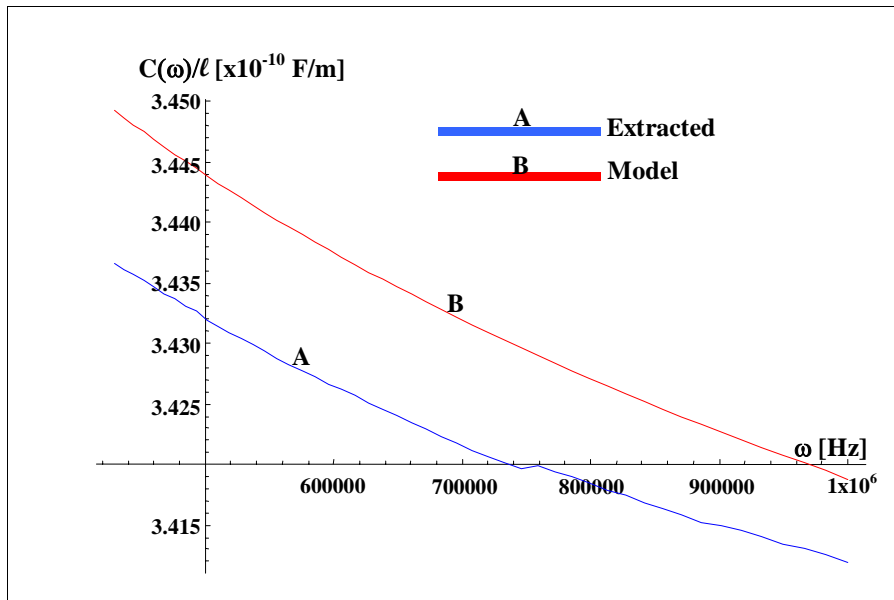


**Figure A-15** Comparison of capacitance per unit length predicted by analytical model to capacitance per unit length extracted from measured impedance for cable with global thermal aging to simulate 20 years of service at 50°C

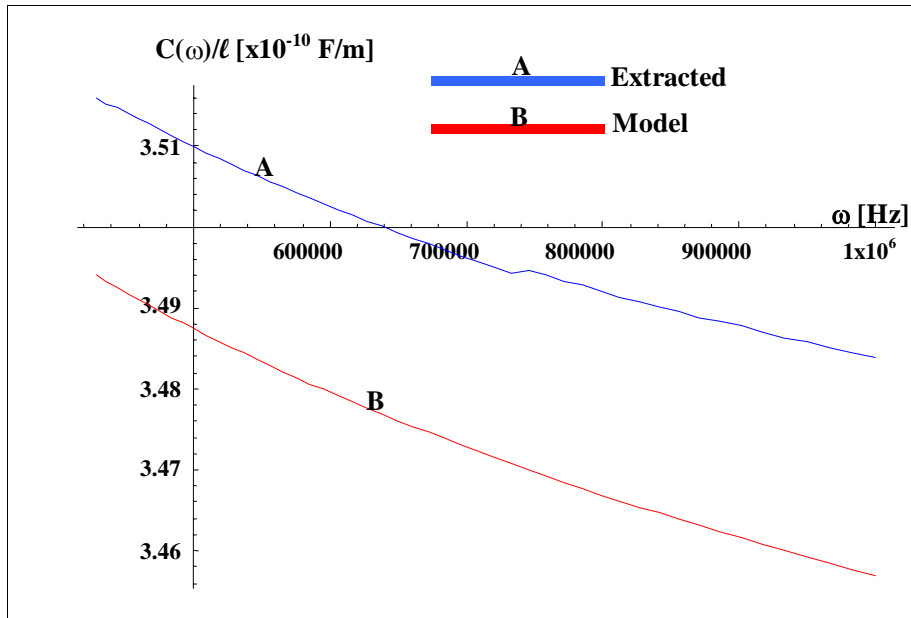


**Figure A-16** Comparison of capacitance per unit length predicted by analytical model to capacitance per unit length extracted from measured impedance for cable with global thermal aging to simulate 20 years of service at 70°C

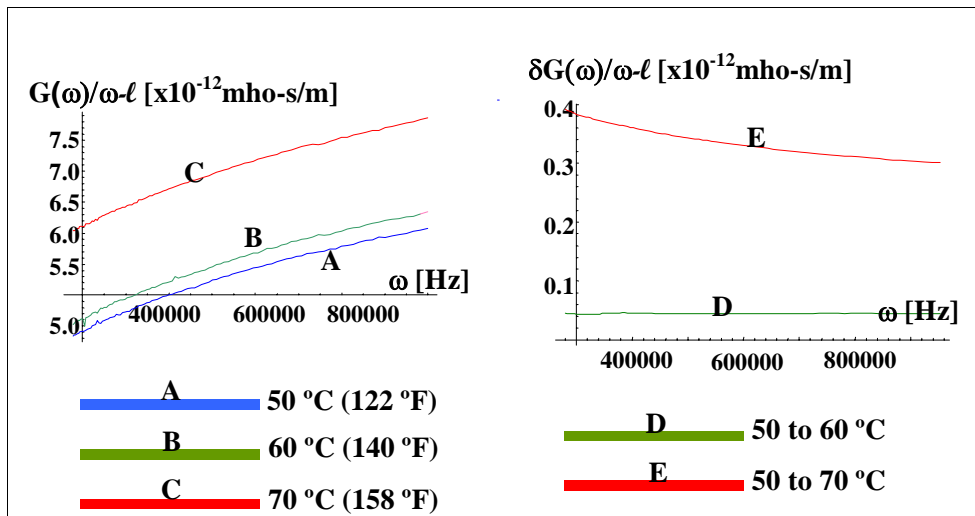


**Figure A-17** Conductance-to-frequency ratio per unit length and change in conductance-to-frequency ratio per unit length for cables with global thermal aging to simulate 20 years of service at various service temperatures

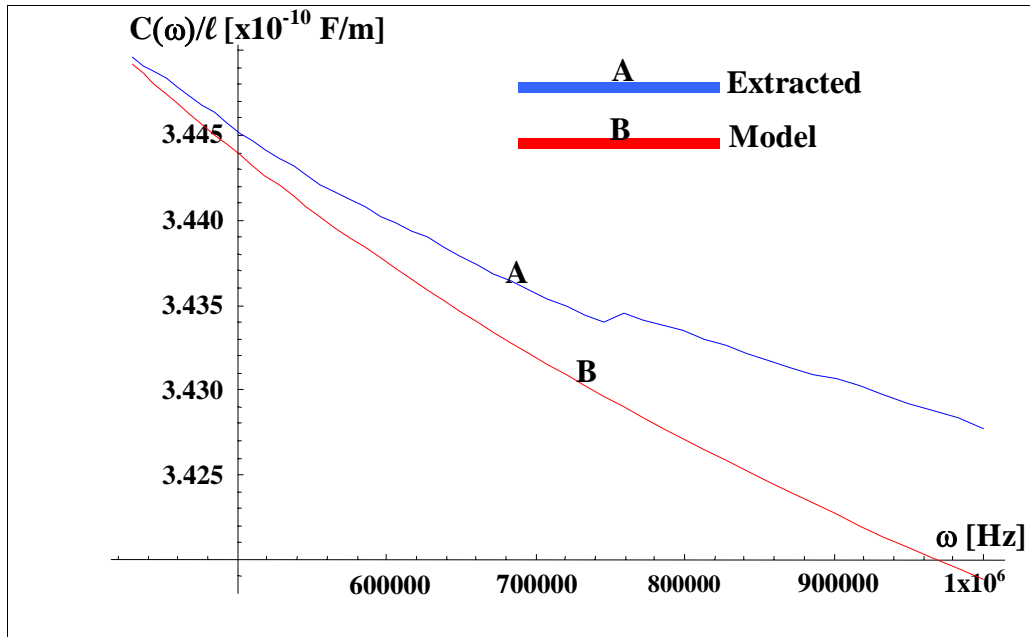


**Figure A-18** Comparison of capacitance per unit length predicted by analytical model to capacitance per unit length extracted from measured impedance for cable with global thermal aging to simulate 20 years of service at 60°C

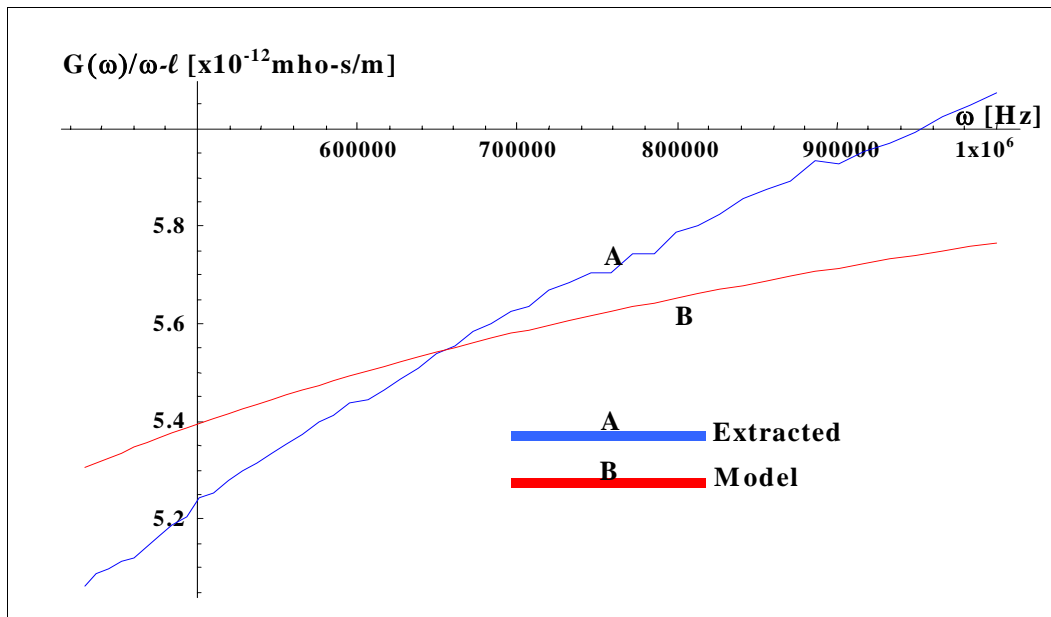


**Figure A-19** Comparison of conductance-to-frequency ratio per unit length predicted by analytical model to that extracted from measured impedance for cable with global thermal aging to simulate 20 years of service at 50°C

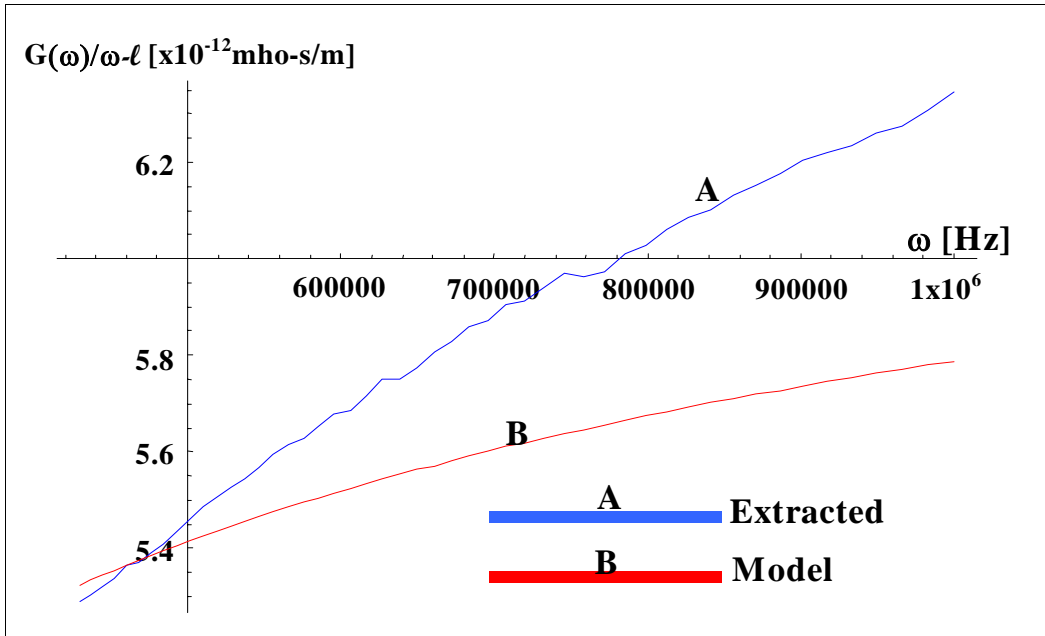


**Figure A-20** Comparison of conductance-to-frequency ratio per unit length predicted by analytical model to that extracted from measured impedance for cable with global thermal aging to simulate 20 years of service at 60°C

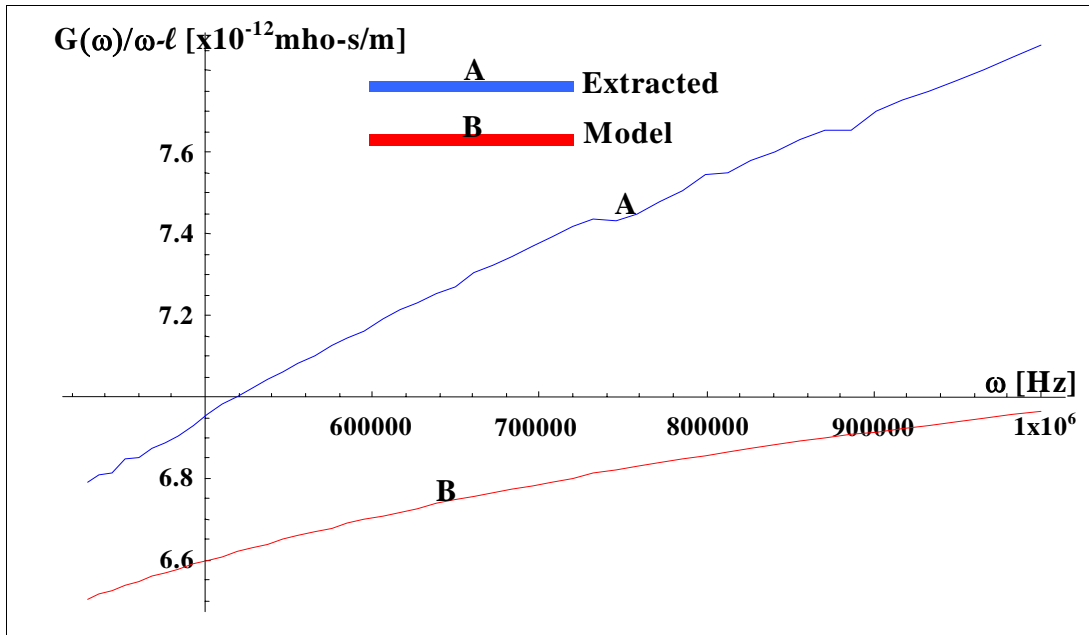


**Figure A-21** Comparison of conductance-to-frequency ratio per unit length predicted by analytical model to that extracted from measured impedance for cable with global thermal aging to simulate 20 years of service at 70°C

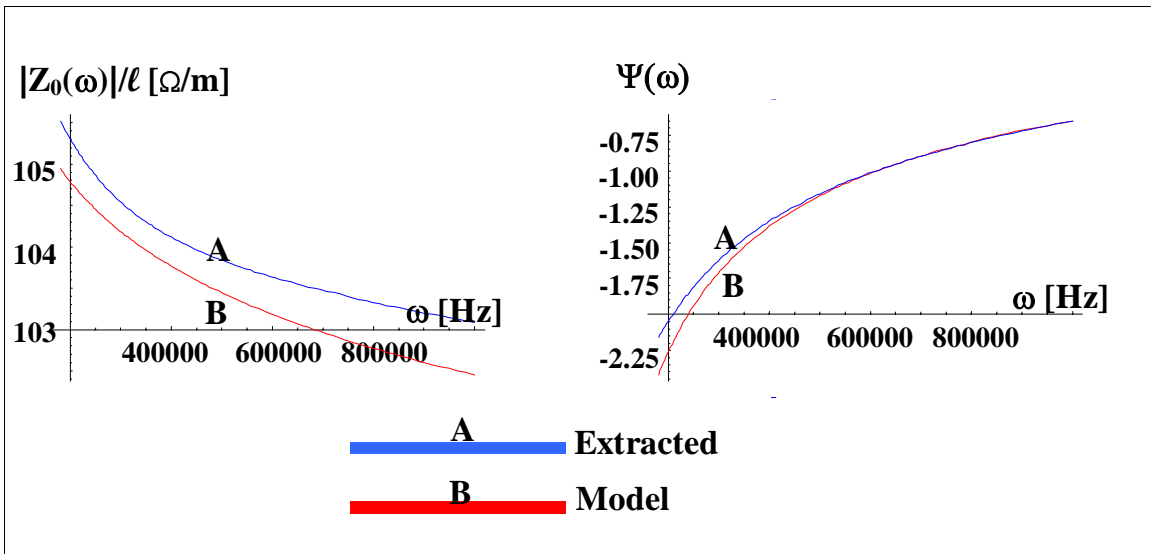


**Figure A-22** Comparison of characteristic impedance magnitude per unit length and phase spectra predicted by analytical model to that extracted from measured impedance for cables with global thermal aging to simulate 20 years of service at 50°C

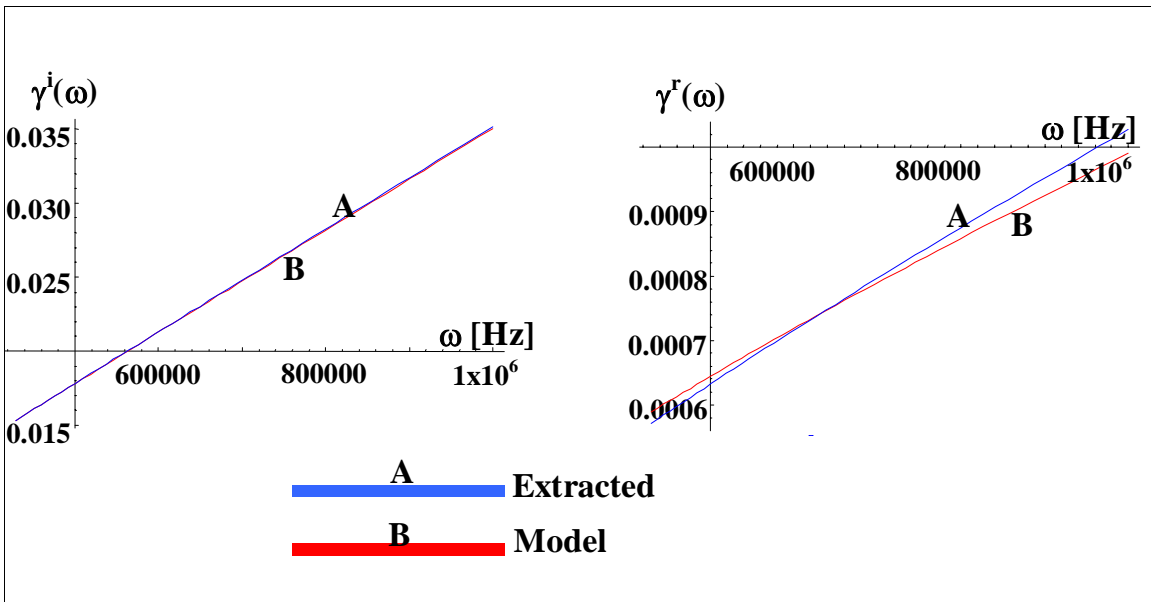


**Figure A-23** Comparison of imaginary and real components of the propagation function predicted by analytical model to that extracted from measured impedance for cable with global thermal aging to simulate 20 years of service at 50°C



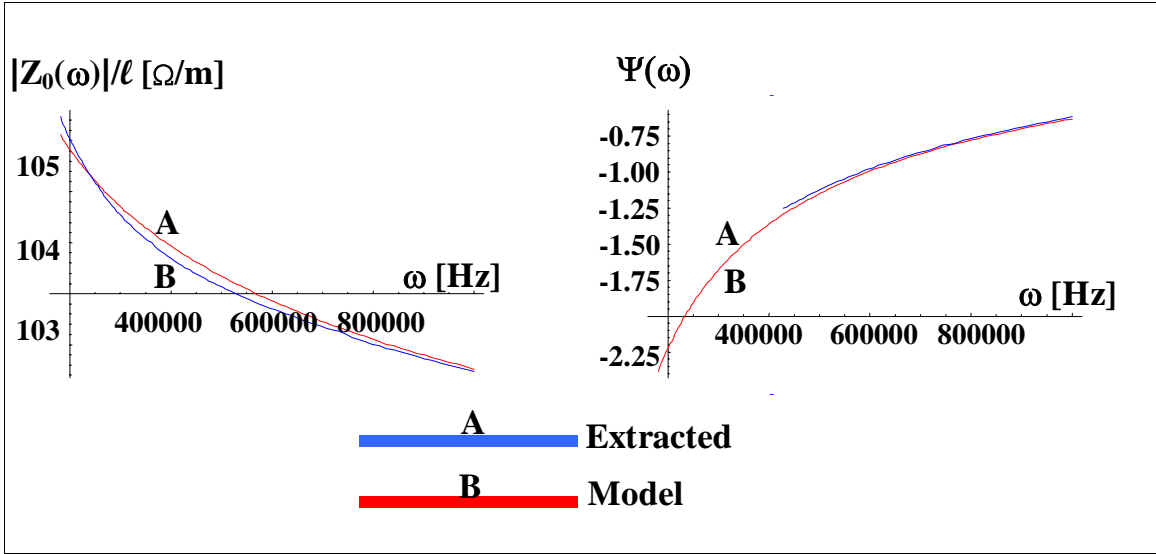


**Figure A-24** Comparison of characteristic impedance magnitude and phase spectra predicted by analytical model to that extracted from measured impedance for cable with global thermal aging to simulate 20 years of service at 60°C

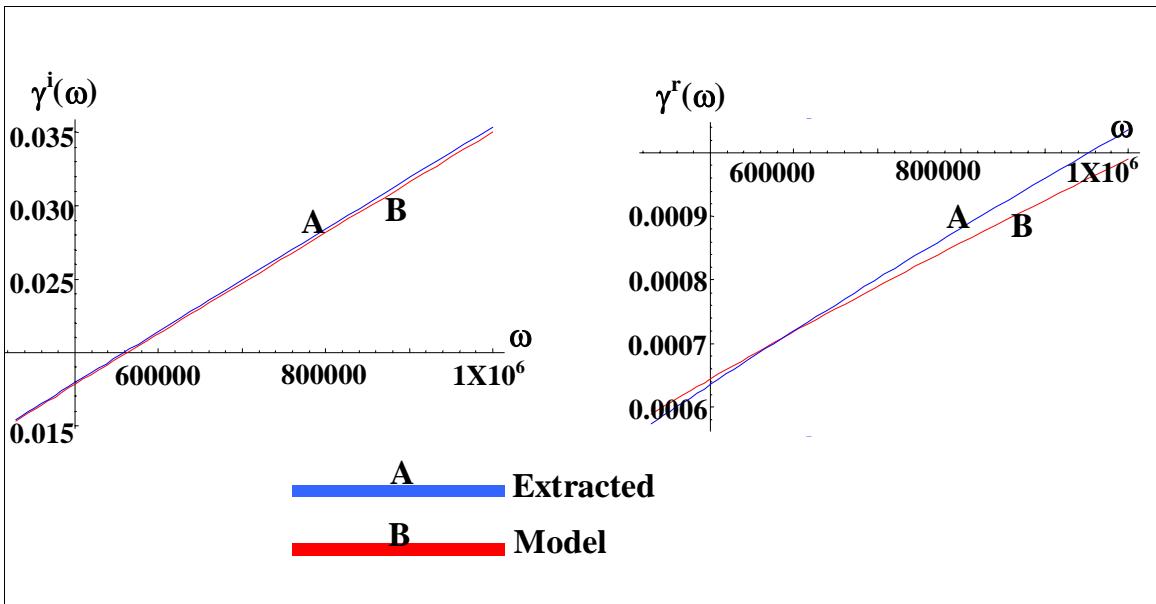


**Figure A-25** Comparison of imaginary and real components of the propagation function predicted by analytical model to that extracted from measured impedance for cable with global thermal aging to simulate 20 years of service at 60°C

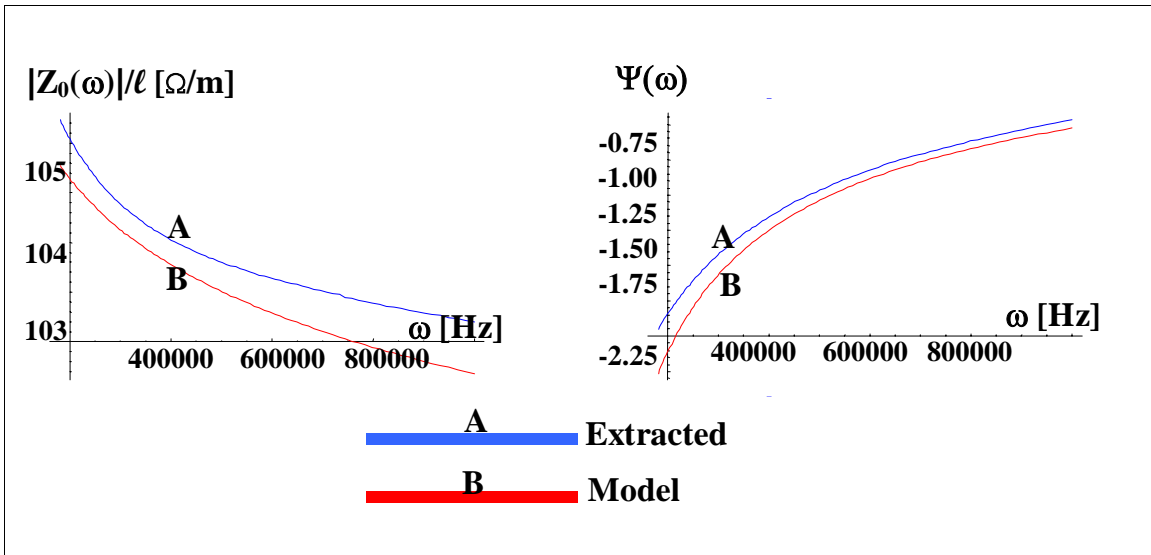


**Figure A-26** Comparison of characteristic impedance magnitude per unit length and phase spectra predicted by analytical model to that extracted from measured impedance for cable with global thermal aging to simulate 20 years of service at 70°C

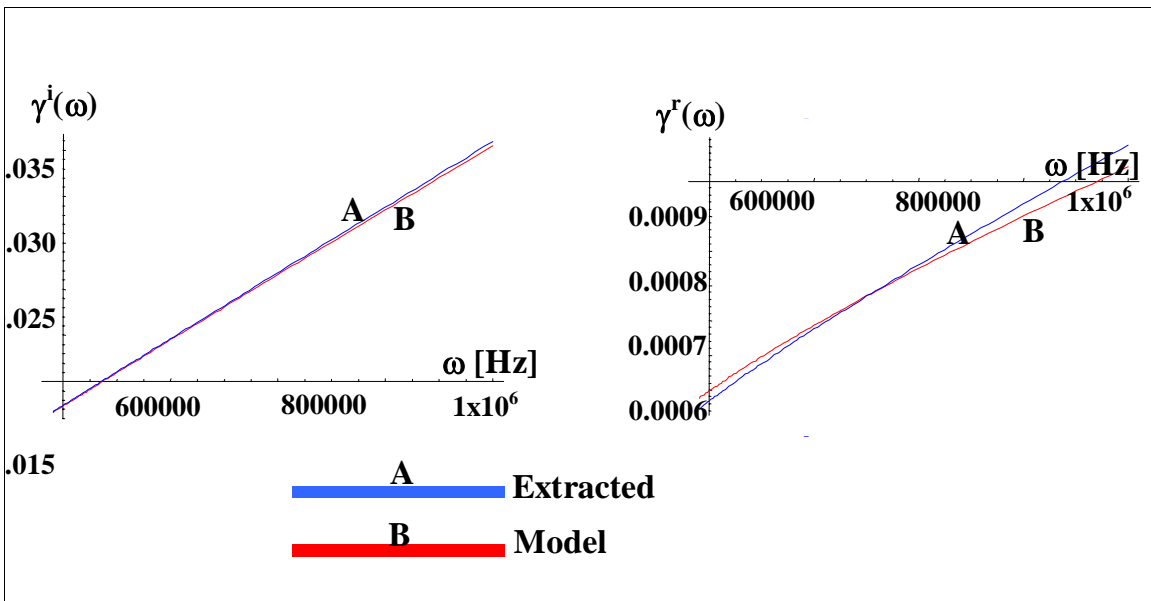


**Figure A-27** Comparison of imaginary component and real component of the propagation function for cable with global thermal aging to simulate 20 years of service at 70°C

## A.2 Test Results for Cables with Global Thermal Aging to Simulate 40 Years of Service

The following figures present the results of broadband impedance tests performed on cables with global thermal aging to simulate 40 years of service in a nuclear power plant at service temperatures of 50°C (122°F), 60°C (140°F), and 70°C (158°F). These results supplement the data presented in Section 5 of this report.

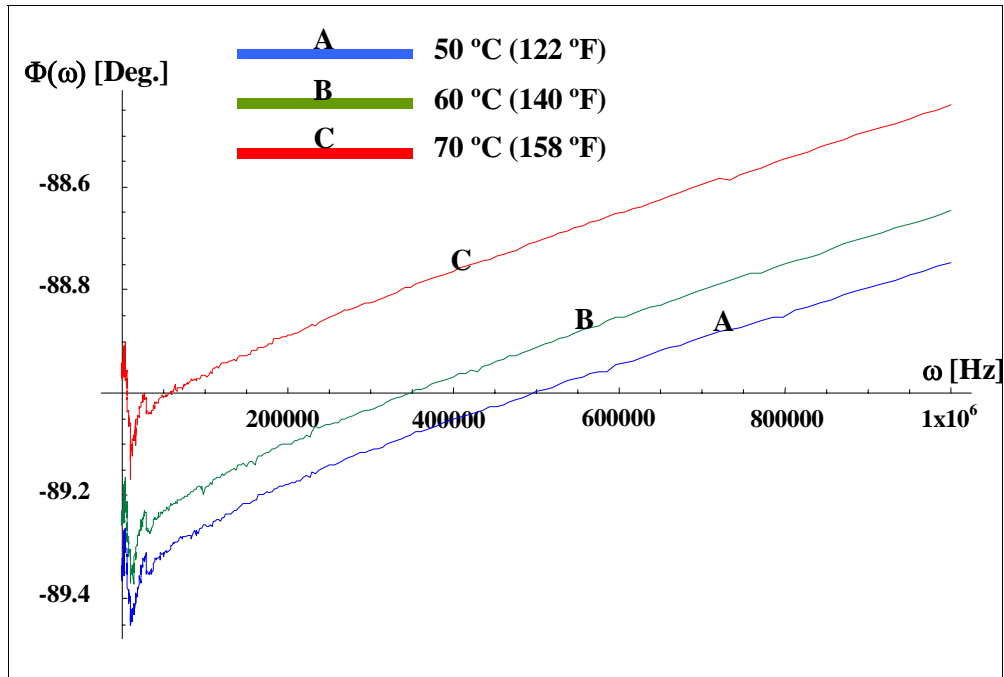


**Figure A-28** Low frequency impedance phase spectra for cables with global thermal aging to simulate 40 years of service at various service temperatures

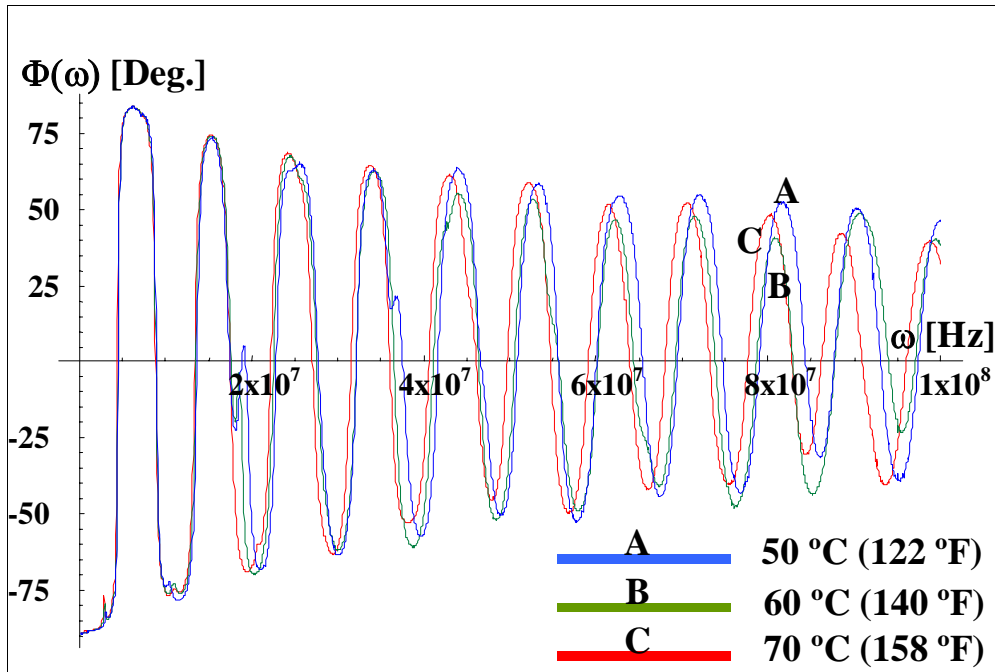


**Figure A-29** High frequency impedance phase spectra for cables with global thermal aging to simulate 40 years of service at various service temperatures

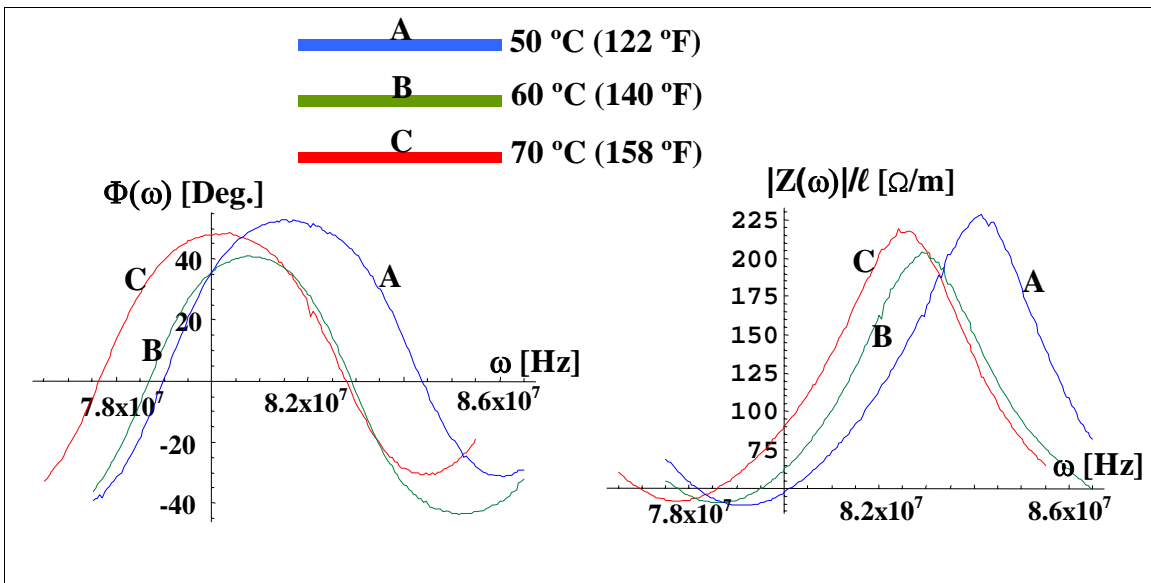


**Figure A-30** Expanded view of impedance phase and magnitude per unit length spectra over the frequency range from 78 MHz to 86 MHz for cables with global thermal aging to simulate 40 years of service at various service temperatures

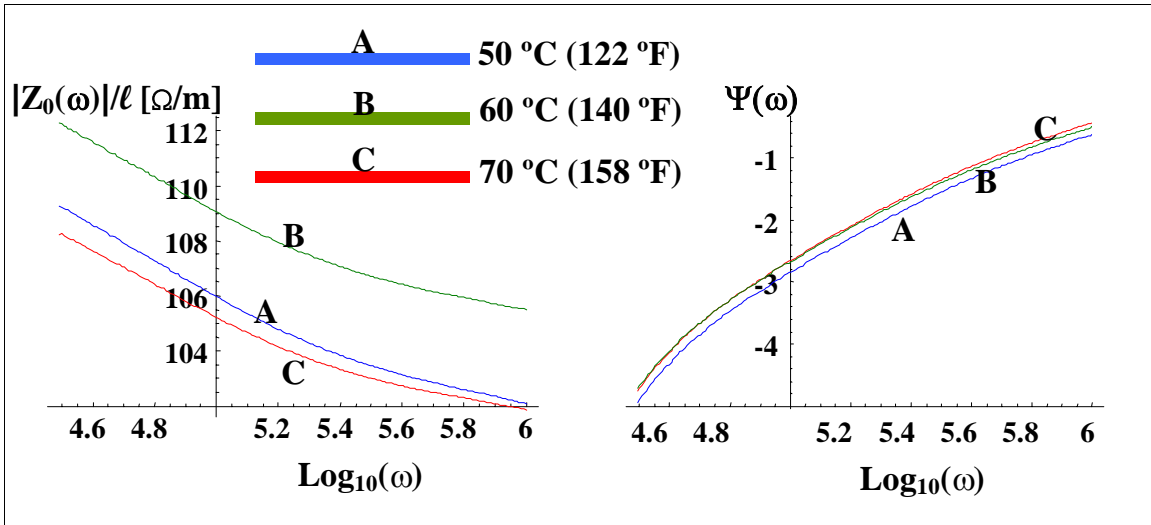


**Figure A-31** Characteristic impedance magnitude and phase spectra for cables with global thermal aging to simulate 40 years of service at various service temperatures

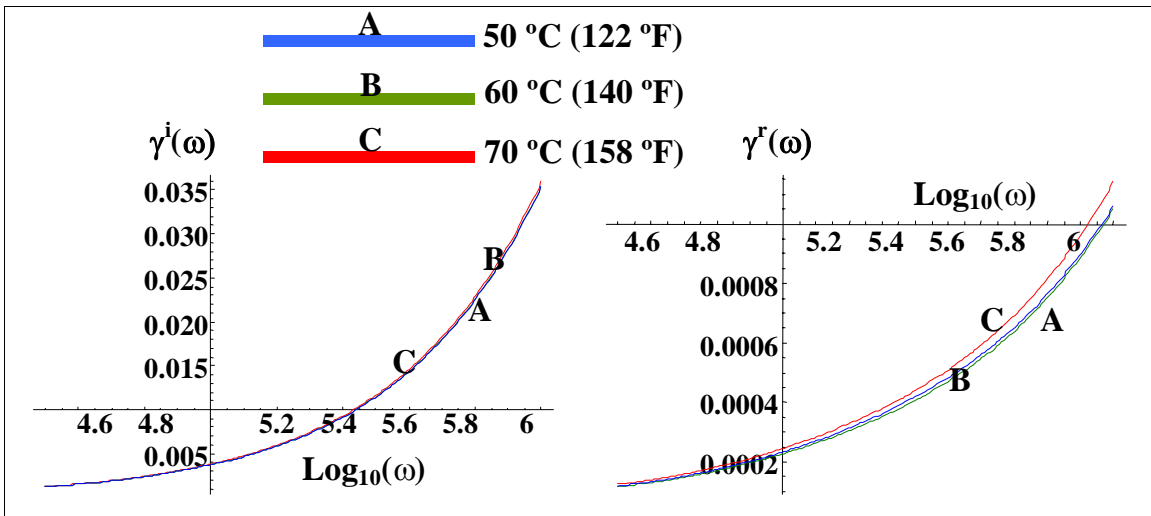


**Figure A-32** Imaginary and real components of the propagation function for cables with global thermal aging to simulate 40 years of service at various service temperatures

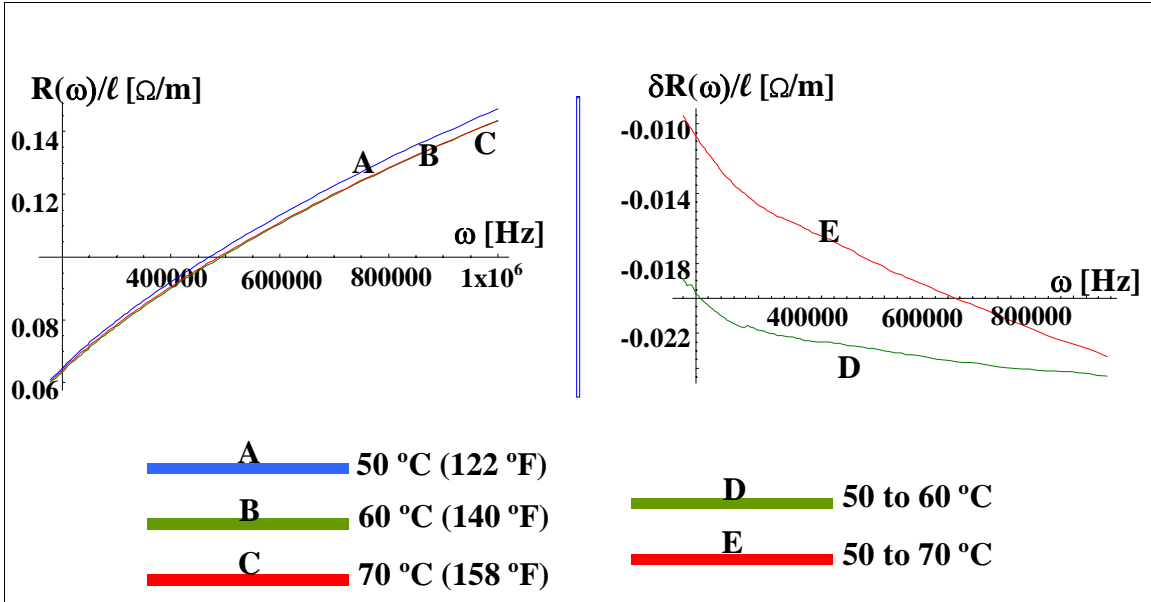


**Figure A-33** Resistance per unit length and change in resistance per unit length for cables with global thermal aging to simulate 40 years of service at various service temperatures

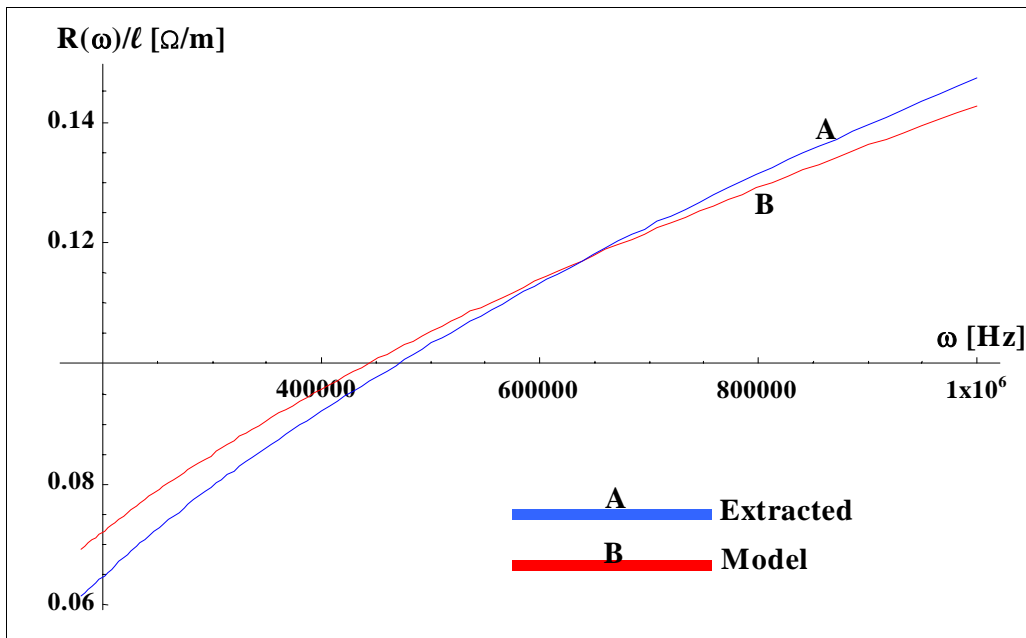


**Figure A-34** Comparison of resistance per unit length predicted by analytical model to that extracted from measured impedance for cable with global thermal aging to simulate 40 years of service at 50°C

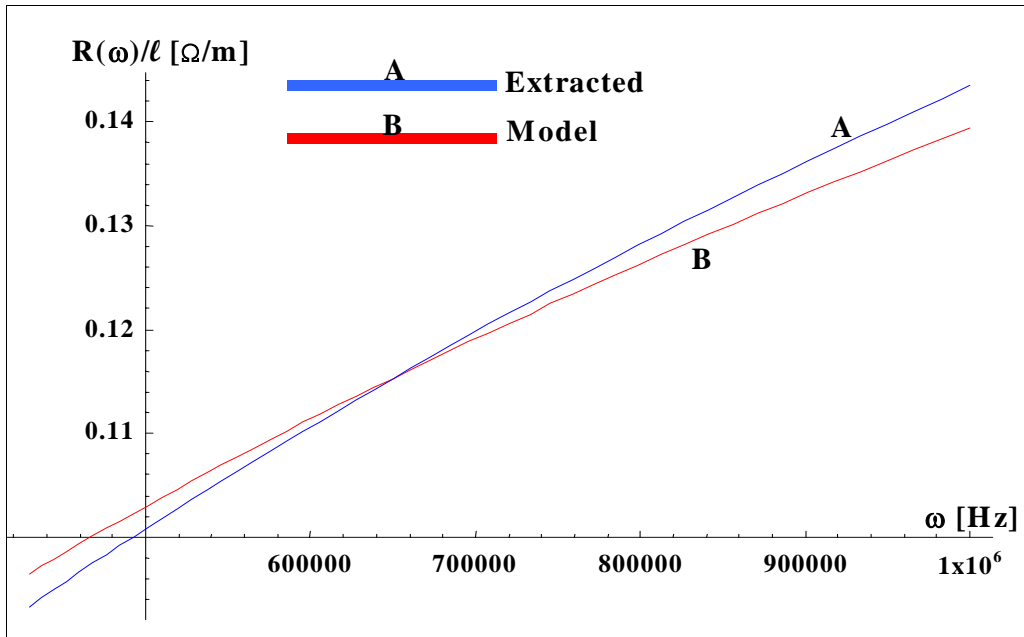


**Figure A-35** Comparison of resistance per unit length predicted by analytical model to that extracted from measured impedance for cable with global thermal aging to simulate 40 years of service at 60°C

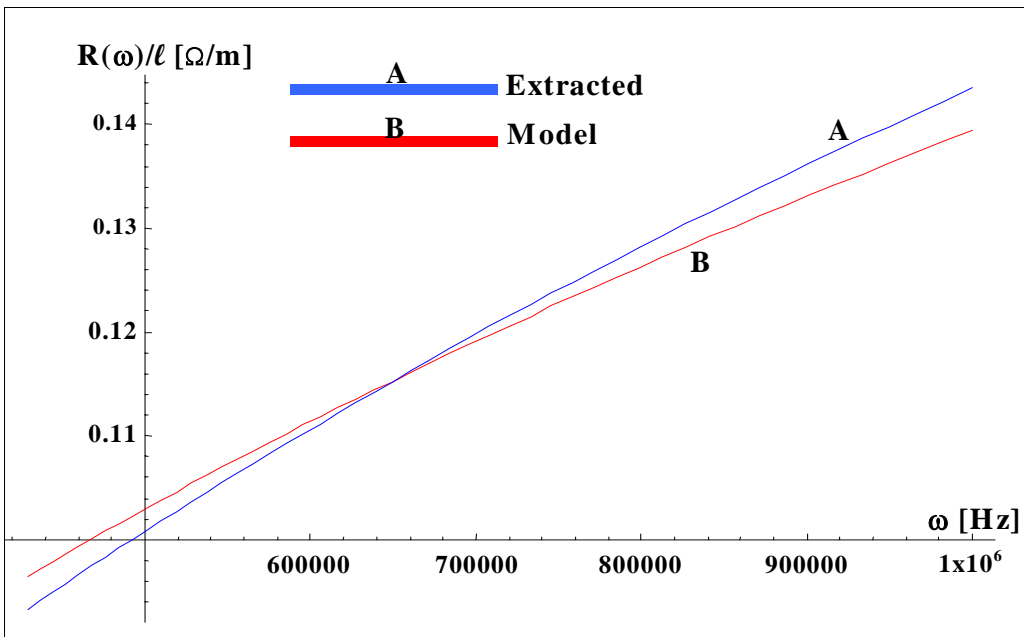


**Figure A-36** Comparison of resistance per unit length predicted by analytical model to that extracted from measured impedance for cable with global thermal aging to simulate 40 years of service at 70°C

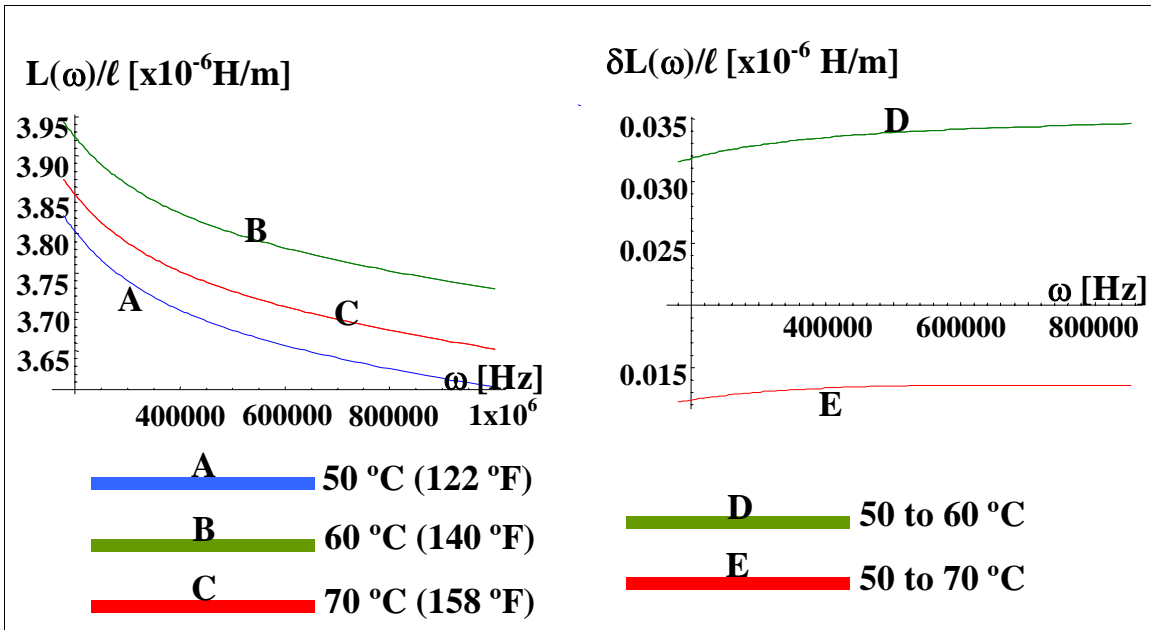


**Figure A-37** Inductance per unit length and change in inductance per unit length for cables with global thermal aging to simulate 40 years of service at various service temperatures

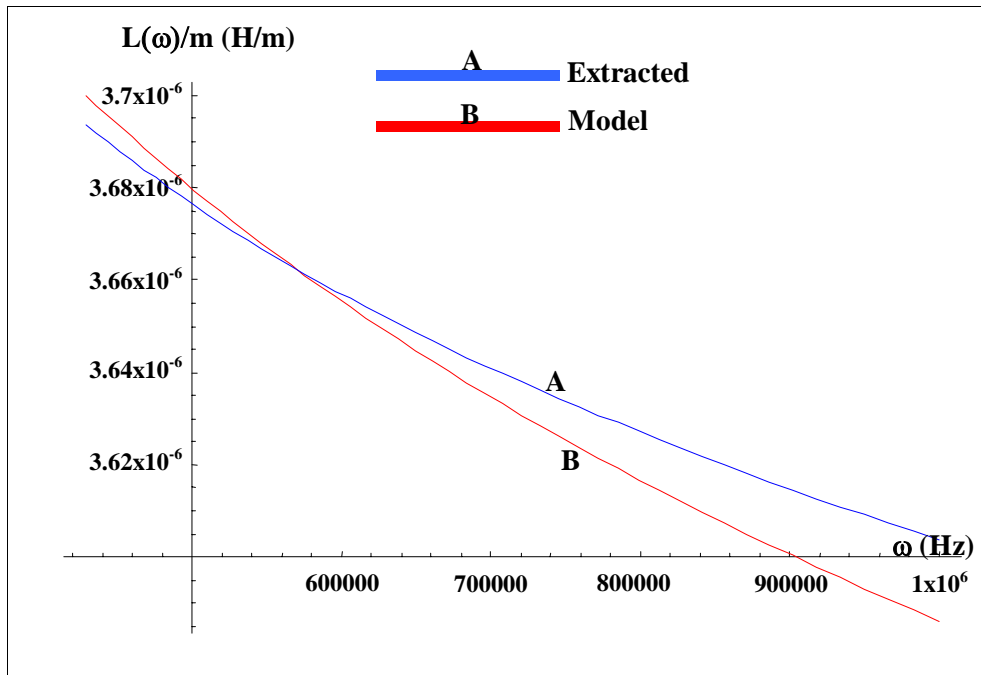


**Figure A-38** Comparison of inductance per unit length predicted by analytical model to that extracted from measured impedance for cable with global thermal aging to simulate 40 years of service at 50°C



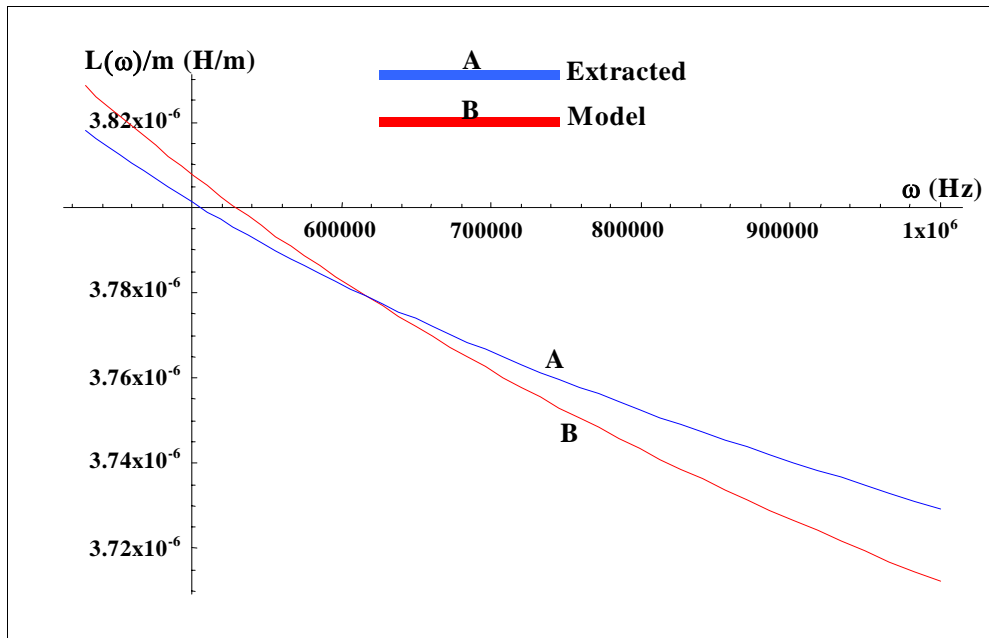


**Figure A-39** Comparison of inductance per unit length predicted by analytical model to that extracted from measured impedance for cable with global thermal aging to simulate 40 years of service at 60°C

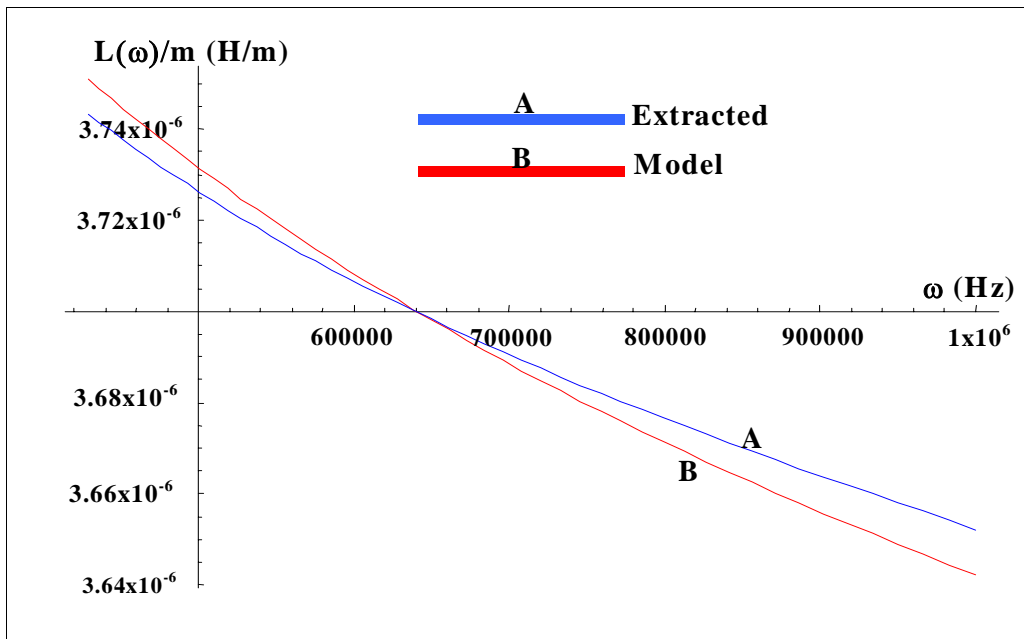


**Figure A-40** Comparison of inductance per unit length predicted by analytical model to that extracted from measured impedance for cable with global thermal aging to simulate 40 years of service at 70°C

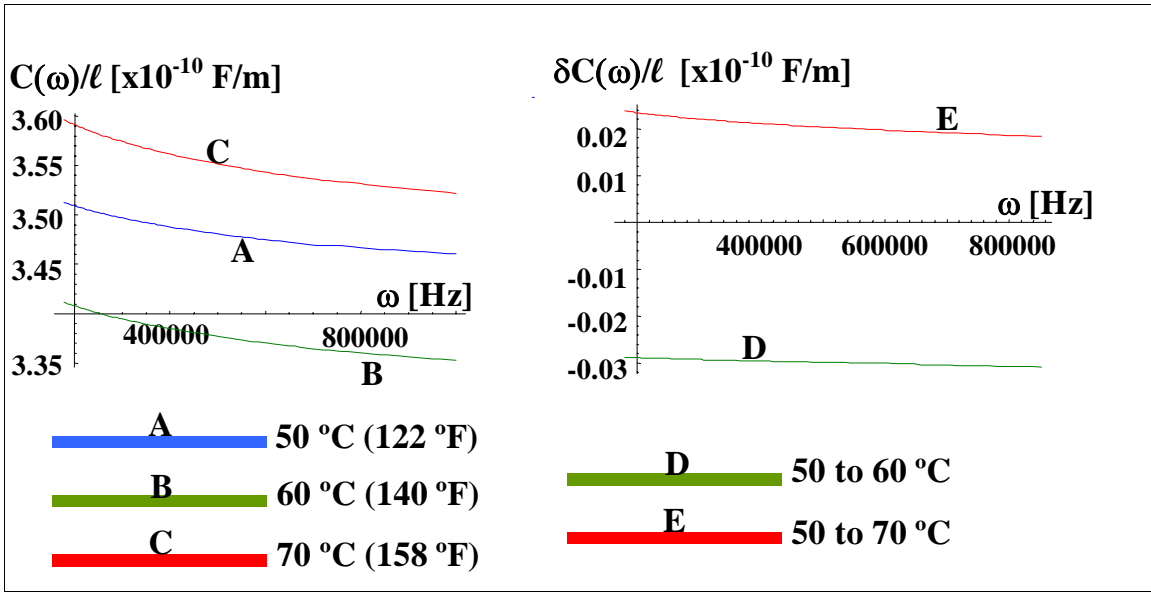


**Figure A-41** Capacitance per unit length and change in capacitance per unit length for cables with global thermal aging to simulate 40 years of service at various service temperatures

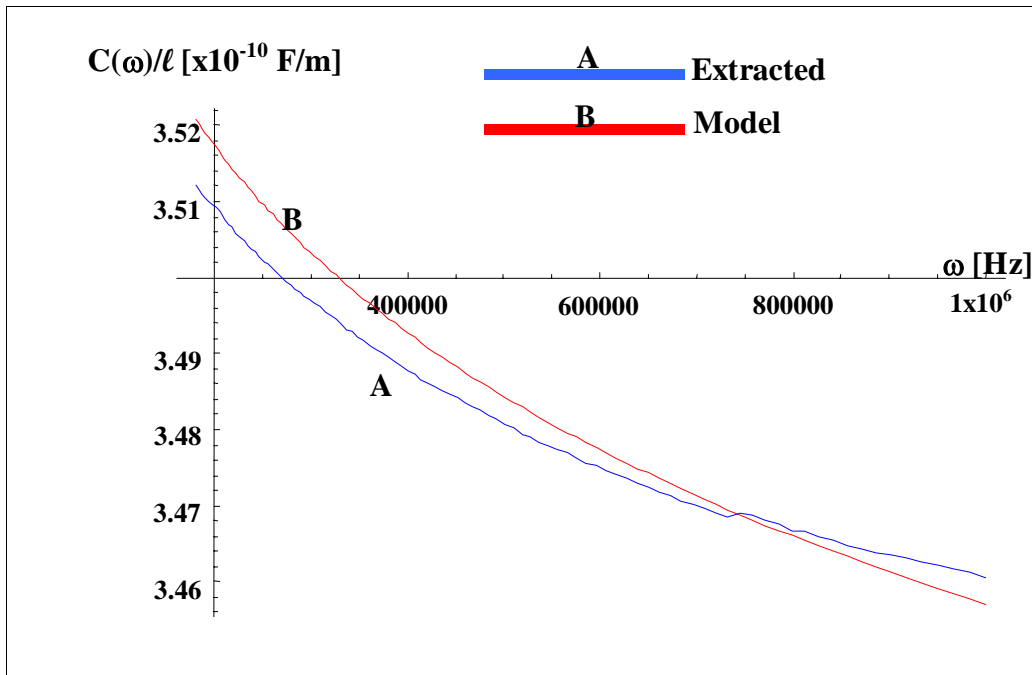


**Figure A-42** Comparison of capacitance per unit length predicted by analytical model to that extracted from measured impedance for cable with global thermal aging to simulate 40 years at 50°C

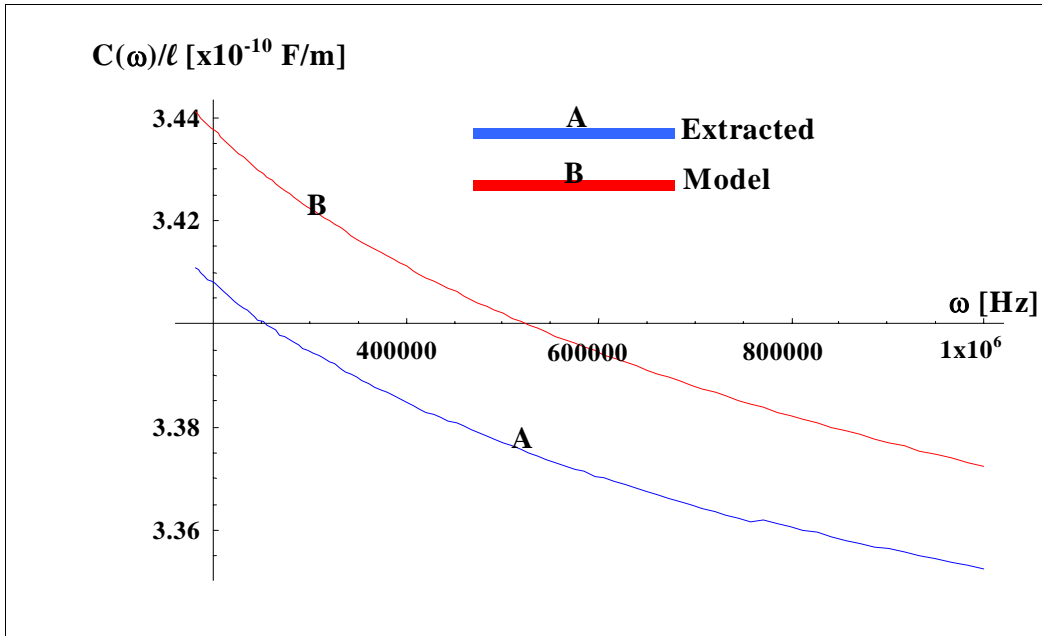


**Figure A-43** Comparison of capacitance per unit length predicted by analytical model to that extracted from measured impedance for cable with global thermal aging to simulate 40 years of service at 60°C

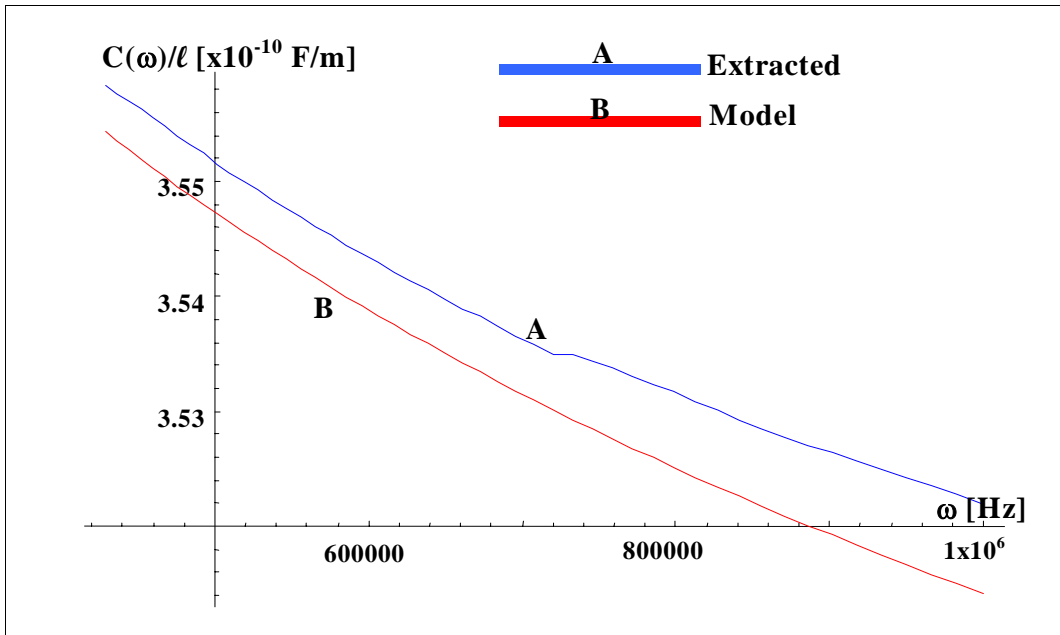


**Figure A-44** Comparison of capacitance per unit length predicted by analytical model to that extracted from measured impedance for cable with global thermal aging to simulate 40 years of service at 70°C

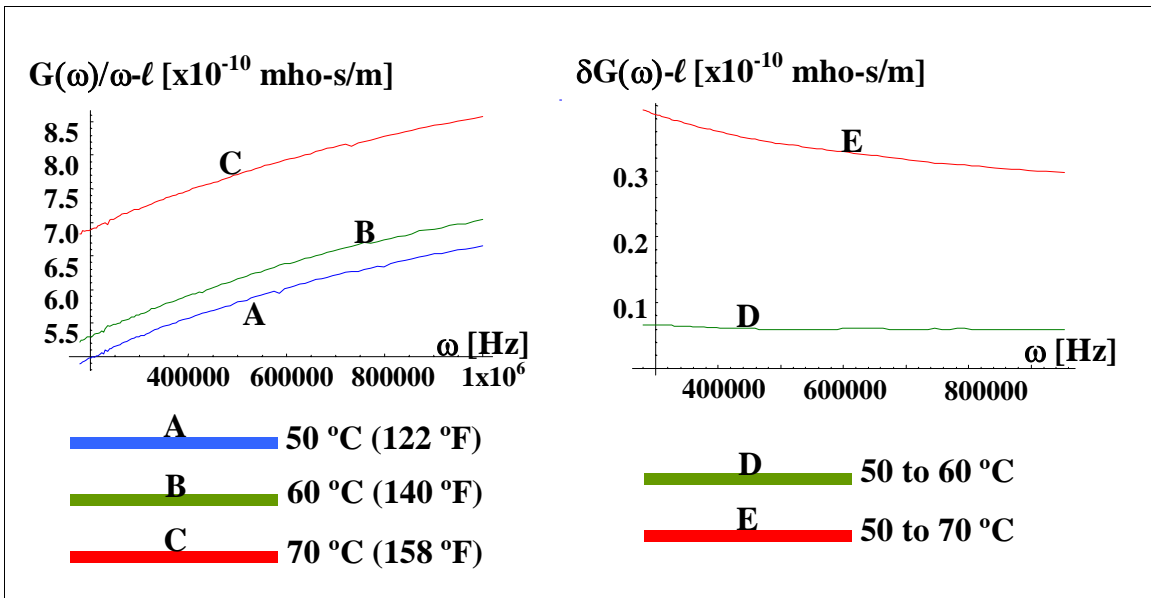


**Figure A-45** Conductance-to-frequency ratio per unit length and change in conductance-to-frequency ratio per unit length for cables with global thermal aging to simulate 40 years of service at various service temperatures

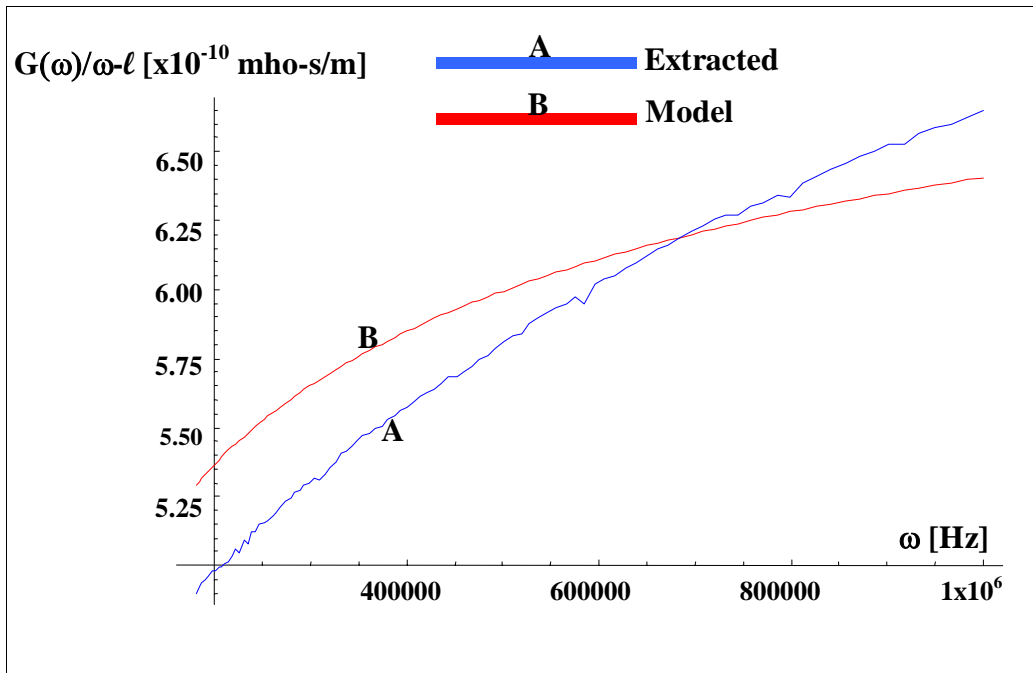


**Figure A-46** Comparison of conductance-to-frequency ratio per unit length predicted by analytical model to that extracted from measured impedance for cable with global thermal aging to simulate 40 years of service at 50°C

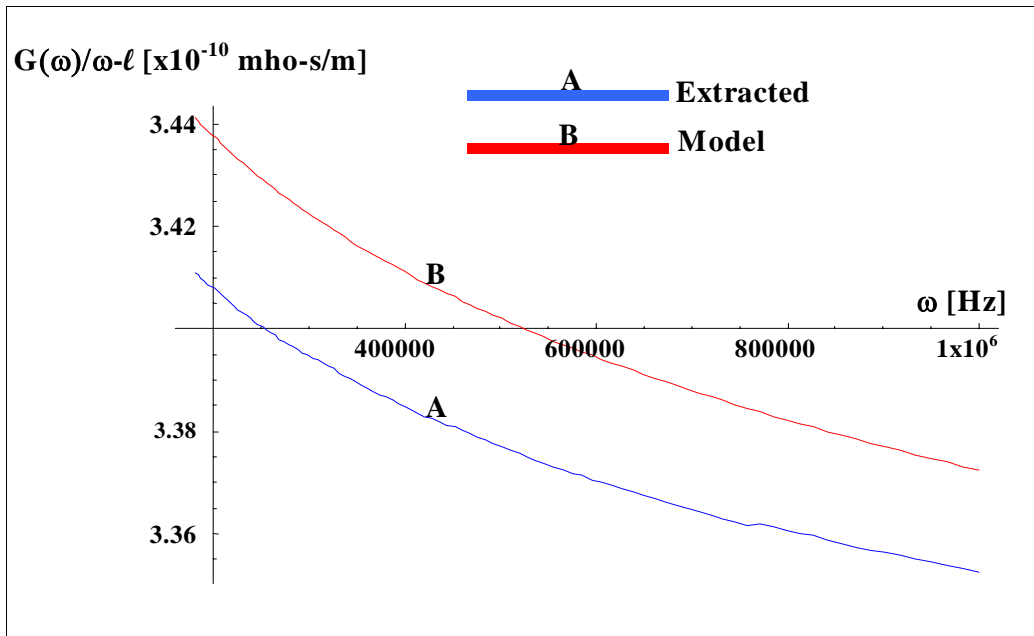


**Figure A-47** Comparison of conductance-to-frequency ratio per unit length predicted by analytical model to that extracted from measured impedance for cable with global thermal aging to simulate 40 years of service at 60°C

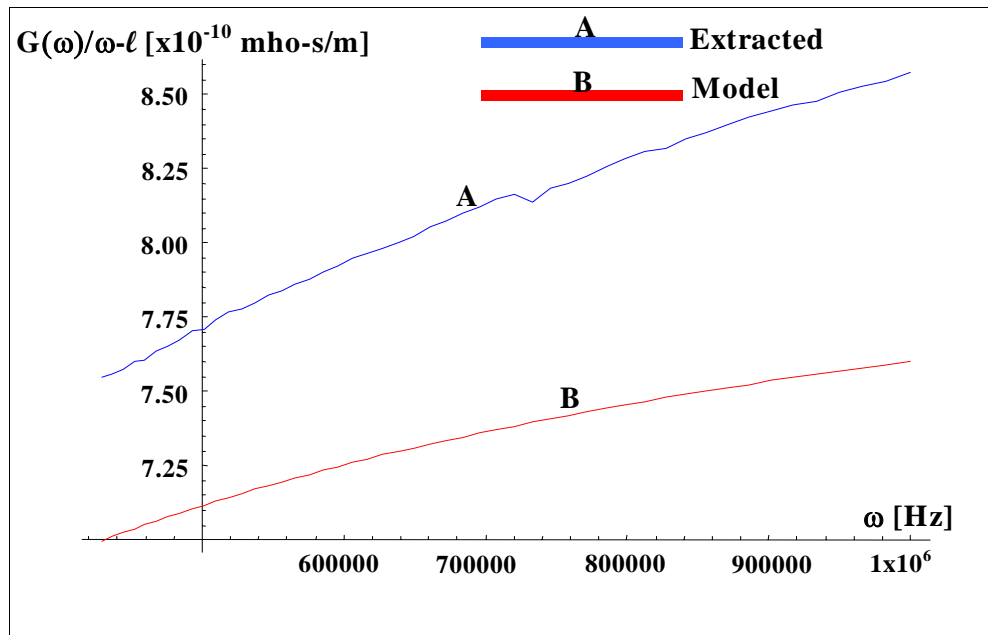


**Figure A-48** Comparison of conductance-to-frequency ratio per unit length predicted by analytical model to that extracted from measured impedance for cable with global thermal aging to simulate 40 years of service at 70°C

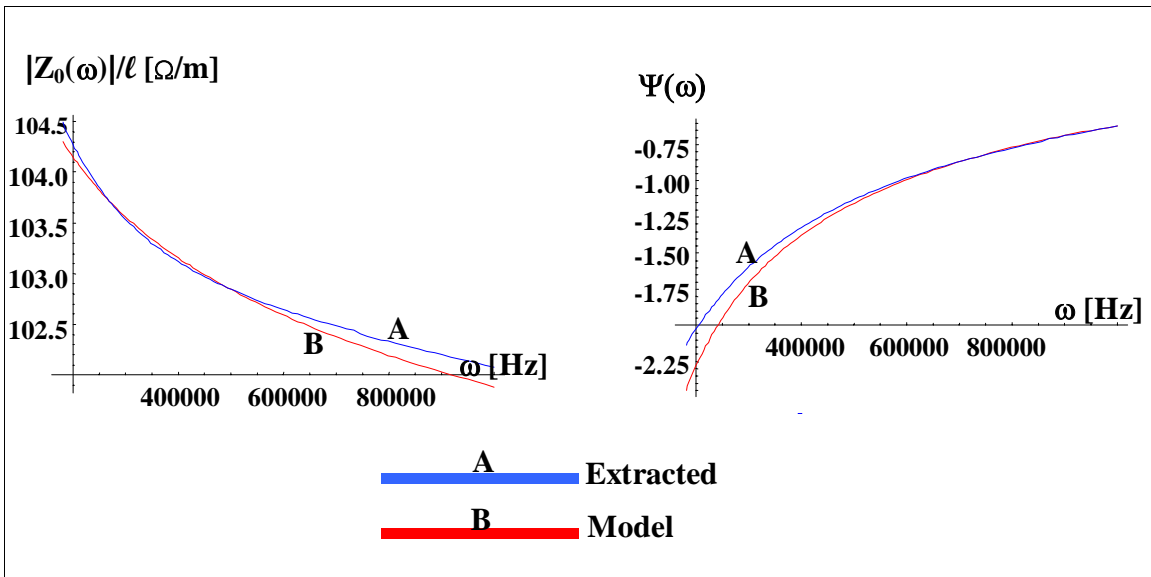


**Figure A-49** Comparison of characteristic impedance magnitude per unit length and phase spectra predicted by analytical model to that extracted from measured impedance for cable with global thermal aging to simulate 40 years of service at 50°C

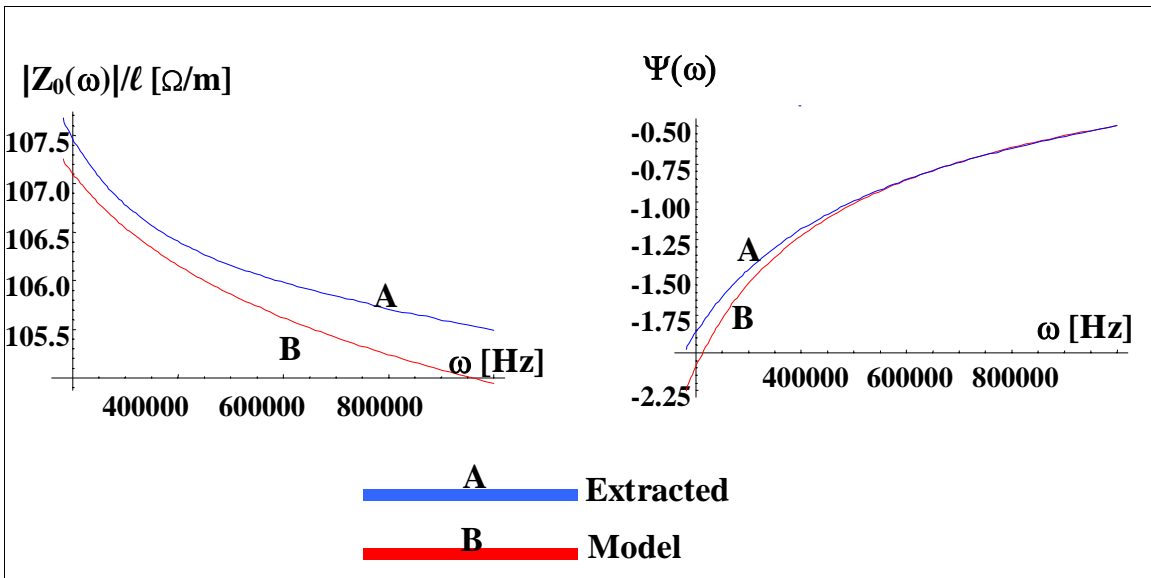


**Figure A-50** Comparison of characteristic impedance magnitude per unit length and phase spectra predicted by analytical model to that extracted from measured impedance for cable with global thermal aging to simulate 40 years of service at 60°C

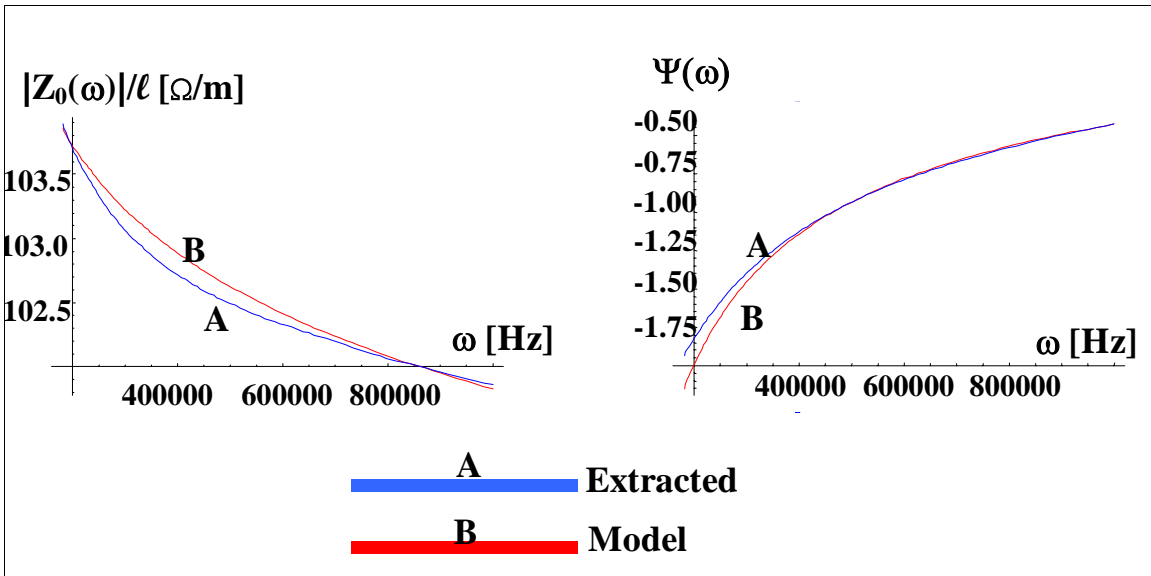


**Figure A-51** Comparison of characteristic impedance magnitude per unit length and phase spectra predicted by analytical model to that extracted from measured impedance for cable with global thermal aging to simulate 40 years of service at 70°C

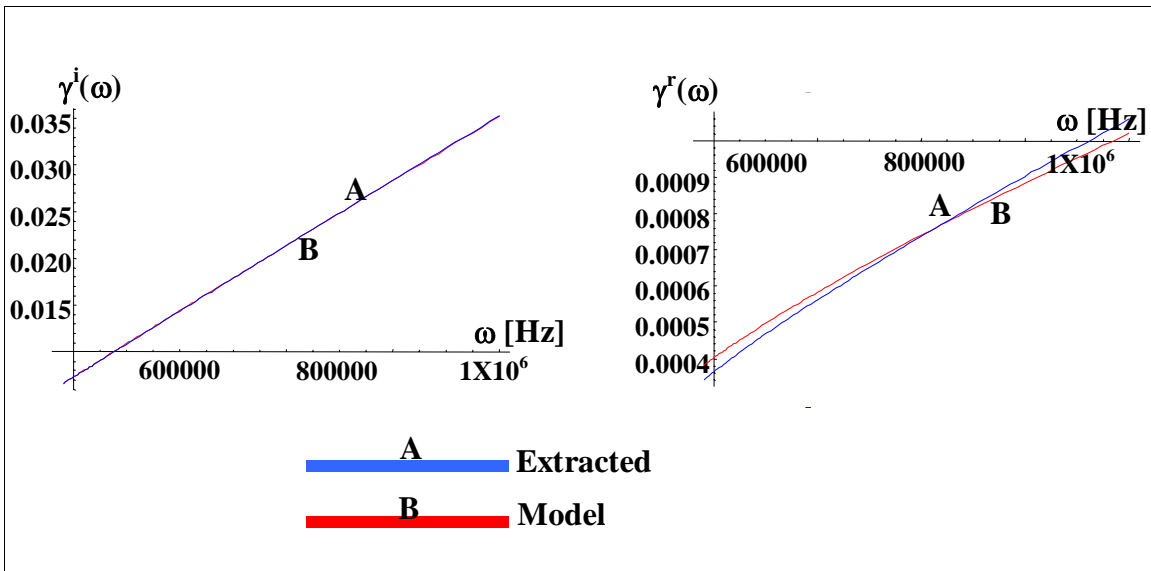


**Figure A-52** Comparison of the imaginary component and real component of the propagation function predicted by analytical model to that extracted from measured impedance for cable with global thermal aging to simulate 40 years of service at 50°C

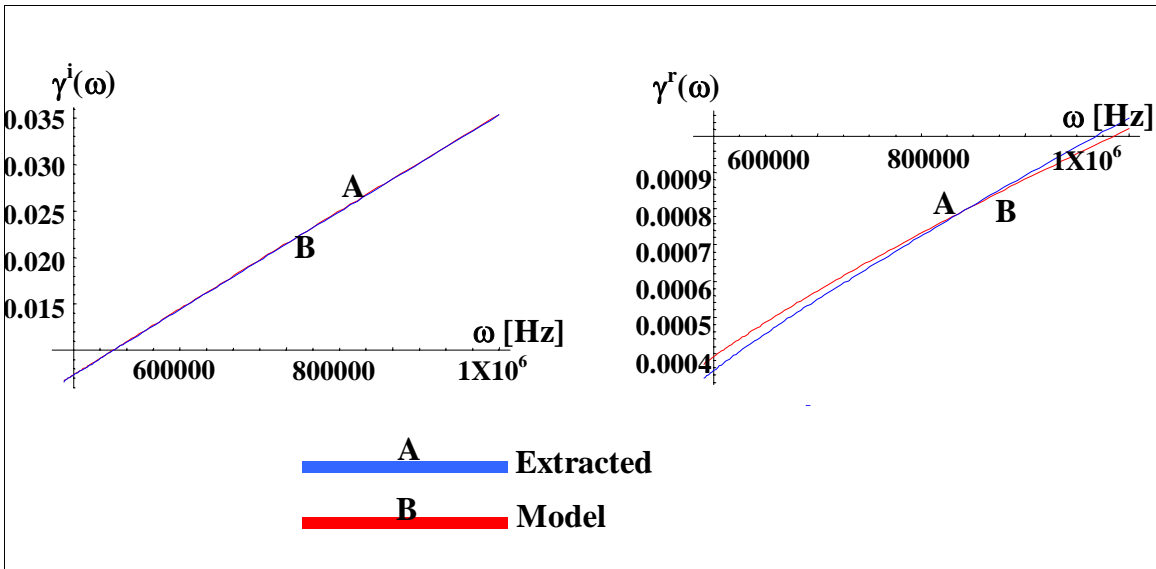


**Figure A-53** Comparison of the imaginary component and real component of the propagation function predicted by analytical model to that extracted from measured impedance for cable with global thermal aging to simulate 40 years of service at 60°C

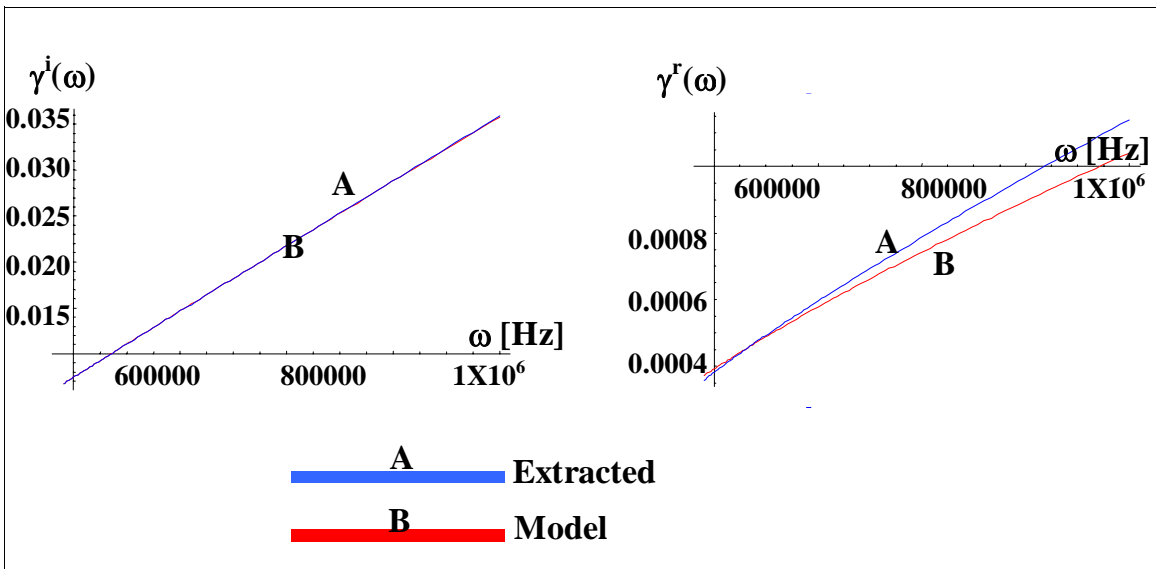


**Figure A-54** Comparison of the imaginary component and real component of the propagation function predicted by analytical model to that extracted from measured impedance for cable with global thermal aging to simulate 40 years of service at 70°C

### A.3 Test Results for Cables with Global Thermal Aging to Simulate 60 Years of Service



The following figures present the results of broadband impedance tests performed on cables with global thermal aging to simulate 60 years of service in a nuclear power plant at service temperatures of 50°C (122°F), 60°C (140°F), and 70°C (158°F). These results supplement the data presented in Section 5 of this report.

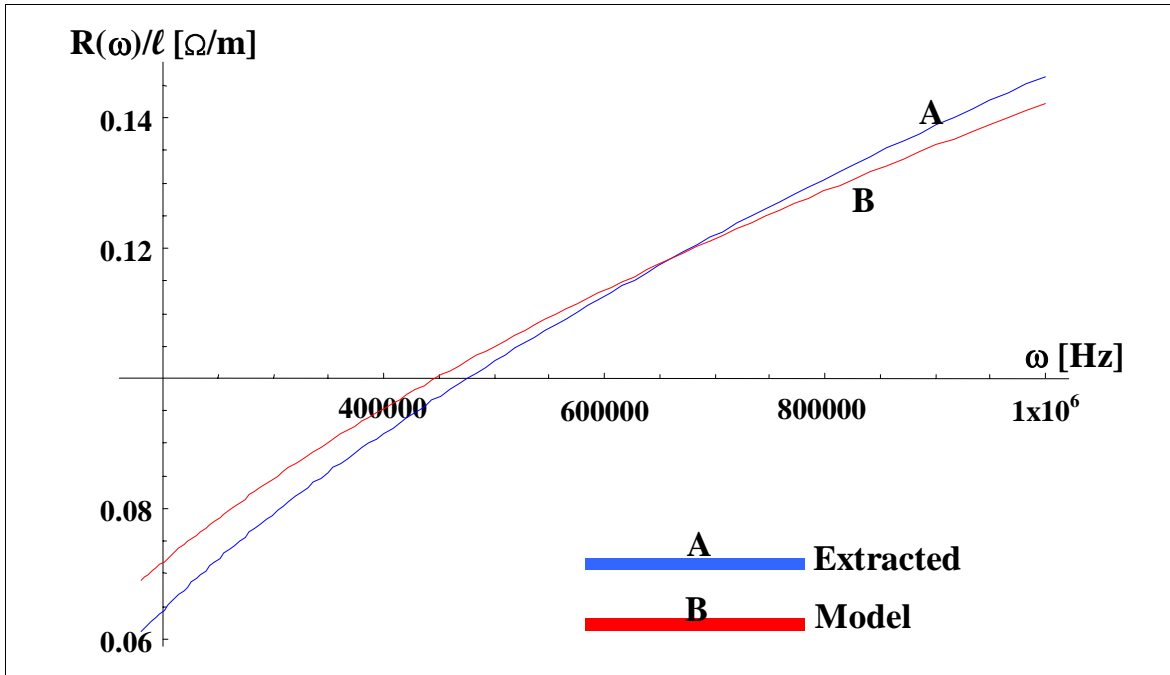


**Figure A-55** Comparison of resistance per unit length predicted by analytical model to that extracted from measured impedance for cable with global thermal aging to simulate 60 years of service at 50°C

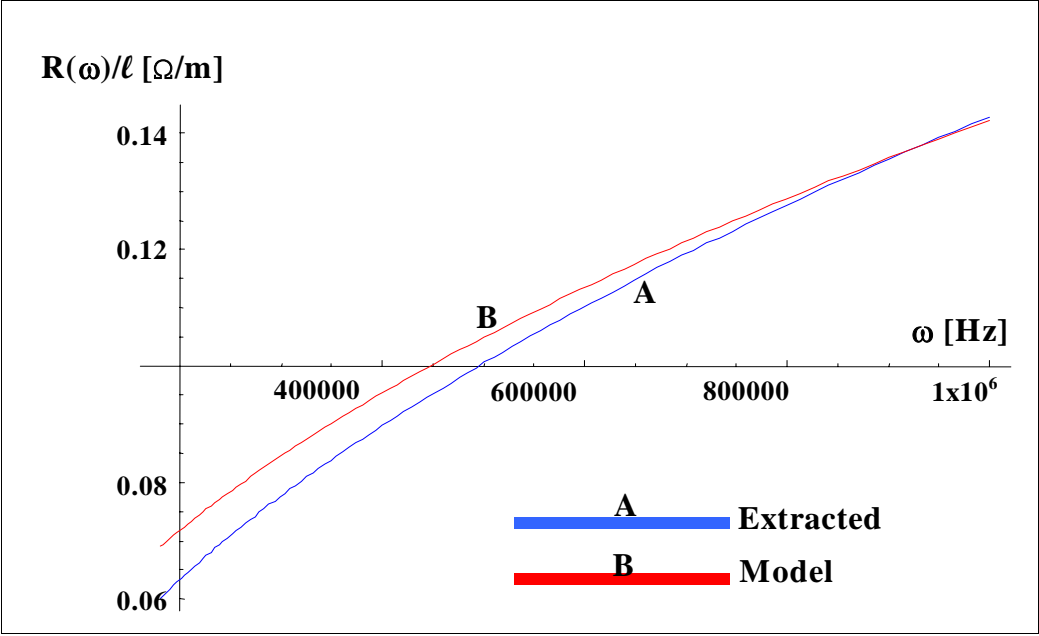


**Figure A-56** Comparison of resistance per unit length predicted by analytical model to that extracted from measured impedance for cable with global thermal aging to simulate 60 years of service at 60°C

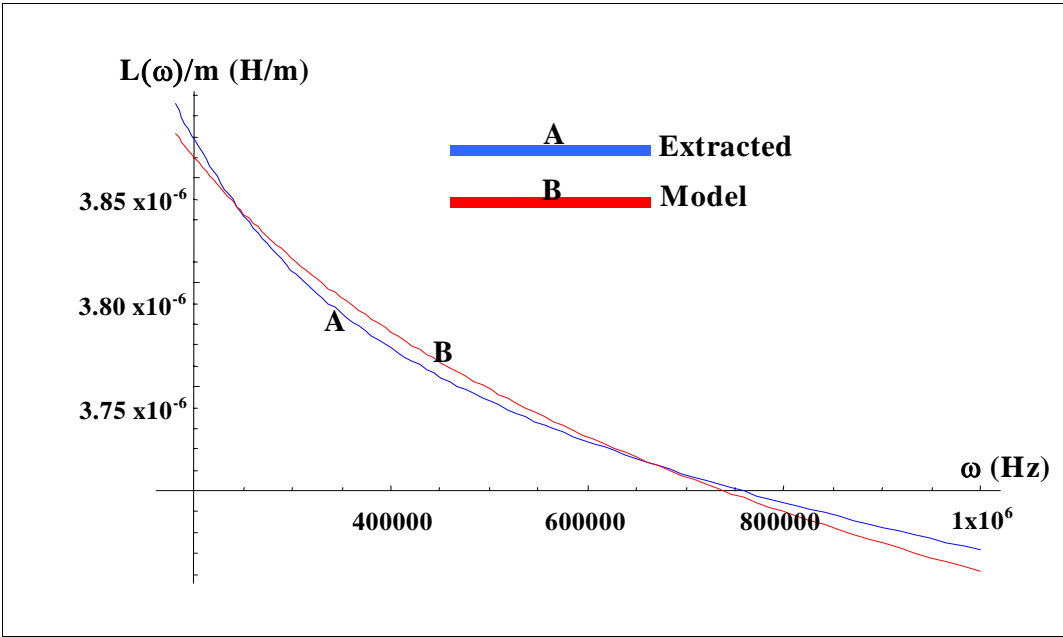


**Figure A-57** Comparison of inductance per unit length predicted by analytical model to that extracted from measured impedance for cable with global thermal aging to simulate 60 years of service at 50°C

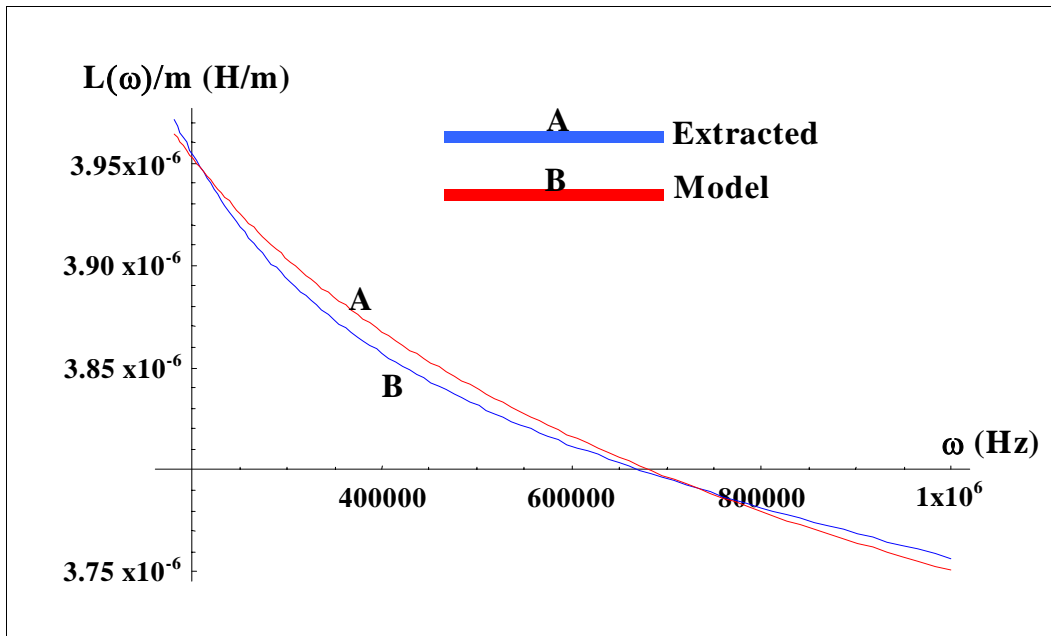


**Figure A-58** Comparison of inductance per unit length predicted by analytical model to that extracted from measured impedance for cable with global thermal aging to simulate 60 years of service at 60°C

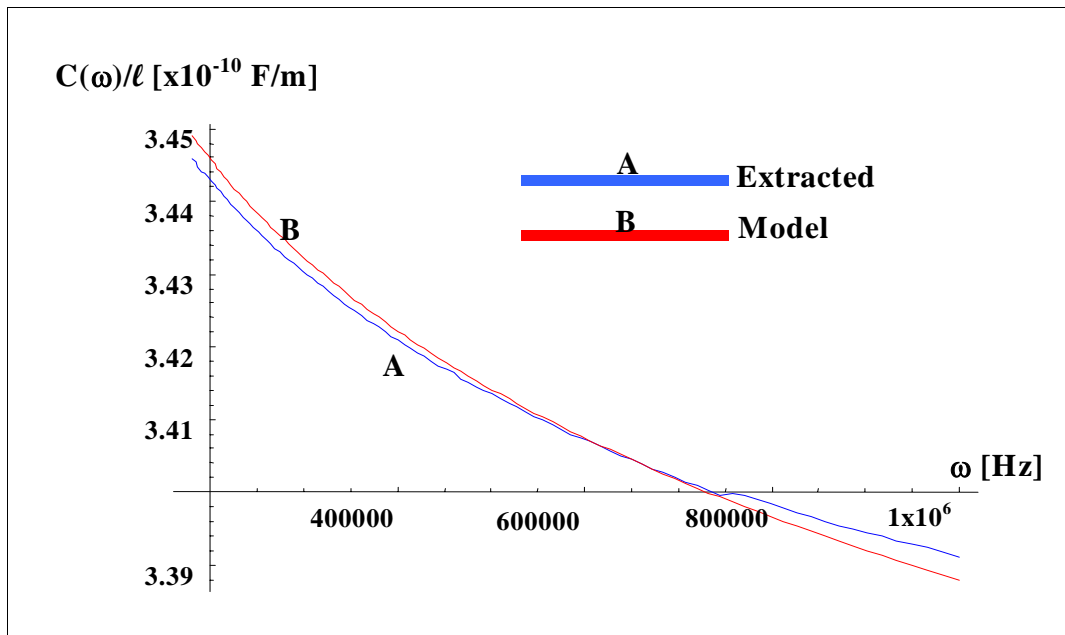


**Figure A-59** Comparison of capacitance per unit length predicted by analytical model to that extracted from measured impedance for cable with global thermal aging to simulate 60 years of service at 50°C

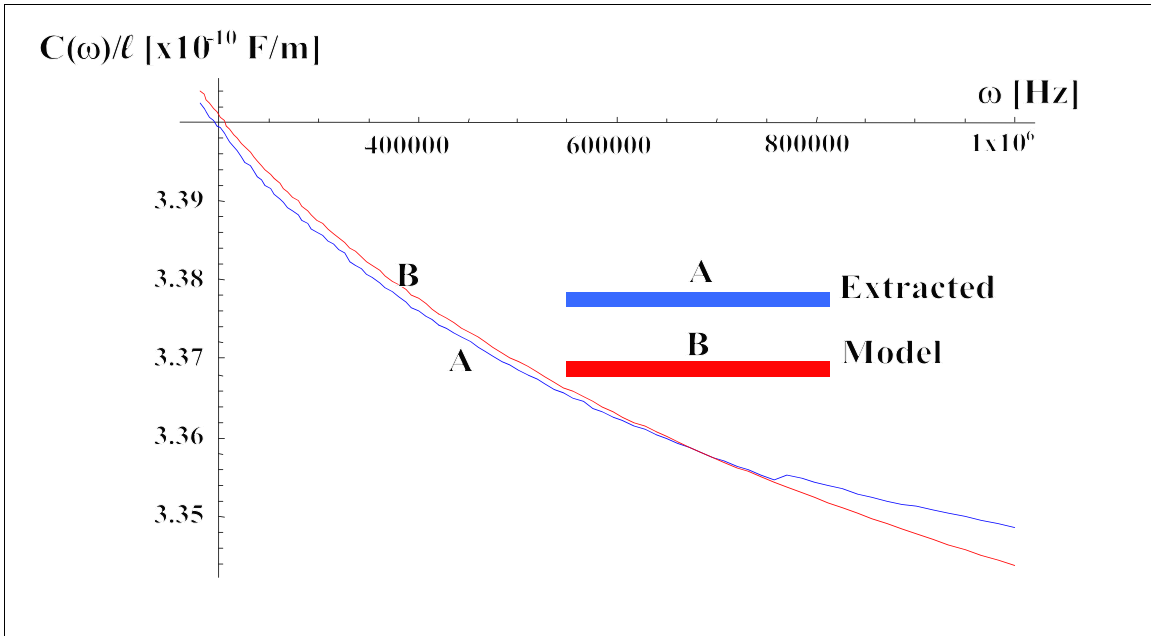


**Figure A-60** Comparison of capacitance per unit length predicted by analytical model to that extracted from measured impedance for cable with global thermal aging to simulate 60 years of service at 60°C

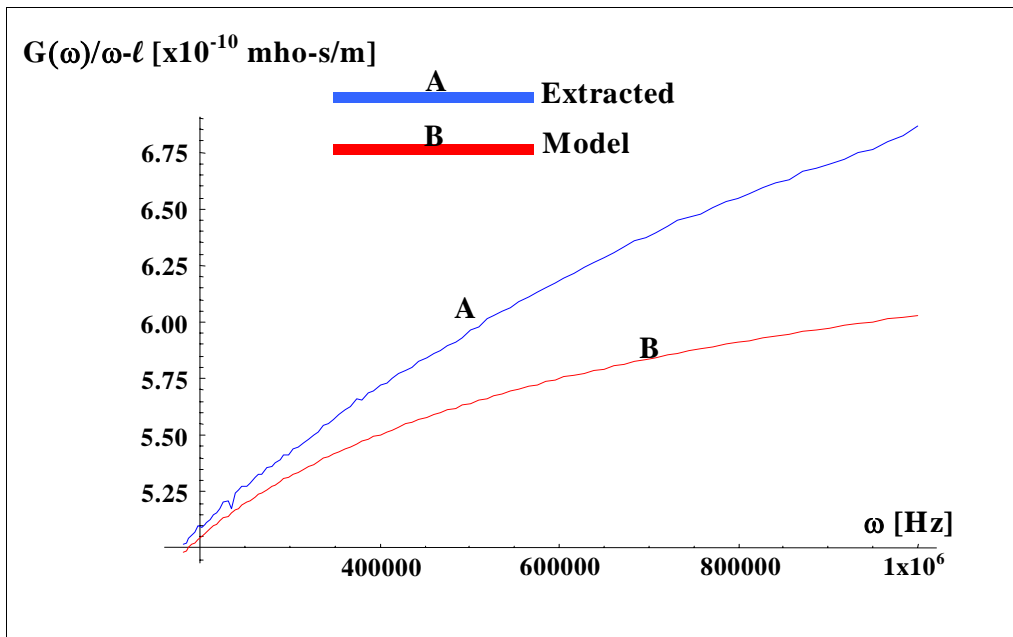


**Figure A-61** Comparison of conductance-to-frequency ratio per unit length predicted by analytical model to that extracted from measured impedance for cable with global thermal aging to simulate 60 years of service at 50°C

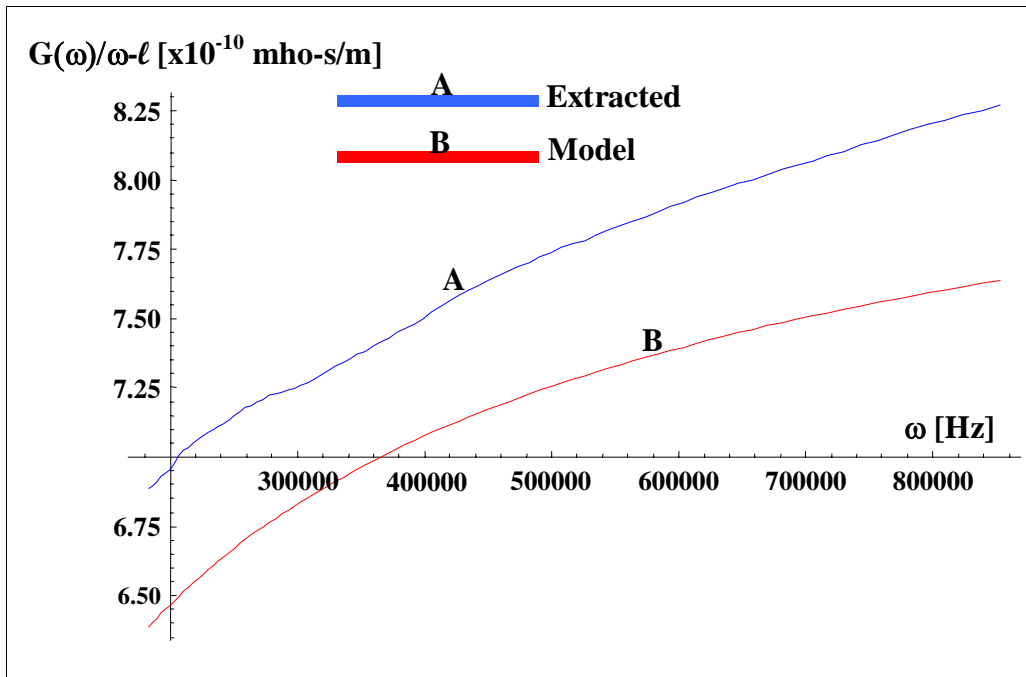


**Figure A-62** Comparison of conductance-to-frequency ratio per unit length predicted by analytical model to that extracted from measured impedance for cable with global thermal aging to simulate 60 years of service at 60°C

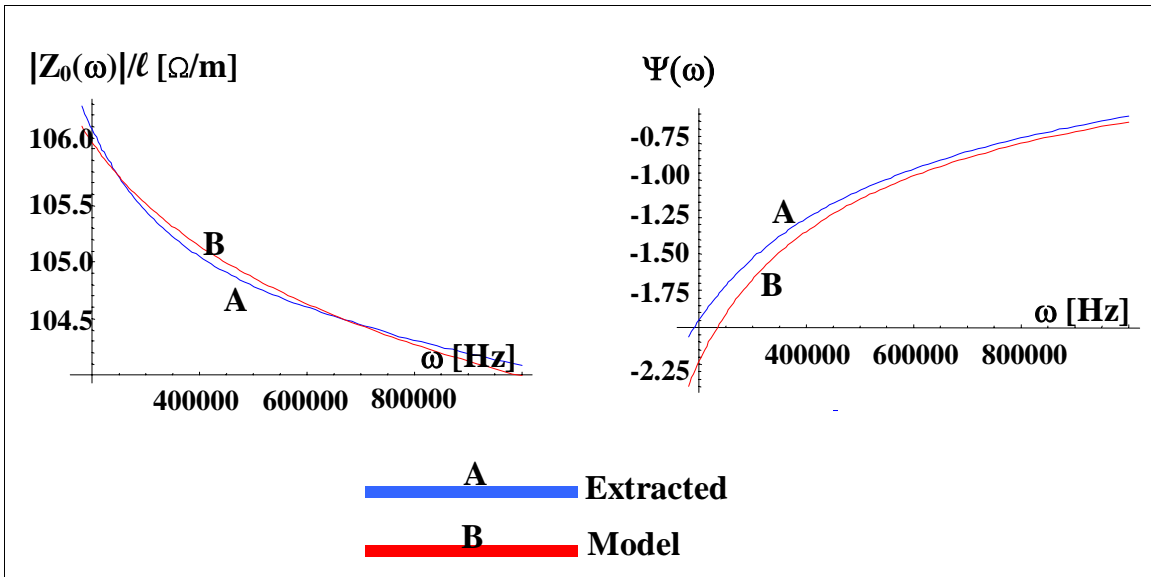


**Figure A-63** Comparison of characteristic impedance magnitude per unit length and phase spectra predicted by analytical model to that extracted from measured impedance for cable with global thermal aging to simulate 60 years of service at 50°C

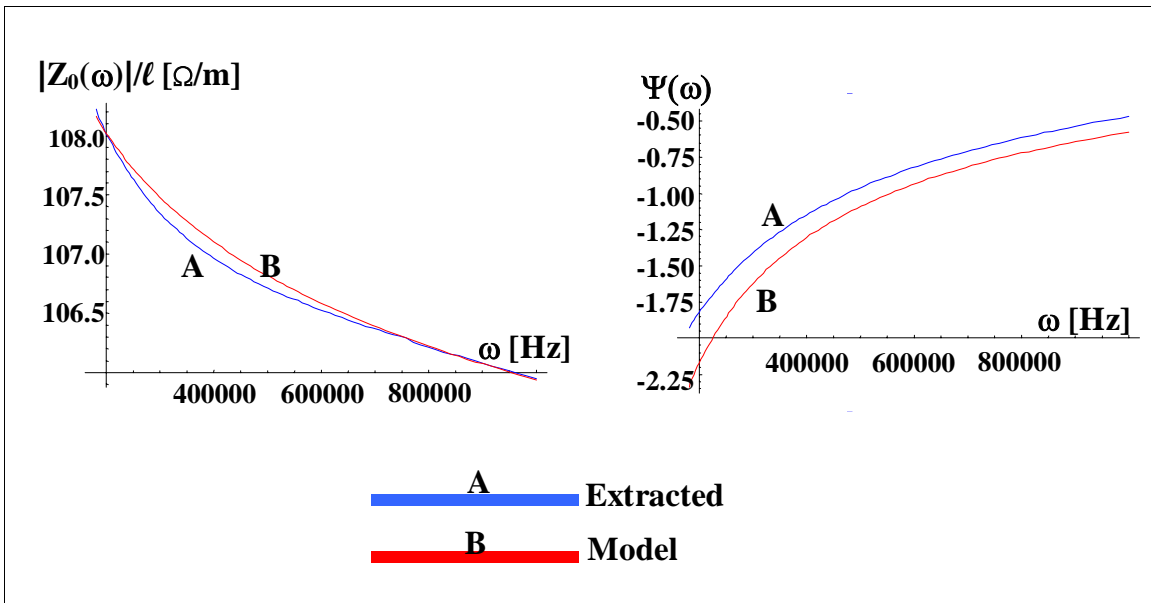


**Figure A-64** Comparison of characteristic impedance magnitude per unit length and phase spectra predicted by analytical model to that extracted from measured impedance for cable with global thermal aging to simulate 60 years of service at 60°C

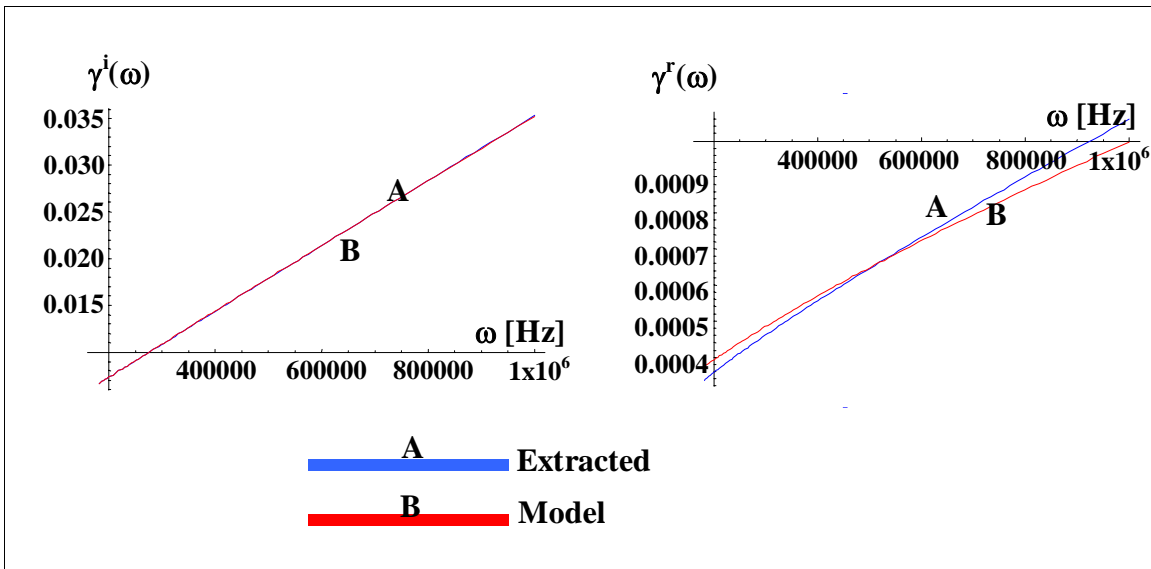


**Figure A-65** Comparison of the imaginary component and real component of the propagation function predicted by analytical model to that extracted from measured impedance for cable with global thermal aging to simulate 60 years of service at 50°C

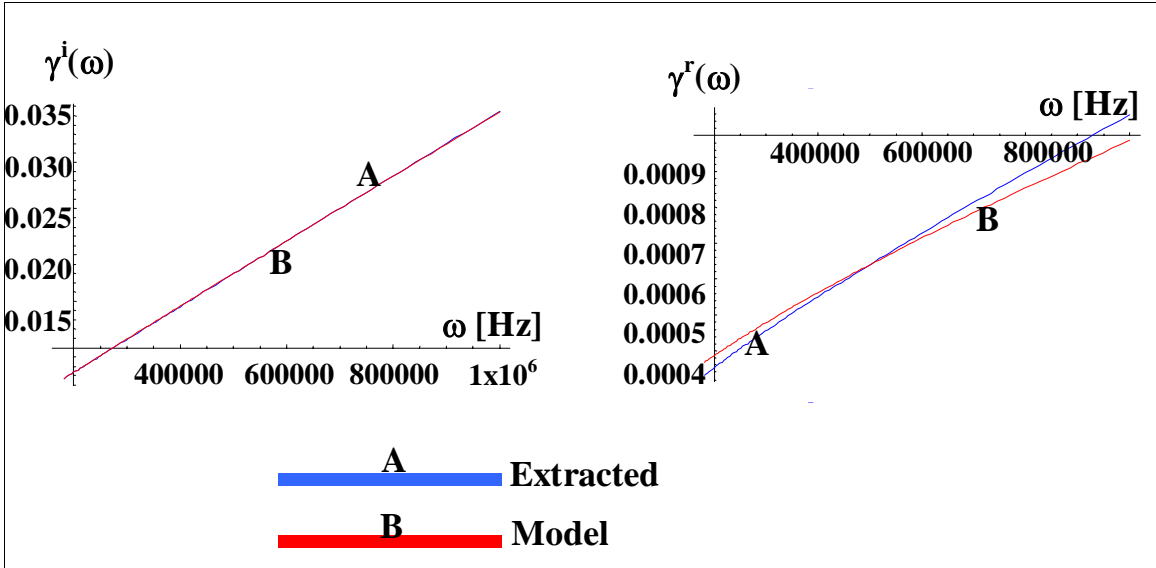


**Figure A-66** Comparison of the imaginary component and real component of the propagation function predicted by analytical model to that extracted from measured impedance for cable with global thermal aging to simulate 60 years of service at 60°C

## **Appendix B**

### **BIS Test Results for Cables with Localized Thermal Aging (Hot Spots)**



(This page intentionally left blank)

## List of Figures

	<u>Page No.</u>
<b>Figure B-1</b> Characteristic impedance magnitude per unit length and phase spectra over the frequency range from 1MHz to 100MHz for cables with global thermal aging to simulate 20 years of service at various temperatures .....	207
<b>Figure B-2</b> Imaginary and real components of the propagation function over the frequency range from 1MHz to 100MHz for cables with global thermal aging to simulate 20 years of service at various temperatures .....	207
<b>Figure B-3</b> Impedance magnitude per unit length and phase spectra over the frequency range from 39MHz to 45 MHz for cables with global thermal aging to simulate 20 years of service at 50°C, plus additional thermal aging to simulate hot spots of different severity .....	208
<b>Figure B-4</b> Imaginary and real components of the propagation function over the frequency range from 1MHz to 100MHz for cables with global thermal aging to simulate 40 years of service at various temperatures .....	208
<b>Figure B-5</b> Characteristic impedance magnitude per unit length and phase spectra over the frequency range from 1MHz to 100MHz for cables with global thermal aging to simulate 40 years of service at various temperatures .....	209
<b>Figure B-6</b> Impedance magnitude per unit length and phase spectra over the frequency range from 14MHz to 22 MHz for cables with global thermal aging to simulate 20 years of service at 50°C, plus additional thermal aging to simulate hot spots of different severity .....	209
<b>Figure B-7</b> Impedance magnitude per unit length and phase spectra over the frequency range from 14MHz to 22 MHz for cables with global thermal aging to simulate 20 years of service at 50°C, plus additional thermal aging to simulate hot spots of different size .....	210
<b>Figure B-8</b> Impedance magnitude per unit length and phase spectra over the frequency range from 41MHz to 42 MHz for cables with global thermal aging to simulate 20 years of service at 50°C, plus additional thermal aging to simulate hot spots of different size .....	210
<b>Figure B-9</b> Impedance magnitude per unit length and phase spectra over the frequency range from 39MHz to 45 MHz for cables with global thermal aging to simulate 20 years of service at 50°C, plus additional thermal aging to simulate hot spots at different locations .....	211

<b>Figure B-10</b>	Impedance magnitude per unit length and phase spectra over the frequency range from 14MHz to 22 MHz for cables with global thermal aging to simulate 20 years of service at 50°C, plus additional thermal aging to simulate hot spots at different locations .....	211
<b>Figure B-11</b>	Impedance magnitude per unit length and phase spectra over the frequency range from 39MHz to 45 MHz for cables with global thermal aging to simulate 40 years of service at 50°C, plus additional thermal aging to simulate hot spots of different severity .....	212
<b>Figure B-12</b>	Impedance magnitude per unit length and phase spectra over the frequency range from 14MHz to 22 MHz for cables with global thermal aging to simulate 40 years of service at 50°C, plus additional thermal aging to simulate hot spots of different severity .....	212
<b>Figure B-13</b>	Impedance magnitude per unit length and phase spectra over the frequency range from 14MHz to 22 MHz for cables with global thermal aging to simulate 40 years of service at 50°C, plus additional thermal aging to simulate hot spots of different size .....	213
<b>Figure B-14</b>	Impedance magnitude per unit length and phase spectra over the frequency range from 41MHz to 42 MHz for cables with global thermal aging to simulate 40 years of service at 50°C, plus additional thermal aging to simulate hot spots of different size .....	213
<b>Figure B-15</b>	Impedance magnitude per unit length and phase spectra over the frequency range from 39MHz to 45 MHz for cables with global thermal aging to simulate 40 years of service at 50°C, plus additional thermal aging to simulate hot spots at different locations .....	214

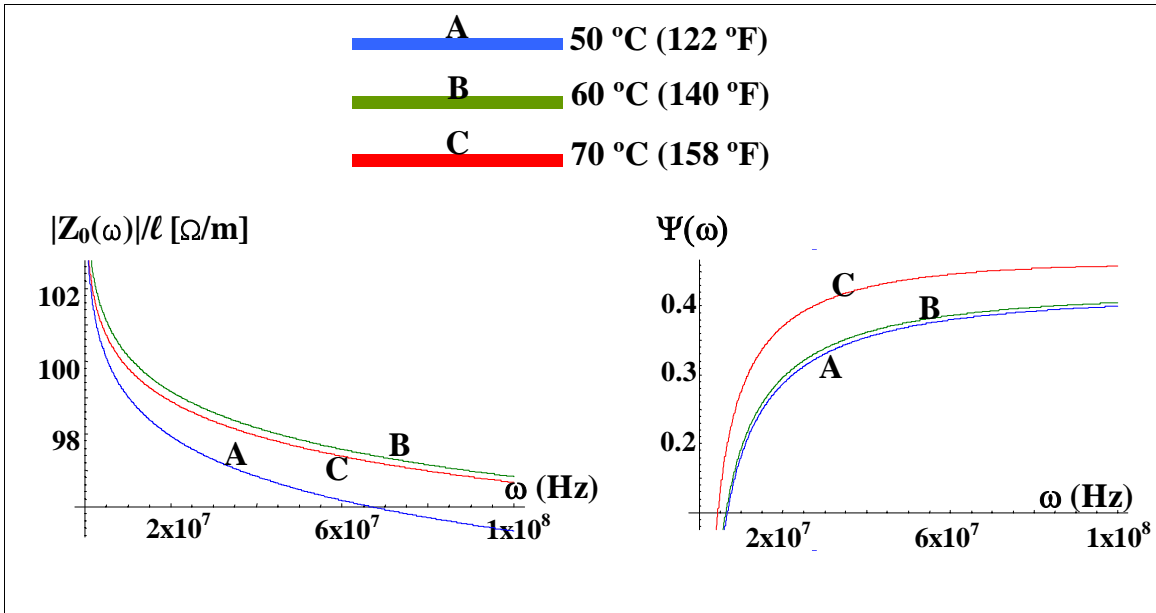


**Figure B-1** Characteristic impedance magnitude per unit length and phase spectra over the frequency range from 1MHz to 100MHz for cables with global thermal aging to simulate 20 years of service at various temperatures

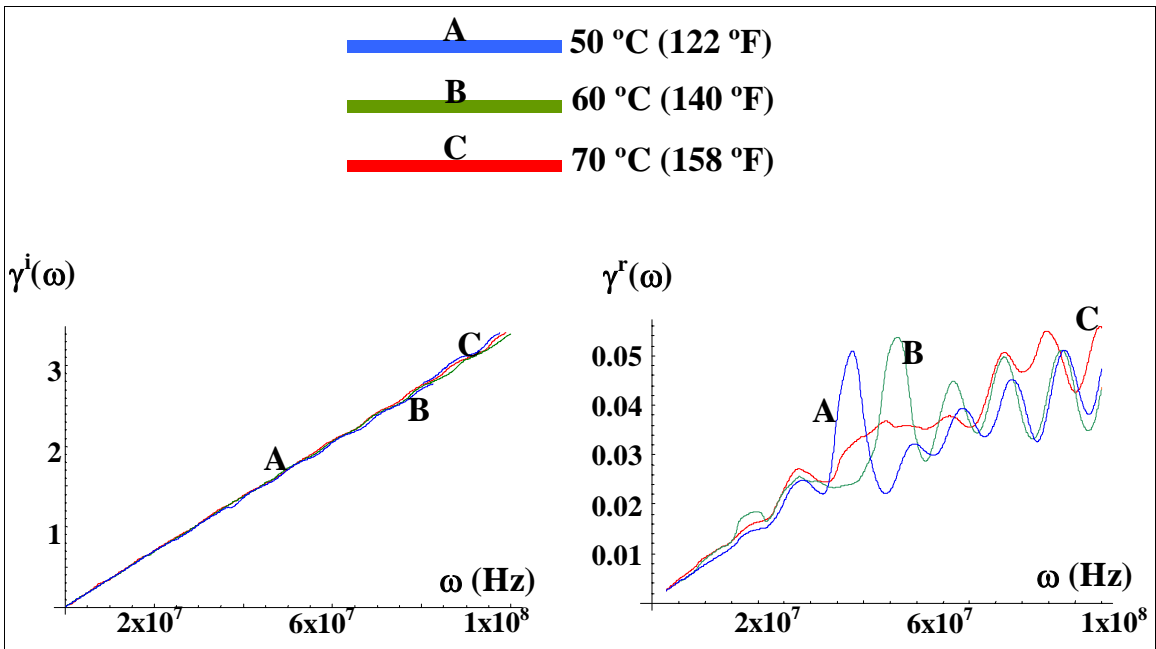


**Figure B-2** Imaginary and real components of the propagation function over the frequency range from 1MHz to 100MHz for cables with global thermal aging to simulate 20 years of service at various temperatures

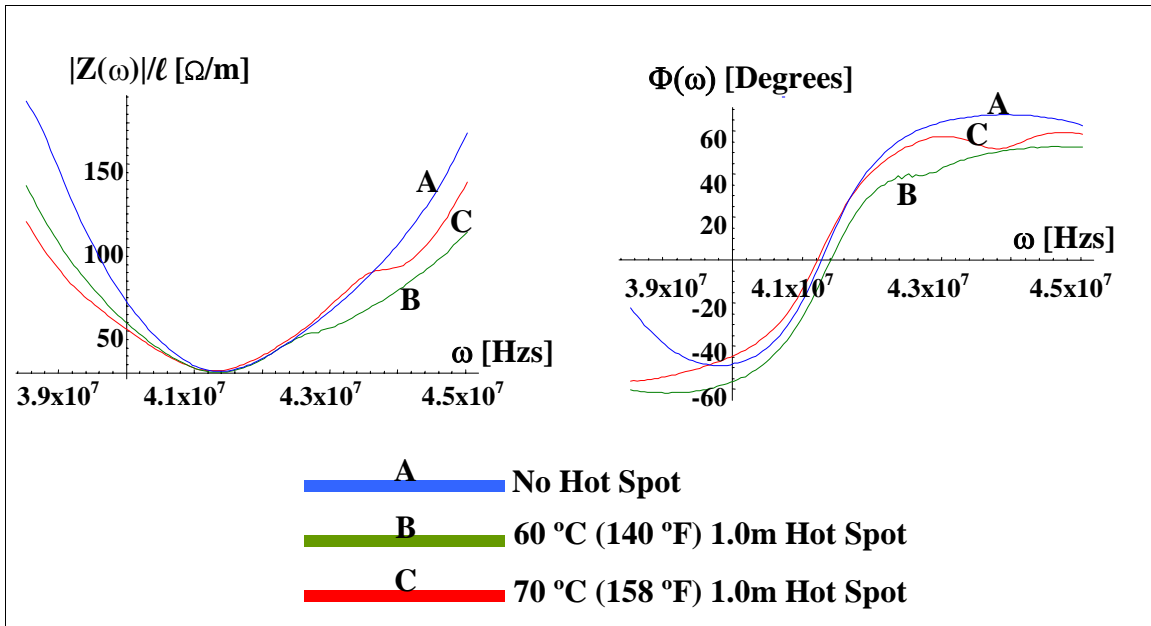


**Figure B-3** Impedance magnitude per unit length and phase spectra over the frequency range from 39MHz to 45 MHz for cables with global thermal aging to simulate 20 years of service at 50°C, plus additional thermal aging to simulate hot spots of different severity

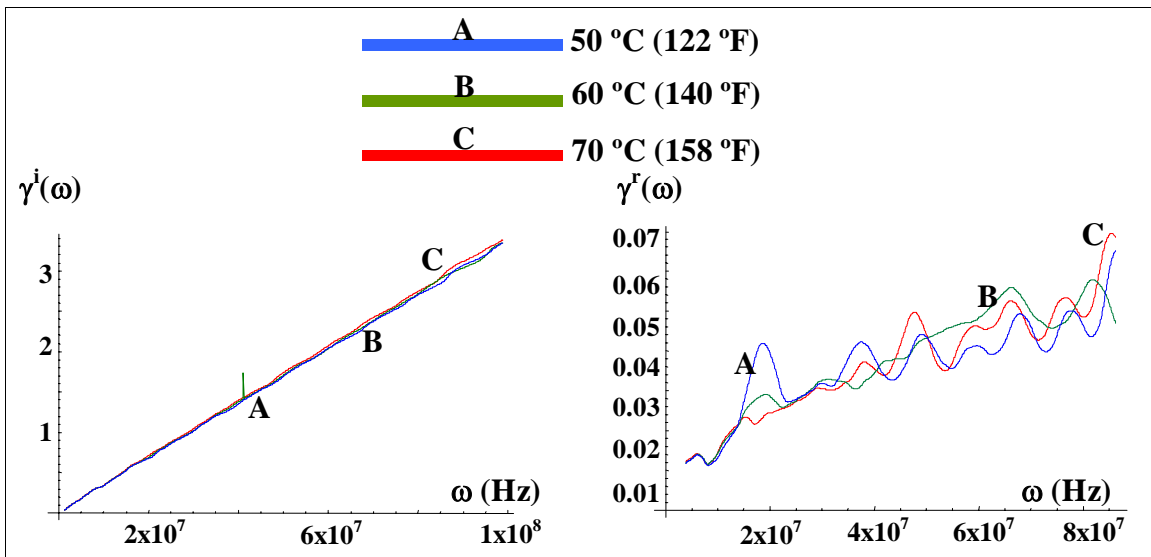


**Figure B-4** Imaginary and real components of the propagation function over the frequency range from 1MHz to 100MHz for cables with global thermal aging to simulate 40 years of service at various temperatures

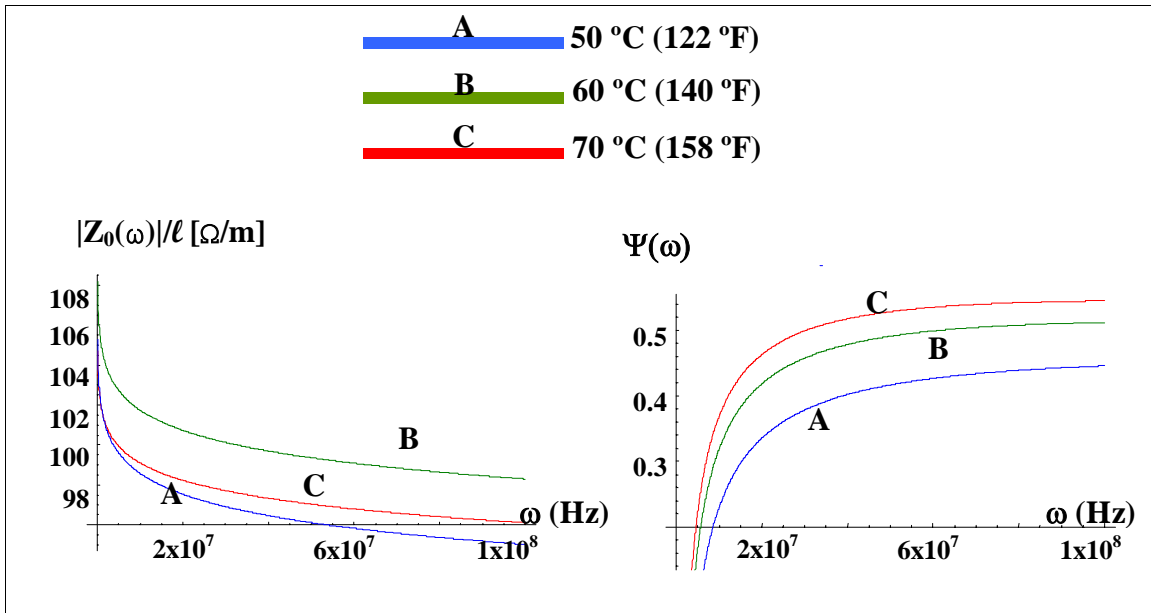


**Figure B-5** Characteristic impedance magnitude per unit length and phase spectra over the frequency range from 1MHz to 100MHz for cables with global thermal aging to simulate 40 years of service at various temperatures

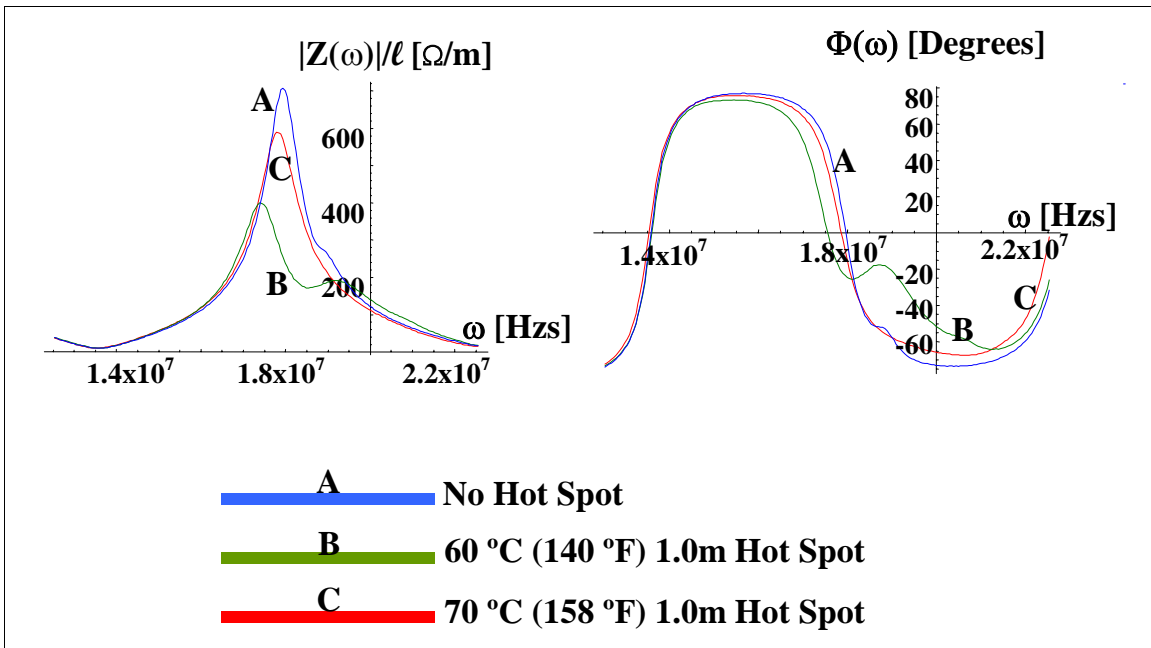


**Figure B-6** Impedance magnitude per unit length and phase spectra over the frequency range from 14MHz to 22 MHz for cables with global thermal aging to simulate 20 years of service at 50°C, plus additional thermal aging to simulate hot spots of different severity

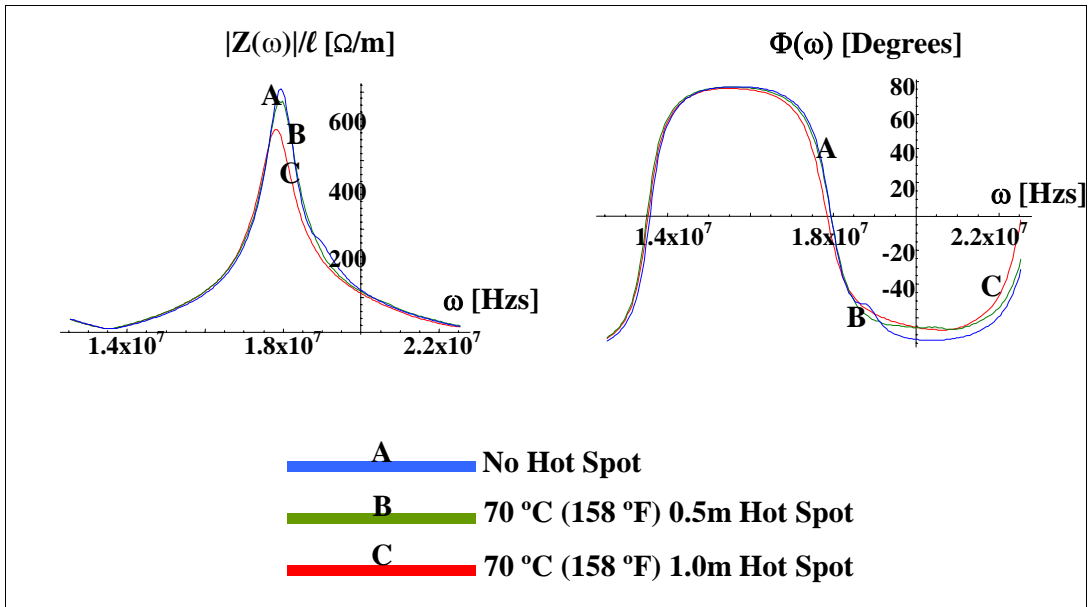


**Figure B-7** Impedance magnitude per unit length and phase spectra over the frequency range from 14MHz to 22 MHz for cables with global thermal aging to simulate 20 years of service at 50°C, plus additional thermal aging to simulate hot spots of different size

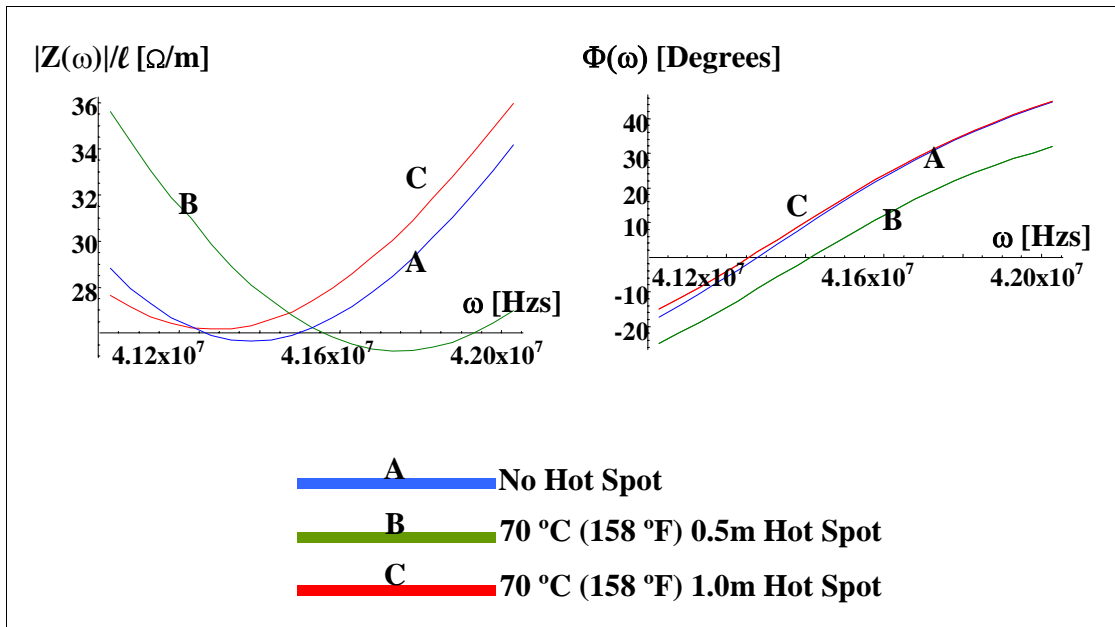


**Figure B-8** Impedance magnitude per unit length and phase spectra over the frequency range from 41MHz to 42 MHz for cables with global thermal aging to simulate 20 years of service at 50°C, plus additional thermal aging to simulate hot spots of different size

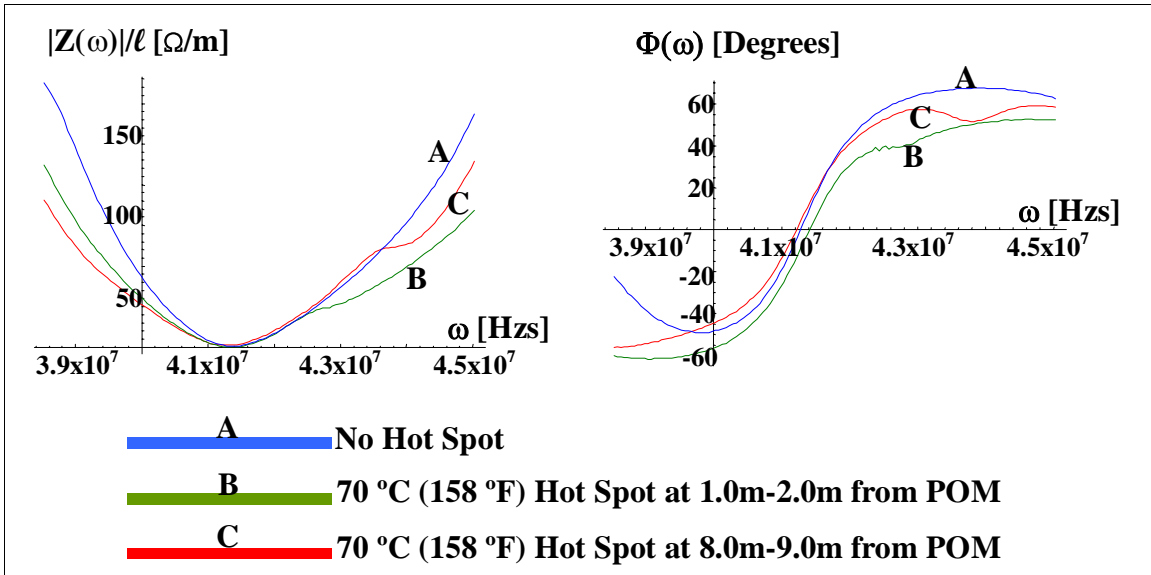


**Figure B-9** Impedance magnitude per unit length and phase spectra over the frequency range from 39MHz to 45 MHz for cables with global thermal aging to simulate 20 years of service at 50°C, plus additional thermal aging to simulate hot spots at different locations

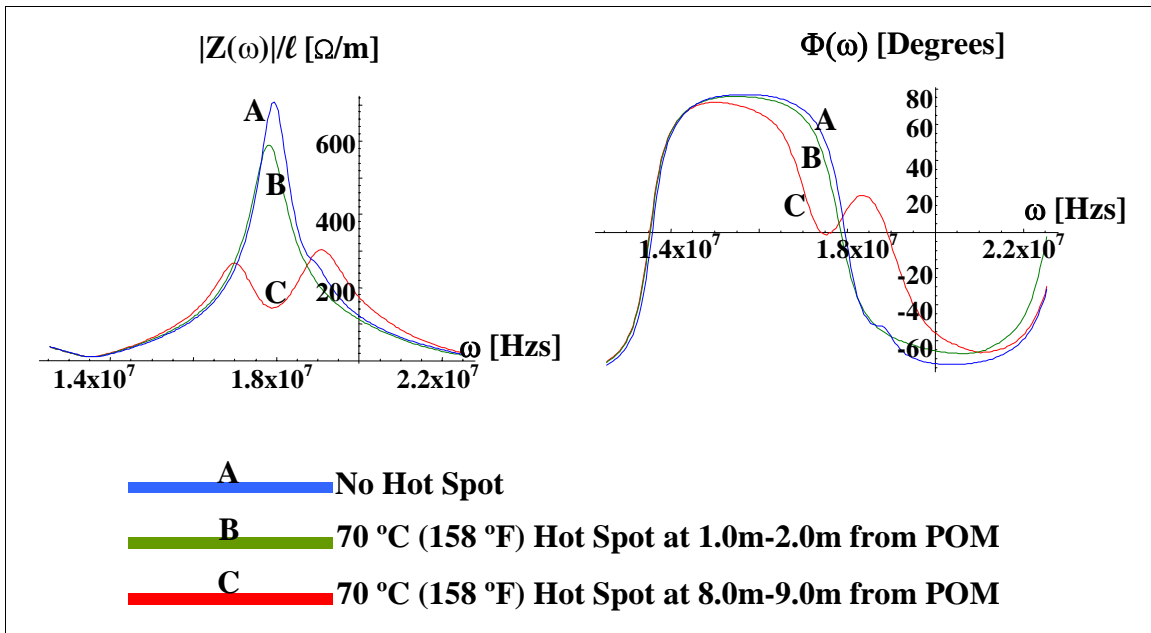


**Figure B-10** Impedance magnitude per unit length and phase spectra over the frequency range from 14MHz to 22 MHz for cables with global thermal aging to simulate 20 years of service at 50°C, plus additional thermal aging to simulate hot spots at different locations



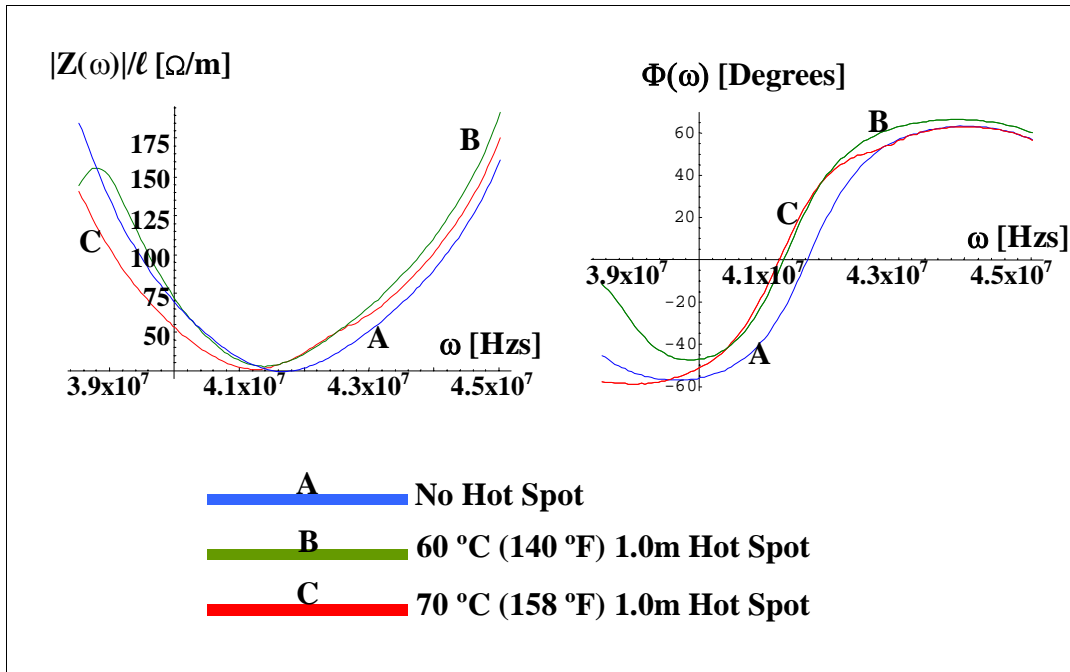


**Figure B-11** Impedance magnitude per unit length and phase spectra over the frequency range from 39MHz to 45 MHz for cables with global thermal aging to simulate 40 years of service at 50°C, plus additional thermal aging to simulate hot spots of different severity

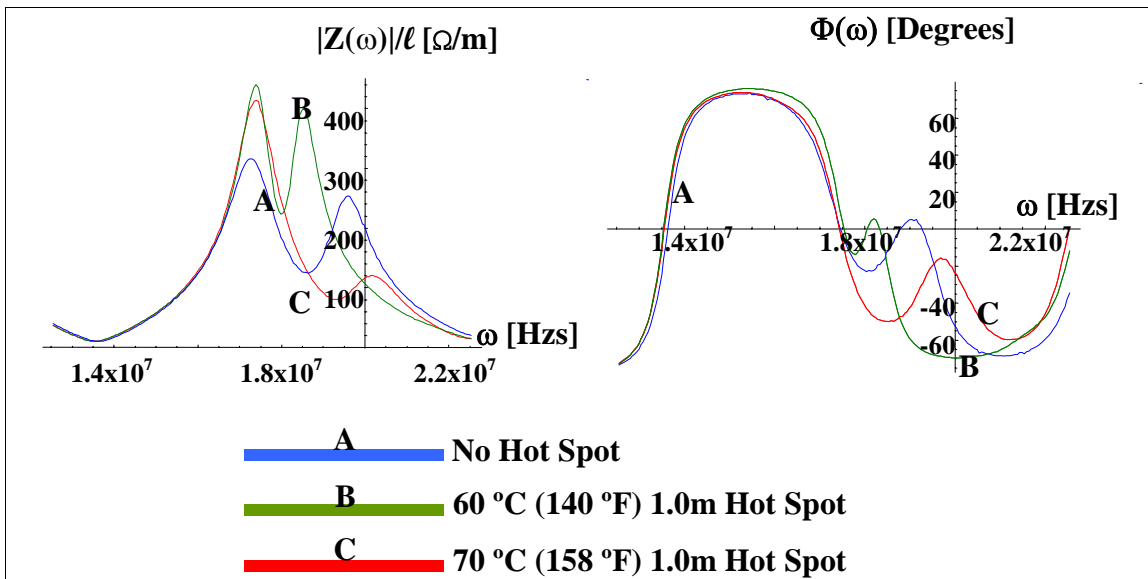


**Figure B-12** Impedance magnitude per unit length and phase spectra over the frequency range from 14MHz to 22 MHz for cables with global thermal aging to simulate 40 years of service at 50°C, plus additional thermal aging to simulate hot spots of different severity

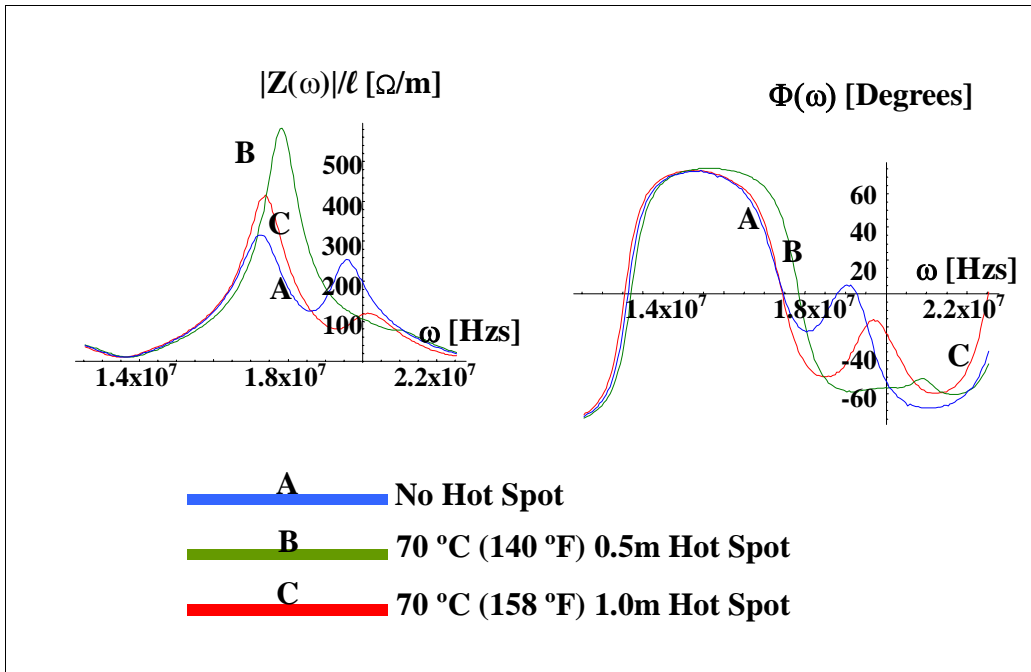


**Figure B-13** Impedance magnitude per unit length and phase spectra over the frequency range from 14MHz to 22 MHz for cables with global thermal aging to simulate 40 years of service at 50°C, plus additional thermal aging to simulate hot spots of different size

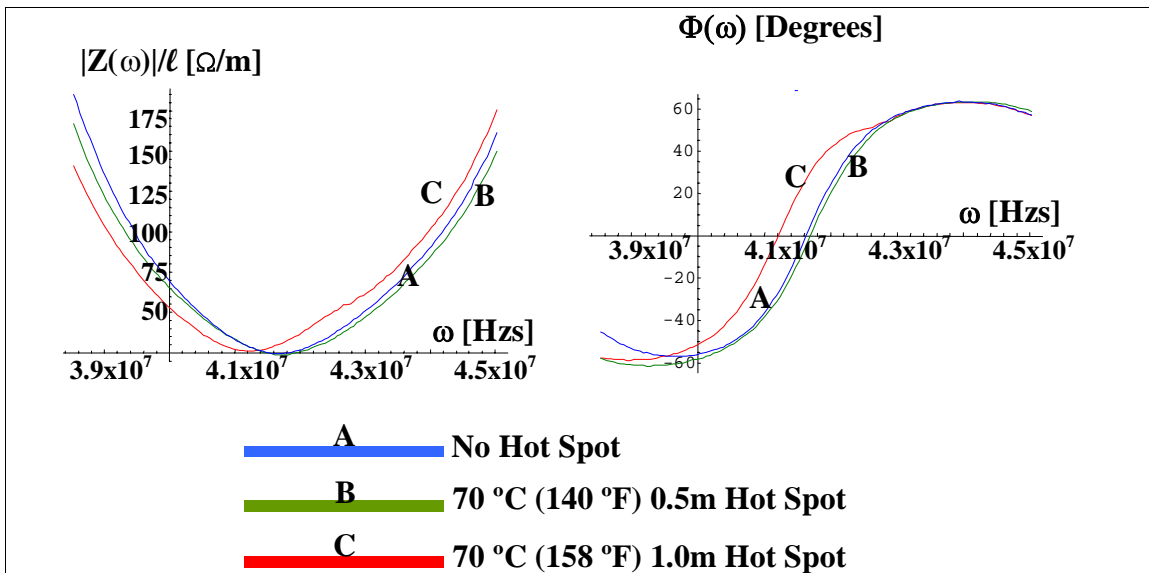


**Figure B-14** Impedance magnitude per unit length and phase spectra over the frequency range from 41MHz to 42 MHz for cables with global thermal aging to simulate 40 years of service at 50°C, plus additional thermal aging to simulate hot spots of different size

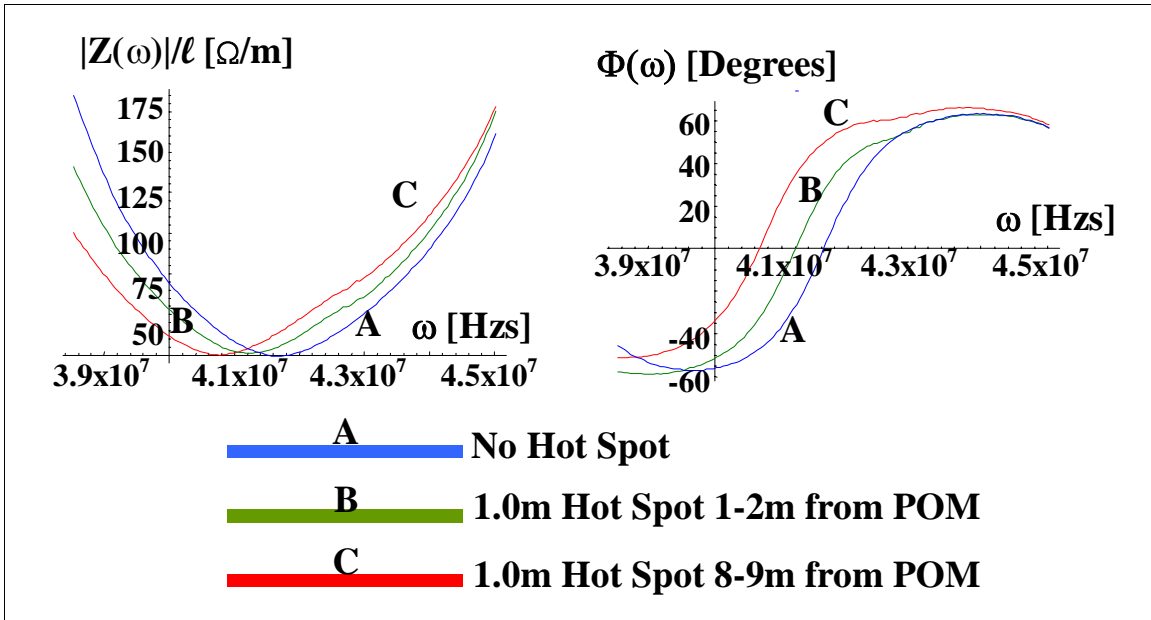


**Figure B-15** Impedance magnitude per unit length and phase spectra over the frequency range from 39MHz to 45 MHz for cables with global thermal aging to simulate 40 years of service at 50°C, plus additional thermal aging to simulate hot spots at different locations

**BIBLIOGRAPHIC DATA SHEET**

(See instructions on the reverse)

NUREG/CR-6904  
BNL-NUREG-75208-2005

2. TITLE AND SUBTITLE

Evaluation of the Broadband Impedance Spectroscopy Prognostic/Diagnostic Technique for Electric Cables Used in Nuclear Power Plants

3. DATE REPORT PUBLISHED

MONTH	YEAR
June	2006

4. FIN OR GRANT NUMBER

Y6410

5. AUTHOR(S)

D. Rogovin, The Boeing Company  
R. Lofaro, Brookhaven National Laboratory

6. TYPE OF REPORT

Technical

7. PERIOD COVERED (Inclusive Dates)

06/11/2001-11/30/2005

8. PERFORMING ORGANIZATION - NAME AND ADDRESS (If NRC, provide Division, Office or Region, U.S. Nuclear Regulatory Commission, and mailing address; if contractor, provide name and mailing address.)

Brookhaven National Laboratory, Upton, NY, 11973  
The Boeing Company, Huntington Beach, CA, 92647

9. SPONSORING ORGANIZATION - NAME AND ADDRESS (If NRC, type "Same as above"; if contractor, provide NRC Division, Office or Region, U.S. Nuclear Regulatory Commission, and mailing address.)

Division of Fuel, Engineering and Radiological Research  
Office of Nuclear Regulatory Research  
U.S. Nuclear Regulatory Commission  
Washington D.C., 20555-0001

10. SUPPLEMENTARY NOTES

Jitendra P. Vora, NRC Project Manager

11. ABSTRACT (200 words or less)

Aging mechanisms can lead to degradation of electric cables and resultant failures of critical functions, as well as losses of essential information for the decision-making process. Consequently, it would be highly desirable to have a single universally effective prognostic, diagnostic technique that can be used in situ to monitor the condition and predict the remaining useful life of installed electric cables of all types, in operating nuclear power plant applications and environments.,

To address this need, the U.S. Nuclear Regulatory Commission (NRC), Office of Nuclear Regulatory Research (RES), in collaboration with the Federal Aviation Administration (FAA) and the Boeing Company, initiated a research study to evaluate the effectiveness of the broadband impedance spectroscopy (BIS) technique for use in nuclear power plant cable diagnostics and condition monitoring. The results demonstrate the effectiveness of this nonintrusive, nondestructive technique, which uses low-voltage signals at varying frequencies to scan the length of an installed cable system to locate anomalies and degradation. Based upon this study's promising results, RES is considering follow-on collaborative research to demonstrate the effectiveness of the BIS technique in operating nuclear power plant environments.

12. KEY WORDS/DESCRIPTORS (List words or phrases that will assist researchers in locating the report.)

Cables, Diagnostics and Condition Monitoring, Remaining Useful Life, Collaborative Research, Broadband Impedance Spectroscopy

13. AVAILABILITY STATEMENT

unlimited

14. SECURITY CLASSIFICATION

(This Page)

unclassified

(This Report)

unclassified

15. NUMBER OF PAGES

16. PRICE

